FUNDAMENTAL INVESTIGATION ON LAMINAR PREMIXED COMBUSTION AND FLAME DYNAMICS OF BIO-SYNGAS

ZHOU QUAN

PhD

The Hong Kong Polytechnic University

2020

The Hong Kong Polytechnic University

Department of Mechanical Engineering

FUNDAMENTAL INVESTIGATION ON LAMINAR PREMIXED COMBUSTION AND FLAME DYNAMICS OF BIO-SYNGAS

ZHOU Quan

A thesis submitted in partial fulfillment of the requirements for the degree of Doctor of Philosophy

October 2019

CERTIFICATE OF ORIGINALITY

I hereby declare that this thesis is my own work and that, to the best of my knowledge and belief, it reproduces no material previously published or written, nor material that has been accepted for the award of any other degree or diploma, except where due acknowledgement has been made in the text.

_____(Signed)

ZHOU QUAN (Name of student)

ABSTRACT

Biomass, as one of the important renewable energy resources for maintaining sustainable energy development and reducing air pollutions as well as greenhouse gas emissions, has attracted global attention in recent years. The synthesis gas obtained from the gasification of biomass, known as bio-syngas, has complex fuel composition due to the different feedstocks and processing techniques and thereby it is increasingly difficult to control the combustion process of bio-syngas in practical combustion systems. Many studies have been conducted on the laminar burning characteristics of single-component fuels such as H_2 and CH_4, or binary fuels such as H_2-CO and H_2-CH_4 mixtures, but the related investigation of bio-syngas, which is composing of H_2/CO/CH_4/N_2/CO_2, is rarely conducted. Therefore, a comprehensive understanding of the laminar premixed combustion characteristics of bio-syngas is the most important issue at present.

In this study, the laminar premixed combustion and flame dynamics of bio-syngas has been systematically studied using a constant volume combustion bomb at an initial temperature of 303 K, equivalence ratios of 0.6-1.5 and initial pressures of 0.1-0.5 MPa for a wide range of H_2/CO/CH_4 fuel compositions and N_2/CO_2 dilution ratios (0%-45%). The research includes investigating the laminar flame speeds, analyzing the instability of the flame front propagation, and studying the explosion characteristics of the bio-syngas/air mixtures. Moreover, a one-dimensional freely

propagating flame was simulated using the PREMIX code in the CHEMKIN package with the Li mechanism for analyzing the experimental results. The main conclusions and innovative achievements are as follows:

For the laminar flame speeds of various bio-syngas/air mixtures, the experimental data and predicted results show good agreement with each other under various fuel compositions and dilution ratios at atmospheric pressure, while there exists discrepancy in the laminar flame speeds at elevated pressures between the experimental data and predicted results. The laminar flame speed decreases with the increase of initial pressure under the tested equivalence ratios which is mainly due to the increasing unburned mixture density and decreasing key radicals (H, OH, and O) concentrations. With the increase of H_2 fraction in the fuel, the laminar flame speed increases significantly, but the CH_4 enrichment flame has the lowest laminar flame speed. With the increase of CO fraction in the fuel, the laminar flame speed does not change much. The thermal and chemical kinetic analyses indicate that the CO addition has more effect on the adiabatic flame temperature but only plays a small role in the chemical effect compared to that of the H_2 addition. Moreover, the laminar flame speed decreases with the increase of N_2/CO_2 dilution ratio in the fuel mixture. CO_2 dilution has stronger dilution effect, thermal effect, and chemical effect than those of N_2 dilution, and thereby it can substantially decrease the laminar flame speeds of $H_2/CO/CH_4$/air mixtures.

For the intrinsic instability of the flame front propagation at atmospheric pressure for various bio-syngas/air mixtures, the results of flame morphology and Markstein length show that, the flame front can remain fairly smooth at atmospheric pressure except for some large wrinkles caused by the ignition disturbance. The Markstein length is decreased with the increase of H_2 fraction in the fuel mixture indicating the decrease of stability of the flame front, while the Markstein length is slightly increased with CH_4 or CO addition suggesting the enhancement of the flame front stability. With N_2/CO_2 dilution, the Markstein length decreases at all dilution ratios, suggesting that the addition of N_2/CO_2 promotes the flame instability at atmospheric pressure.

For the intrinsic instability of the flame front propagation at elevated pressures for various bio-syngas/air mixtures, the results clearly show that with the increase of initial pressure, irregular wrinkles appeared at the flame surface and the higher the initial pressure, the more advance the onset of cellular instability of the flame is observed. The cellular instability of the flame front is significantly promoted with the increase of H_2 fraction in the fuel mixture and the earlier onset of cellular flame structure is also observed, while the cellular instability is suppressed and the moment for onset of cellular flame structure is postponed with the increase of CO fraction in the fuel mixture. With increasing CH_4 concentration in the fuel mixture, the cellular instability is found to be significantly inhibited and the moment for onset

of cellular flame structure is also significantly delayed. On the other hand, the suppression effect of cellular instability with N_2/CO_2 dilution is observed and CO_2 dilution has stronger effect in suppressing the cellular instability at elevated pressures.

For the explosion characteristics of various bio-syngas/air mixtures, the results show that the concentration of H_2 or CH_4 in the fuel mixture has a great influence on the explosion characteristics of bio-syngas/air mixtures, while the concentration of CO in the fuel mixture plays a mild role in affecting the explosion behaviors. Moreover, it is observed that the addition of N_2/CO_2 to the fuel mixture can significantly reduce the potential of explosion hazards of bio-syngas/air mixtures, and CO_2 dilution has stronger suppression effect on the explosion characteristics due to its larger negative influence on the thermal effect and the chemical effect in comparison to that of N_2 dilution. The corresponding correlations of $P_{max}/P_0=f(Z_{dilution})$, $t_c=f(Z_{dilution})$, and $(dP/dt)_{max}=f(Z_{dilution})$ are developed for predicting the explosion behaviors of N_2/CO_2 diluted bio-syngas/air mixtures at various dilution ratios.

In conclusion, since the diverse biomass feedstock and processing techniques lead to considerable variations in the fuel composition of bio-syngas, its fundamental combustion characteristics should be well understood because the components of a bio-syngas and their proportions have significant influences on the laminar flame speed, flame instabilities and explosion characteristics of the bio-syngas. It can be

concluded that H_2-enriched condition has much higher laminar flame speed than other conditions, but the intrinsic instabilities of flame and explosion hazard are significantly prompted. For the CH_4-enriched condition, the behaviors are quite the contrary to that of the H_2-enriched condition. CO addition is found to play a mild role in affecting the laminar burning and explosion characteristics of bio-syngas. On the other hand, it can be concluded that N_2/CO_2 diluted bio-syngas has much lower laminar flame speed and suppressed intrinsic flame instabilities as well as explosion hazard than that of non-diluted bio-syngas. Therefore, the different combustion behaviors of diverse bio-syngas fuels need to be fully considered for optimizing the combustion of bio-syngas in practical combustors.

PUBLICATIONS ARISING FROM THE THESIS

1. **Zhou Q.**, Cheung C.S., Leung C.W., Li XT, Li XJ, Huang ZH. Effects of fuel composition and initial pressure on laminar flame speed of H_2/CO/CH_4 bio-syngas. ***Fuel***, 2019, 238: 149-158.

2. **Zhou Q.**, Cheung C.S., Leung C.W., Li XT, Huang ZH. Effects of diluents on laminar burning characteristics of bio-syngas at elevated pressure. ***Fuel***, 2019, 248: 8-15.

3. **Zhou Q.**, Cheung C.S., Leung C.W., Li XT, Huang ZH. Explosion characteristics of bio-syngas at various fuel compositions and dilutions in a confined vessel. ***Fuel***, 2020, 259: 116254.

4. **Zhou Q.**, Cheung C.S., Leung C.W., Huang ZH. Effect of fuel composition on OH distribution of bio-syngas/air inverse diffusion flame (5476). The 15th International Conference on Flow Dynamics, Sendai, Miyagi, Japan, 7 November-9 November, 2018.

ACKNOWLEDGEMENTS

I would like to express my sincerest appreciation to my supervisors, Prof. C.S. Cheung (The Hong Kong Polytechnic University), Prof. C.W. Leung (CPCE, The Hong Kong Polytechnic University), and Prof. Zuohua Huang (Xi'an Jiaotong University) for their patient guidance and valuable suggestions throughout my study in the past three years. Their expertise is admirable and their dedication to research work always inspires me to overcome difficulties in the research study. Without their help, I would not be able to successfully finish this thesis.

I would also like to thank The Hong Kong Polytechnic University for the stipend and research fund for this study. Additionally, I would like to give my sincere thanks to the technical officer Mr. K.S. Tsang, who has provided me helpful advices and considerable assistance during my study. Also, I would like to thank the lab members: Dr. Chun Guan, Dr. Haishen Zhen, Dr. Jin Fu, Dr. Jing Miao, Dr. Zhilong Wei and Mr. Long Wei who have kindly supported me in my experiments and research.

I would like to express my great appreciation to all the lab members in Xi'an Jiaotong University for their kind assistance and full support in the experiments and research. I am particularly grateful for the assistance given by Prof. Erjinang Hu, Prof. Jinhua Wang, Dr. Xiaotian Li, Mr. Xiaojie Li, Mr. Jinfeng Ku, Mr. Weijie

Zhang, Ms. Min Chang, Mr. Shilong Guo, Mr. Xiao Cai, Ms. Yemiao Zhang, Dr. Ke Yang, Dr. Fuquan Deng, Dr. Feiyu Yang, and Dr. Meng Zhang.

I am also very grateful to my dear friends, Ms. Meng Wang, Dr. Qi Hu, Mr. Yaozhong Liao, Dr. Menglong Liu, Dr. Kai Wang, Dr. Zhibo Wang, Dr. Hao Zhang, Ms. Qin Lei, and Mr. Yu Fang for sharing the inspired discussions and accompanying me to have an unforgettable and valuable campus life.

Lastly, and most importantly, I would like to express my special thanks to my family members. Their unconditional love and support are the significant driving force of my study.

TABLE OF CONTENTS

LIST OF FIGURES

LIST OF TABLES

NOMENCLATURE

A_f	Area of flame surface/ m^2
B_C	Collision frequency factor/ $gm.s.cm^{-3}$
C_p	Constant pressure specific heat capacity/ $kJ.(kg.K)^{-1}$
Da_c	Collision Damköhler number
D	Diffusion coefficient/ $m^2.s^{-1}$
D_{ij}	Binary diffusion coefficient for species (i) to (j)/ $m^2.s^{-1}$
$(dp/dt)_{max}$	Maximum rate of pressure rise/ $MPa.s^{-1}$
E_a	Global activation energy/ $kJ.mol^{-1}$
f^0	Laminar burning flux/ $kg.(m^2.s)^{-1}$
L_b	Markstein length/ mm
l_f	Laminar flame thickness/ mm
Le	Lewis number
Le_{eff}	Effective Lewis number
P_{max}	Explosion pressure/ Pa
Pe_{cr}	Critical Peclet number
q_c	Heat release per unit mass/ $J.kg^{-1}$
R^0	Universal gas constant/ $J.(mol.K)^{-1}$
R_f	Flame radius/ mm
R_{cr}	Critical flame radius/ mm
S_b	Stretched flame speed/ $m.s^{-1}$
S_b^0	Unstretched flame speed/ $m.s^{-1}$
S_u^0 / S_L	Laminar flame speed/ $m.s^{-1}$
T_{ad}	Adiabatic flame temperature/ K
T_u	Unburned fuel mixture temperature/ K
T_b	Burned fuel mixture temperature/ K
t_c	Explosion time/ ms

Ze	Zel'dovich number
α	Thermal diffusion coefficient/ $m^2.s^{-1}$
κ	Flame stretch rate/ s^{-1}
λ	Thermal conductivity/ $W.(m.K)^{-1}$
ρ_u	Density of unburned fuel mixture/ $kg.m^{-3}$
ρ_b	Density of burned fuel mixture/ $kg.m^{-3}$
σ	Thermal expansion ratio
ω	Reaction rate/ $kg.(m^3.s)^{-1}$

CHAPTER 1 INTRODUCTION

1.1 Background

Energy is essential to our existence on this planet. Every great progress in productivity and economy of the world has been accompanied by an explosion in energy demand. According to the production process, energy can be divided into primary energy and secondary energy. Primary energy refers to the natural energy that forms naturally during the evolution of earth. Most of the primary energy sources can be converted and used directly. Secondary energy refers to the energy derived from the transformation of primary energy sources, including petrol, electric energy, and hydrogen, and so on. In general, primary energy can be divided into the following categories.

1) Conventional non-renewable fossil fuels such as coal, oil, and natural gas;
2) Renewable energy sources such as solar energy, wind energy, and water energy;
3) Emerging energy sources such as nuclear energy.

Since 1970, with the continuous and fast development of the world's economy, the demand for energy continues to explode. According to the BP Statistical Review of World Energy 2018 [1], global primary energy consumption grew strongly in 2017, by 2.2% on average. Figure 1.1 shows the outlook of global primary energy consumption and shares of primary energy [2].

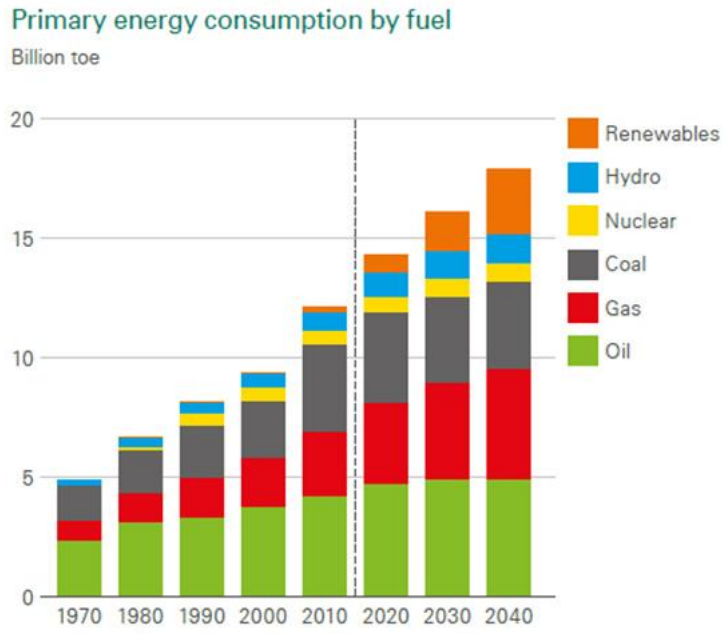

(a) Primary energy consumption by fuel, 1970-2040

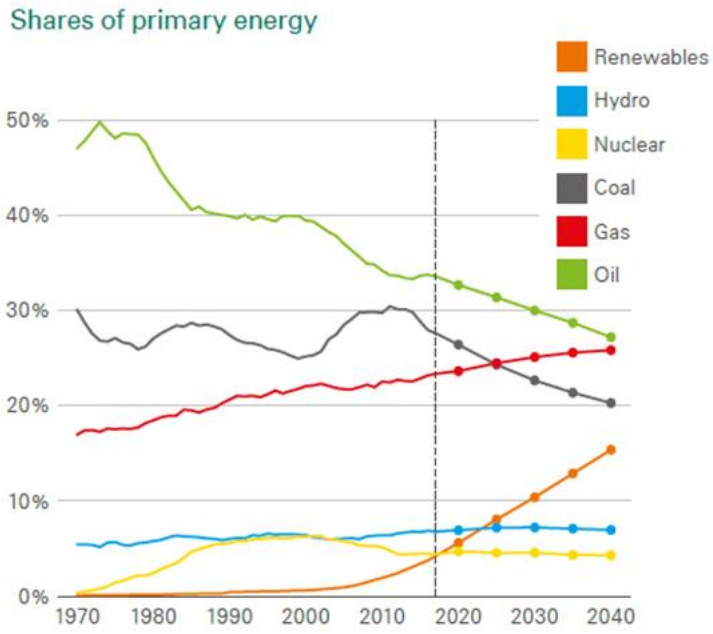

(b) Shares of primary energy , 1970-2040

Figure 1.1 Outlook of global primary energy consumption and shares of each kind of primary energy (2019 edition) [2]

A quick glance at the past forty years, because of the widespread convenience and availability of fossil fuels, including oil, coal and natural gas, there is increasing

reliance on them to fulfill the global energy demand with respect to electricity generation, transportations, and heating appliances. At present, the world's energy system is still dominated by the use of non-renewable fossil fuels. However, when we look at the downside issue associated with energy usage, there are serious problems coming along such as environmental deterioration due to air pollution emissions and global warming due to greenhouse gas emissions. In addition, it is acknowledged that the formation of fossil fuels requires millions of years typically, thus the reserve of existing fossil fuels is considered difficult to accommodate the increase of world energy demand in the future. The drastic increasing consumption of fossil fuels leads to a large amount of pollutant emissions released into the atmosphere, for instance, unburned and partially burned hydrocarbons, nitrogen oxides (NO and NO_2), sulfur oxides (SO_2 and SO_3), carbon dioxide (CO_2), carbon monoxide (CO), and particulate matter in various forms. To achieve the worldwide goal of energy conservation and air pollution control, massive efforts have been made in recent decades to develop more efficient energy conversion techniques and replace fossil fuel utilization as much as possible with sustainable and environmentally friendly alternative fuels. It is seen from Figure 1.1(b) that renewable energy resources are playing increasingly important roles in the world's energy system, while the roles of oil and coal in energy supply are decreasing gradually. In the next 20 years, the transition to a low-carbon energy system will continue in global energy supply, with renewable energy and natural gas gaining in

more importance relative to oil and coal. The BP Company indicates that renewable energy is the fastest growing source of energy, contributing half of the growth in global energy, with its share in primary energy increasing from 4% by 2018 to around 15% by 2040 [1].

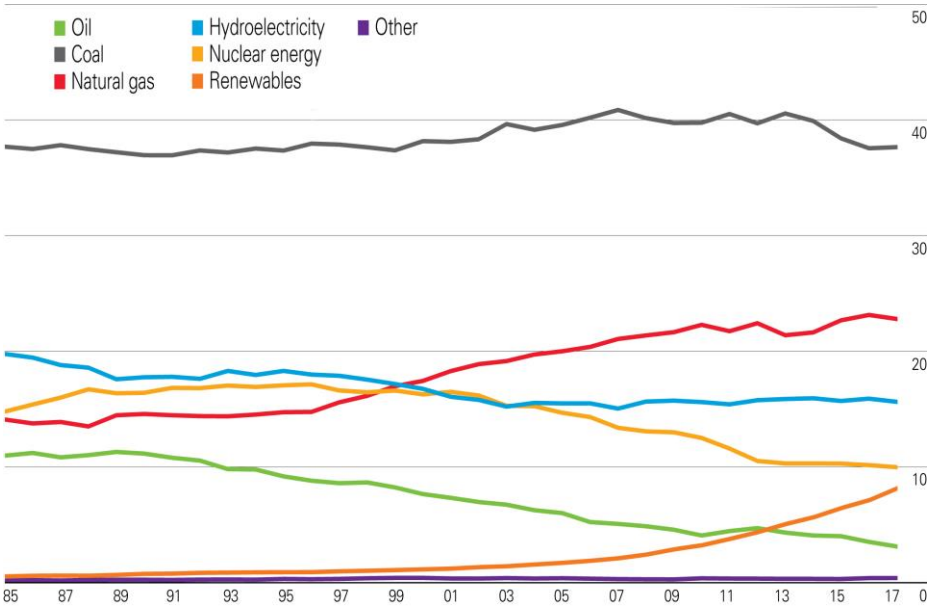

Figure 1.2 Share of global electricity generation by fuel [1]

According to the statistical results of the BP Company, over 40% of primary energy went into the power generation sector in 2017. The power generation sector plays a central role in the development of global energy markets. It is not only the single biggest market for energy consumption by far, but also accounting for over a third of carbon emissions in 2017 [1]. Therefore, it is at the leading edge of the energy transition, in terms of both improvements in energy efficiency and the shift toward a lower-carbon fuel mix. Figure 1.2 shows the share of global electricity generation by different fuels. In the past, the world's electricity needs are met primarily by burning

coal. Because of the huge efforts to encourage a shift away from coal into cleaner and sustainable fuels, the share of renewable energy sources in power generation has risen 6% since 2007. However, it is seen that coal is still the world's dominant source for power generation, with a share of 38% in 2017. Therefore, the search for sustainable and clean fuels is still a crucial factor in economic development and environmental protection.

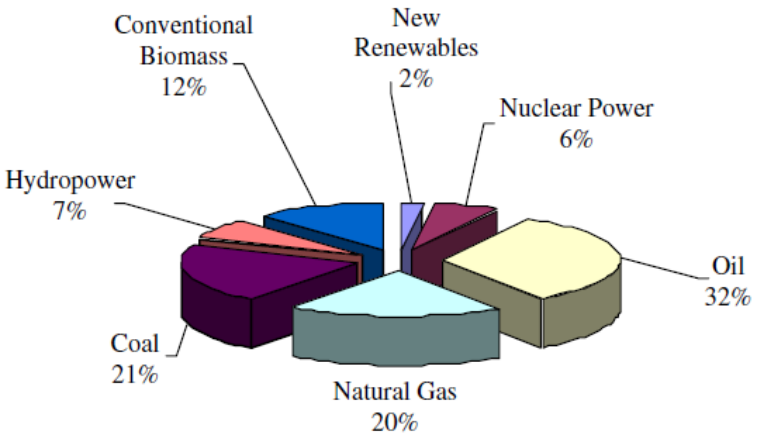

Figure 1.3 Distribution of the world's primary energy consumption [3]

Among the various renewable energy sources, biomass has been widely recognized as one of the most promising alternative fuels and will play a vital role in the global energy supply system in the near future. At present, worldwide biomass ranks fourth as primary energy and its share in the world's total primary energy consumption is about 12%, as shown in Figure 1.3 [3]. With the deterioration of environment as well as the global warming issues due to heavily dependent on fossil fuels, the utilization of biomass in the energy supply system is constantly growing due to the needs for alternative energy sources and low emissions [4]. Many studies [3-7]

indicate that biomass is neutral in CO_2 circulation, that is, the amount of CO_2 it consumed through photosynthesis is the same as that given off by combustion, and therefore contributing to mitigate greenhouse gas emissions. Moreover, biomass offers some important advantages as feedstock for combustion due to its wide availability and contribution to diversification of energy supply and rural development. Since the use of biomass fuels provides substantial benefits as far as the environment is concerned, it is essential to conduct a comprehensive investigation of using such kind of fuels.

1.2 Bio-syngas

Formerly, biomass was usually used in direct combustion. In recent years, conversion technologies such as pyrolysis, gasification, anaerobic digestion and alcohol production have widely been applied to biomass in order to obtain its energy content [6]. In a gasification process, the solid biomass can be converted to gaseous products, namely bio-syngas, containing major components H_2, CO, CH_4, and other species such as N_2, CO_2, and very small amount of high order hydrocarbons (C_{2+}). Because of the production of cleaner gaseous fuel as well as the almost complete conversion of biomass, the gasification process in converting biomass is becoming progressively attractive [8]. The synthesis gas obtained from gasification of biomass fuel is called bio-syngas. The diverse biomass feedstock and gasification techniques lead to considerable variations in the composition of a bio-syngas.

Figure 1.4-1.7 show the statistical results of various compositions of bio-syngas reported in the literature [8-16]. It is seen that a bio-syngas mostly has high concentrations of H_2 and CO but a relatively low concentration of CH_4. The volumetric fraction of H_2 in the main fuel components H_2/CO/CH_4 can vary from 20% to 80%. The H_2/CO ratio in a bio-syngas varies from 1:5 to 5:1 or so. In general, the other species such as N_2 and CO_2 are about half of the total composition, but they can be removed through purification processes such as pressure swing adsorption, amine scrubbing, and membrane reactors [17].

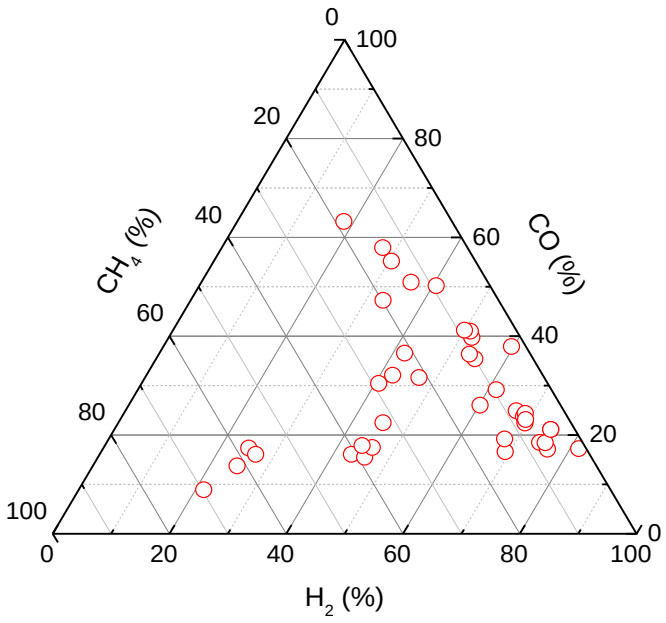

Figure 1.4 Statistical results of bio-syngas composition for the main species H_2/CO/CH_4 on volumetric basis [8-16]

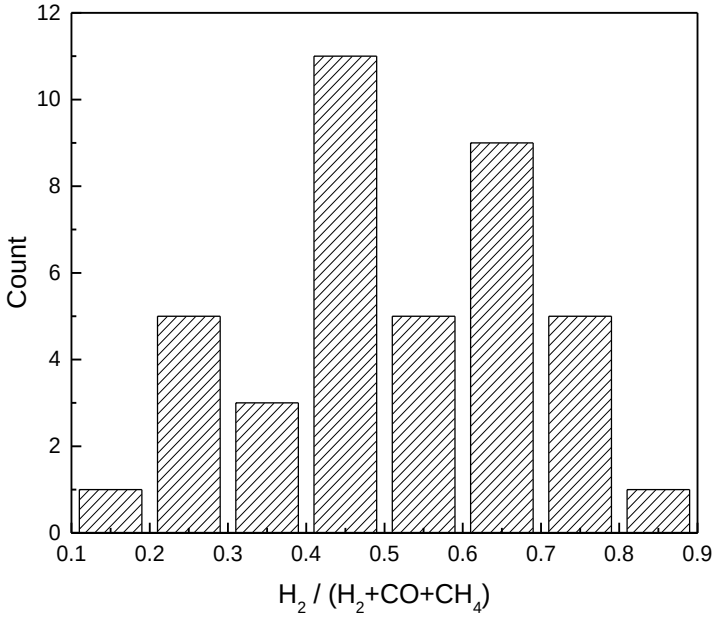

Figure 1.5 Statistical results of bio-syngas composition for H_2/ (H_2+CO+CH_4) ratio [8-16]

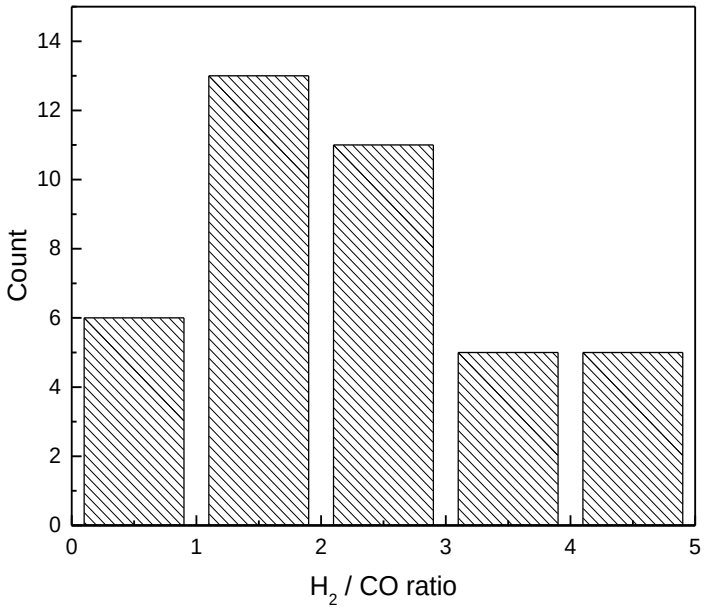

Figure 1.6 Statistical results of bio-syngas composition for H_2/ CO ratio [8-16]

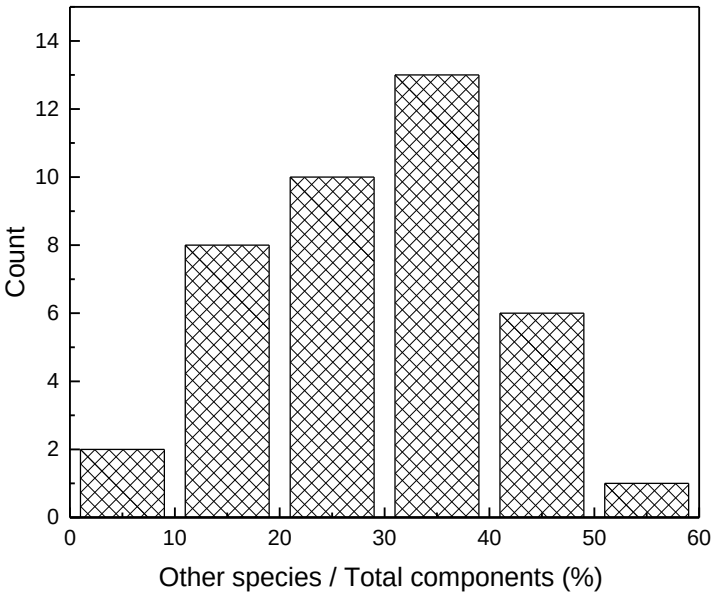

Figure 1.7 Statistical results of bio-syngas composition for the ratio between other species (CO_2, N_2, C_{2+}) and total components [8-16]

The variable fuel compositions in bio-syngas lead to unpredictable combustion performance and increasing difficulties of combustion control and chamber design. Therefore, it is necessary to carry out the fundamental research on bio-syngas combustion to understand its combustion behaviors under various fuel compositions and operating conditions.

1.3 Laminar premixed flame

Today, our dependence on the service of combustion is almost total, ranging from heating and lighting our homes to powering the various modes of transportation vehicles. Combustion transforms energy stored in chemical bonds to heat that can be utilized in a variety of ways [18]. It is comprised of branches of nonlinear science,

such as thermodynamics, chemical kinetics, fluid mechanics, and transportation phenomena. According to different classification methods, fundamental combustion phenomena can be divided into laminar versus turbulent combustion, premixed versus non-premixed combustion, subsonic versus supersonic combustion, and homogenous versus heterogeneous combustion [19]. Combustion occurring in a practical combustor is a complex turbulent combustion process involving a wide range of coupled problems such as fluid mechanics, transport phenomena, detailed chemical reaction schemes, and heat transfer. The accurate control of turbulent flames is a real challenge since all the aspects of the problem are not fully addressed in the present state [20]. In order to deal with this problem, simplified combustion modes are often adopted to study the local combustion characteristics and mechanisms.

For turbulent premixed combustion, the turbulence and chemical reactions are coupled intimately in the flame with a wide range of time scale and length scale. On the one hand, the turbulence affects the structure of the flame and the affected flame structure adversely influences the flow characteristics of the turbulence due to the changes in physical quantities such as the temperature field. Figure 1.8 shows the regime of turbulent premixed combustion [21]. On the basis of velocity and length scale ratios, three regimes of turbulent premixed combustion can be defined, namely, the broken reaction zone, the thin reaction zone, and the flamelet zone. In practical combustors, turbulent premixed combustion is mainly located in the flamelet zone,

where chemical reactions proceed in a thin layer owing to its fast reaction rate while the turbulence can only distort this reaction layer and enlarge the flame front rather than entering the reaction zone [21]. Since the chemical reactions in this thin layer are unaffected by the turbulent fluctuations, the turbulent premixed flame front can be considered to be composed of continuous quasi-steady laminar premixed flamelets which can reveal the global combustion features of turbulent premixed flame to some extent.

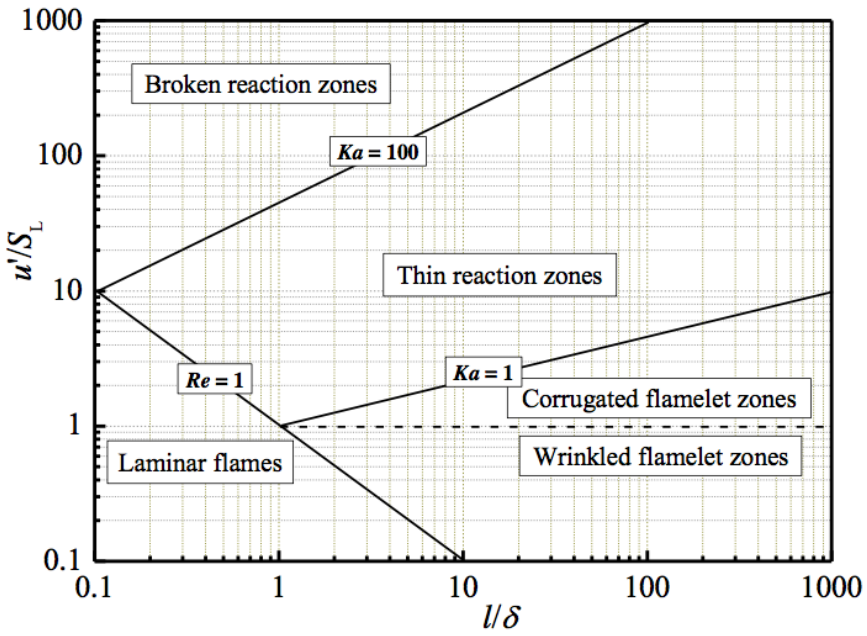

Figure 1.8 Regime diagram for premixed turbulent combustion [19]

Therefore, laminar premixed flame is a common combustion mode adopted in massive researches to simplify problems related to real complex combustion processes. The study of laminar premixed flame is a prerequisite to the study of turbulent flames since in both laminar and turbulent flows, the same physical processes are active, but the flow in a laminar flame is relatively simple and can be

clearly quantified and defined. In addition, qualitatively describing the essential characteristics of laminar premixed flames and developing simplified analysis of these flames can directly reflect the essential characteristics of the fuel utilized and allow us to identify the factors influencing the important combustion parameters such as laminar flame speed and flame thickness.

Flame dynamics, which mainly involved in the flame stretch, intrinsic flame instability, and cellular structure of wrinkled flame front, is also an interesting and important topic for laminar premixed flame propagation [22]. The wrinkled flame front is mostly due to the interaction among stretch, chemical reaction and transport [23]. Moreover, it has been indicated by previous studies [24, 25] that intrinsic flame instability will have a great influence on turbulent premixed flame and the turbulent premixed flame may be induced as cellular flame structures continuously evolve. Therefore, investigations on the intrinsic flame instability and cellular structure of the wrinkled flame front of bio-syngas under various operating conditions can help improve the understanding of the fundamental flame dynamics for utilization of bio-syngas.

Moreover, safety issues are also very important for production, transportation, storage, and usage of bio-syngas due to the variability of bio-syngas composition. Explosion characteristics of a combustible mixture can provide a basis for assessing the hazards of a chemical process and the design of explosion-proof vessels to avoid

damage from gaseous explosions [26, 27]. In this regard, understanding the pressure history during combustion in a constant volume combustion bomb can help evaluate the hazards of bio-syngas explosion and provide fundamental data for the design of bio-syngas combustion system.

1.4 Scope and objectives of the present study

Due to global environmental threats as well as heavy reliance on fossil fuels, it is very urgent to either improve the combustion efficiency with considerable reductions in fuel consumption and pollutant emissions, or more significantly, to replace fossil fuel utilization as much as possible with other environmentally friendly, clean, and renewable energy resources. Synthesis gas derived from biomass (bio-syngas) is expected to have the potential to substitute fossil fuel in heating and power generation, as it allows for a reduction in environmental impact as well as offering a diverse solution to sustainable development. Thus, it is of vital importance to have a comprehensive investigation and in-depth understanding of the laminar premixed combustion and flame dynamics of bio-syngas. Unlike the single-component fuel, it is increasingly difficult to control the combustion process of bio-syngas due to its diversity in fuel composition. A detailed study on the combustion characteristics of bio-syngas can not only improve the understanding of this kind of fuel regarding energy utilization and combustion behavior but also provide some useful information and guidelines for its practical application. The

objectives of the present study are shown below:

1. To obtain laminar flame speeds of various bio-syngas/air mixtures using a constant volume combustion bomb system. To investigate the effect of equivalence ratio, initial pressure, the variation of fuel composition (H_2:CO:CH_4), and dilution ratio (CO_2/N_2/CO_2+N_2 : total fuel components) on laminar flame characteristics of bio-syngas (H_2/CO/CH_4/CO_2/N_2).
2. To numerically study the chemical kinetics of bio-syngas/air laminar premixed flame using the CHEMKIN software. To verify the chemical mechanism by comparing the experimentally obtained laminar flame speed and simulated results. To analyze the effect of different initial conditions on bio-syngas/air laminar premixed combustion by conducting sensitivity analysis, consumption pathway analysis, and chemical flame structures to identify the key reactions and intermediate species that affect the laminar flame speed of bio-syngas.
3. To observe the propagation of laminar flame front of bio-syngas/air premixed flame at different initial pressures. To analyze the factors for changes in flame morphology at elevated initial pressure and measure the critical flame radius of bio-syngas/air mixtures under different initial conditions. To calculate the critical Peclet number, critical flame radius, and instability parameters such as effective Lewis number, thermal expansion ratio, and flame thickness; and theoretically study the effect of fuel composition variation and diluents on the intrinsic flame instabilities of bio-syngas laminar premixed flame at elevated initial pressure.

4. To investigate the explosion characteristics of bio-syngas/air mixtures at different equivalence ratios, initial pressures, fuel compositions, and dilution ratios. To analyze the effect of these initial conditions on the explosion characteristics parameters, such as the maximum explosion pressure, explosion time, the maximum rate of pressure rise, and the deflagration index.
5. To analyze the effect of each fuel component, including the diluents, on the physics and the chemical kinetics behind that lead to change in the laminar flame speed and the flame dynamics of the bio-syngas.

1.5 Thesis organization

Chapter 1 mainly introduces the research background and the objectives of this study. The related previous researches are reviewed and discussed in Chapter 2. Chapter 3 gives the experimental apparatus and numerical methodology adopted in the present investigation. Detailed experimental and numerical results are given and discussed in Chapter 4, Chapter 5 and Chapter 6, which mainly involve in the laminar flame speeds of bio-syngas in a wide range of conditions, analyzing the instability of the flame front propagation under various initial pressures, and studying the explosion characteristics of the bio-syngas/air mixtures, respectively. Chapter 7 presents the main conclusions of this study, as well as the recommendations emerged from the current study.

CHAPTER 2 LITERATURE REVIEW

A review of the basic theory of laminar premixed combustion is firstly presented to provide the fundamental information for understanding this kind of flame. Specifically, laminar flame speed, intrinsic flame instability, and explosion characteristics are emphasized in this work. Moreover, a detailed review of the current conversion technologies of biomass fuels is conducted to provide information for the investigation of bio-syngas fuel. The recent research progress in the combustion of bio-syngas and the efforts on exploring the combustion characteristics of this fuel are reviewed to identify the blanks and provide a solid foundation for the present study.

2.1 Laminar premixed combustion

Laminar flame has been widely used to study and understand the controlling physics of a variety of phenomena which are difficult to be accessible under turbulent conditions [28]. This section firstly introduces the basic theories related to laminar premixed flame, then introduces the common methods adopted in the laboratory for measuring laminar flame speed.

2.1.1 Basic theory of laminar premixed flame

For an ideal standard laminar premixed flame, which is the simplest combustion mode, the flow field has no influence on the chemical reactions in the flame. Then, the flame structure can be considered at three levels of detail [19], which are given

in Figure 2.1.

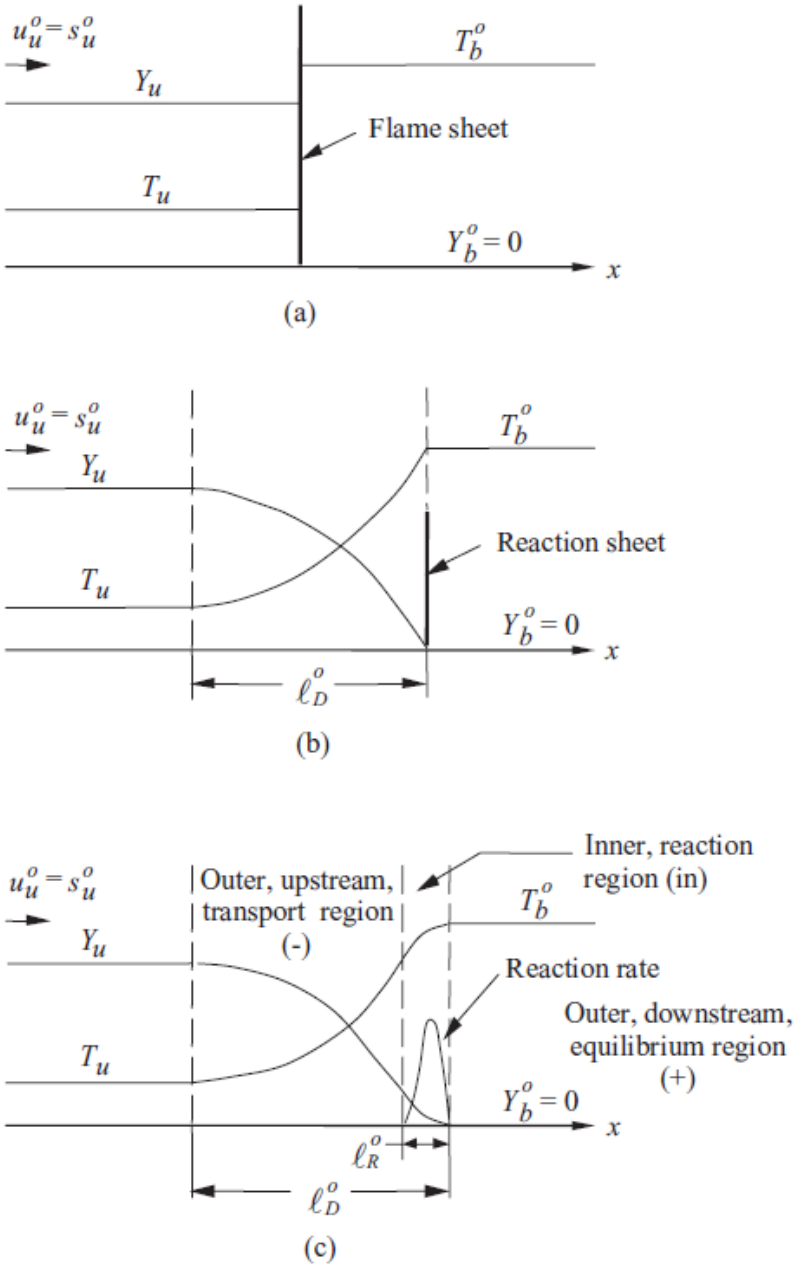

Figure 2.1 Schematic of the laminar premixed flame structure at three levels of detail: (a) The hydrodynamic, flame-sheet level; (b) The transport, reaction-sheet level; (c) Detailed structure including the reaction zone [19].

The first is the hydrodynamic level of the flame structure, as shown in Figure 2.1(a). In the flame-stationary frame, the upstream mixture, namely unburned mixture,

approaches the flame with velocity U_u^0, which is equal to the laminar flame speed S_u^0 (S_L is used interchangeably throughout the present study). The temperature of the unburned mixture is T_u. After passing through the flame sheet, the velocity and temperature of the burned mixture are changed to U_b^0 and T_b^0, respectively. Regardless of the chemical reactions in the flame, the flame sheet is simply an infinitely thin interface separating the unburned and burned gases that are in thermodynamic equilibrium. The unburned gas and burned gas are related by the overall conservation of mass, species concentrations, and energy. However, it can be clearly seen that the temperature T_u and reactant concentration Y_u have a sudden change to T_b^0 and $Y_b^0 = 0$ respectively after passing through the flame sheet, which is discontinuous at this flame sheet.

Figure 2.1(b) gives the second level of the flame structure which is dominated by transport diffusion. In this configuration, the description of the flame structure is more detailed, including a preheat zone and reaction zone. The preheat zone is governed by heat and mass diffusion processes with a characteristic thickness ℓ_D^0. When the unburned gas approaches the flame, it is gradually heated up by the heat conducted forward from the chemical heat release region until the temperature T_b^0 is reached. The continuous heating of the unburned gas will eventually lead to its ignition and subsequent reaction. However, due to the presence of convective transport, the profile of increasing temperature is not linear.

The third description is the most detailed level of the flame structure containing the reaction zone, as shown in Figure 2.1(c). Here, the flame structure can be divided into two distinct zones, namely, the preheat zone in which the convection and diffusion dominate and balance, and the reaction zone in which the reaction and diffusion dominate and balance. The reaction rate profile is a highly peaked function, consisting of a rapid increasing portion due to the activation of the reaction, followed by a rapid decreasing portion due to the depletion of the reactants. Since the characteristic thickness $\ell_R^0 \ll \ell_D^0$, this rapid rate of property change within a narrow region indicates that diffusive transport described by a second-order differential has a greater influence than convective transport described by a first-order differential.

According to the third level of flame structure description, Law [19] theoretically analyzed the process of flame propagation based on a one-reactant reaction hypothesis,

$$\text{Reactant} \rightarrow \text{Products} \tag{2-1}$$

and obtained the following relationship for a laminar premixed flame,

$$\left(f^0\right)^2 = \frac{(\lambda/C_p)LeB_C e^{-T_a/T_b^0}}{Ze^2} \tag{2-2}$$

where f^0 is the mass flow rate of unburned gas, kg.(m^2.s)$^{-1}$; C_p is the constant pressure specific heat capacity, J.(kg.K)$^{-1}$; λ is the thermal conductivity, W.(m.K)$^{-1}$;

Le is the Lewis number, which measures the relative rates of thermal conduction to mass diffusion; B_C is the density-weighted collision rate of the reaction, gm.s.cm^{-3}; *Ze* is the Zel'dovich number, which measures the combined effects of the temperature sensitivity of the reaction and the extent of heat release relative to the initial content of the mixture's sensible energy [19].

It should be noticed that the derivation process uses the assumption of a one-reactant reaction, and there is a clear difference from the practical chemical reactions which contain thousands of elementary reactions. However, Equation (2-2) clearly shows that there is a close correlation between the laminar burning characteristics and the physicochemical properties of the mixture itself for laminar premixed flame.

2.1.2 Laminar flame speed and measurement methods

Laminar flame speed is considered one of the most important physicochemical parameters of a combustible fuel mixture. It is a function of the exothermicity, diffusivity, and reactivity of the mixture and a basic parameter for turbulent flame speed determination [19]. In addition, it can be used to develop and validate the chemical reaction mechanism, and it is of great importance in the design and optimization of practical combustors. Therefore, considerable efforts have been taken towards their determination. In the following, several measurement methods that have been widely used in previous studies are discussed.

2.1.2.1 Bunsen flame method

Bunsen burner plays an important role in studying laminar and turbulent flames in a laboratory. Figure 2.2 shows the schematic diagram of a Bunsen flame. The upstream unburned mixture flow in the Bunsen flame is non-uniform and the flame surface is also curved [29].

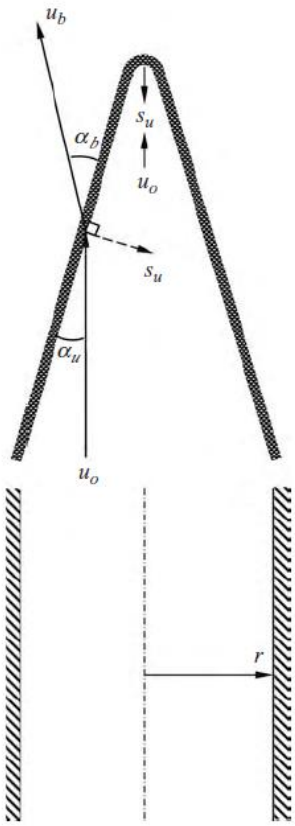

Figure 2.2 Schematic diagram of a Bunsen flame [19]

In general, there are two ways to obtain the laminar flame speed of a fuel from the Bunsen flame. The first way is the flame area method. The laminar flame speed calculated in this method is an area-weighted flame speed over the entire flame

surface A_f. If the mass flow rate of the gas is $\dot{m}$, considering the overall mass conservation, we have

$$\dot{m}=\rho_u S_u A_f \quad \text{or} \quad S_u=\frac{\dot{m}}{\rho_u A_f} \tag{2-3}$$

This method is useful for rough estimation since the area of the photographed flame front can be easily determined graphically [19]. The second way is called the flame angle method. In this method, the determination of S_u can be more accurately achieved by using an aerodynamically contoured nozzle, which gives a uniform exit velocity profile. As shown in Figure 2.2, if the velocity at the nozzle exit is u_0 and the half cone angle is $\alpha = \alpha_u$, the laminar flame speed is given by:

$$S_u=u_0 sin\alpha_u \tag{2-4}$$

The advantage of the Bunsen flame method is that the experimental equipment is very simple and low cost. However, the shortcomings are also obvious that it neglects the influence of the stretch on the measured flame speed. The flame curvature and flame thickness make it difficult to accurately determine the local flame speed.

2.1.2.2 Stagnation flame method

The stagnation flame method was first proposed by Wu and Law [30] and later was widely used to measure the laminar flame speeds of different fuels [31-33]. A typical stagnation flame is shown in Figure 2.3. It can be seen that by impinging two

identical, nozzle-generated combustible flows onto each other, two symmetrical flat flames are situated on the two sides of the stagnation surface.

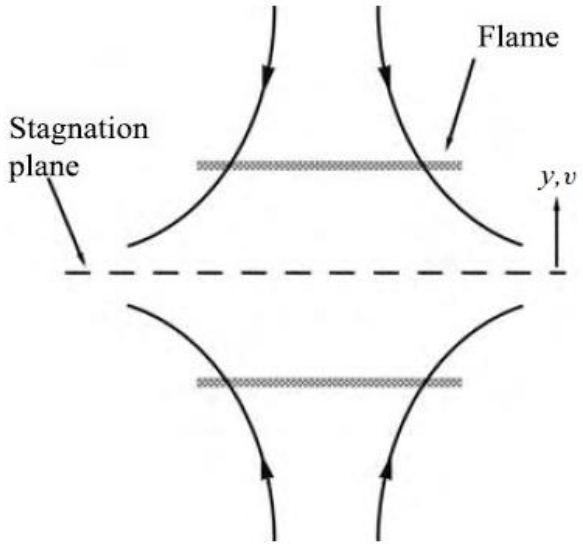

Figure 2.3 Schematic diagram of a typical counterflow, twin stagnation flame [19]

For a typical counterflow flame, it is assumed that the axial velocity v varies linearly, $v=ay$, in accordance with the characteristics of stagnation flow, where $a=\mathrm{d}v/\mathrm{d}y$ is the velocity gradient. It should be noticed that the stagnation flame is also stretched, but for an ideal stagnation flow, the stretch intensity can be represented by the velocity gradient a [34]. Therefore, there are two quantities that can be experimentally measured, namely the velocity gradient a in the hydrodynamic zone and the minimum velocity point v_{min} which can be approximately identified as a reference flame speed $S_{u,ref}$ at the upstream boundary [28]. Then, by extrapolating v_{min} to zero a, the intercept of v_{min} at $a=0$ can be identified as the laminar flame speed S_u, evaluated at the upstream boundary. This method can greatly reduce the effects of

heat transfer on flame propagation and laminar flame speed measurement because the upstream heat loss from the nozzle-generated flow is small while the downstream heat loss is also small due to the symmetry. The stagnation flame method is very convenient for controlling the fuel mixture and is capable of obtaining the stretched laminar flame speed at a fixed stretch intensity. However, the biggest disadvantage of this method is that it is difficult to conduct the experiments under elevated pressure condition.

2.1.2.3 Flat and one-dimensional flame method

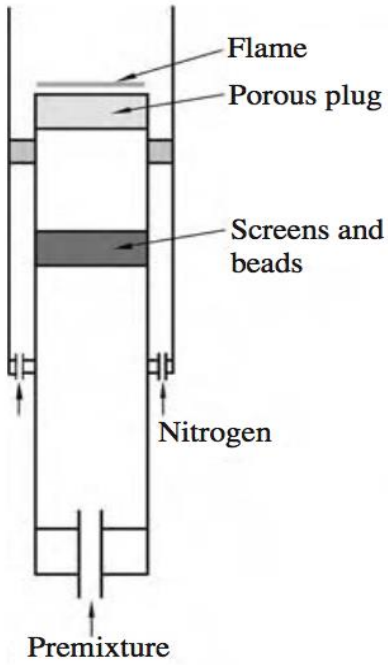

Figure 2.4 Schematic diagram of a typical flat flame burner [19]

The flat flame method was firstly proposed by Botha and Spalding [35] in 1954. As shown in Figure 2.4, they manipulated the heat loss rate by cooling the porous plug. Thus, by continuously varying the mixture flow rate and noting the corresponding

cooling rate needed to obtain a flat flame, the burning velocity without heat loss can be estimated by extrapolating the cooling rate to zero. However, there are certain difficulties in measuring the heat loss rate, and the flame is inherently non-adiabatic relative to the enthalpy of the free stream. Therefore, the burning velocity determined by this method is lower than S_u^0 based on the free stream.

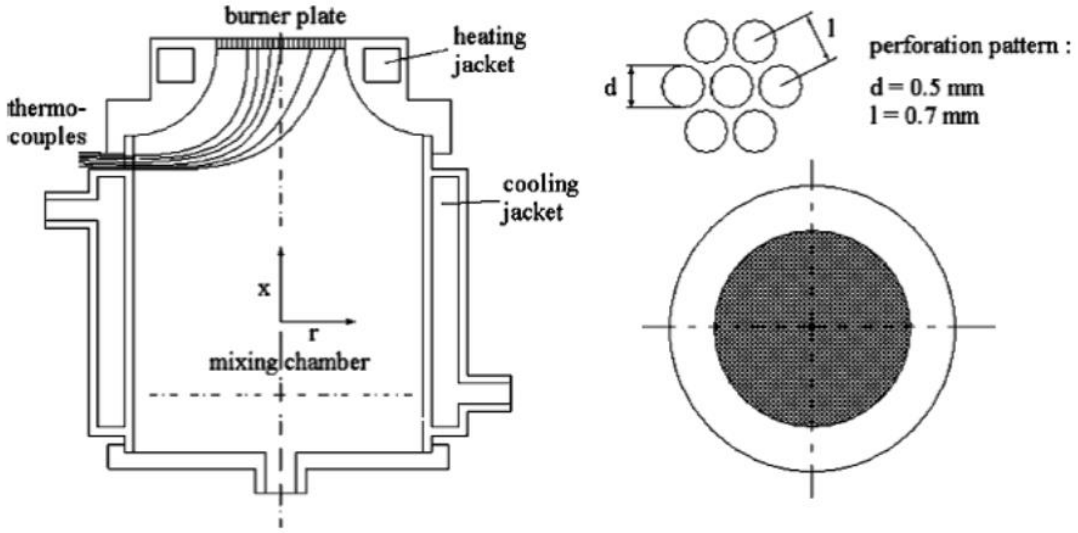

Figure 2.5 Schematic diagram of a flat flame experimental system using heat flux method [37]

De Goey et al. [36] improved this method by providing additional heat to the unburned mixture to compensate for the heat loss of the flame, keeping the stabilized flame in an approximately adiabatic state. Figure 2.5 shows the schematic diagram of the flat flame experimental system. This method is also called the heat flux method. The advantage of this improved method is that instead of estimating the heat loss by extrapolating the cooling rate like the traditional flat flame method,

it is possible to directly measure the laminar flame speed and improve the reliability and accuracy of the experimental results. However, the main drawback of this method is similar to the stagnation flame method that it is difficult to obtain the laminar flame speed at elevated pressures.

2.1.2.4 Outwardly propagating spherical flame method

The outwardly propagating spherical flame method has been widely used for measuring the laminar flame speed of a fuel. This method was firstly proposed by Stevens [38] in the 1920s. In 1934, Lewis and Von Elbe [39] first proposed a method in determination of the laminar flame speed using a spherical propagating flame from time-pressure explosion records. However, the method of calculating the laminar flame speed based on the pressure curve ignores the influences of the stretch rate and the flame instability on the burning velocity, so that there is a large difference between the measured laminar flame speed and the actual value.

With the development and improvement of flame dynamics theory, the concept of the stretch rate in a flame has been developed in 1980s [40-42]. Moreover, with the development of optical equipment and high-speed camera technology, high-frequency flame front images can be obtained through experiments. Currently, the laminar flame speed can be determined mainly by taking images of the flame propagation process and extrapolating using a linear or nonlinear method. Figure 2.6 shows a typical constant volume combustion bomb system developing outwardly

propagating spherical flame.

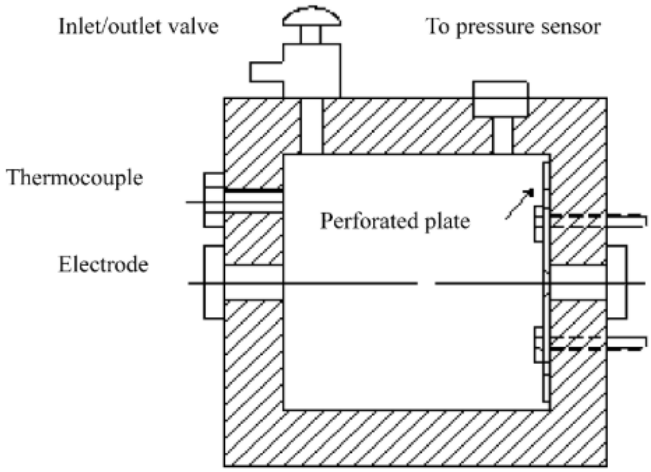

Figure 2.6 Schematic diagram of a constant volume combustion bomb developing outwardly propagating spherical flame [43]

The outwardly expanding spherical flame method has the following disadvantages. First, when the burning velocity is very low, the flame is easily deformed by the influence of buoyancy. Therefore, conventional outwardly expanding spherical flame method is not suitable for a fuel having a relatively low laminar flame speed. Second, the electrodes used for ignition can cause a disturbance in the propagation of the flame, and there is radiative heat loss from the large volume of the burned gas behind the flame. These factors affect the propagation of the flame, especially in the early stage of flame propagation. Third, the development of intrinsic pulsating and cellular instabilities over the flame surface leads to self-acceleration of the flame propagation, which cannot be used to measure the laminar flame speed at this point. However, this method has unparalleled advantages compared to other measurement

methods. Since a spherical propagating flame can usually be produced in a confined vessel, the design of the experimental equipment can be relatively simple and the amount of gas consumed is small. It is also particularly suitable for the determination of laminar flame speeds at high temperatures and pressures. Therefore, the outwardly propagating spherical flame method is also adopted in the present study to study the laminar burning characteristics of bio-syngas under various initial conditions.

2.2 Biomass fuels

2.2.1 Biomass sources

As introduced in Chapter 1, renewable energy sources play an increasingly important role in the world's energy system not only for fulfilling the growing energy demand for sustainable development of society but also for mitigating environmental pollution and greenhouse gas emission. Among various forms of renewable energy sources, including solar, wind, water, and biomass, biomass has notable advantages in terms of its wide availability and capability for producing different useful chemicals that can be modified according to various conversion technologies which are absent in other sources of energy [44].

In general, biomass is defined as living matters on earth in which solar energy is stored through the photosynthesis process [45, 46]. To be specific, biomass is essentially biological material from agriculture, forestry, and related industries and

municipal solid waste (MSW), which excludes the material embedded in geological formations and transformed into fossil fuel. [47, 48]. The energy stored in these substances can be accessed in a variety of ways, ranging from direct burning to complex conversion processes. A wide-accepted classification of biomass sources is based on their origination, which is shown in Table 2-1 [47]. It gives a detailed classification of biomass sources and examples of representative materials of every type.

Table 2-1 Classification of biomass sources according to their origination [47]

Categories		Representative materials
Terrestrial	Carbohydrate	Sugar cane; Corn; Sweet sorghum
	Starch	Maize; Cassava; Sweet potato
	Cellulose	Tropical grasses; Poplar; Sycamore
	Hydrocarbon	Eucalyptus; Green coral
	Grease	Oil palm; Rapeseed; Sunflower
Aquatic	Freshwater	Water hyacinth
	Ocean	Large kelp
	Microorganism	Green algae; Photosynthetic bacteria
Residues from Agriculture/Forestry/Husbandry	Agriculture	Wheat bran; Straw; Vegetable residues; Processing residues
	Animal Husbandry	Animal manure; Farm residues
	Forestry	Secondary forest; woodland remnants; Crippled material in plants
Waste	Fisheries	Jettisoned and dead fish
	Municipal Waste	Municipal and pulp sludge
	Garbage	Family garbage; Feces

The use of biomass as feedstock for conversion to various biofuels depends on its chemical constituents and physical properties. In fact, the varied feedstock types can affect the carbon content of the biofuels and require different treatment for the conversion of biomass to biofuel, and consequently changing the processing techniques and product quality. If we restrict the feedstock to include only the plant material, vegetation, or agricultural waste, these types of biomass chemically consist of three major components, namely, (1) cellulose; (2) hemicellulose; and (3) lignin, with a small amount of proteins, sugars, aliphatic acids, and fats [44-46, 48]. The combustion behaviors and degradation patterns of these components are so different that the energy released depends on the type of biomass and its composition.

Figure 2.7 gives a schematic diagram of cellulose, hemicellulose, and lignin in plant cells [48]. As shown in Figure 2.7, cellulose, hemicellulose, and lignin are unevenly distributed in the cell wall, and the structure they formed is called microfibril. Cellulose is the main structural component in plant cells, which consists of a long linear chain of glucose molecules linked by β(1-4)-glycosidic bonds. Cellulose connects with hemicellulose and lignin mainly through hydrogen bonds. Hemicellulose, the second abundant constituent of biomass, is a complex mixture of polysaccharides, composed of various 5- and 6-carbon sugars such as glucose, mannose, xylose, galactose, and arabinose [45]. Hemicellulose links cellulose fibers into microfibrils and cross links with lignin, forming a complex network of bonds that provide structural strength [49]. Lignin is a highly branched, substituted,

mononuclear aromatic polymer consisting of phenolic components, and often found to be adjacent to cellulose fibers working like cellular glue to provide compressive strength and stiffness [50].

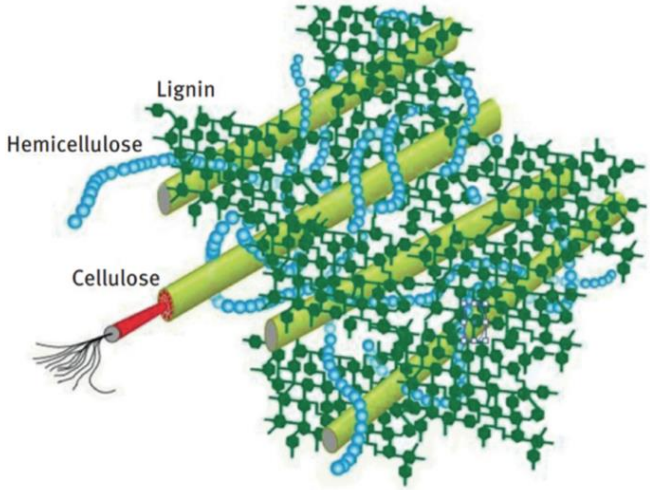

Figure 2.7 Cellulose, hemicellulose, and lignin in plant cells [48]

All these components of biomass have different reaction behaviors upon degradation into different chemicals, and their contents in biomass also vary significantly, depending on the type of biomass. Normally, the cellulose content can reach 40%-60%, which is the largest fraction followed by hemicellulose (15%-30%) and lignin (10%-25%) [48]. Thus, an appropriate conversion technology has to be designed according to the different types of biomass as feedstock for conversion to meet the desired needs.

2.2.2 Current biomass conversion technologies

Biomass can be utilized by either direct combustion or converted to solid, liquid,

and gaseous fuels and chemical products through thermochemical and biochemical processes. Direct combustion is the old way of using biomass to obtain its energy content in the form of heat [6]. The flame temperature can be beyond 2000 ^{o}C, depending on various factors such as the heating value and moisture content of the biomass [51]. Some researches [52, 53] show that co-firing of biomass with coal can reduce the emissions and lower the cost per unit energy produced in comparison to single coal firing. The thermochemical processes mainly include pyrolysis, gasification, hydrogenation, and liquefaction [46, 54]. On the other hand, digestions such as anaerobic and aerobic fermentation are typical biochemical processes used to produce biofuels and chemical products [55, 56].

Figure 2.8 shows the different processing technologies for biomass and the respective products [44]. All these processing techniques have been extensively developed and reported in the past decades, and the biofuels generated from diverse biomass have been improved through various treatments and procedures such as reduced pressurized distillation and purification processes. According to the origination of biomass source, the produced biofuels can be divided into two types, namely, (1) conventional or first-generation biofuel; and (2) advanced or second/third/fourth generation biofuel [57].

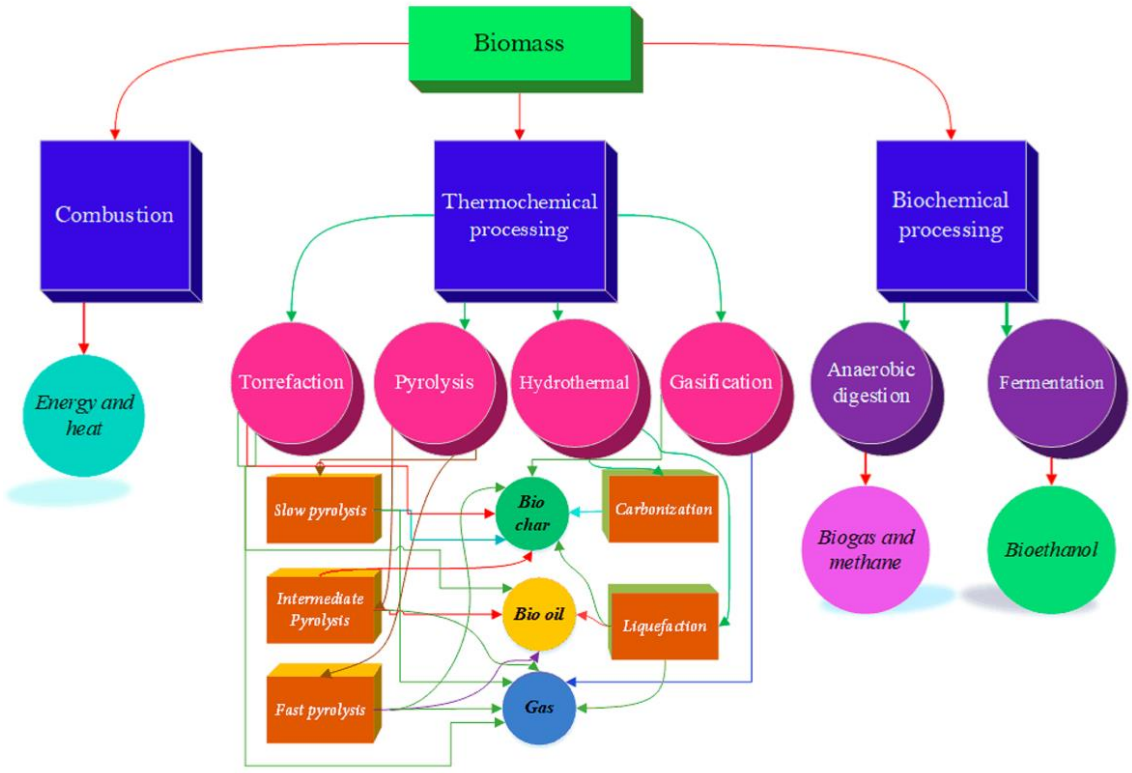

Figure 2.8 Biomass processing technologies and respective products [44]

For biochemical processes, the biomass can firstly be subjected to acid, alkaline or steam explosion pre-treatments to break the cellulose-hemicellulose-lignin structures to make biomass more accessible to microbial reactions [58]. The organic matter is then decomposed by various groups of microorganisms in an environment with or without oxygen [55]. However, biochemical processes face several challenges such as high cost of pre-treatment, low fermentability of mixed sugar stream in biomass, and generation of inhibitory soluble compounds [59]. There are two thermochemical conversion processes, namely pyrolysis and gasification. Both of them can divert the end-products' yield according to the desired outcome with properly selected feedstock [44]. Pyrolysis is a process of heating the organic materials in biomass in a

limited or oxygen-free environment at an elevated temperature (< 700 ºC) [44, 60]. It mainly contains three subcategories, namely, (1) fast pyrolysis; (2) intermediate pyrolysis; and (3) slow pyrolysis. On the other hand, the gasification of biomass also plays an important role in converting biomass into diverse biofuels, and it is regarded as one of the most effective techniques for the utilization of carbon-based feedstock [61]. In a gasification process, biomass is converted into not only a gaseous biofuel which can be further burned to release energy but also chemical feedstock which can be used to produce valued-added chemical products by using the Fischer-Tropsch (FT) process or by using fermentation.

2.2.3 Gasification of biomass

The gasification of biomass is a process of partial oxidation of biomass at high temperature (700-900 ºC) yielding mainly combustible producer gas/syngas, in the presence of insufficient supply of air [46]. The principal steps of a gasification process are (1) drying; (2) pyrolysis; (3) oxidation; and (4) reduction. Despite the relative similarity between gasification and pyrolysis, gasification is not only simply pyrolysis of biomass but also involves sub-stoichiometric combustion of the pyrolysis products (oxidation), and further react with char (reduction), leading to a typical product—a gas mixture of hydrogen (H_2), carbon monoxide (CO), methane (CH_4), carbon dioxide (CO_2), as well as some light hydrocarbons generated through tar decomposition, higher molecular compounds such as tars, and remaining nitrogen (N_2) or water vapor (H_2O), in proportions depending on the feedstock and

gasifying agents used [62].

Most of the gasifiable biomass sources are chemically composed of cellulose, hemicellulose, and lignin [63]. The reactors used to gasify the biomass are usually called gasifiers. According to their configurations, they can be divided into four main categories: (1) moving bed; (2) fixed bed; (3) fluidized bed; (4) entrained flow gasifier. Henrich and Weirich [64] indicated that an entrained flow gasifier produces cleaner bio-syngas compared to other types of gasifiers, but it also requires more pre-treatment steps to achieve the size reduction of biomass which significantly increases the cost. More detail on the advantages and disadvantages of different gasifiers have been reported in previous studies [51, 57, 62, 65]. Moreover, the influence of different gasifying agents on the efficiency of a gasification process has been widely investigated in previous literature [66-69]. There are three commonly used gasifying agents, namely, air, steam, and carbon dioxide. If air is the gasifying agent, the conversion pathway moves toward the oxygen-driven reactions, leading to more CO production with a relatively low amount of oxygen content or more CO_2 production with a relatively high amount of oxygen content. Gasification is a sub-stoichiometric oxidation process, which means fuel-rich condition is needed for producing the combustible gases (H_2/CO/CH_4). Therefore, if the amount of oxygen exceeds the stoichiometric level, the overall process moves from gasification to combustion. On the other hand, if steam is the gasifying agent, the conversion pathway moves toward the hydrogen-dominated reactions, leading to more hydrogen

production with a higher H/C ratio. Steam gasification of biomass has been extensively adopted to generate hydrogen-rich bio-syngas [70-72]. The influence of CO_2 as a gasifying agent also has been studied [73, 74]. Under an atmosphere of CO_2, the production of CO_2 is drastically decreased and the production of CO is increased as a result of the positive promotion of the reaction: $C + CO_2 \leftrightarrow 2CO$.

Since biomass diversifies in various parameters, such as chemical composition, moisture content, and ash content, the composition of the produced bio-syngas varies significantly depending on the feedstock, the gasification technologies, and operating conditions. It is important to select an appropriate gasification technology according to different chemical and physical properties of diverse biomass sources to improve the efficiency of the thermochemical conversion process.

2.3 Research progress in combustion of bio-syngas

2.3.1 Applications of bio-syngas in power plants and IC engines

Bio-syngas produced by thermochemical conversion of biomass has been widely investigated for use in practical combustors such as internal combustion engines and power generation sectors. Gupta et al. [75] developed a catalytic combustion system for use with syngas (20% H_2, 20% CO, 2% CH_4, 12% CO_2 and 46% N_2) of a hybrid heating source for solar-thermal power generation. The system exhibited stable operation, quick startup and high turndown ratio, which confirmed the suitability of the syngas fuel as an important component of a hybrid heating source for

solar-thermal power generation. Kohsri et al. [76] evaluated the potential of a hybrid solar PV/biomass syngas system with battery energy storage for off-grid application. They found that the combination of two renewable energy sources can guarantee a continuous 24h electricity supply in case of shortage of solar energy. In addition, many researchers tried to find efficient coupling between the gasification of biomass and fuel cells [77-80]. Donolo et al. [78] numerically studied energy production from biomass by molten carbonate fuel cells (MCFC). They indicated that the efficiency obtained by coupling the biomass gasifier and the MCFC system is around 36%-40%, depending on the type of biomass used. Tomasi et al. [79] investigated a molten carbonate fuel cell (MCFC) power plant fed with a biomass syngas. They found that the proposed coupling of a recirculated fluidized-bed gasifier with an MCFC system had high conversion efficiencies of 43%-49%, which is better than those reached by traditional fossil-fuel plants of the same size.

On the other hand, bio-syngas produced through gasification of biomass can also be fed to internal combustion (IC) engines to obtain its energy content. Indrawan et al. [81] developed a small scale power generation unit which consisted of a downdraft gasifier and an internal combustion engine to generate electricity by co-gasification of municipal solid wastes (MSW) and agricultural biomass. They demonstrated that the co-gasification system could provide a basis for the future development of small-scale power generation to utilize local wastes. Kohn et al. [82] studied the performance of an internal combustion engine operating on landfill gas and the

effect of syngas addition. Their results showed that as the quality of landfill gas decreased due to the increase of CO_2 content, the CO and unburned hydrocarbon emissions significantly increased while NO_x emissions slightly decreased. Syngas addition to the landfill gas could not only reduce the pollutant emissions but also improve the fuel conversion efficiency due to the positive effect of H_2 and CO in syngas. Hagos et al. [83] comparatively studied the effect of methane-enrichment of syngas (H_2/CO) on combustion, performance, and emissions of a spark ignition direct injection engine. They stated that methane-enriched syngas could extend the operation, maintain the faster and smoother combustion compared to the syngas or compressed natural gas (CNG) single mode operating at the same engine speed. Kan et al. [84] investigated the utilization of biogas and syngas respectively generated from biomass waste through the anaerobic digestion process and gasification process in a premixed spark ignition engine. They found that the utilization of syngas and biogas under blended-fuel mode could lead to a reduction of engine knocking and NO_x emissions.

Integrated gasification combined cycle (IGCC) is one of the most promising technologies for designing bio-power plants assisted with the biomass gasification process. The principal advantage of IGCC is the ability to use diverse fuels and lower emissions [85]. In IGCC power plant, the post-treatment of the produced syngas is considered to ensure the versatility of the process to be employed for a variety of applications such as power and heat generation, production of chemicals,

liquid fuels and hydrogen fuel. Many researchers studied the feasibility of biomass utilization in IGCC power plants based on the biomass gasification/gas turbine concept [86-91]. Minguez et al. [90] studied the behavior of an IGCC power plant fueled with different kinds of biomass waste by simulation. They indicated that the high overall waste to power process efficiency (45-48% with no CO_2 capture and 38-42% with CO_2 capture) made bio-IGCC power plant one of the most promising technologies for large-scale power generation from waste. Baratieri et al. [92] comparatively investigated the use of biomass syngas in IC engines and combined cycle gas turbine (CCGT) plants and studied several types of biomass feedstock to assess their potential energy production and effect on the environment. They found that the use of biomass syngas in these two power generators is a valid way to reduce environmental impact and compared with application of biomass syngas in IC engine, CCGT plants using biomass syngas has better electrical efficiency (about 40%).

Co-gasification of coal and biomass in IGCC power plants offers a better prospect for cleaner coal utilization and a way to dispose of wastes/biomass in an economical, safe, and environmentally acceptable manner [93]. The most attractive benefit of co-firing coal and biomass is certainly the reduction of greenhouse gas emissions and environmental pollution, considering biomass is a carbon-neutral sustainable energy source [94, 95]. Reichling and Kulacki [96] comparatively studied the biomass utilization via Fischer-Tropsch (FT) conversion process and IGCC power

plant. In the IGCC system, biomass was co-firing with coal, comprising 10% of the fuel input by energy content. Based on the overall performance of the two processes, they suggested that co-fired with coal conversion for electrical generation has lower capital costs compared to the biomass-only FT fuel plants. Bhattacharaya and Datta [97] investigated the effects of supplementary biomass firing on the performance of a natural gas fired combined cycle (NGCC) and IGCC power plant. They identified a critical degree of supplementary firing for the slag free operation of the biomass combustor. Wu and Ouyang [98] analyzed co-gasification of coal and biomass based on the IGCC system with a two-staged entrained-flow bed gasifier. They found a nonlinear correlation of biomass blending ratio and technical, economic indicators. In addition, the content of H_2 and CO both increased and reached the maximum at 10% biomass blending ratio. Thallam Thattai et al. [99] experimentally and numerically investigated a high percentage (up to 70%) biomass co-gasification with coal in an IGCC system. Such a high percentage of biomass co-gasification at a large scale power plant demonstrated that existing coal-based IGCC system can be operated with an increasing percentage of biomass substitution without extensive modification of the power plant.

2.3.2 Laminar burning characteristics of bio-syngas

2.3.2.1 Laminar flame speed

Laminar flame speed, as a fundamental physiochemical parameter, is critical to

understand the combustion characteristics of a combustible fuel mixture, since it determines the flame burning rate and the flame stability in practical combustors. In addition, it is an important target for validating chemical reaction mechanisms and developing surrogate fuel models. In section 2.1, we have introduced the definition of laminar flame speed and various experimental approaches for the measurement of laminar flame speed. In the open literature, plenty of experiments have been conducted to investigate the laminar flame speed of various fuel mixtures, such as H_2-air mixtures [100-102], CH_4-air mixtures [103-106], high order hydrocarbon-air mixtures [107-111], H_2-CH_4-air mixtures [43, 112-116], and syngas (H_2/CO)-air mixtures [117-123].

Hydrogen has a much higher laminar flame speed than that of hydrocarbon fuels [124]. In fact, pure hydrogen combustion is restricted considerably in practical applications for safety consideration due to its high reactivity and diffusivity. Therefore, hydrogen is generally adopted as an excellent addition to adjust the combustion performance of hydrocarbon fuels. One of the effective methods to solve the problem of the slow burning velocity of methane is to mix the methane with a fuel that has higher burning velocity, such as hydrogen [112]. Halter et al. [115] investigated the effect of initial pressure and hydrogen concentration on the laminar burning velocities of CH_4-H_2-air mixtures using the spherical flame method. Their results showed that the laminar burning velocity increased with increasing hydrogen content in the fuel blends and decreases with increasing initial pressure.

Tang et al. [125] experimentally studied the effects of hydrogen addition on the laminar flame speed of hydrocarbon-air mixtures. They found that hydrogen addition could affect the laminar flame speed of a fuel mixture via three mechanisms, including thermal effect, diffusion effect, and chemical kinetic effect. Among these mechanisms, the kinetic effect was found to be the most important, which enhances the burning intensity due to the strong reactivity of hydrogen.

On the other hand, the combustion characteristics of CO, which is one of the major species in bio-syngas, are different from those of hydrogen and hydrocarbons. According to previous literature [126, 127], the "dry" oxidation of CO: $CO + O_2 \rightarrow CO_2 + O$, $CO + O + M \rightarrow CO_2 + M$ is not observed in practical combustion processes because the concentrations of hydrogen-containing species are always sufficiently high that the reaction: $CO + OH \rightarrow CO_2 + H$ is much more rapid. Many researchers studied the laminar burning velocities of H_2-CO-air mixtures. Li et al. [119] measured the laminar burning velocities and Markstein lengths of lean and stoichiometric syngas premixed flames under various hydrogen fractions. Their experimental results showed that the unstretched burning velocities of lean and stoichiometric syngas premixed flames increased with the increase of hydrogen fraction and equivalence ratio. Varghese et al. [121] experimentally and numerically investigated the effect of CO content (15%, 20%, 25% by volume) on the laminar burning velocities of syngas-air premixed flames at elevated temperatures using an externally heated diverging channel method. They found that the laminar burning

velocity increased with the increase of CO content. The effects of initial pressure and temperature on the laminar flame speed and Markstein length of syngas were studied by Ai et al. [128]. They found that the laminar flame speed increased with the increase of the initial temperature, and decreased with the increase of the initial pressure. Moreover, the Marksein length decreased with the increase of initial pressure and temperature.

As mentioned before, the main fuel component in bio-syngas derived from biomass is normally a mixture of H_2, CO, and CH_4. So far, the laminar flame speeds of H_2/CO/CH_4/air mixtures have rarely been reported. The H_2/CO/CH_4 fuel blend is more complex than a single component fuel or binary fuel in terms of fuel composition and combustion characteristics. Lee et al. [129] investigated the fuel composition effects of H_2/CO/CH_4 syngas on the combustion instability characteristics of a partially premixed swirl-stabilized gas turbine model combustor. They indicated that the combustion frequency appeared to be linearly proportional to the adiabatic flame temperature and laminar flame speed for all test conditions. Vagelopoulos and Egolfopoulos [130] experimentally and numerically studied the effect of H_2 and CH_4 additions on the propagation and extinction of atmospheric CO/air opposed-jet flames. They found that the addition of a small amount of H_2 or CH_4 to CO flames increased the laminar flame speeds and extinction strain rates by accelerating the main CO oxidation reaction. Wu et al. [131] also studied the effect of CO addition on the characteristics of premixed CH_4/air opposed-jet flames.

Detailed analysis of the calculated chemical kinetic structures revealed that as the CO content in the fuel was increased from 0% to 80%, the "wet" oxidation of CO: $CO + OH \leftrightarrow H + CO_2$ increased significantly and contributed to a significant level of heat-release rate, while the chemistry of CO consumption shifted to the dry oxidation kinetics when CO content was over 80%. Yan et al. [132] measured the laminar burning velocities of four biomass-derived gases at atmospheric pressure over a range of equivalence ratios using the heat flux method on a perforated flat flame burner. The studied gases were bio-methane (upgraded landfill gas), two gasification gases (one from an industry demonstration plant, and one model gas studied in the literature), and one co-firing gas made up of an industry gasification gas and methane. They found that the peak burning velocities of the two gasification gases/air mixtures and the co-firing gases/air mixtures were higher than that of the bio-methane/ air mixtures due to the presence of H_2 and CO in the gasification gases. Monteriro et al. [133] also experimentally determined the laminar burning velocities and Markstein numbers of three types of syngas produced from wood gasification using spherical flame method at normal temperature and pressure. The Markstein number results showed that the three syngas-air flames were generally unstable and the maximum laminar flame speeds were observed at stoichiometric equivalence ratio.

Some researchers [134-136] numerically studied the physicochemical properties and laminar flame speed of bio-syngas (H_2/CO/CH_4) combustion using GRI Mech 3.0

[137] and San Diego Mech [138]. The results demonstrated that the different chemical kinetic mechanisms gave reasonable agreement with each other and with experimental data. Vu et al. [139] experimentally and numerically studied the laminar burning characteristics of three biomass-derived gases. They reported that the experimental results and predicted results using GRI Mech 3.0 agreed well at lean and stoichiometric conditions, and the peak burning velocity was found at the equivalence ratio of 1.4. Cheng et al. [17] experimentally and numerically investigated the effect of variations in fuel composition on the characteristics of H_2/CO/CH_4/air opposed-jet flames. They found that the laminar burning velocity increased with increasing H_2 or CO addition to the CH_4/air flame. Moreover, they stated that the increase in the laminar flame speed with H_2 addition was most likely due to an increase in active radicals during combustion (chemical effect), rather than from changes in the adiabatic flame temperature (thermal effect).

In addition, bio-syngas usually contains a considerable amount of diluents such as N_2 and CO_2. These diluents can be removed by post treatment process, such as pressure swing adsorption, amine scrubbing, and membrane reactors. However, the dilution gas can be deliberately introduced into the unburned mixtures to reduce the NO_x emissions [140]. In previous literature, researchers have studied the effect of different diluents on the laminar burning velocities of H_2-air, CH_4-air, or syngas (H_2/CO)-air mixtures [140-147]. Zhang et al. [140] pointed out that with N_2 or CO_2 dilution in the fuel mixture, the thermal effect dominated the reduction of laminar

flame speed while the diffusivity change effect was negligible for both N_2 and CO_2 dilution. Prathap et al. [146, 147] investigated the N_2/CO_2 dilution effect on the laminar burning velocity of syngas at atmospheric condition. They found that the laminar burning velocity decreased with N_2 dilution in the syngas due to the reduction of thermal diffusivity and flame temperature of the mixture with N_2 dilution. In addition, according to their results, CO_2 has a stronger inhibiting effect on the laminar burning velocity than N_2. Shang et al. [148] also studied the laminar flame speeds of syngas with N_2 and CO_2 dilution. According to their results, CO_2 dilution has stronger the negative effect on the flame propagation than that of N_2 dilution due to its stronger thermal and chemical kinetic effects. In fact, Liu et al. [149] stated that unlike other dilution gases, such as N_2, CO_2 can directly participate in the chemical reaction primarily through the intermediate reaction $CO + OH \leftrightarrow H + CO_2$ rather than acting as an inert gas in the overall reaction process.

2.3.2.2 Laminar flame front instabilities

One of the most fascinating phenomena in flame dynamics is the presence of instabilities in the forms of cells and ridges of characteristics size over the flame surface [19, 150-152]. The formation of laminar flame front cellular instabilities will increase the flame speed and enhance the engine knock [153]. At present, the theoretical study of laminar flame front instabilities suggests that there are three mechanisms generating cellular instabilities, namely buoyancy-driven instability,

hydrodynamic instability [154, 155], and diffusional-thermal instability [156, 157].

First, buoyancy-driven instability is commonly known as the Rayleigh-Taylor instability [19, 158] which occurs for two fluids with different densities. For an expanding spherical flame, there is a large amount of unburned mixture outside the burned mixture region. Since the density of the burned mixture is significantly lighter than the density of the unburned mixture, the buoyancy caused by the density difference pushes the burned mixture to the opposite direction of gravity. If the flame propagates slowly, the velocity of the burned mixture region in the direction of gravity is also slow, and then the body force caused by buoyancy from the unburned to the burned mixtures will obviously affect the stability of the flame surface. However, this instability usually occurs when the corresponding laminar flame speed is slow (<0.15 m/s).

Second, the hydrodynamic instability, also known as the Landau-Darrieus instability [154, 155], is caused by the density jump across a flame. It is assumed that an infinitely thin flame surface separates the unburned mixture of constant density ρ_u from the burned mixture of constant density ρ_b, and the flame surface propagates with a constant flame speed, which is the laminar flame speed, S_u^0. Therefore, as long as there is a thermal expansion ratio between the burned and unburned mixtures, the flame front is absolutely unstable in the hydrodynamic mode to disturbances of all wavelengths.

Third, the diffusional-thermal instability is mainly caused by the competition between the thermal diffusivity and the mass diffusivity [159]. Due to different influences of heat diffusion (smoothing effect) and mass diffusion (enhancement effect) on the flame wrinkles [19], the combined effect of heat diffusion and mass diffusion depends on the relative magnitudes of thermal diffusivity (α) and mass diffusivity (D_m). The ratio between the thermal and mass diffusivities is called the Lewis number ($Le=\alpha/D_m$). For a $Le > 1$ flame, the heat diffusion is stronger than the mass diffusion, leading to the suppression of the flame surface wrinkles. Conversely, if $Le < 1$, the mass diffusion is stronger than the heat diffusion, then the flame surface wrinkles are enhanced.

Laminar flame front instabilities of various fuel mixtures with or without diluents have been widely studied, including H_2-air flame [101, 160-164], CH_4-air flame [105, 161], syngas (H_2/CO)-air flame [23, 165-168], H_2-air flame or syngas (H_2/CO)-air flame with addition of various hydrocarbons [114, 153, 159, 169-173], and other alternative fuels such as n-butanol [108, 174]. Many studies indicated that with the increase of H_2 fraction in the fuel mixture, the cellular instabilities of the flame front were significantly promoted by enhancing both the hydrodynamic and diffusional-thermal instabilities [114, 139, 172, 175]. Law and Kwon [169] and Law et al. [170] studied the effects of hydrocarbon substitution (CH_4/C_2H_4/C_3H_8) on H_2-air spherical premixed flames propagation at atmospheric and elevated pressures respectively. They found that a small or moderate amount of hydrocarbon addition

would suppress the propensity of onset of both diffusional–thermal instability and hydrodynamic cellular instability in H_2–air flames. Lapalme et al. [159] studied the characterization of thermodiffusive and hydrodynamic mechanisms on cellular instability of syngas fuel blended with CH_4 or CO_2. The results showed that the variation of critical radius was mostly controlled by the variation in the laminar flame thickness for the near-equidiffusive H_2/CO/CH_4 flames, where *Le*~1. Vu et al. [139] investigated the flame instabilities of three biomass derived gases. According to their experimental results, the cellular instability was promoted with hydrogen enrichment but diminished with methane enrichment. Meanwhile, similar behavior was observed for CO enrichment condition.

Moreover, Tse et al. [164] examined the cellular structures of H_2/O_2 flames diluted with nitrogen or helium at initial pressure up to 60 atm. They found that helium dilution was able to suppress cellular instabilities for H_2/O_2/He flames from lean to rich conditions. The effect of various diluents (N_2/CO_2/He) on cellular instabilities of syngas-air spherical premixed flames was studied by Vu et al. [168] at elevated pressure. They stated that the cellular instabilities for the N_2-diluted and CO_2-diluted syngas-air flames were not suppressed compared to that of the He-diluted syngas-air flames. Li et al. [167] studied the flame intrinsic instability of N_2/CO_2 diluted H_2/CO/air mixtures under different hydrogen fractions. They stated that for 30% H_2/70% CO premixed flames, the flames became more stable with increasing dilution fractions. Lapalme et al. [159] pointed out that adding CO_2 to the syngas

promoted thermodiffusive instability through a decrease in Lewis number, but this instability would be counterbalanced by the hydrodynamic one through an increase in the laminar flame thickness, leading to a net result of a nearly constant critical radius.

In the literature, it is seen that studies related to laminar flame front instabilities of bio-syngas (H_2/CO/CH_4/N2/CO_2) have rarely been investigated, especially at elevated pressures. As mentioned before, a deep understanding of combustion behavior of cell formation in laminar premixed flames is very important in designing combustion devices since the formation of flame front cellular instabilities will increase the flame speed and promote the engine knock. Therefore, it is meaningful to investigate the laminar flame front instabilities of bio-syngas at various fuel compositions and initial pressures.

2.3.2.3 Explosion characteristics

Explosion characteristics of a combustible mixture are very essential and useful for the evaluation of the hazards of a chemical process and design of explosion-proof vessels to avoid damage from gaseous explosions [26]. The pressure history during explosion in a confined vessel can provide a basis for explosion hazard assessment. The characteristic parameters of a confined vessel explosion are the explosion pressure (P_{max}), the explosion time (t_c), the rate of pressure rise (dP/dt), and the deflagration index (K_G) [176]. These parameters are strongly affected by initial

pressure, initial temperature, fuel composition, volume and shape of the combustion vessel, ignition style and level of turbulence [177-182]. It has been reported that the maximum rate of pressure rise and the deflagration index depend to a small extent on the initial temperature, but are strongly influenced by the initial pressure [180, 183]. This is primarily due to a higher amount of flammable mixture with the increase of initial pressure, which delivered an increased amount of heat [184]. Kindracki et al. [177] experimentally studied the influence of ignition position and obstacles on explosion development. According to their results, the position of the ignition can affect the maximum combustion pressure and the rate of pressure rise. Compared to central ignition, the maximum combustion pressure decreased for bottom/top ignition because of a longer time of heat exchange between the combustion products and the vessel walls. Razus et al. [182] reported the rates of pressure rise of propylene-air explosions in spherical and cylindrical vessels. They found that the maximum rates of pressure rise $(dP/dt)_{max}$ and the deflagration index K_G observed during explosions in a cylindrical vessel were systematically lower than that of a spherical vessel. This is consistent with the observation of Movileanu et al. [176] that in comparison to the spherical vessel, the heat loss starts much earlier in the case of cylindrical vessel because the flame front comes into contact with the side wall long before the end of the combustion. Therefore, the heat loss is higher in a cylindrical vessel compared to that of a spherical vessel, and the larger the L/D ratio of the cylindrical vessel is, the larger amount of heat loss will be observed.

Massive researches have been conducted to study the explosion characteristics of various fuels, such as H_2 [27, 185-188], different hydrocarbon fuels [176, 184, 189-197], H_2-CH_4 mixture [183, 198-200], and H_2-CO mixture [201-204], for providing hazard and risk assessment. It is acknowledged that hydrogen has higher flammability and explosive hazard compared to the traditional fuel sources of gasoline and methane. H_2 leakage in a confined space is very dangerous due to its wide flammability limits and high burning velocity [185]. Faghih et al. [183] also found that for H_2-CH_4 mixtures with hydrogen blending level above 70%, the deflagration index was observed to increase exponentially with hydrogen blending level. For syngas fuel mixture, increasing H_2 content in the fuel blends also significantly increased the maximum rate of pressure rise and deflagration index and shortened the explosion time [202]. Dupont et al. [205] experimentally studied the explosion characteristics of a synthesized biogas (50%CH_4-50%CO_2) at atmospheric pressure and various initial temperatures. Their results showed that the biogas had less violent explosion than pure methane due to the presence of CO_2. Tran et al. [206] investigated the effects of hydrocarbon additions (CH_4 and C_3H_8) and diluent additions (He and N_2) on the explosion behaviors of syngas/air mixtures. They found that for hydrocarbon additions, both the maximum explosion pressure and the explosion time increased linearly with the increase of hydrocarbon concentration, while the maximum rate of pressure rise decreased nonlinearly. For diluent additions, the maximum explosion pressure decreased linearly, the explosion time increased

linearly, and the maximum rate of pressure rise reduced significantly with the increase of dilution ratio. Razus et al. [191] also indicated that the addition of diluents could effectively decrease the peak explosion pressures, rates of pressure rises and severity factors at all initial pressures.

In regard to the safety issues for production, transportation, storage and use of bio-syngas, knowledge of its pressure history during the explosion in a confined vessel is very essential and useful. So far, the explosion characteristics of bio-syngas (H_2/CO/CH_4/N_2/CO_2)/air mixtures have rarely been reported in publications. Safety problems persist in using bio-syngas due to the damages of the fire and explosion resulting from gas leakage. In addition, the variability of bio-syngas composition has a significant influence on its combustion and explosion characteristics, making the design of combustion chamber and the prevention of bio-syngas explosion hazards even more complex. Therefore, investigations on the explosion characteristics of bio-syngas at various fuel compositions are of great importance to understand the safety issues for its production, transportation, and utilization.

2.4 Summary

From the above literature review, it can be found that the combustion of bio-syngas (H_2/CO/CH_4/N_2/CO_2) has both merits and demerits in various aspects. Bio-syngas can be used in many applications ranging from industrial process heaters to IGCC for power generation. However, the diversity of the fuel composition in bio-syngas

leads to increasing difficulty of the combustion control and chamber design. In order to solve this problem, it is necessary to carry out the fundamental research of bio-syngas combustion to understand the combustion behaviors under various fuel composition and conditions.

A lot of investigations have been conducted by different researchers to study the laminar burning characteristics of pure hydrogen, pure methane, methane/hydrogen mixture and traditional syngas (H_2/CO mixture) using various experimental and numerical methods, but the related investigations of bio-syngas-air mixtures are rarely conducted. A literature survey indicates that systematic investigations, especially on the laminar flame speed, the flame structures, the flame front instabilities, and explosion characteristics of the H_2/CO/CH_4/N_2/CO_2 blended fuels are still deficient, since most of the previous investigations on the combustion characteristics of H_2/CO/CH_4 fuel blends are limited by the variability of fuel composition or elevated pressure conditions. The variability of fuel composition in bio-syngas can lead to different combustion performance, and thereby impose considerable technological challenge in the designing of practical systems. Detailed investigations on the laminar premixed combustion characteristics of bio-syngas can not only improve the comprehensive understanding of this kind of fuel in the aspect of combustion behaviors but also provide useful information and guidelines for its practical utilization. Moreover, analysis on the effect of each fuel component on the physics and the chemical kinetics behind that affect the laminar flame speed and

flame dynamics will provide fundamental knowledge on the combustion characteristics of the multi-component fuel.

CHAPTER 3 EXPERIMENTAL APPARATUS AND NUMERICAL METHODOLOGY

3.1 Introduction

This chapter introduces the experimental apparatus and numerical methodology adopted in the present study. A constant volume combustion bomb combined with a high-speed schlieren system was utilized to develop an expanding spherical flame for investigating the laminar burning characteristics of bio-syngas/air mixtures under various operating conditions. In addition, a numerical model of one-dimensional freely propagating plane premixed flame was used to calculate the laminar flame speed for comparison with the measured values and for analysis on the influences of fuel composition and initial conditions. The procedures of experimental measurements, an introduction of the fuel blends used in the present study, and uncertainty analysis are also provided in this chapter.

3.2 Experimental apparatus

In the present study, the experiments were conducted in a constant volume combustion bomb system, which consisted of a constant volume combustion bomb, gas control system, ignition system, high-speed schlieren photography system, and data acquisition system, as shown in Figure 3.1.

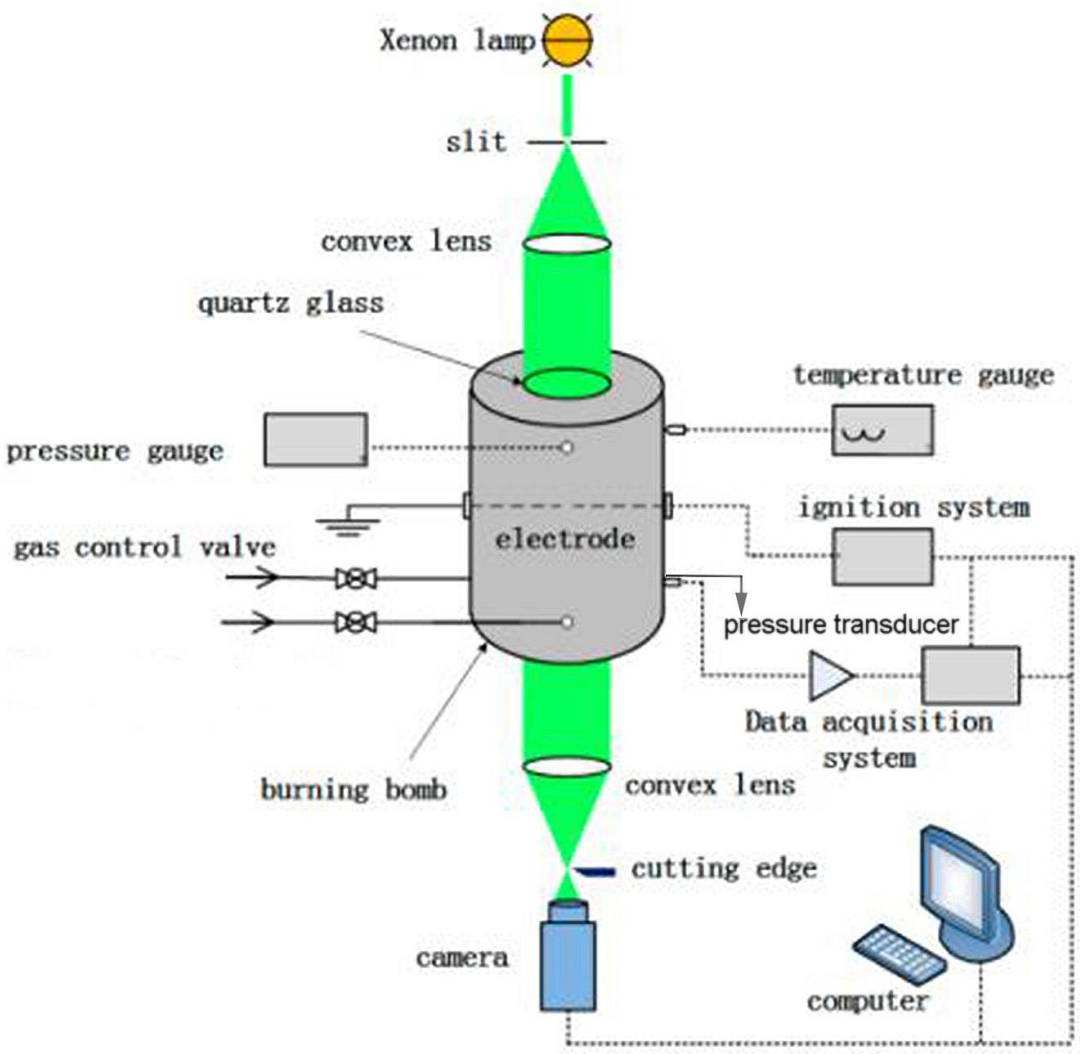

Figure 3.1 Experimental setup of constant volume combustion bomb system

The constant volume combustion bomb was in a cylindrical shape and made of stainless steel with an inner diameter and length of 180 mm and 210 mm, respectively. The detailed structure of the combustion bomb is shown in Figure 3.2. Two quartz windows with diameters of 80 mm each were located at the two sides of the combustion chamber for optical access. The high-pressure seal between the two quartz glasses and the combustion chamber was achieved by the high temperature-resistance fluoroelastomer gasket and the preload force provided by the

bolts. A K-type thermocouple was mounted on the combustion chamber to measure the temperature with an uncertainty of ±3 K. Moreover, pressure transmitter, pressure transducer, inlet and outlet valves were mounted on the chamber body. Two ignition electrodes with diameters of 1 mm were symmetrically located at the center of the bomb to create a uniform controllable spark to ignite the combustible mixture.

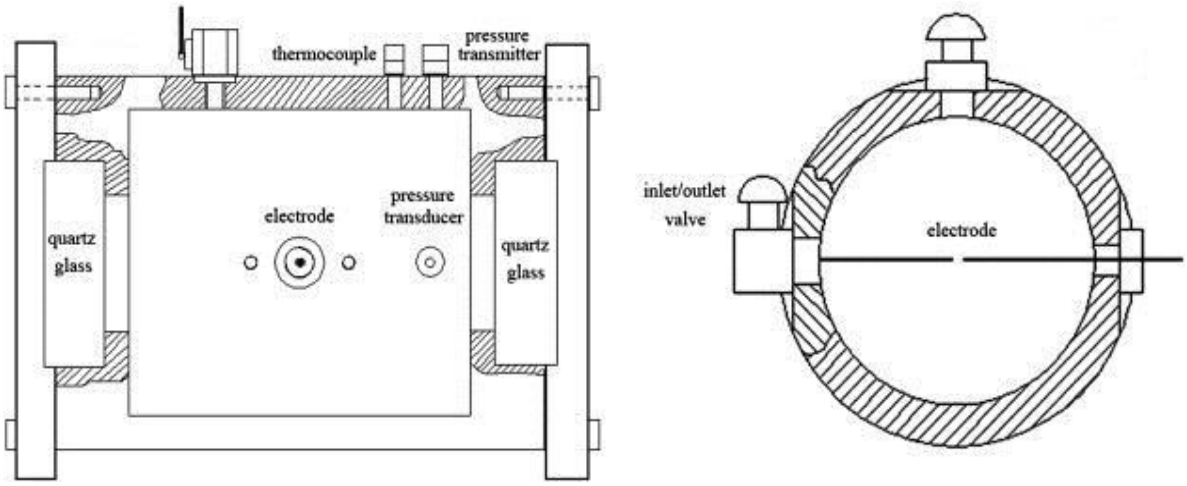

Figure 3.2 Schematic of the constant volume combustion bomb

The gas control system included gas distribution pipelines, vacuum pump, and a gas mixing tank which was made of stainless steel with the maximum working pressure of 2 MPa. Two static pressure gauges (Rosemount 3051 TG1) with an error of 0.075% were installed in the combustion chamber and the gas mixing tank respectively to measure the pressure.

The pressure acquisition system consisted of a pressure transducer (Kistler 7001) mounted on the inner wall of the combustion chamber, a charge amplifier (Kistler 5011), and a data collector (YOKOGAWA DL850) for recording the pressure data.

The charge amplifier output signal ratio is 10 V~ 5 MPa, and the frequency of the data collector sampling is 1 MHz.

The high-speed schlieren photography system included a high-speed digital camera (Phantom V611) and a schlieren optical system. The schlieren method is based on the principle that the refractive index gradient of light in the measured flow field is proportional to the gas density in the flow field, and then the change of the density gradient in the flow field is transformed into the change of the relative light intensity on the recording plane, so that the regions with a sharp change in density such as the flame front can be distinguished and observed through the flame images [170]. The maximum sampling frequency of the high-speed digital camera is 680,000 frames per second. To ensure the resolution of the captured images, the sampling frequency used in the present study was set as 10,000 frames per second.

The high-speed schlieren photography system, the pressure acquisition system, and the ignition system were controlled by a digital delay pulse generator (Model DG535). The trigger signals for the high-speed schlieren photography system and the pressure acquisition system were sent simultaneously, and the ignition system was delayed for 1 ms.

3.3 Experimental procedures

In the present study, the initial temperature was set as 303 K, and the initial pressure

was set as 0.1, 0.3, and 0.5 MPa, respectively. The equivalence ratio ranged from 0.6 to 1.5. Before the start of each set of experiment, it was first necessary to calculate the partial pressure of each component according to the operating condition. The procedures of the experiment are shown below:

(1) The vacuum pump and the connected valves were opened to pull out all the air in the combustion chamber and the pipelines. The vacuum pump was kept working until the reading of the pressure gauge no longer changed. Then, the vacuum pump and the connected valves were closed, and the reading of the pressure gauge was recorded for calibration. Then, the inlet valve was open on the side of the combustion bomb. Both fuel and air (N_2:O_2 = 3.762:1) were supplied into the bomb through the inlet valve. Since all the reactants were gases, the fuel mixture was prepared by delivering the reactants one by one into the combustion bomb according to the pre-calculated partial pressure of each component until the total pressure inside the combustion chamber reached the preset initial pressure of 0.1 MPa/0.3 MPa/0.5 MPa. After finishing the intake process, all the valves were closed and a 5-minute interval was spent before ignition to allow the reactants to become fully mixed with each other.

(2) A trigger signal was given using a digital delay pulse generator (Model DG535). Then the high-speed schlieren photography system and the pressure acquisition system were activated. After 1 ms, the fuel mixture in the combustion bomb was

ignited by the centrally located electrodes to form an outwardly propagating spherical flame. The flame images and pressure data were saved through the computer and the pressure data collector, respectively.

(3) After combustion, the exhaust valve was opened immediately to expel the high-temperature and high-pressure combustion products. Then, the vacuum pump was turned on to pull out the remaining combustion products. During the pumping process, the valve for atmospheric air on the top of the combustion bomb was opened intermittently to allow fresh air to enter in and flush away the residual combustion products until no residual gas was remained, and the temperature inside the combustion bomb was reduced to around 303 K. After flushing the combustion bomb, a near vacuum condition was created again by the vacuum pump, then, the next experiment could be conducted. Each operating condition was repeated at least three times to inspect the repeatability of the experimental results and the average data were used in the analysis.

3.4 Fuels

In the present study, the main fuel components in bio-syngas were prepared by mixing the appropriate amount of pure H_2 (99.99% purity), CO (99.99% purity), and CH_4 (99.99% purity). The main oxidizer used was air, which was prepared by mixing 21% O_2 (99.995% purity) and 79% N_2 (99.995% purity) volumetrically. For the measurements of laminar flame speed at elevated pressure conditions (0.3 MPa

and 0.5 MPa), helium (He, 99.99% purity) was utilized as a substitution for N_2 to suppress cellular instabilities and acquire more accurate experimental data. The ratio of helium and oxygen was fixed at 7:1 which was widely used in previous studies [164, 207, 208] to produce adiabatic flame temperature comparable to that of the flames combusted in the air (N_2/O_2).

The volumetric percentage of a specific fuel component (i) in a $H_2/CO/CH_4$ fuel blend, $\alpha(i)$, is defined as,

$$\alpha(i)=\frac{X_i}{X_{H_2}+X_{CO}+X_{CH_4}} \times 100\% \tag{3-1}$$

where X_i is the volume fraction of the specific fuel component (i). According to the statistical results of fuel composition of bio-syngas shown in section 1.2, we found that bio-syngas mostly has high concentration of H_2 and CO, but relatively low concentration of CH_4. The ratio between H_2 and CO usually equals to 1. Therefore, in the present study, the basic condition ($H_2/CO/CH_4$ = 2:2:1), namely $\alpha Basis$, was set as a reference for the convenience of variable control. When the proportion of one of the three fuel components was changed, the mole ratio between the other two fuel components was kept constant to examine the effect of fuel composition variation on flame characteristics. Besides the basic condition, six other fuel blends were also studied, namely, αH_2-60, αH_2-80, αCO-60, αCO-80, αCH_4-60, and αCH_4-80. Detailed compositions and properties of the investigated fuel blends are shown in Table 3-1.

For the dilution gas study, the diluents used in the present study were pure N_2 (99.995% purity) and CO_2 (99.995% purity). In each case, the ratio of the main fuel components H_2/CO/CH_4 in the fuel blend was kept constant at *αBasis* (40%/40%/20% by volume fraction) condition and the air was also introduced by mixing 21% O_2 and 79% N_2. Therefore, the equivalence ratio is not affected by the percentage of diluents added. The dilution ratio is defined as the volumetric fraction of diluents added to the fuel blend,

$$Z_{dilution} = \frac{V_{dilution}}{V_{dilution} + V_{fuel}} \times 100\% \tag{3-2}$$

where $V_{dilution}$ and V_{fuel} are the volumetric fractions of diluents (N_2 or CO_2) and fuel (H_2/CO/CH_4) in the fuel mixture, respectively. The dilution ratio was changed from 0% to 45%, at an interval of 15%. Moreover, for $Z_{dilution}$ =30% condition, there was an extra condition for $Z_{N_2\text{-}CO_2}$, which means that N_2 and CO_2 coexisted in the bio-syngas mixture at a ratio of 1:1.

Table 3-1 The fuel blends investigated

Flame	Fuel mixture (vol%)			Fuel mixture density (g/L)	Stoichiometric air/fuel ratio
	X_{H2}	X_{CO}	X_{CH4}		
αBasis	40	40	20	0.604	3.808
αH_2-60	60	26.7	13.3	0.429	3.332
αH_2-80	80	13.3	6.7	0.255	2.856
αCO-60	26.7	60	13.3	0.773	3.332
αCO-80	13.3	80	6.7	0.943	2.856
αCH_4-60	20	20	60	0.621	6.664
αCH_4-80	10	10	80	0.629	8.092

3.5 Data processing method

3.5.1 Extraction of laminar flame speed

By using the experimental apparatus introduced in section 3.2, an outwardly propagating spherical flame was developed, and the data of flame radius R_f versus time t were collected from the flame images captured by the high-speed digital camera, as shown in Figure 3.3 and Figure 3.4, respectively. It can be noticed that there is a large bright circle in the pictures which is the combustion bomb, and the two horizontally placed black lines are the electrodes. After ignition, combustion starts from the center of the combustion bomb, which is located between the two electrodes. The flame gradually propagated and expanded from the burned gas to the unburned gas. The smaller bright circle found in the figure is the flame front.

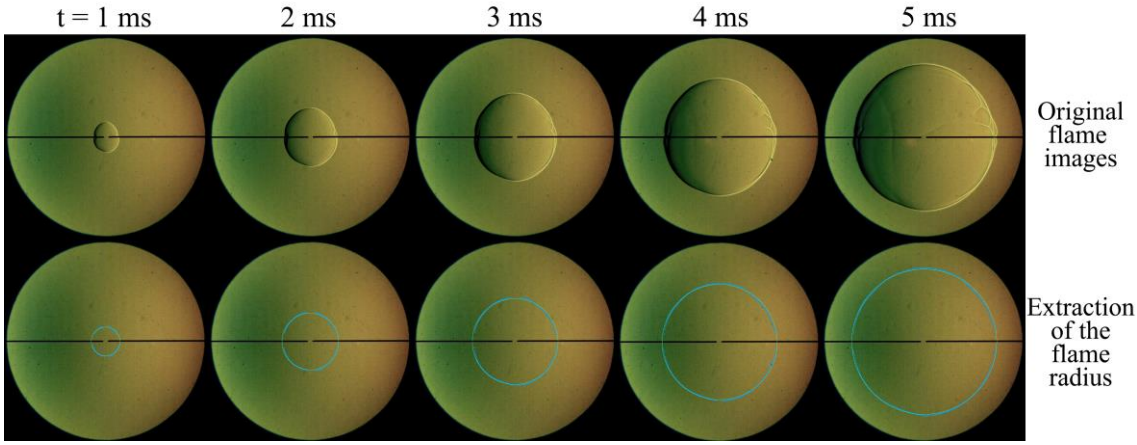

Figure 3.3 Images of measuring the flame radius

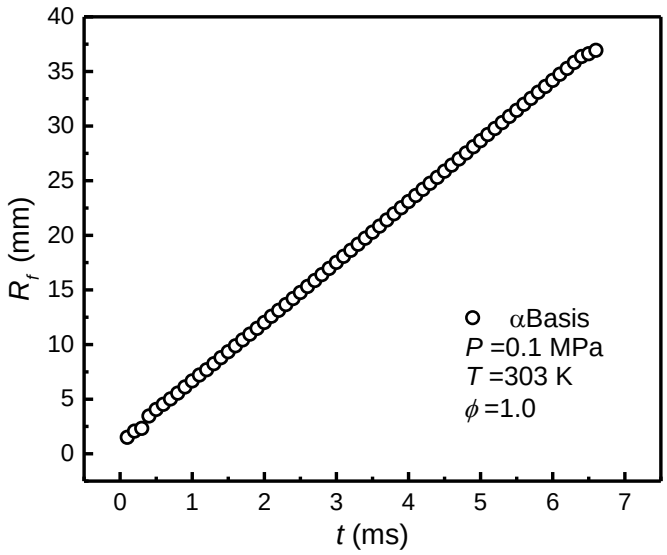

Figure 3.4 Typical relationship between flame radius and time

According to the theoretical assumptions of an expanding spherical flame, the flame is close to an adiabatic condition and the unburned gas remains stationary during its propagation. When the flame radius is small, the pressure inside the combustion bomb is almost unchanged, which can be considered as the isobaric developing process [209]. The stretched flame speed S_b, also known as the flame propagation speed, can be calculated using Equation (3-3) [210, 211]:

$$S_b = dR_f / dt \tag{3-3}$$

where S_b is the stretched flame speed (m.s^{-1}); R_f is the flame radius of the spherical flame (mm).

However, a practical expanding spherical flame possesses a curvature in the flame front during its propagation [19]. A general definition of the stretch rate κ at any point on the flame surface is the Lagrangian time derivative of the logarithm of the area A_f of an infinitesimal element of the surface [30]. For an outwardly propagating

spherical flame, the flame stretch rate can be derived in the following Equation:

$$\kappa = \frac{d(\ln A_f)}{dt} = \frac{1}{A_f} \cdot \frac{dA_f}{dt} = \frac{2}{R_f} \cdot \frac{dR_f}{dt} = \frac{2}{R_f} \cdot S_b \tag{3-4}$$

where A_f is the area of the flame surface (m^2); κ is the flame stretch rate (s^{-1}). A typical relationship between the flame propagation speed S_b and the flame stretch rate κ is shown in Figure 3.5.

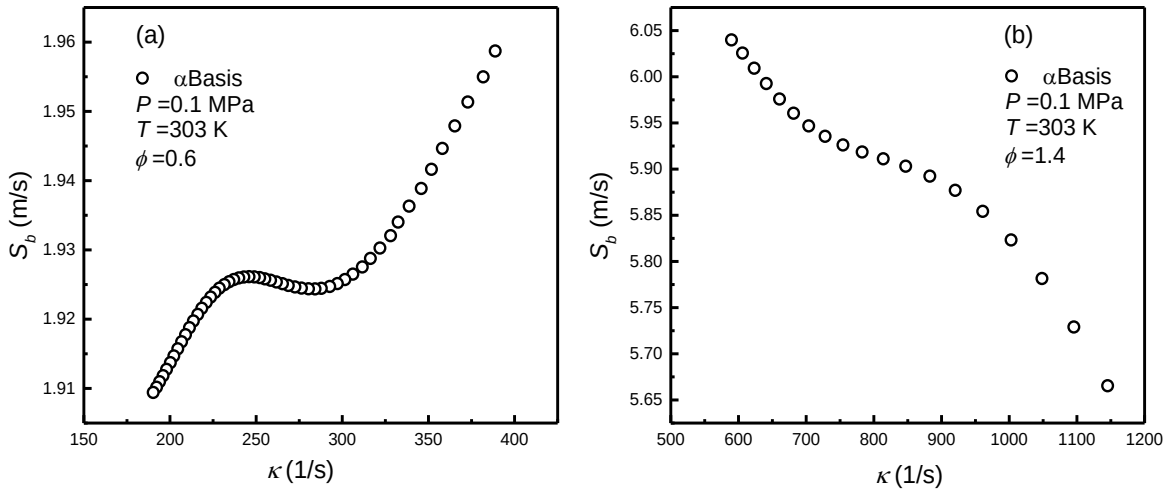

Figure 3.5 Typical relationship between flame propagation speed and the flame stretch rate: (a) ϕ=0.6; (b) ϕ=1.4

In addition to the effect of flame stretch rate, ignition disturbance could also affect the propagation of a flame at the early stage of expanding spherical flame development [101, 212]. According to Bradley et al. [210] and Lamoureux et al. [213], the measured values of laminar flame speed using the outwardly propagating spherical flame method are independent of disturbance from ignition energy when the flame radius is larger than 5 mm. On the other hand, the pressure increment at

the early stage of flame propagation can be neglected since the total volume of burned gas is less than 0.5 % of the volume of the combustion bomb [214], however, with the pressure rise in the combustion chamber, the confinement effect is stronger when the flame radius is large enough to approach the wall [215]. Kelley and Law [216] indicated that there are three distinct periods in the flame propagation process, namely, the initial period which is influenced by the ignition energy input, followed by a quasi-steady period of stretched flame propagation process which is suitable for the extraction of laminar flame speed, and the final period which is affected by the chamber confinement effect. Figure 3.6 shows these three periods of the flame propagation process. In a previous study, the upper limit of the extraction data range was found to be 25% of the combustion bomb radius [217]. According to the specification of the constant volume combustion bomb used in the present study, the flame images with flame radius ranging from 10 mm to 20 mm were chosen to measure the laminar flame speed for eliminating the influences of ignition disturbance and chamber confinement.

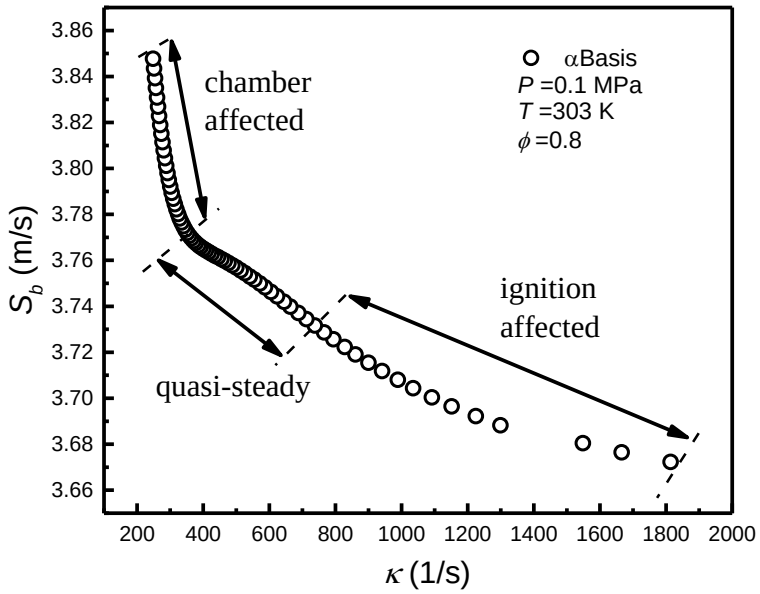

Figure 3.6 Three periods of the flame propagation process

After determining the appropriate extraction data range, the post processing of data is applied to eliminate the stretch rate and obtain the unstretched flame speed S_b^0, and then the laminar flame speed S_L can be calculated according to the law of mass conservation [19]:

$$S_L = S_b^0 \frac{\rho_b}{\rho_u} \tag{3-5}$$

where S_L is the laminar flame speed ($m.s^{-1}$); S_b^0 is the unstretched flame speed ($m.s^{-1}$); ρ_u and ρ_b ($kg.m^{-3}$) are the densities of unburned and burned mixtures, respectively.

There are several theoretical models for the extraction of laminar flame speed. The linear model proposed by Wu and Law [30] suggested that for a moderate stretch rate, there exists a linear relationship between the unstretched flame speed S_b^0 and the stretch rate κ at the early stage of flame expansion:

$$S_b^0 = S_b - L_b \cdot \kappa \tag{3-6}$$

where L_b is the Markstein length with respect to the burned mixture. This linear model has been widely adopted in previous investigations [43, 101, 105, 115, 164, 218, 219]. However, based on the assumption of a weakly stretched flame, the linear model sometimes performs unsatisfactorily in situations such as high stretch rates or strong non-equidiffusion mixtures [220].

The first nonlinear model was proposed by Markstein [221] and theoretically verified by Frankel and Sivashinsky [222], suggesting that the flame propagation speed S_b changes linearly with the flame curvature, $2/R_f$:

$$S_b = S_b^0 - S_b^0 L_b \cdot 2/R_f \tag{3-7}$$

Another nonlinear model was used by Kelly and Law [216] in the extraction of S_b^0 and L_b:

$$\ln(S_b) = \ln(S_b^0) - S_b^0 L_b \cdot 2/(R_f S_b) \tag{3-8}$$

This model describes that $\ln(S_b)$ changes linearly with $2/(R_f S_b)$. Then S_b^0 and L_b can be obtained through linear extrapolation based on the plot of $\ln(S_b)$ versus $2/(R_f S_b)$. The accuracies of these three models were found to strongly dependent on the Lewis number of the fuel mixture [212, 223, 224]. Chen [223] presented a detailed analysis of these three extrapolation methods. It was demonstrated that the first nonlinear model as shown in Equation (3-7) is the most accurate for mixtures with large Lewis numbers. This nonlinear model was also used in the present study to obtain the S_b^0

and L_b results.

3.5.2 Parameters for intrinsic flame instability

Thermal expansion ratio (σ), laminar flame thickness (l_f), Lewis number (Le), and global activation energy (E_a) are considered as the four most important parameters in inducing hydrodynamic instability and diffusional-thermal instability. The calculations of these four parameters are specified as follows.

Hydrodynamic instability is mainly caused by the density jump across the flame, which is represented by the thermal expansion ratio (σ), the ratio between the densities of the unburned mixture and the burned mixture:

$$\sigma = \rho_u / \rho_b \tag{3-9}$$

The thermal expansion ratio is the most sensitive parameter controlling the onset of hydrodynamic instability. In addition to the thermal expansion ratio, the laminar flame thickness l_f also has a strong influence on the hydrodynamic instability since a thinner flame weakens the stabilizing effect of curvature on the flame surface and increases the density gradient and the pressure gradient along with the flame, leading to the enhancement of hydrodynamic instability [225]. Herein, the laminar flame thickness was calculated on the basis of the temperature distribution [170, 174]:

$$l_f = \frac{T_{ad} - T_u}{(dT/dx)_{\max}} \tag{3-10}$$

where T_{ad} and T_u are the adiabatic flame temperature and initial temperature, respectively. $(dT/dx)_{max}$ is the maximum gradient of the temperature profile of the flame extracted from the PREMIX calculations.

On the other hand, the development of diffusional-thermal instability is caused by the competition between thermal diffusivity and mass diffusivity. An appropriate parameter representing the effect of non-equidiffusion is the Lewis number, which can be calculated by Equation (3-11), as shown below:

$$Le_i = \alpha / D_{ij} = \lambda / \rho C_p D_{ij} \tag{3-11}$$

where α is the thermal diffusivity of the fuel-air mixture; D_{ij} is the binary mass diffusivity of the deficient species (i) into the abundant species (j), and the deficient species (i) means the fuel or the oxidizer for lean and rich fuel mixtures respectively; λ is the thermal conductivity; C_p is the mixture specific heat; ρ is the mixture density.

It should be noticed that the definition of *Le* in a single-component fuel mixture is quite straightforward, while in a multi-component fuel mixture, the calculation of *Le* is more complex since the diffusivity of each component in the fuel mixture needs to be considered. There are three calculation methods proposed in the literature regarding *Le* for multi-component fuel mixtures, namely the volume-based method [226], the diffusion-based method [227], and the heat release-based method [170]. Lapalme et al. [173] performed an investigation to assess these three methods for

calculating the *Le* of H_2/CO/CH_4 mixtures and the volume-based method was found to be the most accurate one for all the investigated fuel blends. Therefore, the volume-based method was adopted in the present study to calculate the Le_f based on the volume fraction (χ_i) of the fuel (*i*) in the multi-component fuel mixture, as shown below:

$$Le_f = \sum_{i=1}^{f} \chi_i Le_i \tag{3-12}$$

where χ_i is the volume fraction of the fuel (*i*) in the multi-component fuel mixture and Le_i was calculated using Equation (3-11).

The effective Lewis number Le_{eff} was used in the present study to calculate a weighted average of the Lewis numbers of a fuel-air mixture, which is the combination of the Lewis number of the fuel with oxidizer [228]:

$$Le_{eff} = 1 + \frac{(Le_{exc} - 1) + (Le_{def} - 1)A_1}{1 + A_1} \tag{3-13}$$

where Le_{exc} and Le_{def} are the Lewis numbers of the excessive and deficient reactants in the fuel-air mixture, respectively. That is to say, for the fuel-lean condition, the excessive reactant is the oxidizer and the deficient reactant is the fuel in the fuel-air mixture, and vice versa. The parameter A_1 is a measurement of the mixture strength, which can be represented by $A_1 = 1 + Ze(\Phi - 1)$. Here, Φ is defined as the ratio of the mass of excess-to-deficient reactants in the unburned fuel mixture relative to their

stoichiometric ratio (Φ =1/ϕ for $\phi \leq 1$; $\Phi = \phi$ for $\phi > 1$) [114, 168]. *Ze* is the Zel'dovich number given by $Ze=E_a(T_{ad}-T_u)/R^0T_{ad}^2$. E_a is the global activation energy shown in Equation (3-14),

$$E_a=-2R^0\left\{\frac{\partial(\ln\rho_u S_u^0)}{\partial(1/T_{ad})}\right\}_{p,\varphi} \tag{3-14}$$

where R^0 is the universal gas constant; S_u^0 is the unstretched laminar flame speed of the unburned gas, also means the laminar flame speed S_L.

Moreover, the critical conditions for the onset of cellular instabilities can be expressed by introducing a critical Peclet number given by Law et al. [170]:

$$Pe_{cr}=\omega^{-1}\{Q_1+\beta(Le_{eff}-1)Q_2/(\sigma-1)+PrQ_3\} \tag{3-15}$$

where the *Pr* is the Prandtl number. The constants ω, Q_1, Q_2, and Q_3 depend on the wavenumber, n, which can be found in Addabbo et al. [228]. Then, the corresponding critical radius, R_{cr}, can be obtained from:

$$R_{cr}=Pe_{cr}*l_f \tag{3-16}$$

3.5.3 Uncertainty analysis

According to previous studies [28], various factors can affect the uncertainty of the measurement of laminar flame speed using the outwardly propagating spherical flame method, including the effects of ignition [43, 210, 229, 230], buoyancy [231, 232], radiation [217, 233-236], flame instability [164, 237, 238], chamber

confinement [215, 239-241], mixture preparation [136, 242, 243], and nonlinear stretch behavior [216, 224, 244-246]. As mentioned in section 3.5.1, the present study chose the experimental data within the flame radius of 10 to 20 mm and abandoned the data of full-fledged cellular flames to minimize the effects of ignition, chamber confinement, and flame instability. Therefore, the total experimental uncertainty of the laminar flame speed measurements can be evaluated through the method proposed by Moffat [247], which takes both systematic uncertainty and random uncertainty into account. This method has been widely used to evaluate the overall uncertainty in experimental laminar flame speed measurements [248-252], and can be expressed as:

$$\delta_{S_L}=\sqrt{(B_{S_L})^2+\left(\frac{t_{M-1.95}S_{S_L}}{\sqrt{M}}\right)^2} \tag{3-17}$$

where S_{S_L} is the standard deviation of S_L at each condition, derived from the laminar flame speeds of repeated experiments; M represents the repeat times for each experimental condition; $t_{M\text{-}1.95}$ is the student's value at the confidence interval of 95% with the freedom degrees of M-1; B_{S_L} is the total systematic uncertainty of the measurement method, and can be calculated by,

$$B_{S_L}=\sqrt{\sum_{i=1}^{n}\left(\frac{\partial S_L(x_i)}{\partial x_i}u_i\right)^2} \tag{3-18}$$

where x_i indicates each factor affecting the uncertainty of the laminar flame speed

measurement; u_i represents the fixed error of each factor x_i.

Then, with the experimental data at various operating conditions, the laminar flame speed can be correlated with equivalence ratio, initial temperature and pressure through Equation (3-19) [110]:

$$S_L=S_L(\phi)\left(\frac{T_u}{T_{u_0}}\right)^{\alpha_T(E,\ \phi)}\left(\frac{P_u}{P_{u_0}}\right)^{\beta_P(E,\ \phi)} \tag{3-19}$$

where the subscript *0* refers to the initial conditions, in which T_{u_0}=303 K and P_{u_0}=0.1/0.3/0.5 MPa according to the actual operating conditions. $S_L(\phi)$ is the laminar flame speed under the referenced condition. $\alpha_T(E, \phi)$ and $\beta_P(E, \phi)$ are the temperature and pressure exponents, respectively, which can be obtained by fitting with the experimental data. It should be noticed that the uncertainty of ϕ is mainly caused by the measurement of partial pressure when introducing the fuel (H_2, CO, CH_4) and the oxidizer (O_2 and N_2), which was estimated to be ±0.003~0.12. The accuracies of the initial temperature and pressure are controlled to within ±3 K and ±3 KPa, respectively. Finally, the overall experimental uncertainty was estimated to be in the range of ±0.8-4.6 cm/s by using Equation (3-17) for all the investigated fuel mixtures.

3.6 Numerical methodology

3.6.1 Introduction to CHEMKIN code

In the present study, a one-dimensional freely propagating plane premixed flame

was adopted to numerically study the laminar burning characteristics of premixed bio-syngas/air flames using the PREMIXED code [253] in the CHEMKIN package [254]. In 1980, Kee et al. [255] at the Sandia National Laboratory first developed the CHEMKIN software package to simulate gas-phase chemical reactions. After continuous development and improvement, the latest CHEMKIN package contains various modules that can simulate a variety of chemical reaction devices. Figure 3.7 shows the structure of the CHEMKIN package and the basic process for the simulation of one-dimensional laminar premixed flame using the PREMIXED code in the CHEMKIN package. The operation process of CHEMKIN is mainly divided into three parts, namely, gas-phase chemical reactions, transport, and fundamental equations for solving the laminar premixed combustion. During operation, the complier first obtained the reaction rates and thermal properties of each substance and the elementary reactions from the user-supplied mechanism file, and stored them in the linked file. Then, the software obtained transport data including viscosity, thermal conductivity, and diffusion coefficient from the transport file and the linked file generated in the previous step, and stored all the data in another linked file. Finally, the energy and momentum equations of the premixed combustion were solved based on the input parameters that the user defined according to the initial conditions, transport linked file, and chemical reaction linked file.

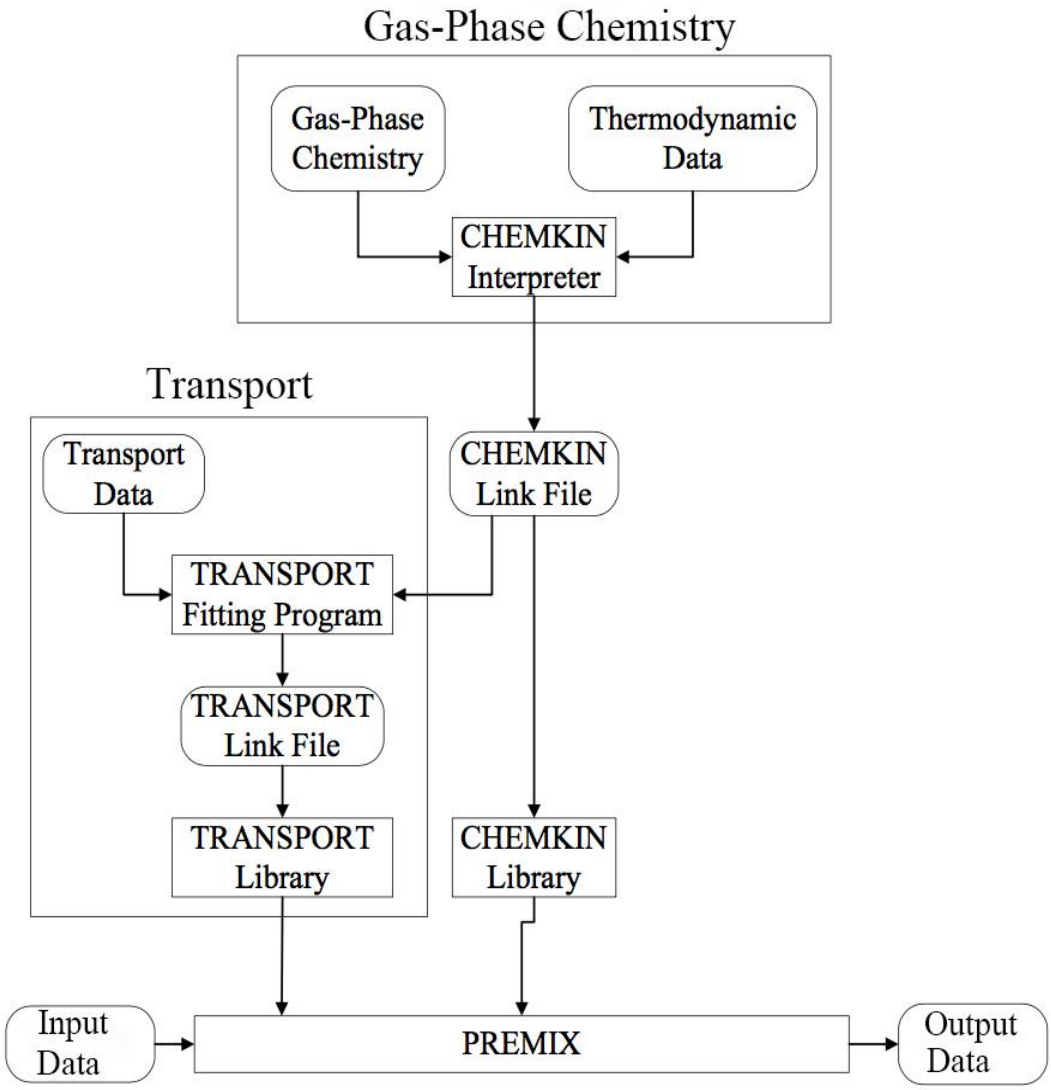

Figure 3.7 Flow chart of laminar premixed flame simulation using the CHEMKIN package

3.6.2 Numerical simulation and mechanisms

In the present study, the Li mechanism [256] was adopted for comparing the experimental data with simulated results. This mechanism was updated from the sub-mechanism for the hydrogen-oxygen [257, 258], carbon monoxide (CO), formaldehyde (CH_2O), and methanol (CH_3OH) kinetics. The detailed reaction

mechanism consists of 84 reversible reactions and 21 species. This mechanism has been compared against a wide range of experimental results, such as laminar flame speed, shock tube ignition delay data, and species profiles measured in flow reactors [256, 259]. For the present calculation, the Soret effects and multicomponent diffusion model were taken into consideration in the simulation. To assure a fully converged flame speed prediction, above 900 grid points were imposed in the PREMIX calculation. Moreover, the GRAD and CURV values were set at 0.02 to ensure the independence of grid solution.

CHAPTER 4 LAMINAR FLAME SPEEDS OF BIO-SYNGAS/AIR MIXTURES

4.1 Introduction

This Chapter presents the experimental and numerical results of laminar flame speeds of bio-syngas/air mixtures under various operating conditions [260, 261]. The effect of fuel composition, initial pressure, and dilution were studied experimentally and numerically. A constant volume combustion bomb combined with a high-speed schlieren system was utilized to measure the laminar flame speeds of bio-syngas/air mixtures. Moreover, by using the PREMIXED code in the CHEMKIN package with the Li mechanism, the thermochemical parameters including thermal diffusivity and adiabatic flame temperature were calculated. Chemical kinetic analyses were also conducted to identify the chemical effects of fuel composition, initial pressure, and dilution on the laminar flame speeds of bio-syngas/air mixtures.

4.2 Effect of fuel composition variation

4.2.1 Experimental conditions

For this part of the study, seven H_2/CO/CH_4 fuel blends were investigated at the initial temperature and pressure of 303 K and 0.1 MPa, respectively. The composition of the fuel blends can be found in Table 3-1. The equivalence ratio ranged from 0.6 to 1.5.

4.2.2 Flame and stretch interaction

Figure 4.1 shows the schlieren photographs of stoichiometric H_2/CO/CH_4/air flame at αBasis fuel composition. It can be seen that at the initial temperature and pressure of 303 K and 0.1 MPa, the expanding spherical flame propagates outward smoothly from the center of the combustion bomb, which is located between the two electrodes. At the early stage of flame development, the two electrodes are found to impede the combustion of fuel mixture due to the cooling effect [112], leading to a relatively slow flame propagation speed along the direction of the electrodes. This cooling effect of the electrodes becomes negligible when the flame radius has developed to a certain value.

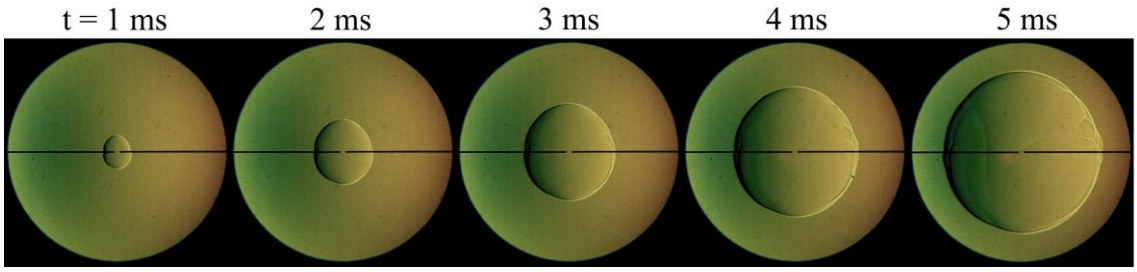

Figure 4.1 Schlieren photographs of H_2/CO/CH_4/air flame at αBasis condition, T=303 K, P=0.1 MPa, ϕ=1.0

Figure 4.2 and Figure 4.3 show the variation of flame radius with time at different equivalence ratios and fuel compositions. It can be noticed that there exists a linear relationship between the flame radius against the time after ignition start, except for the very early stage of flame propagation when the flame radius is smaller than 5 mm, when the flame propagation is influenced by the ignition energy and the

electrodes. As shown in Figure 4.2, the slope of the radius versus time line increases with increase of the equivalence ratio especially from the fuel-lean conditions to the stoichiometric condition. For the fuel-rich conditions, the maximum value of the slope is found at ϕ= 1.2. Then, the slope of the radius-time line slightly decreases with the increase of equivalence ratio to 1.4.

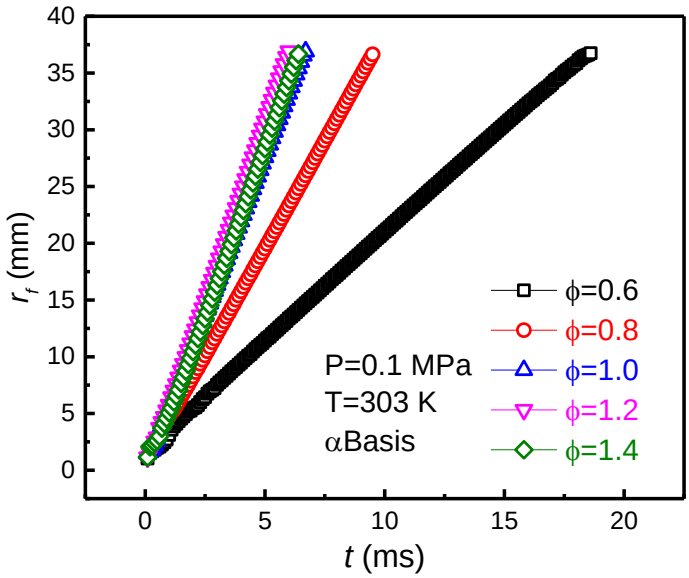

Figure 4.2 Flame radius versus time at different equivalence ratios

On the other hand, it can be seen from Figure 4.3 that with the increase of hydrogen fraction in the fuel mixture, the slope of the radius-time line increases significantly, which indicates the increase of flame propagation speed as hydrogen concentration is increased. Both the CO-enriched and CH_4-enriched fuel mixtures have smaller slopes compared to that of the αBasis condition, indicating smaller flame propagation speeds of the CO-enriched and CH_4-enriched flames. The increase of CH_4 fraction in the fuel mixture leads to an evident decrease of slope of the

radius-time line, while the slopes of the radius-time lines of αCO-60 and αCO-80 conditions decrease slightly compared to the αBasis condition.

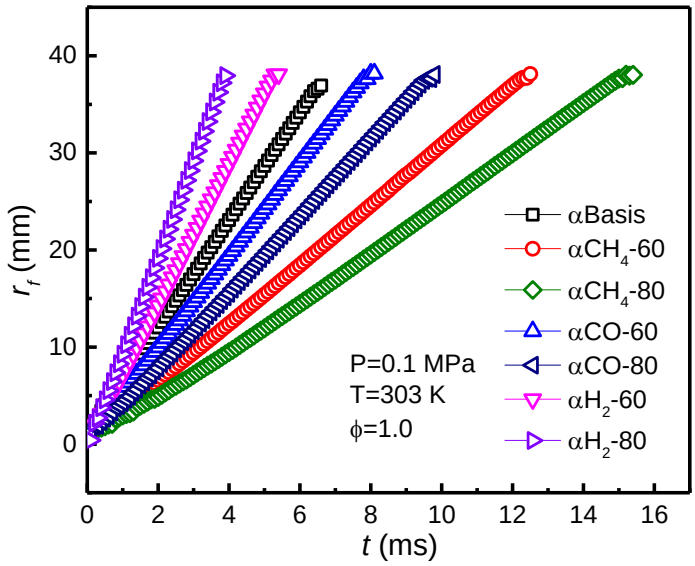

Figure 4.3 Flame radius versus time at different fuel compositions

The variations of stretched flame propagation speed S_b with flame radius at different equivalence ratios and fuel compositions are shown in Figure 4.4 and Figure 4.5, respectively. As stated in section 3.5.1, the stretched flame propagation speed is the derivative of the flame radius with respect to time. For the flame radius ranging from 10 mm to 20 mm selected in the present study, it can be seen that in the case of ϕ<1.0 under αbasic condition, the stretched flame propagation speed fluctuates slightly when the flame radius is relatively small. For stoichiometric and fuel-rich conditions, there is a slight increase in the stretched flame propagation speed with the increase of flame radius. The maximum value of the stretched flame propagation speed is also found at ϕ= 1.2. When ϕ < 1.2, the flame propagation speed increases

significantly with the increase of equivalence ratio. But for ϕ > 1.2, the flame propagation speed is slightly decreased with the increase of equivalence ratio to 1.4.

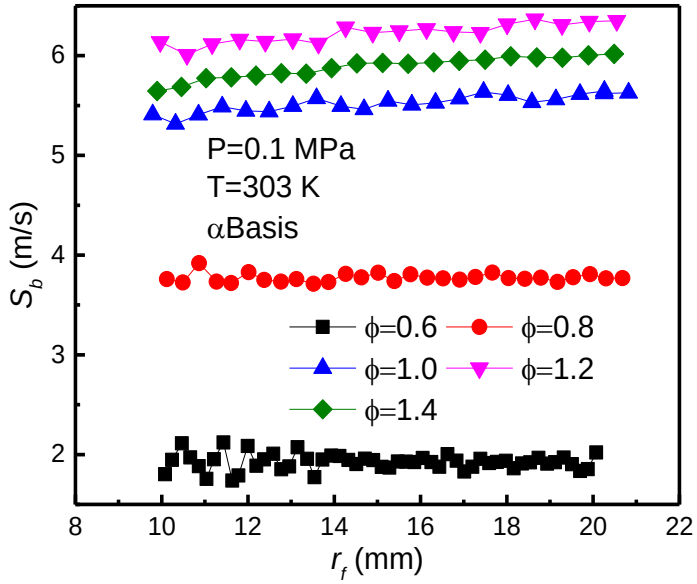

Figure 4.4 Stretched flame propagation speed versus flame radius at different equivalence ratios

As shown in Figure 4.5, there is no evident change of the stretched flame propagation speed with the increase of flame radius for different fuel compositions at stoichiometric equivalence ratio. S_b increases significantly with the increase of hydrogen content in the fuel mixture especially when the hydrogen fraction is larger than 60%, while for the CO-enriched and CH_4-enriched fuel mixtures, S_b decreases evidently with the increase of CH_4 fraction and decreases slightly with the increase of CO fraction.

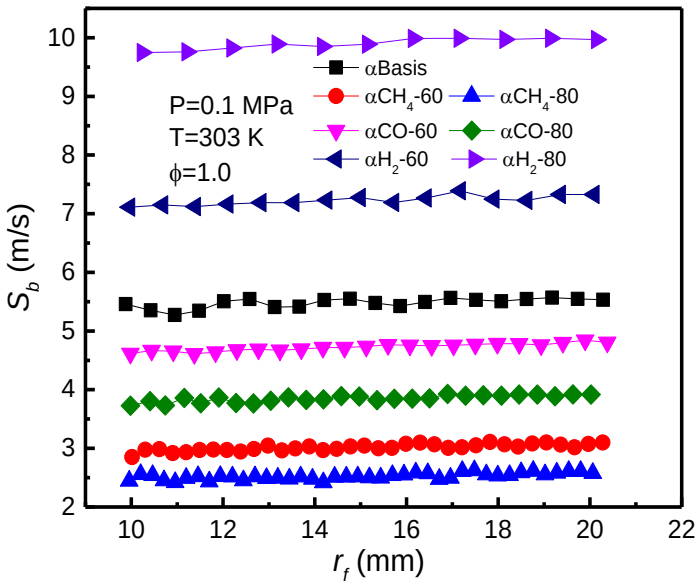

Figure 4.5 Stretched flame propagation speed versus flame radius at different fuel compositions

Figure 4.6 and Figure 4.7 show the variation of stretched flame propagation speeds with flame stretch rate at different equivalence ratios and fuel compositions respectively. In the early stage of flame development when the flame radius is small, the stretch rate of the flame surface is very large [262]. As the flame propagates outward, the stretch rate is decreased. After removing the data obtained at the early stage of flame development which is affected by the ignition energy and the electrodes, and the data obtained at large flame radius which is affected by the confinement effect, an approximately linear correlation between the stretched flame propagation speed and the flame stretch rate can be found at different equivalence ratios and fuel compositions. It is seen from Figure 4.6 that in the case of $\phi > 0.8$, the flame propagation speed is slightly decreased with the increase of the flame stretch rate, while for the case of $\phi < 0.8$, the flame propagation speed is slightly

increased with the increase of the flame stretch rate. At ϕ = 0.8, the variation of stretched flame propagation speed with flame stretch rate is insignificant.

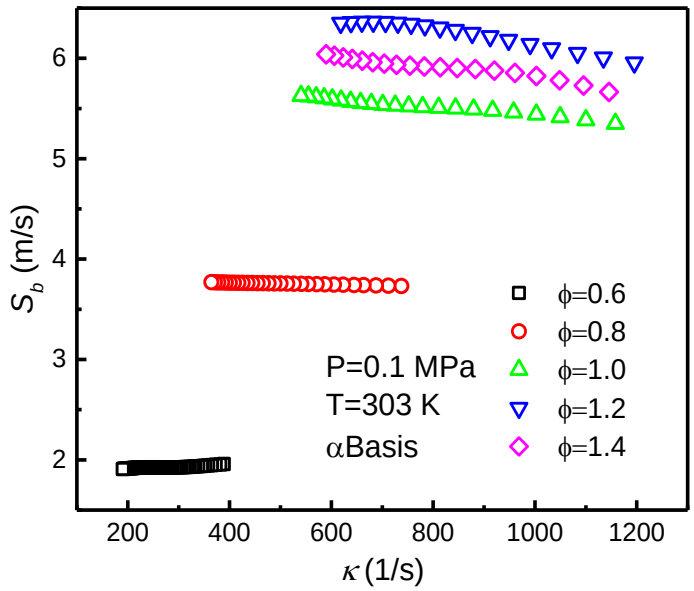

Figure 4.6 Stretched flame propagation speed versus flame stretch rate at different equivalence ratios

In regard to the variation of stretched flame propagation speed with flame stretch rate for different fuel compositions at the stoichiometric equivalence ratio, it can be seen from Figure 4.7 that the stretched flame propagation speed decreases with the increase of stretch flame rate for all fuel compositions. The results also show that the stretched flame propagation speed is increased significantly with the increase of hydrogen content in the fuel mixture. However, for the CO-enriched and CH_4-enriched flames, the stretched flame propagation speed is decreased compared to that of the αBasis condition. Thus, it can be seen that the flame stretch rate is lower with the increase of CO and CH_4 concentration in the fuel mixture at the same

flame radius, and the stretched flame propagation speed varies with a narrower range of flame stretch rate compared to the H_2-enriched condition.

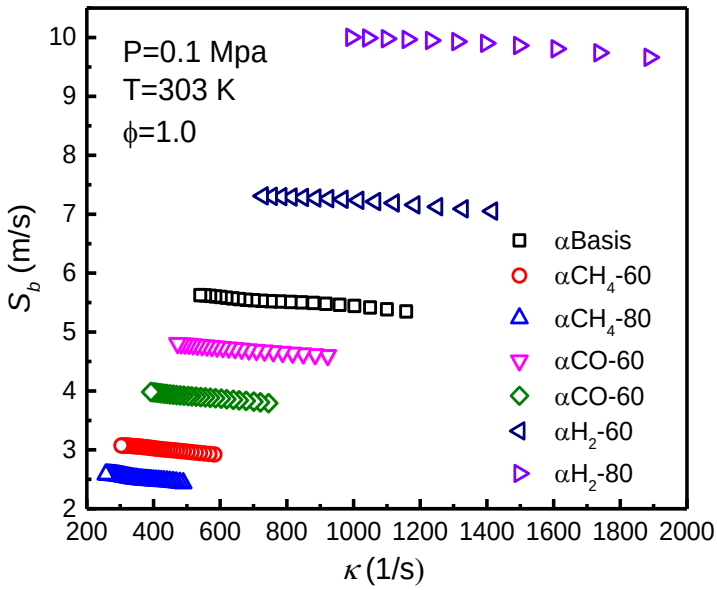

Figure 4.7 Stretched flame propagation speed versus flame stretch rate at different fuel compositions

4.2.3 Laminar flame speed

Figure 4.8 gives the variation of laminar flame speed of premixed H_2/CO/CH_4/air mixtures with equivalence ratio for different fuel compositions. The results predicted by using the PREMIX code in the CHEMKIN package with the Li mechanism are also plotted for comparison. A comparison of the experimental and predicted results shows that the Li mechanism can have a good prediction on the laminar flame speed of the H_2/CO/CH_4/air mixtures, especially in fuel-lean conditions. For fuel-rich conditions, differences between the experimental and predicted results are small. Previous studies [120, 259] also indicated that the Li mechanism was better in

predicting the laminar flame speed in fuel-lean conditions for syngas (H_2/CO) /air mixtures. In general, this good agreement between the experimental and the predicted results using the Li mechanism is considered to be satisfactory in the determination and prediction of laminar flame speeds of bio-syngas/air mixtures.

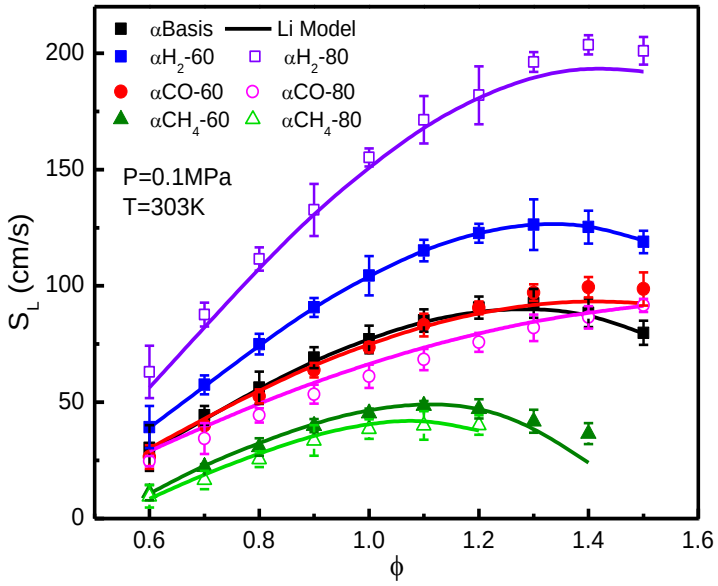

Figure 4.8 Laminar flame speed of H_2/CO/CH_4/air mixtures versus equivalence ratio at different fuel compositions

For the effect of fuel composition, the following results are observed. First, compared to the αBasis condition, the laminar flame speed increases significantly with the increase of H_2 fraction in the fuel mixture for the tested equivalence ratios. Second, the difference in laminar flame speed between the αCO-60 and the αBasis conditions is small, while the laminar flame speed for the αCO-80 condition is slightly decreased compared to that of the αBasis condition. Third, with the increase of CH_4 fraction in the fuel mixture, the laminar flame speed decreases evidently

compared to that of the αBasis condition. It can be observed that the laminar flame speeds for the CH_4-enriched conditions are lower than that of the CO-enriched conditions, which is consistent with results presented by Wu et al. [131] that the addition of an appropriate amount of CO to a CH_4/air mixture could increase the propagation speed of premixed CH_4/CO/air flame. Finally, the maximum laminar flame speed always occurs on the fuel-rich side for all the tested fuel blends. The peak laminar flame speeds for the CH_4-enriched conditions occur at ϕ=1.1, while with the increase of CO and H_2 fraction in the fuel mixture, the peak values of S_L shifts toward more fuel-rich condition, especially for the H_2-enriched cases, as a result of the higher diffusivity of hydrogen [169].

4.2.4 Numerical simulation and analysis

4.2.4.1 Thermal diffusivity and adiabatic flame temperature

The thermal diffusivity and adiabatic flame temperature of the tested fuel mixtures are shown in Figure 4.9, calculated by using STANJAN [263] and EQUIL [255] respectively. The thermochemical and transport properties were provided by the CHEMKIN thermodynamic database [264]. According to the classic laminar flame theory [265], $S_L \propto (\alpha RR)^{1/2}$, the laminar flame speed is proportional to the thermal diffusivity (α) and the reaction rate (RR), which has a positive correlation with the adiabatic flame temperature (T_{ad}). Law [19] also stated that the adiabatic flame temperature could not only indicate the exothermicity and maximum attainable

temperature of the fuel mixture when equilibrium was attained, but also represent the reactivity of the various chemical processes.

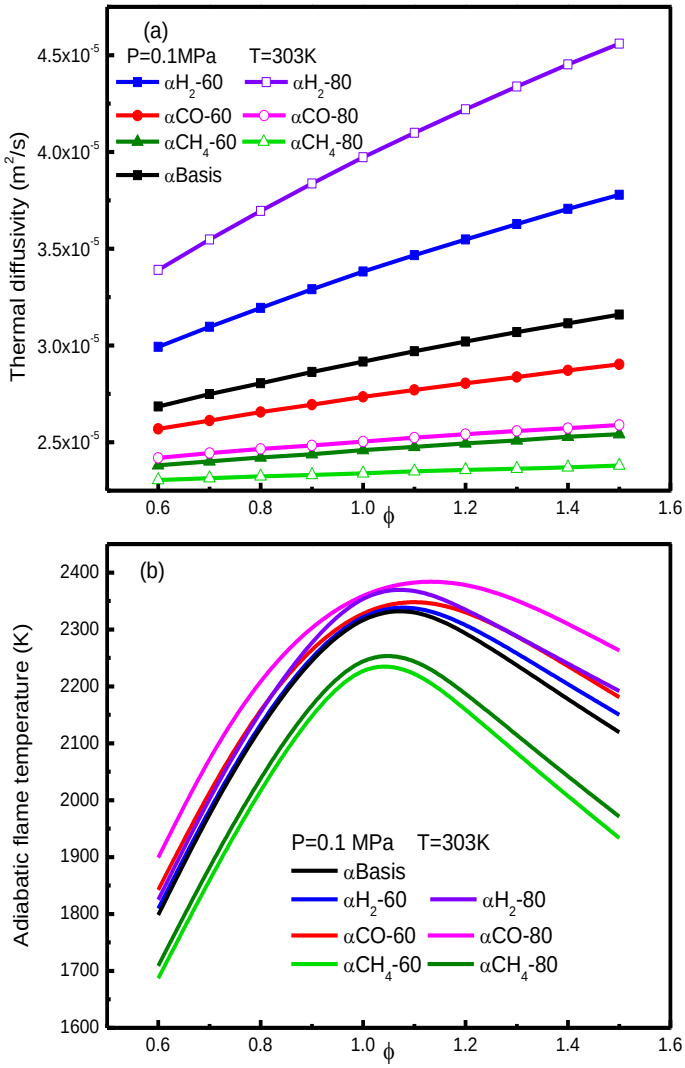

Figure 4.9 Thermal diffusivity and adiabatic flame temperature versus equivalence ratio for different fuel compositions

It is seen from Figure 4.9 that the adiabatic flame temperature always reaches its peak value at around ϕ=1.1 regardless of the variation of fuel composition, while the thermal diffusivity monotonically increases with the increase of equivalence ratio from ϕ=0.6 to ϕ=1.5. With the increase of H_2 fraction in the fuel mixture, the

thermal diffusivity increases significantly with increasing equivalence ratio, leading to the right shift of the peak laminar flame speed of H_2-enriched flames as observed in Figure 4.8. On the contrary, with the increase of CO or CH_4 fraction in the fuel mixture, the thermal diffusivity increases modestly or changes little with increasing equivalence ratio, and thereby the peak laminar flame speed for the CO-enriched or the CH_4-enriched flames shift left compared to the H_2-enriched flames. Moreover, compared with the αBasis case, the thermal diffusivity and adiabatic flame temperature both increase for the H_2-enriched flames but decrease for the CH_4-enriched flames. This is consistent with the results in Figure 4.8 in which the laminar flame speed increases with the increase of H_2 fraction but decreases with the increase of CH_4 fraction in the fuel mixture. However, for the CO-enriched flames, the thermal diffusivity is decreased compared to that of the αBasis case, while the adiabatic flame temperature is increased with the increase of CO fraction in the fuel mixture. The adiabatic flame temperatures of the CO-enriched flames are even higher than that of the H_2-enriched flames. This is different from the laminar flame speed results which indicate that the laminar flame speeds of the CO-enriched flames are lower than that of the H_2-enriched and αBasis flames. Xie et al. [145] also found that the adiabatic flame temperature increased with the increase of CO/H_2 ratio in the fuel mixture. This is consistent with the results found in the present study which indicate that the addition of CO in the $H_2/CO/CH_4$ mixture has more influence on the adiabatic flame temperature than that of H_2 addition. However, it is

noted that the variation of laminar flame speed for a multi-component fuel cannot be determined solely based on the adiabatic flame temperature [131]. Chemical effect analysis will be presented in the following sections to clarify the factors that influence the complicated variation of laminar flame speed of H_2/CO/CH_4/air mixtures.

4.2.4.2 Sensitivity analysis

A comprehensive analysis was conducted to identify the most important elementary reactions that affect the variation of laminar flame speed of H_2/CO/CH_4/air mixtures. Figure 4.10 gives the logarithmic sensitivity coefficients of the laminar flame speed of various stoichiometric H_2/CO/CH_4/air flames at different fuel compositions. The sensitivity coefficient (S_i) is defined as the sensitivity of one variable (A) with the change of another variable (B), and the formula is expressed as $S=\partial A/\partial B$. The greater the sensitivity coefficient is, the greater the change of variable A (ΔA) will be when the variable B is changed by a certain amount ΔB. In the present study, the sensitivity analysis was carried out by calculating the sensitivity coefficient of the laminar mass burning rate with respect to the reaction rate constant, as shown in Equation (4-1) using the CHEMKIN package:

$$S=\frac{\partial \ln m^0}{\partial \ln k_i}=\frac{k_i}{m^0}\frac{\partial m^0}{\partial k_i} \tag{4-1}$$

where m^0 is the laminar mass burning rate and k_i is the reaction rate constant for the

elementary reaction *i*.

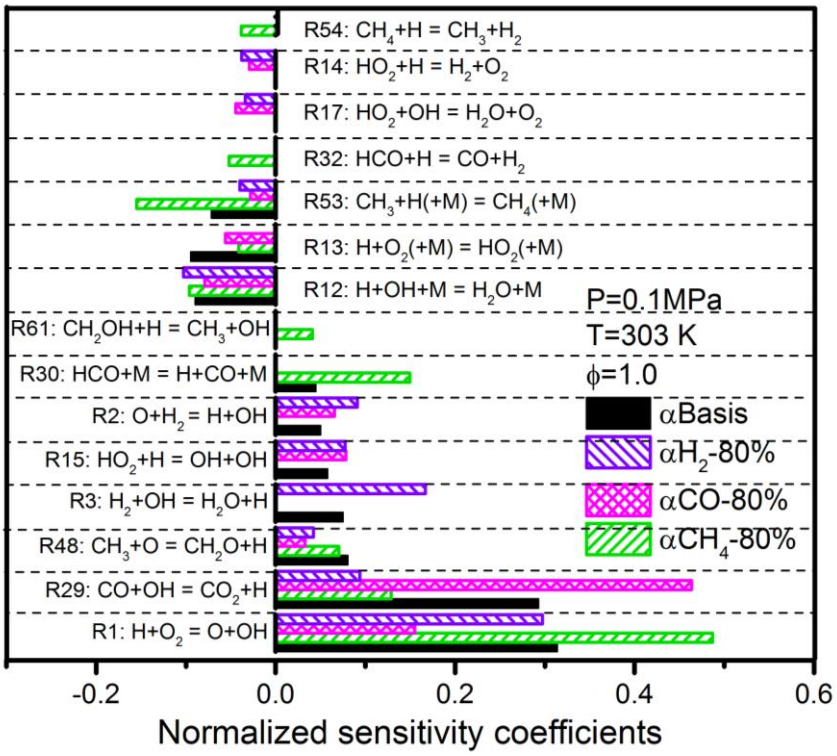

Figure 4.10 Logarithmic sensitivity coefficients of laminar flame speed for various $H_2/CO/CH_4$/air mixtures

In general, the major chemical reactions involved in premixed $H_2/CO/CH_4$/air combustion are the H_2/O_2 reactions, the oxidation of CO and CH_4, and the reactions that lead to the production of intermediate CO. As shown in Figure 4.10, the following three elementary reactions are the most important ones in the $H_2/CO/CH_4$/air flames for all the tested conditions:

$$H+O_2 \leftrightarrow O+OH \quad \text{(R1)}$$

$$CO+OH \leftrightarrow CO_2+H \quad \text{(R29)}$$

$CH_3+O \leftrightarrow CH_2O+H$ (R48)

The reaction (R1) is the dominant chain branching reaction, which produces a lot of OH and O radicals during the combustion. The oxidation of CO through the reaction (R29) and consumption of CH_3 through the reaction (R48) contribute to building up the H radical pool. These reactions contribute significantly to increase the concentration of active radicals (H, OH, and O), and thereby have a positive influence on the laminar flame speed.

With the increase of H_2 fraction in the fuel mixture, besides the reactions (R1), (R29), and (R48), the reactions $H_2+O \leftrightarrow H+OH$ (R2), $H_2+OH \leftrightarrow H_2O+H$ (R3), and $HO_2+H \leftrightarrow OH+OH$ (R15) also play an increasingly important role in promoting the overall reaction process. When the CO fraction in the fuel mixture increases to 80%, it can be seen that the reaction $H+O_2 \leftrightarrow O+OH$ (R1) becomes insignificant, because it has the lowest positive sensitivity coefficient compared to that of the other conditions, while the reaction $CO+OH \leftrightarrow CO_2+H$ (R29) plays a dominant role in the overall reaction process. Chaos and Dryer [266] also indicated that the reaction (29) was of critical importance in the combustion of $H_2/CO/O_2$ mixtures and was responsible for a major fraction of heat release during combustion [259]. Moreover, it is seen that for the αCH_4-80 condition, the reaction (R1) has the highest positive sensitivity coefficient compared to other conditions, and the reaction $HCO+M \leftrightarrow H+CO+M$ (R30) and $CH_2OH+H \leftrightarrow CH_3+OH$ (R61) become more important. The major negative contributors are the reactions $H+OH+M \leftrightarrow H_2O+M$ (R12),

$H+O_2+(M) \leftrightarrow HO_2+(M)$ (R13), and $CH_3+H+(M) \leftrightarrow CH_4+(M)$ (R53), together with the reactions $HCO+H \leftrightarrow CO+H_2$ (R32) and $CH_4+H \leftrightarrow CH_3+H_2$ (R54). They all have negative sensitivity coefficients resulting in an effective termination of the radical chain reaction.

4.2.4.3 Chemical kinetic analysis

To further understand the effect of fuel composition variation on the flame characteristics, detailed chemical kinetic structures of stoichiometric laminar premixed $H_2/CO/CH_4$ flames, including αH_2-60, αH_2-80, αCO-60, αCO-80, αCH_4-60, αCH_4-80, and αBasis, were investigated via numerical simulation using the Li mechanism. Figure 4.11-Figure 4.14 show the profiles of species mole fraction, production rate, net reaction rate, and heat release rate of the major elementary reaction steps at various fuel compositions. First, for the αBasis condition (40% H_2-40% CO-20% CH_4), Figure 4.13(g) shows that the chain cycle (R1)-(R3) of the H_2-O_2 reaction scheme plays an important role in the overall reaction process, contributing to producing abundant amount of H, OH, and O radicals. With these active radicals, the dehydrogenation of CH_4 is achieved by the reactions $CH_4+H \leftrightarrow CH_3+H_2$ (R54), $CH_4+O \leftrightarrow CH_3+OH$ (R55), and $CH_4+OH \leftrightarrow CH_3+H_2O$ (R56). Moreover, it is seen from Figure 4.11(g) that the decrease of H_2 mole fraction occurs earlier than those of CO and CH_4. The consumption of CO starts after the CH_4 has been consumed to a large extent due to the positive

production rate of CO as demonstrated from Figure 4.12(g). With the oxidation of CH_4, the intermediate CO is produced mainly through the following reactions $CH_3+O \leftrightarrow CH_2O+H$ (R48), $CH_2O+H \leftrightarrow HCO+H_2$ (R42), and $HCO+M \leftrightarrow H+CO+M$ (R30) as shown in Figure 4.13(g). This is consistent with the results of Vagelopoulos and Egolfopoulos [130] and Wu et al. [131] who observed the added CO in the fuel mixture would not react until most of the hydrocarbon species had been consumed. On the other hand, it is noteworthy that some CH_3 radicals also react with H through the reaction $CH_3+H+(M) \leftrightarrow CH_4+(M)$ (R53), leading to the termination of the radical chain process. Figure 4.14(g) indicates the major elementary reactions contributing to the positive heat release include the following:

$CH_3+O \leftrightarrow CH_2O+H$ (R48)

$CH_3+H+(M) \leftrightarrow CH_4+(M)$ (R53)

$H_2+OH \leftrightarrow H_2O+H$ (R3)

$CO+OH \leftrightarrow CO_2+H$ (R29)

$HCO+H \leftrightarrow CO+H_2$ (R32)

$H+O_2+(M) \leftrightarrow HO_2+(M)$ (R13)

$H+OH+M \leftrightarrow H_2O+M$ (R12)

$HO_2+H \leftrightarrow OH+OH$ (R15)

$CH_2O+H \leftrightarrow HCO+H_2$ (R42)

The major negative contributor is:

$H+O_2 \leftrightarrow O+OH$ (R1)

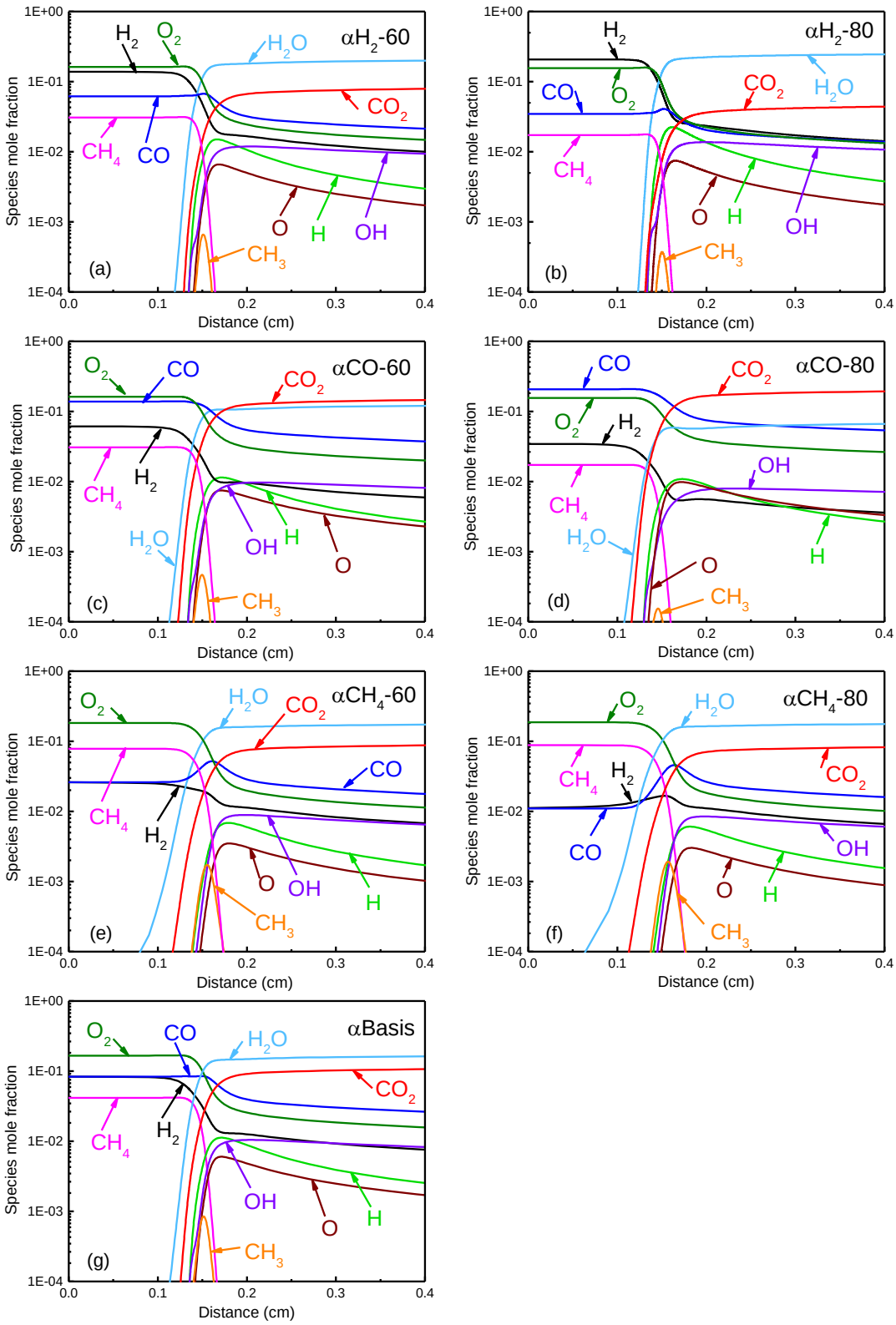

Figure 4.11 Computed species mole fraction of stoichiometric laminar premixed H_2/CO/CH_4/air flames at T=303 K, P=0.1 MPa: (a) αH_2-60; (b) αH_2-80; (c) αCO-60; (d) αCO-80; (e) αCH_4-60; (f) αCH_4-80; (g) αBasis condition

With the increase of H_2 fraction in the fuel mixture, i.e., for αH_2-60 and αH_2-80 cases, it can be noticed from Figure 4.11(a) and (b) that the mole fraction of CH_3 radical decreases gradually compared to that of the αBasis condition due to the lower concentration of CH_4 in the fuel mixture. However, the consumption of CO still does not occur during the stage of CH_4 oxidation, as demonstrated by the positive production rate of CO in the beginning, as shown in Figure 4.12(a) and (b). It is seen from Figure 4.13(a) and (b) that with the increasing H_2 concentration in the fuel mixture, the chain cycle (R1)-(R3) in the H_2-O_2 reaction scheme plays a dominant role in the overall reaction process, and the net reaction rates of these reactions are much higher than that in other conditions. It can be seen that the rate of reaction (R3) increases significantly, contributing to the maximum positive heat release as shown in Figure 4.14(a) and (b). Moreover, the formation and consumption of HO_2 are observed through the reactions $H+O_2+(M) \leftrightarrow HO_2+(M)$ (R13) and $HO_2+H \leftrightarrow OH+OH$ (R15), which also generate the active radicals (H, OH, and O) to again speed up the overall reaction process and contribute to a significant amount of positive heat release. Therefore, with the larger pool of H, OH, and O radicals combined with the increasing reaction rate and heat release, the S_L of H_2-enriched flames are significantly increased compared to that of the αBasis flame.

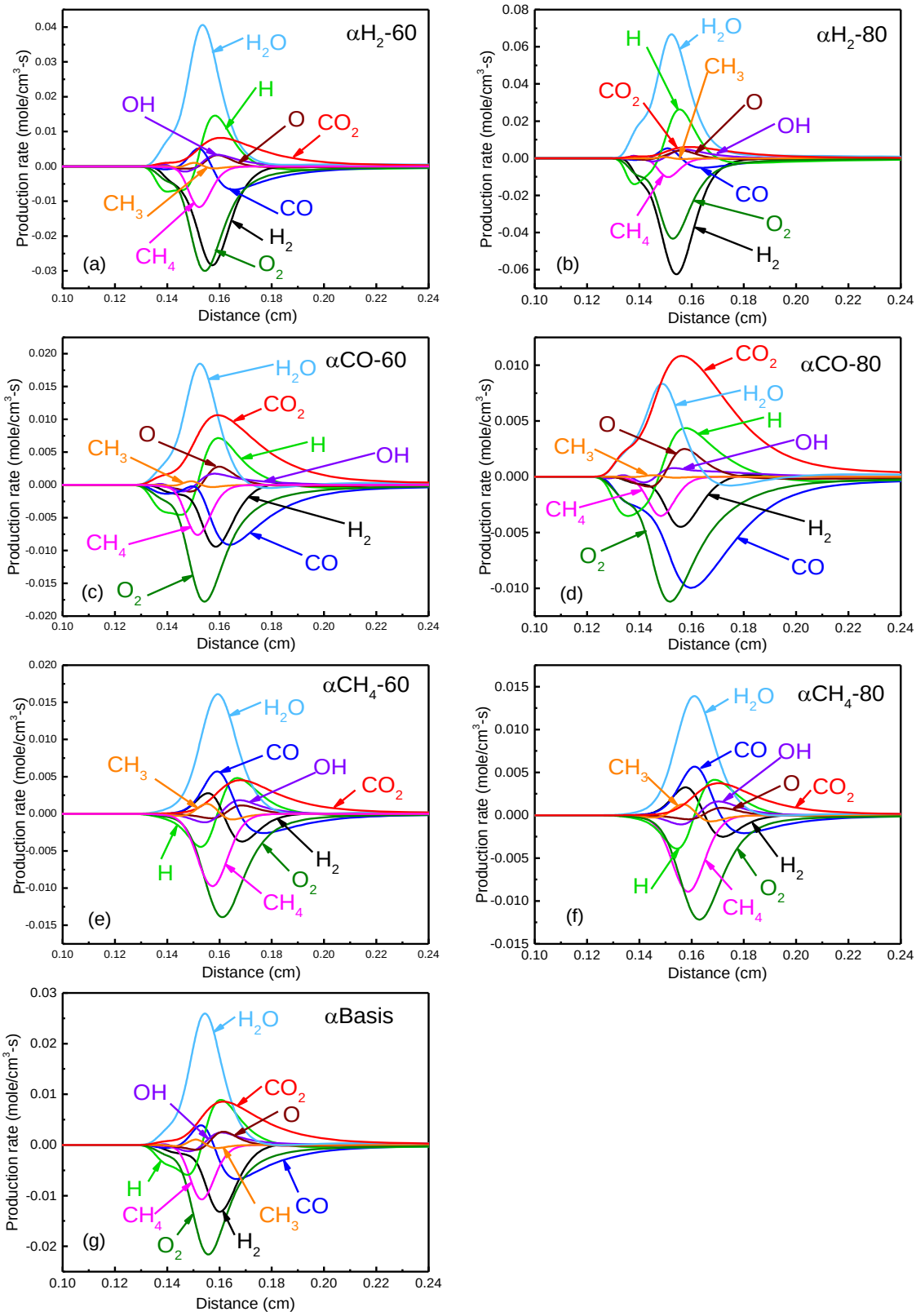

Figure 4.12 Computed production rate of stoichiometric laminar premixed H_2/CO/CH_4/air flames at T=303 K, P=0.1 MPa: (a) αH_2-60; (b) αH_2-80; (c) αCO-60; (d) αCO-80; (e) αCH_4-60; (f) αCH_4-80; (g) αBasis condition

For the CO-enriched flames, i.e., αCO-60 and αCO-80 cases, it can be seen from Figure 4.11(c) and (d) that the mole fraction of CH_3 radical decreases with the increase of CO fraction in the fuel mixture, and is lower than that of the αBasis and H_2-enriched conditions. With the higher CO concentration in the fuel mixture, the dominant chemistry shifts to the CO kinetics as revealed by Figure 4.13(c) and (d). The net reaction rate of CO+OH ↔ CO_2+H (R29) for oxidation of CO increases significantly with increasing CO concentration in the fuel mixture and even exceeds those of the reactions (R1-R3) at αCO-80 condition. The H radicals produced in (R29) can feed the chain branching reactions (R1-R3) together with the formation and consumption of HO_2 (R13, R15), and thereby accelerate the CO oxidation rate contributing to a significant amount of positive heat release as shown in Figure 4.14(d). However, it can be found in Figure 4.13 and Figure 4.14 that the magnitude for both net reaction rates of overall reactions and heat release rates of CO-enriched conditions are lower than those of the αBasis and H_2-enriched conditions. Referring to the results of laminar flame speed shown in Figure 4.8 and adiabatic flame temperature shown in Figure 4.9(b), although the increasing addition of CO to the fuel mixture will slightly increase the adiabatic flame temperature, the chemical effect of CO addition is not comparable to that of H_2 addition. Consequently, there is no significant difference between the S_L of αBasis and αCO-60 conditions, and the S_L of αCO-80 condition is even lower than that of the αBasis condition due to less H_2 in the fuel mixture.

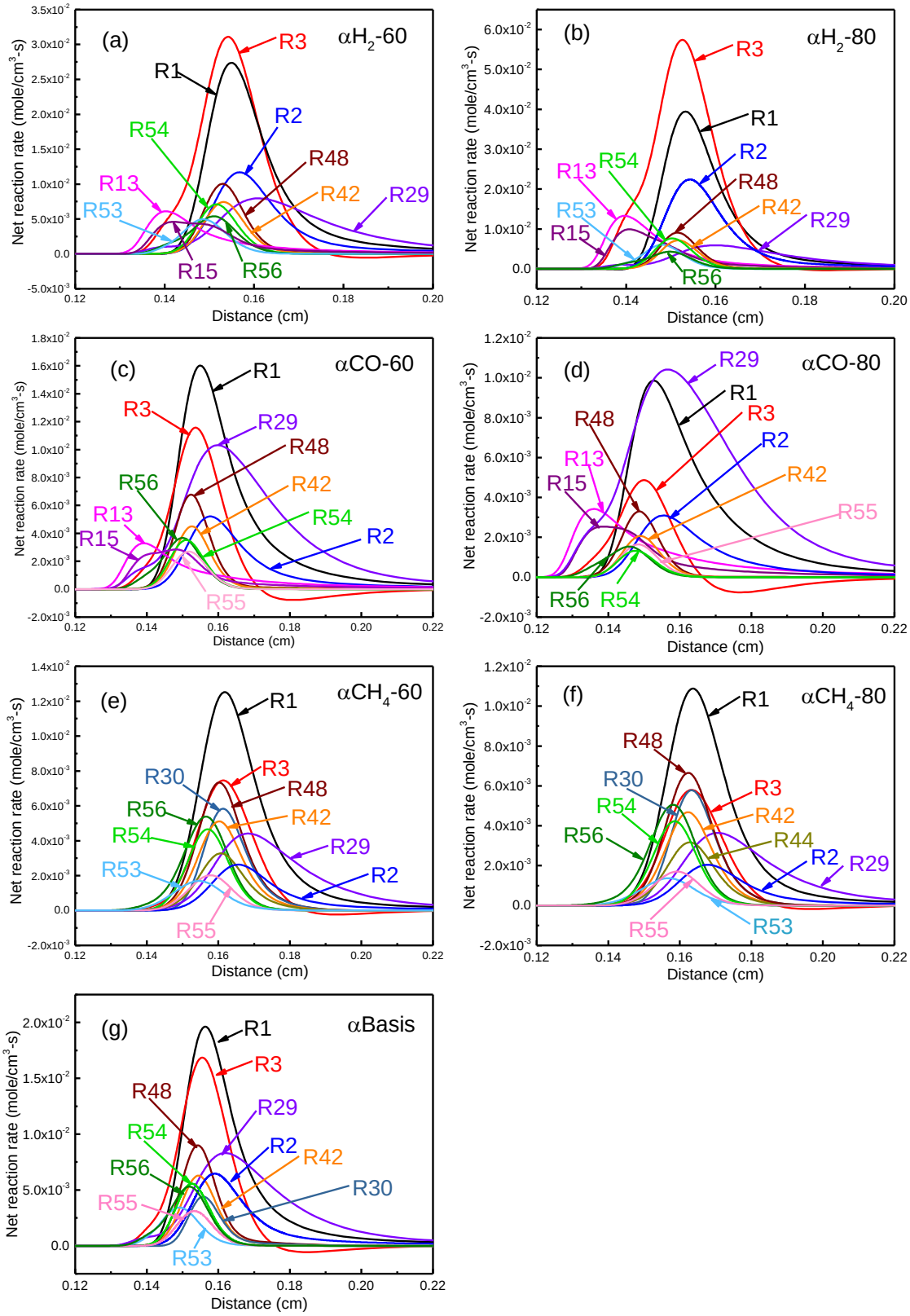

Figure 4.13 Computed net reaction rate of stoichiometric laminar premixed H_2/CO/CH_4/air flames at T=303 K, P=0.1 MPa: (a) αH_2-60; (b) αH_2-80; (c) αCO-60; (d) αCO-80; (e) αCH_4-60; (f) αCH_4-80; (g) αBasis condition

Finally, for the CH_4-enriched flames, i.e., αCH_4-60 and αCH_4-80 cases, it can be noticed from Figure 4.11(e) and (f) that the mole fraction of CH_3 radical increases obviously with the increase of CH_4 concentration in the fuel mixture. Moreover, there is an increasing amount of CO produced mainly through the reactions $CH_3+O \leftrightarrow CH_2O+H$ (R48), $CH_2O+H \leftrightarrow HCO+H_2$ (R42), $CH_2O+OH \leftrightarrow HCO+H_2O$ (R44), and $HCO+M \leftrightarrow H+CO+M$ (R30), as shown in Figure 4.12(e) and (f), and the net reaction rates of these reactions increase accordingly in Figure 4.13(e) and (f). The most significant reaction for the CH_4-enriched flames is still the chain branching reaction $H+O_2 \leftrightarrow O+OH$ (R1), followed by the reaction $H_2+OH \leftrightarrow H_2O+H$ (R3) and the oxidation of CH_4 through the reaction $CH_3+O \leftrightarrow CH_2O+H$ (R48). These reactions provide the necessary active radicals H, OH, and O for proceeding the overall reaction process. The dehydrogenation of CH_4 plays an increasing role with the increase of CH_4 concentration in the fuel mixture by following the reactions $CH_4+OH \leftrightarrow CH_3+H_2O$ (R56), $CH_4+H \leftrightarrow CH_3+H_2$ (R54), and $CH_4+O \leftrightarrow CH_3+OH$ (R55). It can be noticed that in these reactions, the active radicals H, OH and O are exchanged for the less active radical CH_3, leading to a weakening of the reactivity of the overall reaction process and the evident decrease of the laminar flame speed compared to the other cases. Moreover, it is noteworthy that with abundant CH_3 radicals in the reaction pool, some of them can react by themselves through the reaction $CH_3+CH_3+(M) \leftrightarrow C_2H_6+(M)$ (R52), as shown in Figure 4.14(e) and (f). This reaction is a radical termination step, which can inhibit the ignition and

combustion process, and thereby for some fuel-rich conditions, it is hard for the CH_4-enriched fuel mixture to be ignited. Table 4-1 gives a summary of the major reaction steps discussed in this chapter.

Table 4-1 Summary of the major reaction steps

Reaction No.	Reaction step
(R1)	$H+O_2 \leftrightarrow O+OH$
(R2)	$O+H_2 \leftrightarrow H+OH$
(R3)	$H_2+OH \leftrightarrow H_2O+H$
(R12)	$H+OH+M \leftrightarrow H_2O+M$
(R13)	$H+O_2+(M) \leftrightarrow HO_2+(M)$
(R15)	$HO_2+H \leftrightarrow OH+OH$
(R17)	$HO_2+OH \leftrightarrow H_2O+O_2$
(R29)	$CO+OH \leftrightarrow CO_2+H$
(R30)	$HCO+M \leftrightarrow H+CO+M$
(R32)	$HCO+H \leftrightarrow CO+H_2$
(R42)	$CH_2O+H \leftrightarrow HCO+H_2$
(R44)	$CH_2O+OH \leftrightarrow HCO+H_2O$
(R48)	$CH_3+O \leftrightarrow CH_2O+H$
(R52)	$CH_3+CH_3+(M) \leftrightarrow C_2H_6+(M)$
(R53)	$CH_3+H+(M) \leftrightarrow CH_4+(M)$
(R54)	$CH_4+H \leftrightarrow CH_3+H_2$
(R55)	$CH_4+O \leftrightarrow CH_3+OH$
(R56)	$CH_4+OH \leftrightarrow CH_3+H_2O$

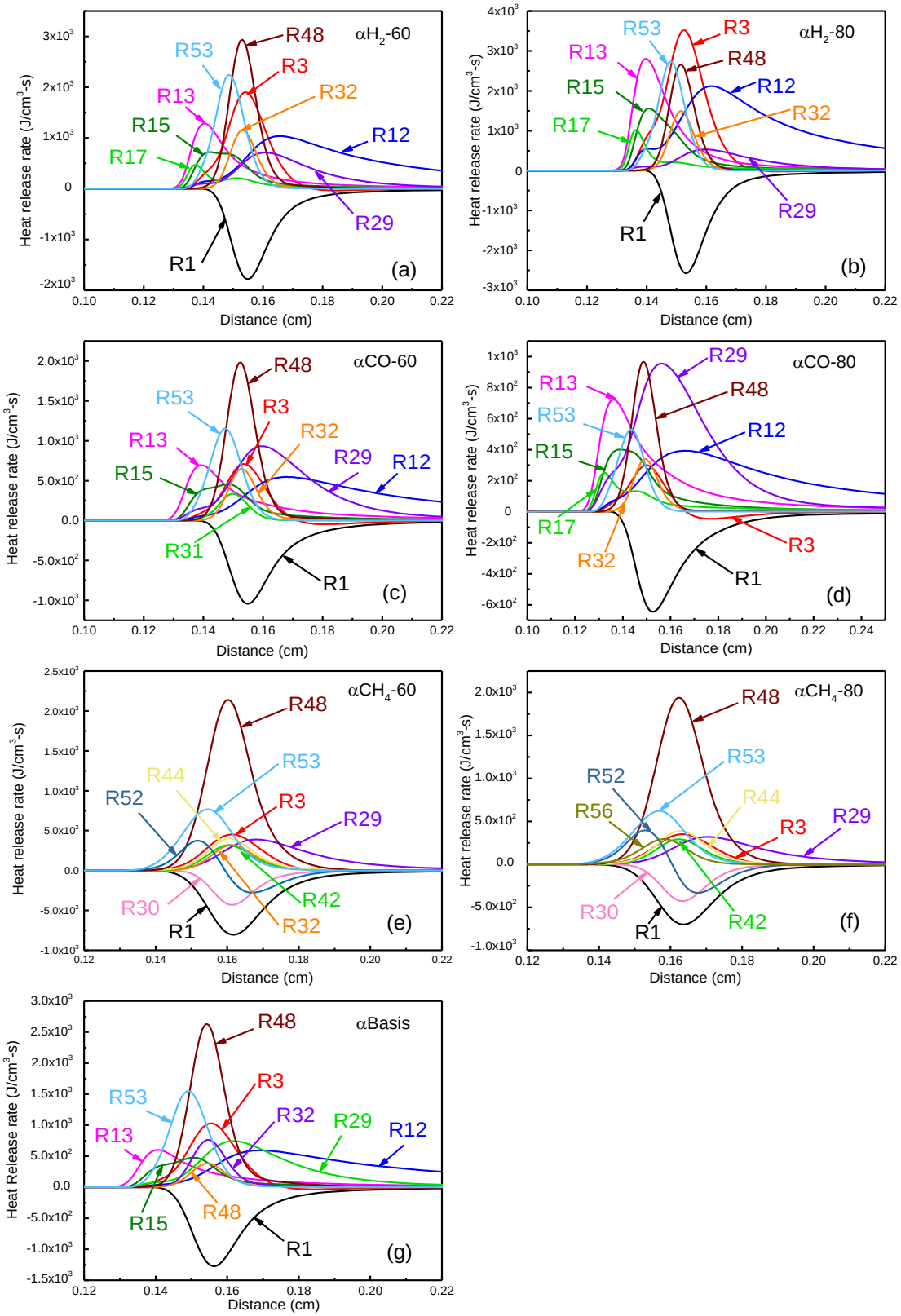

Figure 4.14 Computed heat release rate of stoichiometric laminar premixed H_2/CO/CH_4/air flames at T=303 K, P=0.1 MPa: (a) αH_2-60; (b) αH_2-80; (c) αCO-60; (d) αCO-80; (e) αCH_4-60; (f) αCH_4-80; (g) αBasis condition

4.3 Effect of initial pressure

4.3.1 Experimental conditions

For studying the effect of initial pressure (0.1 MPa, 0.3 MPa, and 0.5MPa) on laminar flame speed, as introduced in section 3.4, in order to acquire accurate experimental results, helium (He) was used as a substitution for N_2 to suppress the cellular instabilities of the premixed H_2/CO/CH_4/air flames, as shown in Figure 4.15. The ratio of He and O_2 was fixed at 7:1 which is widely adopted in the literature [164, 207, 208] to produce the comparable adiabatic flame temperature to that of the fuel mixture burned in air (N_2/O_2). The H_2/CO/CH_4 ratio was kept at the αBasis condition (40%H_2-40%CO-20%CH_4) during all the experiments. All the experiments were carried out at the initial temperature of 303 K.

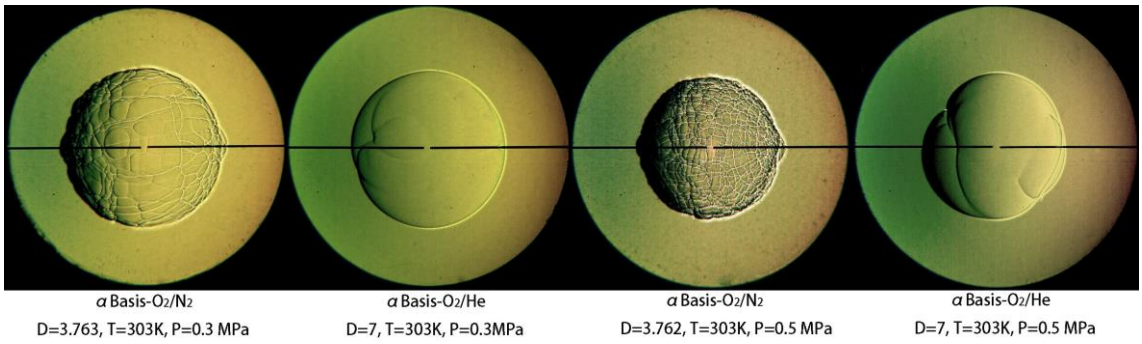

Figure 4.15 Schlieren photographs showing cellular instability of various H_2/CO/CH_4/air and H_2/CO/CH_4/He mixtures at αBasis condition, T=303 K, P=0.3/0.5 MPa, ϕ=1.0

4.3.2 Laminar flame speed

Figure 4.16 gives the variation of laminar flame speed with equivalence ratio for H_2/CO/CH_4/He mixture at different initial pressures. The prediction results of S_L calculated using the CHEMKIN package with the Li mechanism are also plotted for comparison. It shows that the Li mechanism slightly overestimates the laminar flame speeds of H_2/CO/CH_4/He mixtures at fuel-lean conditions but underestimates the laminar flame speeds at fuel-rich conditions for the tested initial pressures. It is seen that the laminar flame speed decreases with the increase of initial pressure under the tested equivalence ratios and S_L reaches its peak value around ϕ=1.0-1.2 under each initial pressure. With the increase of initial pressure, the peak value of laminar flame speed shifts slightly closer to the ϕ=1.0 side due to the slight decrease of thermal diffusivity of the fuel mixture with the increase of initial pressure.

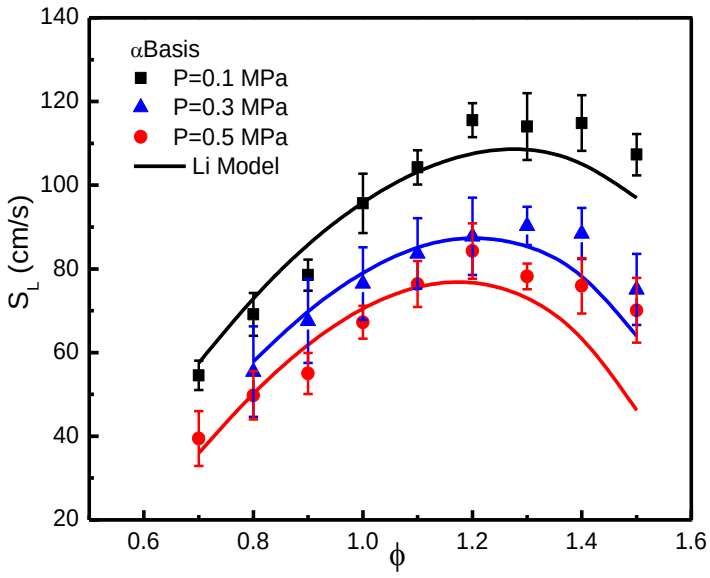

Figure 4.16 Laminar flame speed of H_2/CO/CH_4/He mixtures versus equivalence ratio at different initial pressures

4.3.3 Numerical simulation and analysis

4.3.3.1 Thermal diffusivity and adiabatic flame temperature

Figure 4.17 and Figure 4.18 show the adiabatic flame temperature and thermal diffusivity of H_2/CO/CH_4/He mixtures respectively at different initial pressures. It can be noticed that there is no significant change in the adiabatic flame temperature under different initial pressures and it reaches its peak value at around ϕ=1.0 regardless of variation of the initial pressure. This suggests that the adiabatic flame temperature is not a strong function of the initial pressure [19]. However, it is seen from Figure 4.18 that the thermal diffusivity decreases significantly with the increase of initial pressure. This leads to the slight left shift of the peak laminar flame speed at higher initial pressure.

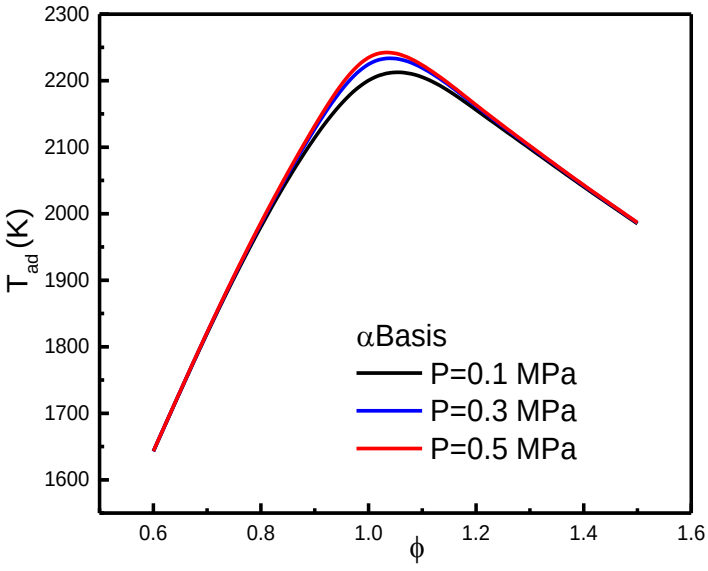

Figure 4.17 Adiabatic flame temperature of H_2/CO/CH_4/He mixtures at different initial pressures

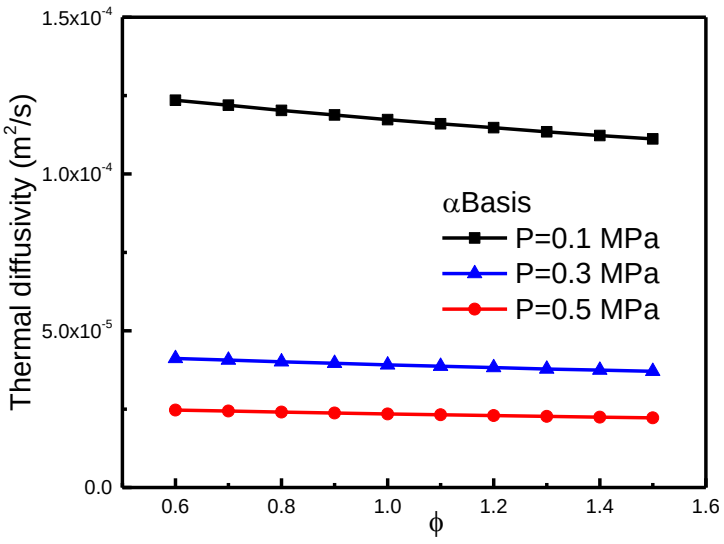

Figure 4.18 Thermal diffusivities of H_2/CO/CH_4/He mixtures at different initial pressures

4.3.3.2 Sensitivity analysis

Figure 4.19 gives the logarithmic sensitivity coefficients of the laminar flame speeds of stoichiometric H_2/CO/CH_4/He flames at different initial pressures. It can be noticed that the positive sensitivity coefficient of the chain branching reaction H+O_2 ↔ O+OH (R1) increases evidently when the initial pressure is increased. Moreover, the positive sensitivity coefficients for the chain carrying reactions CO+OH ↔ CO_2+H (R29) and CH_3+O ↔ CH_2O+H (R48) are also slightly increased with the increase of initial pressure. These results are consistent with the observation found by Law [267] that as the initial pressure is increased, the collision between molecules and free radicals becomes more frequent and reactions are facilitated. However, it should be noted that the three-body, chain termination reactions with large negative sensitivity coefficients, including the reactions CH_3+H+(M) ↔

CH_4+(M) (R53), H+O_2+(M) ↔ HO_2+(M) (R13), and H+OH+M ↔ H_2O+M (R12), play an increasing role in the overall reaction process when the initial pressure is increased. These reactions are found to be sensitive to the variation of initial pressure [268] and they can remove active radicals such as H and OH from the reaction pool, producing the relatively inactive radicals such as HO_2 or stable molecule such as CH_4. A retarding effect is thereby imposed on the overall reaction process, leading to a decrease of laminar flame speed with the increase of initial pressure.

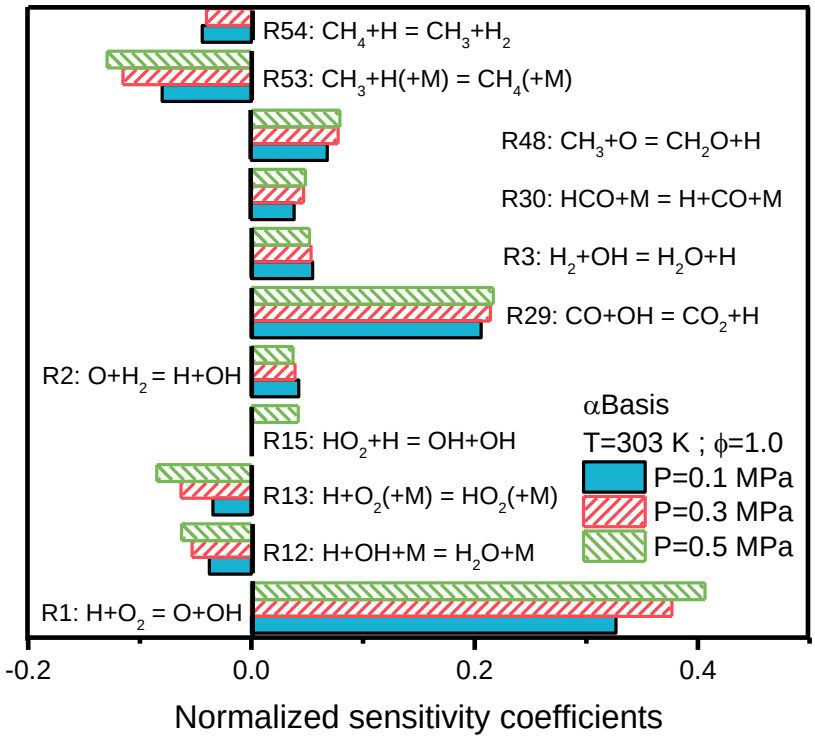

Figure 4.19 Sensitivity analysis for different initial pressures

4.3.3.3 Chemical kinetic analysis

The effect of initial pressure on the chemical kinetic in the flame is further analyzed. Figure 4.20 gives the calculated mole fraction of H, OH and O radicals at different initial pressures under the stoichiometric αBasis condition. Previous studies [145, 269] indicated that there is a strong positive correlation between the laminar flame speed and the concentrations of the key radicals H, OH, and O in the reaction zone. It is seen that the maximum concentrations of H, OH, and O radicals decrease with the increase of initial pressure, indicating that the decrease of laminar flame speed with the increase of initial pressure is indeed related to the reduction of concentrations of H, OH, and O radicals in the reaction pool.

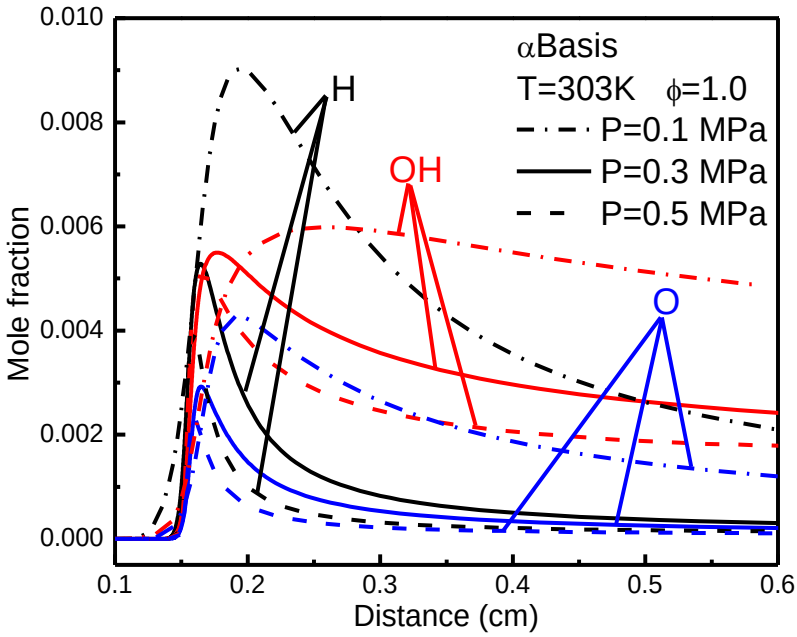

Figure 4.20 Mole fraction of H, OH, and O radicals at different initial pressures

4.3.3.4 Consumption pathway analysis

Figure 4.21 presents the results of integrated species consumption pathway analysis for P=0.1 MPa and P=0.5 MPa under the stoichiometric αBasis condition. The results clearly show that the consumption of H_2 is through the two reactions $H_2+O \leftrightarrow H+OH$ (R2) and $H_2+OH \leftrightarrow H_2O+H$ (R3); the consumption of CO is mainly through the reaction $CO+OH \leftrightarrow CO_2+H$ (R29); and the consumption of CH_4 is through the three reactions $CH_4+H \leftrightarrow CH_3+H_2$ (R54), $CH_4+O \leftrightarrow CH_3+OH$ (R55), and $CH_4+OH \leftrightarrow CH_3+H_2O$ (R56).

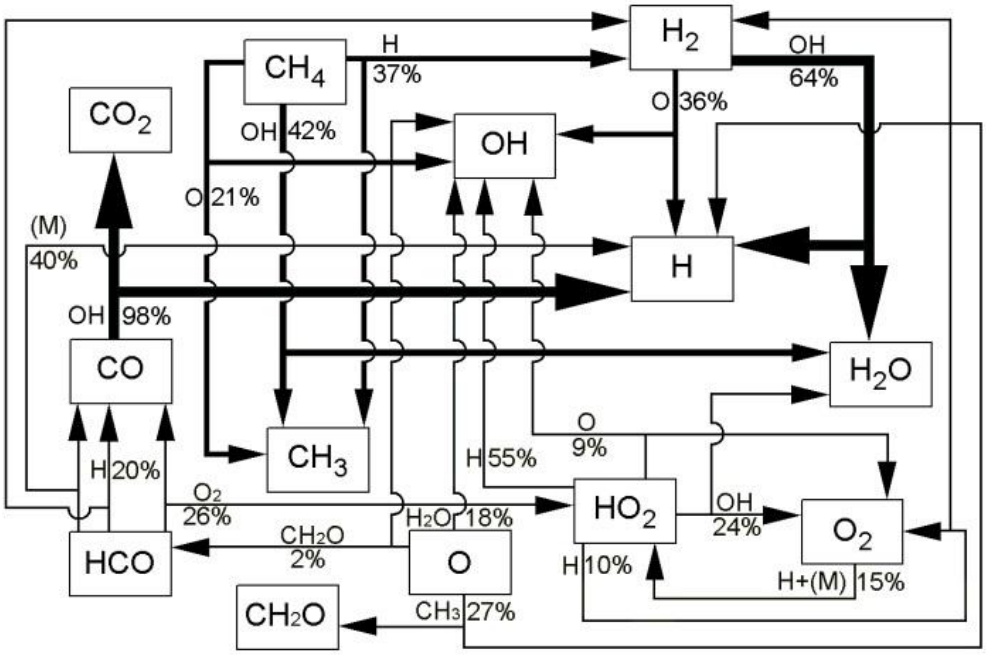

(a) αBasis, P=0.1 MPa

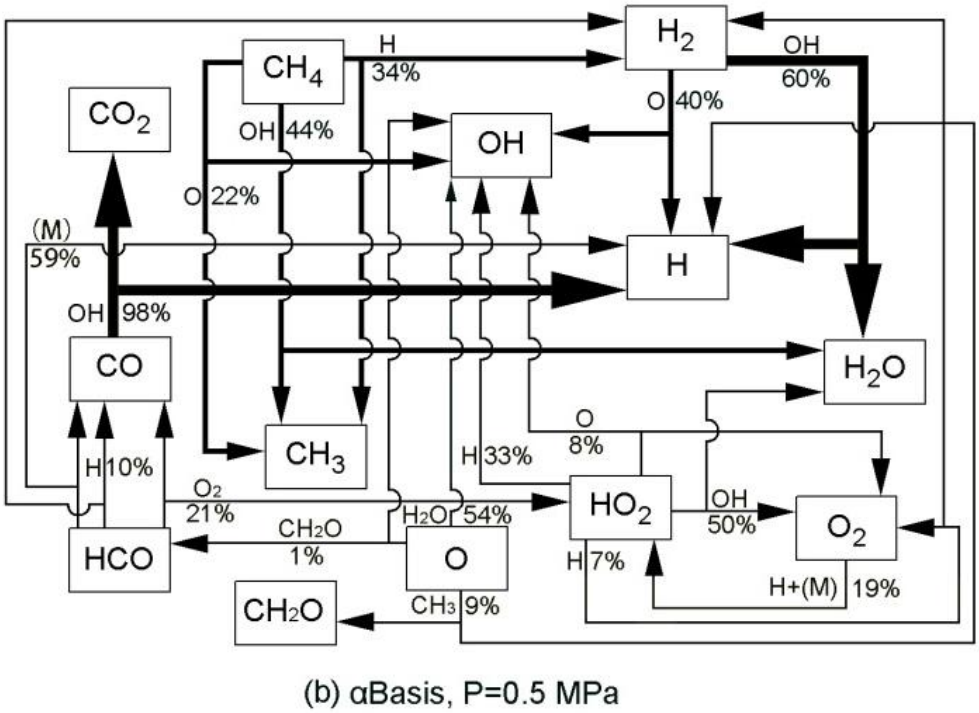

(b) αBasis, P=0.5 MPa

Figure 4.21 Integrated species consumption pathways of stoichiometric $H_2/CO/CH_4$/air mixtures at different initial pressures

As stated above in the sensitivity analysis under different initial pressures, the three-body, pressure-sensitive, chain termination reactions H+OH+M ↔ H_2O+M (R12), H+O_2+(M) ↔ HO_2+(M) (R13), and CH_3+H+(M) ↔ CH_4+(M) (R53) are favored as the initial pressure is increased. The consumption pathway analysis also shows the reduction of concentration of the key radicals. It is seen that although the production of OH radicals is increased through the reaction O+H_2O ↔ OH+OH (R4), marked by an increase in the consumption percentage of O radical from 18% to 54%, the production of OH through the reaction HO_2+H ↔ OH+OH (R15) decreases substantially from 55% to 33%. Moreover, the consumption of OH

radicals through the reaction HO_2+OH ↔ H_2O+O_2 (R17) increases greatly from 24% to 50% as the initial pressure is increased from 0.1 MPa to 0.5 MPa. Similarly, with the increase of initial pressure, H radicals produced by the reaction CH_3+O ↔ CH_2O+H (R48) are reduced from 27% to 9%, and H radicals consumed through the three-body reaction H+O_2+(M) ↔ HO_2+(M) (R13) are increased from 15% to 19%. Consequently, the chain-branching cycle (R1) to (R3) is broken as the initial pressure is increased, leading to a fall in the total concentration of H and OH radicals. Therefore, the radical pool is reduced quantitatively, which has a retarding effect on the overall reaction activity.

4.3.3.5 Laminar burning flux

The sensitivity analysis (Figure 4.19) and chemical kinetic analysis (Figure 4.20 and Figure 4.21) both indicate that a strong retarding effect of the chain termination reactions is imposed on the overall reaction process, and consequently the key radicals responsible for chain branching, namely, H, OH, and O, are diminished with the increase of initial pressure. Previous literature [268, 270] also suggested that the decreasing trend of laminar flame speed with increasing initial pressure is a manifestation of the dominance of the three-body termination reactions at high pressure. On the other hand, according to Law and Sung [211], there is a density-weighted fundamental parameter, the laminar burning flux, $f^0=\rho_u S_L$, which allows for density weighting in the interpretation of combustion phenomena due to

the pressure variation. It can manifest reactivity, diffusivity, and exothermicity of a combustible fuel mixture. Figure 4.22 gives the variation of laminar burning flux of the H_2/CO/CH_4/He mixtures with equivalence ratio at different initial pressures for the αBasis condition.

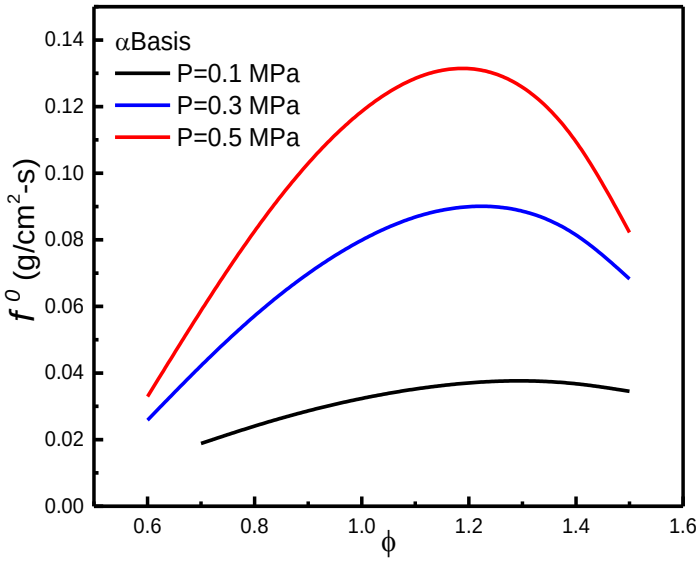

Figure 4.22 Laminar burning flux of H_2/CO/CH_4/He mixtures at different initial pressures

According to Law and Sung [211], we have $S_b^0 \sim [(\lambda/c_p)_b w_b]^{1/2}/\rho_b$, which shows that laminar premixed flame depends on the flame kinetic through the characteristic reaction rate w_b, and on the transport processes through the density-weighted transport coefficient $(\lambda/c_p)_b$. Therefore, it is important to take density into account because the density weighting intrinsically affects the interpretation of the role of diffusive transport as well as that of bulk mass flow rate. Recall that the laminar flame speed decreases with the increase of initial pressure as shown in

Figure 4.16, however, the laminar burning flux f^0 increases with the increase of initial pressure. This is consistent with the result of a previous study [267] which stated that as the initial pressure is increased, the significant increasing density of the fuel mixture could also lead to the decrease of laminar flame speed at elevated pressure.

4.4 Effect of diluents (N_2/CO_2)

4.4.1 Experimental conditions

Experiments were conducted under various dilution ratios $Z_{dilution}$ and equivalence ratios, which ranged from 0% to 45% and 0.6-1.5, respectively. The H_2/CO/CH_4 ratio was fixed at the αBasis condition (40: 40: 20 by volume fraction) and the initial temperature and pressure were set as 303 K and 0.1 MPa respectively.

4.4.2 Laminar flame speed

Figure 4.23 gives the experimental and predicted results of laminar flame speeds of H_2/CO/CH_4/air mixtures with N_2 and CO_2 dilution at various equivalence ratios and dilution ratios. According to a previous study [142], there are mainly three effects that a diluent can impose on the laminar flame speed, namely, dilution effect, thermal-diffusion effect, and chemical kinetic effect. The dilution effect means that the percentage of fuel and oxidant in the fuel mixture is decreased when a diluent is added. The thermal-diffusion effect is that the physical properties of the fuel mixture such as the specific heat capacity and thermal diffusivity are changed as a diluent is

added. The chemical effect means that the diluent can directly participate in the chemical reactions.

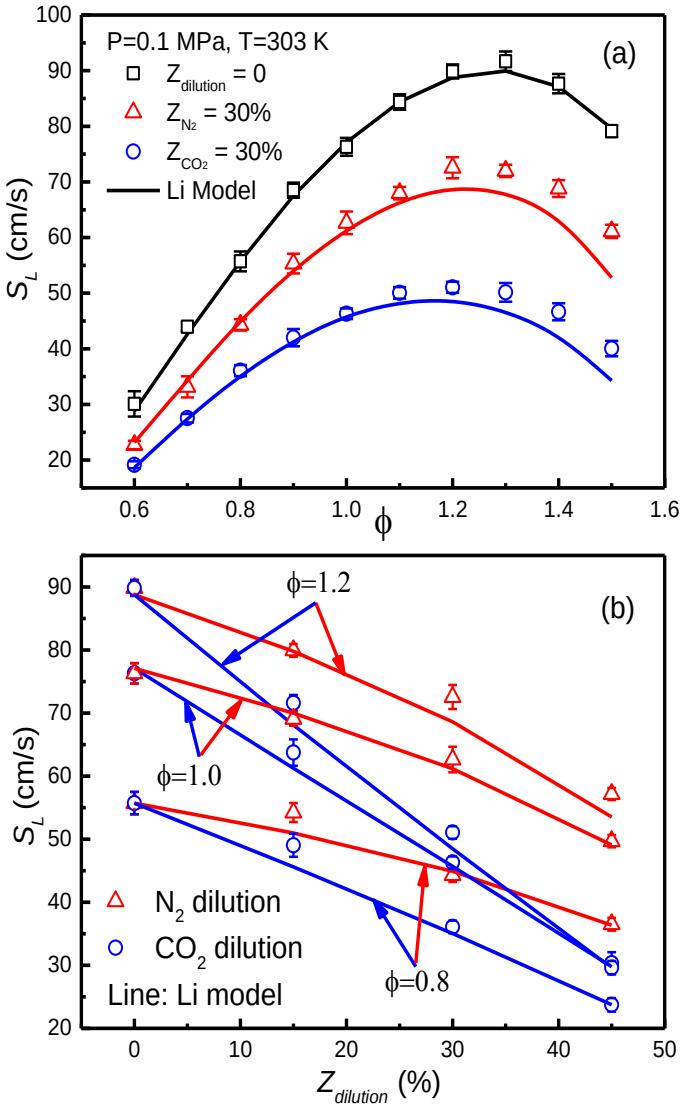

Figure 4.23 Laminar flame speed of H_2/CO/CH_4/air mixture with N_2 and CO_2 dilution at T=303 K, P=0.1 MPa

A comparison of the experimental and calculated results shows that the Li mechanism can have a good prediction of the laminar flame speed of a H_2/CO/CH_4/air mixture especially in the case of no dilution. With the addition of N_2

or CO_2 to the fuel mixture, it is seen that the Li mechanism slightly overestimates the laminar flame speed for the fuel-rich conditions. Moreover, as shown in Figure 4.23(a), the laminar flame speed decreases evidently with the N_2/CO_2 addition at all equivalence ratios and the peak values of S_L for the $Z_{dilution}$=0%, Z_{N_2}=30%, and Z_{CO_2}=30% conditions occur at around ϕ=1.2. Figure 4.23(b) also clearly shows that the laminar flame speed decreases significantly with the increase of dilution ratio. In the following analysis from thermal and chemical kinetics aspects, we can find that the decrease of laminar flame speed of bio-syngas with N_2/CO_2 dilution is mainly due to the evident decrease of thermal diffusivity, adiabatic flame temperature and concentrations of key free radicals with N_2/CO_2 dilution. Moreover, it is seen that the S_L of the CO_2-diluted flames are lower than that of the N_2-diluted flames at all dilution ratios. Hu et al. [142] indicated that the higher specific heat capacity and radiation of CO_2 lead to a more substantial reduction of S_L compared to the case with N_2 dilution.

4.4.3 Numerical simulation and analysis

4.4.3.1 Thermal diffusivity and adiabatic flame temperature

Figure 4.24 and Figure 4.25 give the thermal diffusivity and adiabatic flame temperature of $H_2/CO/CH_4$/air mixture with N_2 and CO_2 dilution at various equivalence ratios and dilution ratios respectively. For the plotted results of the equivalence ratios, i.e., ϕ=0.8, ϕ=1.0, and ϕ=1.2, it can be noticed that for the

N_2-diluted and CO_2-diluted fuel mixtures, the thermal diffusivity increases with the increase of equivalence ratio, while the adiabatic flame temperature reaches its peak value at ϕ=1.0. The combination results of thermal diffusivity and adiabatic flame temperature versus equivalence ratio indicate that the peak value of the laminar flame speed occurs at fuel-rich condition, which is consistent with the results shown in Figure 4.23. Moreover, it is seen that with N_2 or CO_2 dilution, the thermal diffusivity and adiabatic flame temperature of the fuel mixture both decrease approximately linearly with the increase of dilution ratio. At the same dilution ratio and equivalence ratio, the CO_2-diluted flame has both lower thermal diffusivity and adiabatic flame temperature compared to that of the N_2-diluted flame. Therefore, the thermal-diffusion effect of CO_2 dilution is stronger than that of the N_2 dilution in reducing the laminar flame speed of the H_2/CO/CH_4/air fuel mixture.

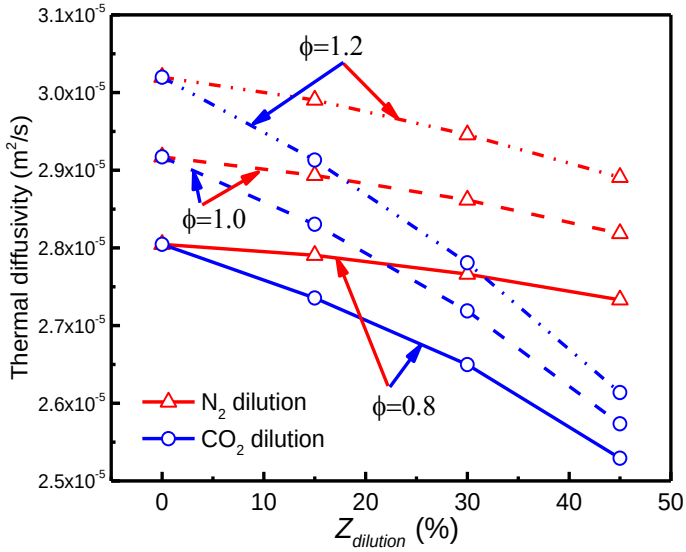

Figure 4.24 Thermal diffusivity of N_2/CO_2 diluted H_2/CO/CH_4/air mixture at various dilution ratios (T=303 K, P=0.1 MPa)

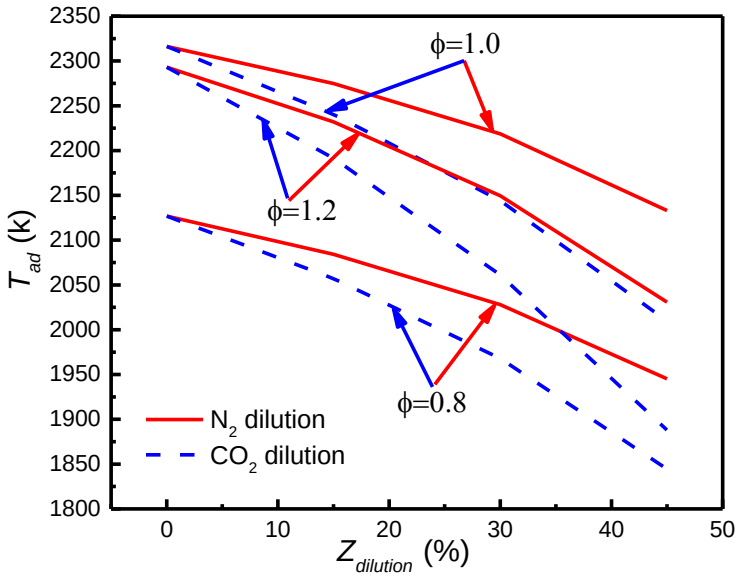

Figure 4.25 Adiabatic flame temperature of N2/CO2 diluted H2/CO/CH4/air mixture at various dilution ratios (T=303 K, P=0.1 MPa)

4.4.3.2 Sensitivity analysis

The logarithmic sensitivity coefficients of stoichiometric N_2/CO_2 diluted $H_2/CO/CH_4$/air flames are shown in Figure 4.26. From the positive sensitivity coefficient side, it is seen that the chain branching and chain carrying reactions play important roles in promoting the combustion process, including the reactions $H+O_2 \leftrightarrow O+OH$ (R1); $O+H_2 \leftrightarrow H+OH$ (R2); $H_2+OH \leftrightarrow H_2O+H$ (R3); $HO_2+H \leftrightarrow OH+OH$ (R15); $CO+OH \leftrightarrow CO_2+H$ (R29); $HCO+M \leftrightarrow H+CO+M$ (R30); $CH_3+O \leftrightarrow CH_2O+H$ (R48). The reaction $H+O_2 \leftrightarrow O+OH$ (R1) has the highest positive sensitivity coefficient, followed by the reaction $CO+OH \leftrightarrow CO_2+H$ (R29). All these reactions contribute to increasing the concentration of the key free radicals (H, OH, and O) in the reaction pool, and thereby they have a positive impact on the laminar

flame speed. For the negative sensitivity coefficient side, the following chain termination reactions are involved: H+OH+M ↔ H_2O+M (R12); H+O_2+(M) ↔ HO_2+(M) (R13); CH_3+H+(M) ↔ CH_4+(M) (R53). These chain termination reactions consume the key free radicals H and OH to produce unreactive intermediates such as HO_2 or stable products such as CH_4, resulting in a retarding effect on the overall reaction process and a negative impact on the laminar flame speed. When the N_2 or CO_2 is added to the fuel mixture, it can be seen that the negative sensitivity coefficients of the chain termination reactions (R12), (R13), and (R53) are substantially increased, and the effect of CO_2 dilution is stronger than that of N_2 dilution. As mentioned above, these three-body chain termination reactions can strongly restrain the reaction process. The increase of the negative sensitivity coefficients of these reactions suggests that with the N_2/CO_2 addition, chain termination reactions play an increasingly important role in the overall reaction process, leading to a decrease in the concentration of the key free radicals, and consequently, the laminar flame speed is decreased. In the case of CO_2-diluted flame, Liu et al. [149] pointed out that the CO_2 dilution can directly participate in the chemical reactions primarily through the reaction CO+OH ↔ CO_2+H (R29), resulting in the competition for H radicals with the most important chain branching reaction H+O_2 ↔ O+OH (R1). Consequently, the CO_2-diluted flames have lower laminar flame speed than that of the N_2-diluted flames at all the reported equivalence ratios and dilution ratios. In fact, some researchers indicated that the

chemical effect of N_2 dilution is so small that it can be neglected compared to its dilution effect [142, 149].

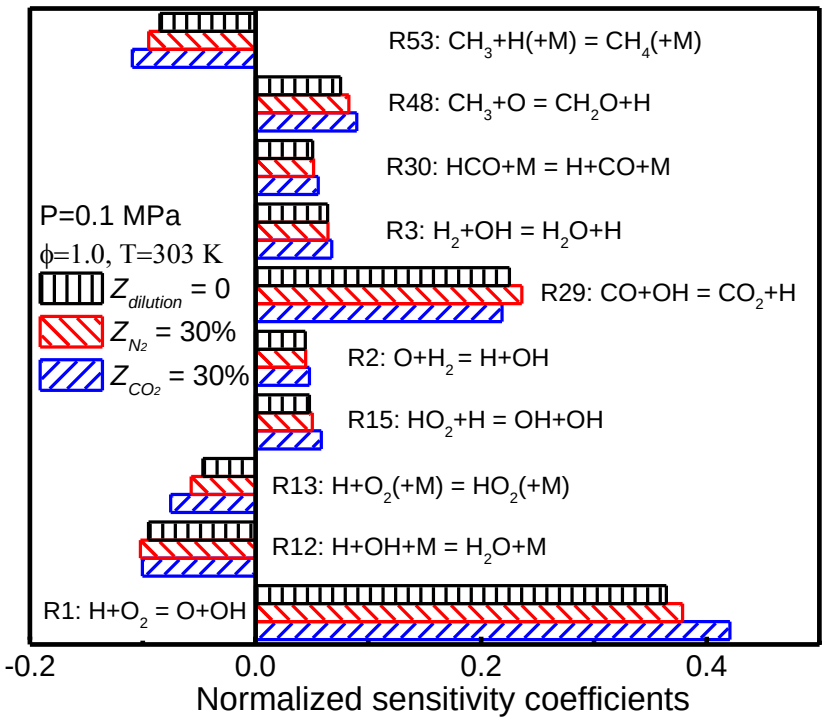

Figure 4.26 Sensitivity analysis for different diluents

4.4.3.3 Chemical kinetic analysis

As mentioned in section 4.3.3.3, there is a strong positive correlation between the laminar flame speed and the concentrations of key free radicals in the reaction zone. Figure 4.27 shows the variation of the maximum H+OH concentrations of N_2/CO_2 diluted $H_2/CO/CH_4$/air flame at various equivalence ratios and dilution ratios. With the N_2/CO_2 addition, it is seen that the maximum H+OH concentration decreases with the increase of dilution ratio. Consequently, there is an inhibiting effect imposed on the overall reaction process, leading to a decrease in the laminar flame

speed. Moreover, compared to the N_2-diluted flames, reduction of the maximum H+OH concentration for the CO_2-diluted flames is more substantial at all the reported equivalence ratios. This is consistent with the results observed in Figure 4.26 that CO_2 dilution has stronger chemical effect on the laminar flame speed than that of N_2 dilution.

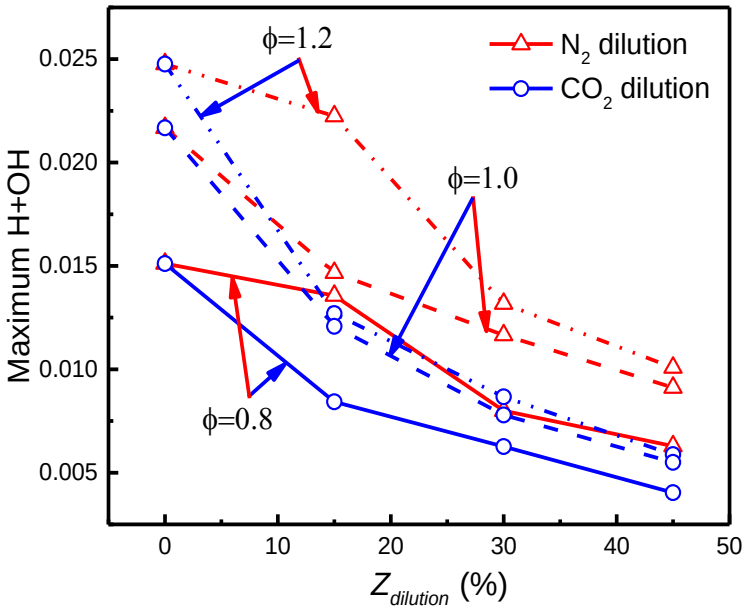

Figure 4.27 Maximum mole fraction of H+OH radicals of N_2/CO_2 diluted $H_2/CO/CH_4$/air mixture at various dilution ratios (T=303 K, P=0.1 MPa)

4.5 Summary

Experiments were conducted to investigate the laminar flame speed of bio-syngas/air mixtures with various fuel compositions ($H_2/CO/CH_4$), initial pressures (0.1 MPa/0.3 MPa/0.5 MPa), and different diluents (N_2/CO_2) under the initial temperature of 303 K and a wide range of equivalence ratios (0.6-1.5).

Besides the experimental study, a numerical simulation was conducted to validate the chemical mechanism and clarify the thermal and chemical effects of these parameters on the variation of laminar flame speed. The following results are obtained:

For the effect of fuel composition variation, the experimental results and predicted results using the Li mechanism show good agreement with each other, especially at fuel-lean conditions. With the increase of H_2 fraction in the fuel mixture, the overall reaction activity is strongly promoted, resulting in a significant increase in the laminar flame speed of H_2-enriched flames compared to that of the αBasis flame. For the CO-enriched flames, the laminar flame speed of the αCO-60 flame changes little compared to that of the αBasis flame, while the laminar flame speed of the αCO-80 flame is slightly decreased. It is observed that CO addition has more impact on the adiabatic flame temperature, but it plays a smaller role in the chemical kinetic effect compared to that of H_2 addition. For the CH_4-enriched flames, the laminar flame speed decreases evidently compared to that of the αBasis flame, and also lower than that of the CO-enriched flames due to the combination of thermal and chemical kinetic effects of CH_4 addition.

Regarding the effect of initial pressure, the Li mechanism slightly overestimates the laminar flame speed for fuel-lean conditions, but slightly underestimates for the fuel-rich conditions at elevated initial pressures. The laminar flame speed decreases

with the increase of initial pressure. This is mainly caused by the growing importance of the chain termination reactions in the overall reaction process and the increase of fuel mixture density as the initial pressure is increased.

For the study of the effect of diluents, the Li mechanism slightly underestimates the laminar flame speed of H_2/CO/CH_4/air mixture with N_2/CO_2 dilution at fuel-rich condition. As N_2/CO_2 is added to the fuel mixture, the laminar flame speed decreases obviously with the increase of dilution ratio. Furthermore, the results show that the reductions of laminar flame speeds for CO_2-diluted flames are more substantial than that of the N_2-diluted flames due to the stronger dilution effect, thermal-diffusion effect, and chemical effect of CO_2 dilution than those of N_2 dilution.

CHAPTER 5 LAMINAR FLAME INSTABILITIES OF BIO-SYNGAS/AIR MIXTURES

5.1 Introduction

The intrinsic flame instability of a laminar flame front has been a classic problem in the field of laminar flame dynamics for a long time. During the propagation of an outwardly expanding spherical flame, the flame front can be relatively smooth at the early stage of development. With the increase of the flame radius, some cracks grow and branch until eventually cellular structure appears over the entire flame surface. The onset of cellularity often depends on the initial conditions including the initial pressure, the fuel composition, and the diluent. As stated in section 2.3.2.2, there are three mechanisms generating cellular instabilities, namely buoyancy-driven instability, hydrodynamic instability, and diffusional-thermal instability. Figure 5.1 shows the three typical instabilities observed in the present study. Buoyancy-driven instability usually occurs when the corresponding laminar flame speed is slow (<0.15 m/s). Diffusional-thermal instability is caused by the competition between the thermal diffusion and the mass diffusion. Hydrodynamic instability is caused by the density jump across the flame front. Moreover, the flame stretch rate also plays an important role in flame instability. At the early stage of flame propagation, hydrodynamic instability is suppressed due to the strong effect of flame stretch while diffusional-thermal instability plays a dominant role in the instability of the

flame. With the propagation of the flame and increase of flame radius, the flame stretch rate decreases and its inhibiting effect on flame instability is weakened. The flame morphology is then determined by both hydrodynamic and diffusional-thermal instabilities [260].

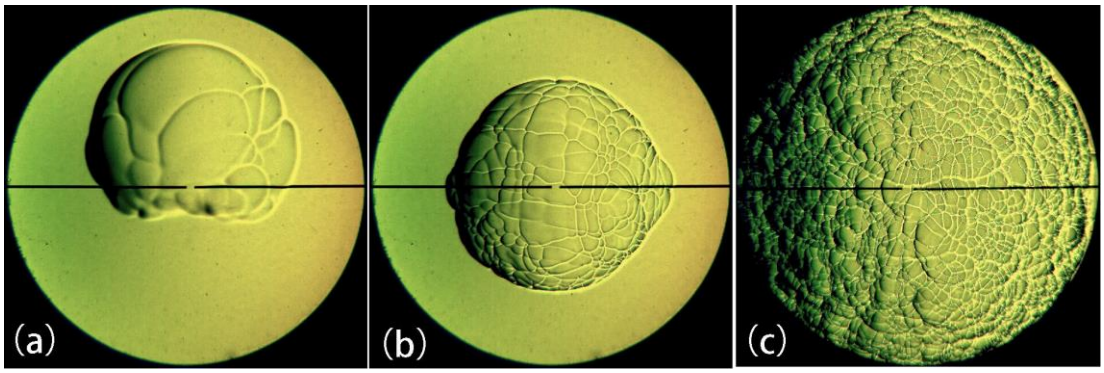

Figure 5.1 (a) Buoyancy-driven instability; (b) Diffusional-thermal instability; (c) Hydrodynamic instability observed in the present study

In this chapter, the flame instability of bio-syngas/air mixtures was quantitatively analyzed by means of experimental measurements and theoretical calculations. The propagation of laminar flame front of bio-syngas/air premixed flame was investigated at various initial pressures. The effects of fuel composition variation and diluents on the intrinsic flame instability of bio-syngas laminar premixed flame were analyzed through the critical Peclet number, the critical flame radius and instability parameters such as effective Lewis number, thermal expansion ratio, and laminar flame thickness.

5.2 Propagation of laminar flame front at atmospheric initial pressure

5.2.1 Effect of fuel composition variation

5.2.1.1 Flame morphology

Figure 5.2-5.4 present the schlieren photographs of various H_2/CO/CH_4 mixtures under fuel-lean (ϕ =0.6), fuel stoichiometric (ϕ =1.0) and fuel-rich (ϕ =1.4) conditions at initial pressure P=0.1 MPa and initial temperature T=303 K. Since the flame propagation speed is greatly influenced by the equivalence ratio, the time slots chosen for the fuel-lean, fuel stoichiometric, and fuel-rich conditions are 1.5-7.5 ms (at an interval of 1.5 ms), 1.5-3.5 ms (at an interval of 0.5 ms) and 1-3 ms (at an interval of 0.5 ms), respectively. The flame instability can be directly observed from the schlieren photographs. The curves and cracks on the flame fronts appearing at the burned zone indicate the instability of the flame front. In general, it can be seen that at the initial pressure P=0.1 MPa, initial temperature T=303 K, usually a single curve is formed on the flame especially in the early stage of flame propagation under each equivalence ratio. There are only a few cracks on the flame normally due to the effect of ignition energy and the influence of the electrodes.

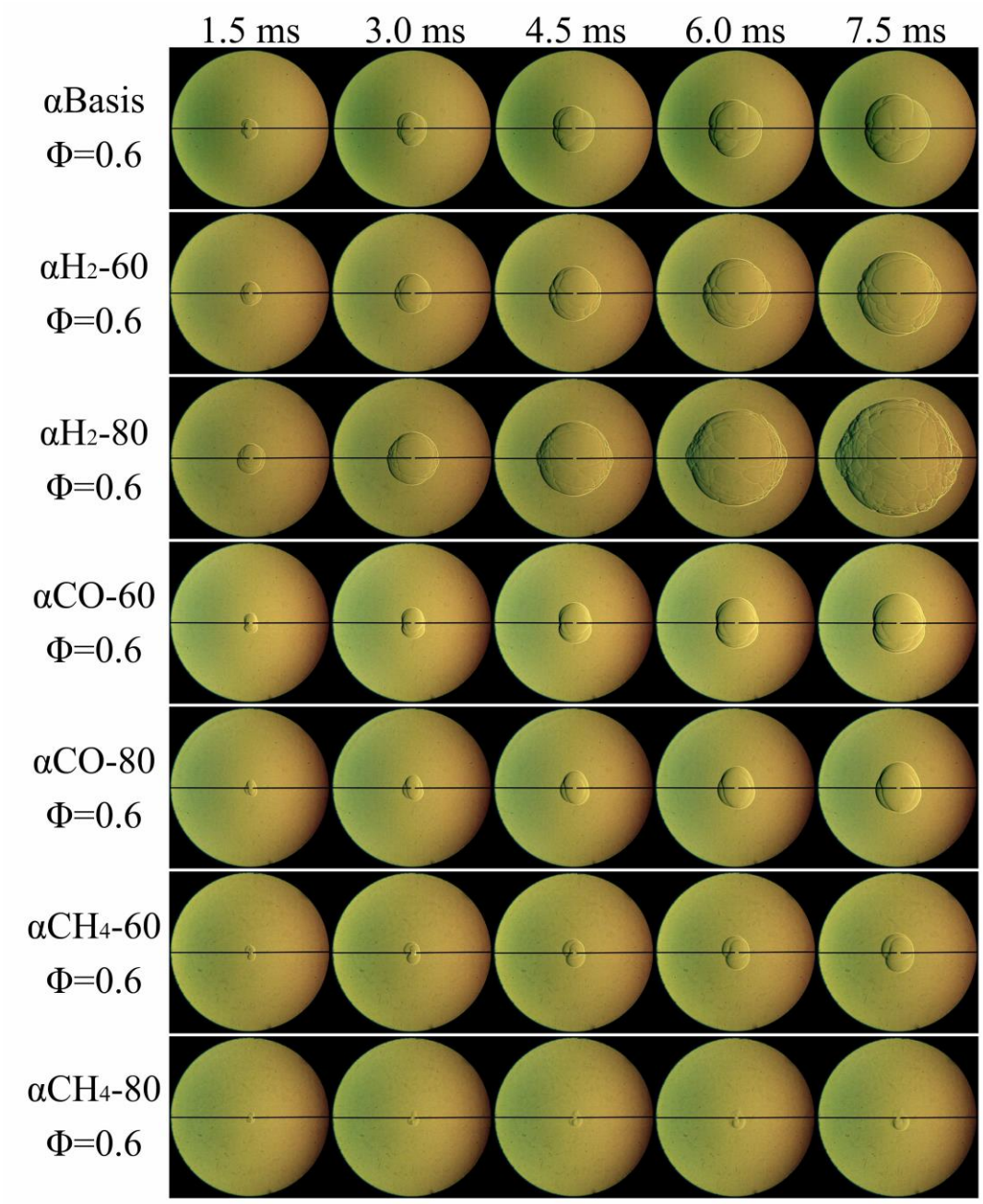

Figure 5.2 Schlieren photograph of various fuel composition of H_2/CO/CH_4/air mixtures under fuel-lean (ϕ=0.6) condition at 0.1 MPa, 303K

For fuel-lean condition, it can be seen from Figure 5.2 that curves and cracks appear at the flame fronts of almost all the fuel compositions. The irregular flame shape also indicates the incomplete combustion of all bio-syngas/air mixtures at ϕ=0.6

condition. Compared with the αBasis condition, fewer wrinkles appear at the flame front for the CO-enriched and CH_4-enriched conditions, while for the H_2-enriched conditions, wrinkle structure appears at the flame front even when the flame radius is still small, which suggests that H_2 addition reduces the flame stability of the bio-syngas/air mixture at atmospheric pressure and fuel-lean condition.

At stoichiometric equivalence ratio, as shown in Figure 5.3, smooth flame fronts appear in different fuel compositions. It seems that the increase of equivalence ratio can slightly weaken the instability of the flame front. However, compared with other conditions, there are still more wrinkles at the flame front for the H_2-enriched conditions. This is consistent with the results of Hu et al. [112] which indicated that with the increase of H_2 fraction in the fuel mixture, the flame behavior tends to be similar to that of pure H_2 flame, which is diffusional-thermally unstable.

When the fuel mixture becomes richer (ϕ=1.4), it is seen from Figure 5.4 that there are fewer curves and cracks at the flame front, indicating that the flame tends to be stable with the increase of equivalence ratio at atmospheric pressure. Moreover, it is noted that as more CH_4 is added to the fuel mixture, the flame propagation speed decreases significantly, leading to a slight upward floating of the flame at αCH_4-60 condition due to the low laminar flame speed of the CH_4-enriched flame. And also, we can notice that due to the significant decrease of reactivity of the overall reaction process with CH_4 addition, the αCH_4-80 fuel mixture cannot be ignited at fuel rich

condition.

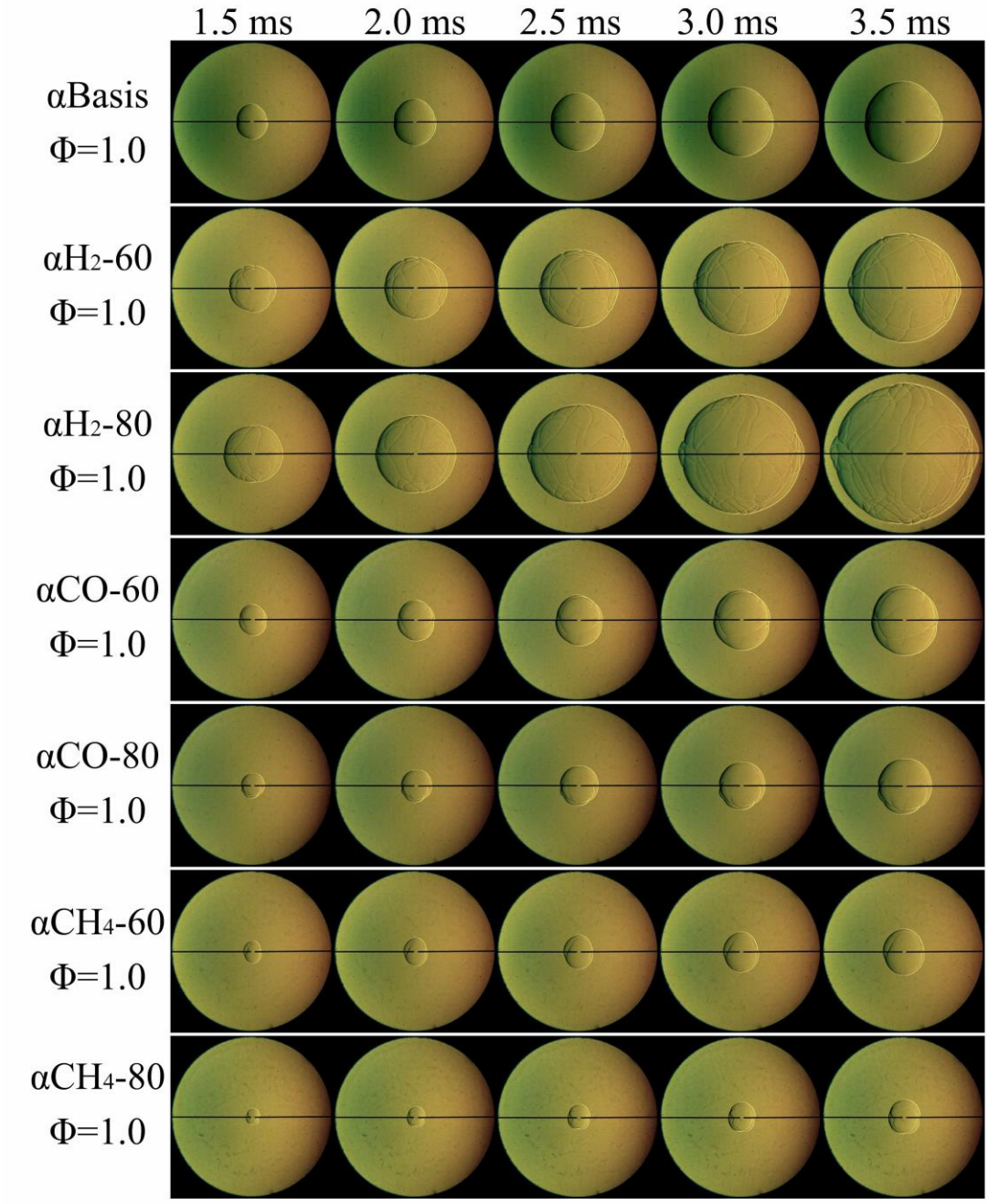

Figure 5.3 Schlieren photograph of various fuel composition of H_2/CO/CH_4/air under fuel stoichiometric (ϕ=1.0) condition at 0.1 MPa, 303K

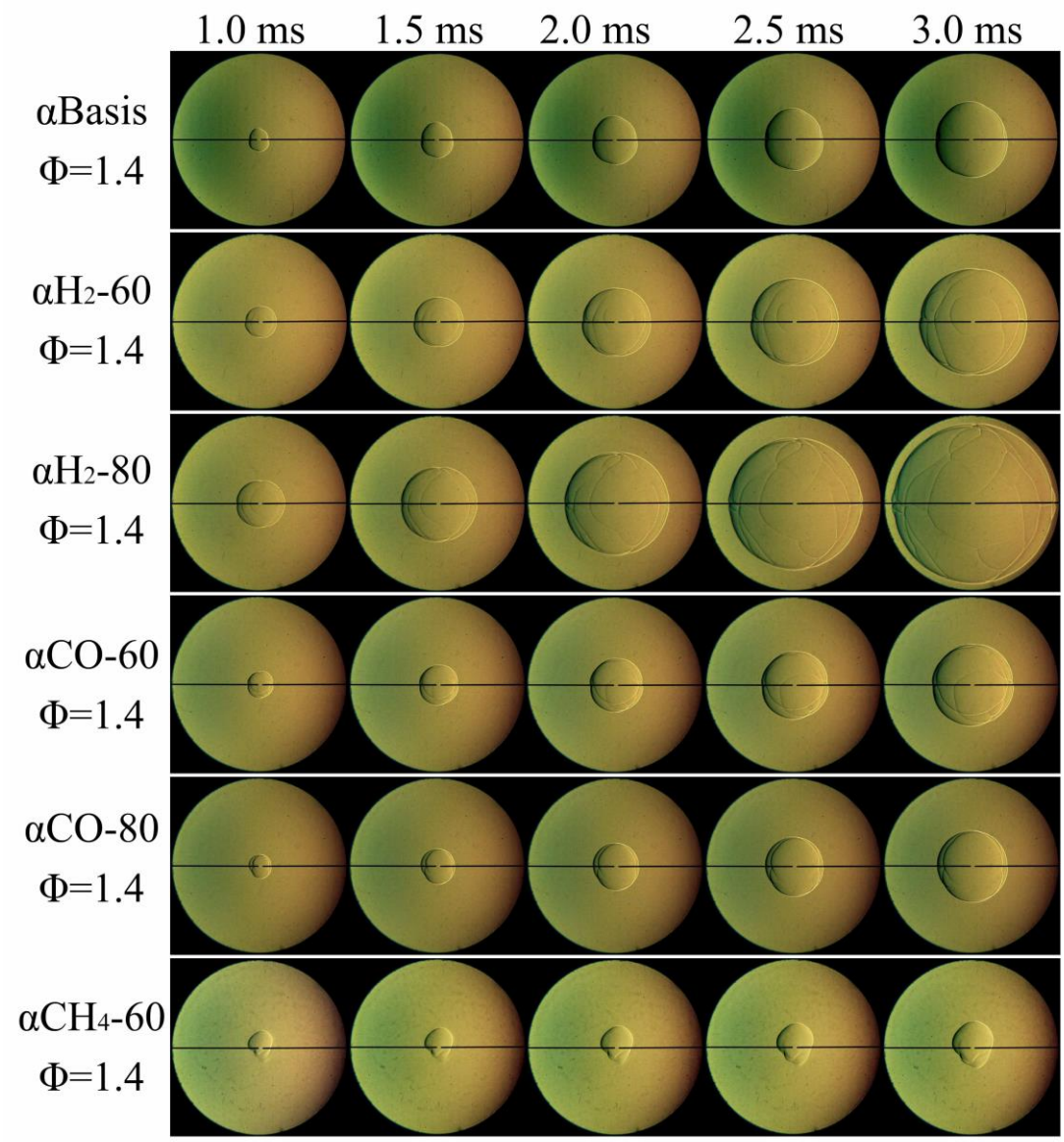

Figure 5.4 Schlieren photograph of various fuel composition of H_2/CO/CH_4/air mixture under fuel rich (ϕ=1.4) condition at 0.1 MPa, 303K

5.2.1.2 Markstein length

As stated in section 3.5.1, the negative value of the slope of the best straight-line fit between the stretched flame speed and the flame stretch rate is defined as the burned gas Markstein length, L_b, which indicates the relationship between the flame speed

and the flame stretch rate. According to previous studies [105, 210], for the case of a negative value of L_b, the flame speed increases with the increase of the flame stretch rate. Therefore, in this case, any disturbance occurring at the flame front can increase the flame speed, leading to the enhancement of instability [139]. On the contrary, if L_b >0, the flame speed decreases with the increase of the flame stretch rate, contributing to the flame stabilization. Figure 5.5 gives the measured Markstein length L_b versus equivalence ratio at different fuel compositions. It is seen that the Markstein length increases with the increase of equivalence ratio under each fuel composition, which suggests that the increase of equivalence ratio contributes to the flame stabilization. However, it is noted that this increase behavior is weakened at a high equivalence ratio condition, and the curve of L_b- ϕ tends to be flat in the rich mixture region. With the increase of H_2 fraction in the fuel mixture, the Markstein length decreases compared to the other conditions. This indicates that the increase of H_2 concentration in the fuel mixture will decrease the stability of the flame front. According to Manton et al. [271] and Markstein [272], the laminar premixed flame tend to be unstable due to the effects of preferential diffusion under the conditions where the fast-diffusing component, such as H_2 in the present study, is deficient, which corresponds to the fuel-lean condition in our study. On the other hand, it is seen that the increase of CH_4 and CO fraction in the fuel mixture slightly increases the Markstein length, and the increases of the CH_4-enriched flames are more substantial than that of the CO-enriched flames, suggesting that the flame front

stability is slightly enhanced with CH_4 addition.

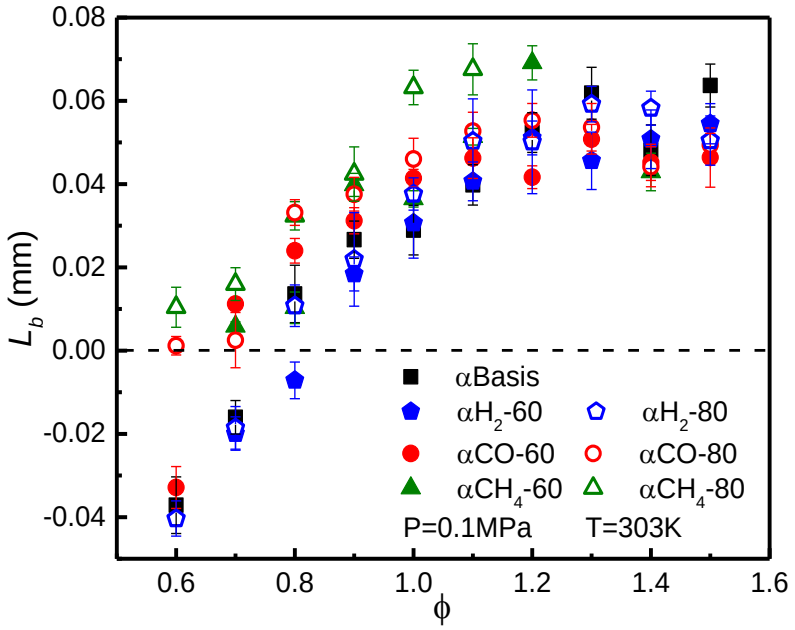

Figure 5.5 Markstein length L_b at different fuel compositions for H_2/CO/CH_4/air mixture

5.2.2 Effect of different diluents (N_2/CO_2)

5.2.2.1 Flame morphology

Figure 5.6-5.8 show the schlieren photographs of N_2/CO_2 diluted H_2/CO/CH_4/air mixtures under fuel-lean (ϕ=0.8), fuel-stoichiometric (ϕ=1.0), and fuel-rich (ϕ=1.2) conditions at 0.1 MPa, 303K. The time slots chosen for the fuel-lean, fuel-stoichiometric, and fuel-rich conditions are 1.5-7.5 ms (at an interval of 1.5 ms), 1.5-5.5 ms (at an interval of 1.0 ms) and 1.5-5.5 ms (at an interval of 1.0 ms), respectively.

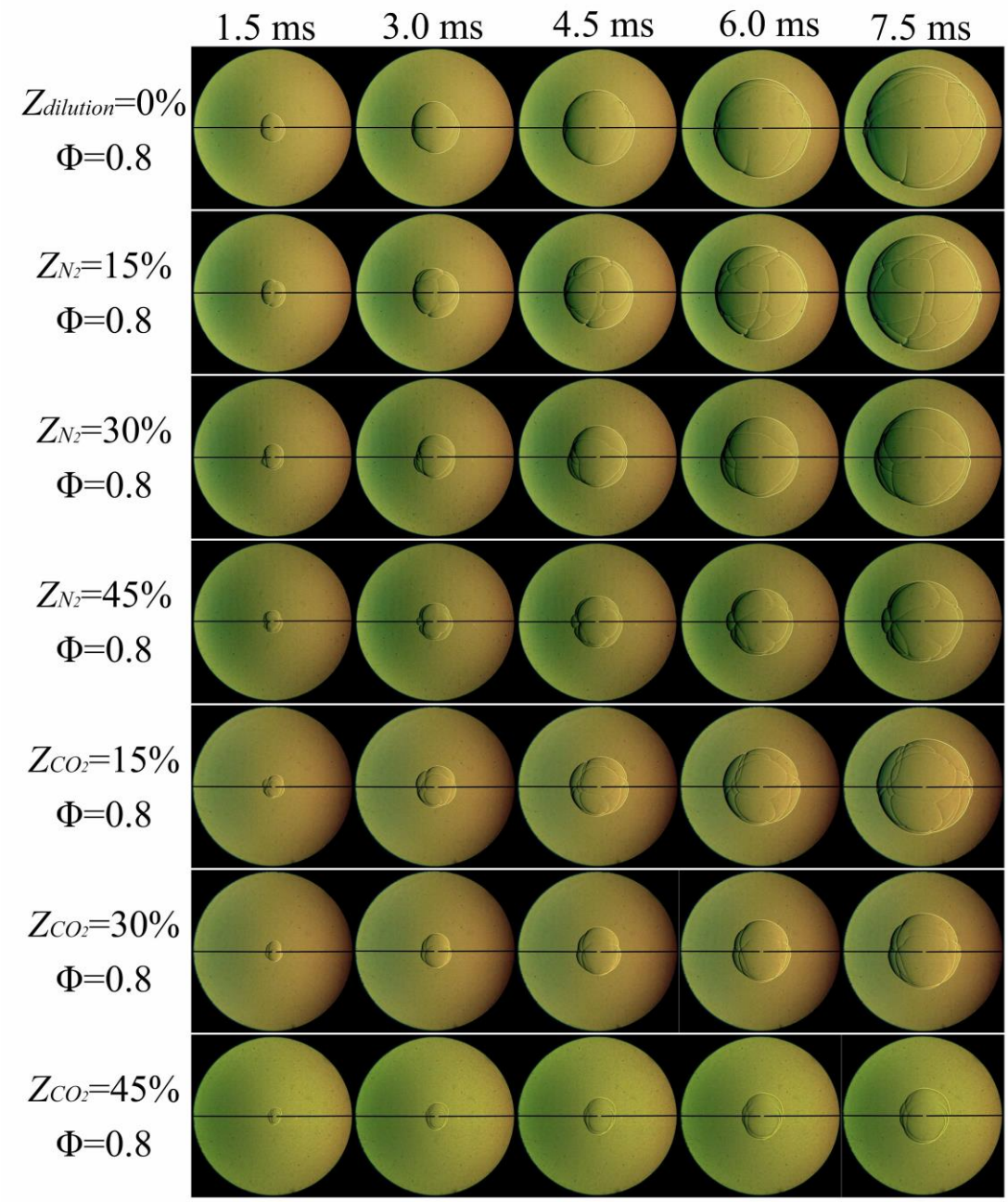

Figure 5.6 Schlieren photograph of N_2/CO_2 diluted $H_2/CO/CH_4$/air mixtures under fuel-lean (ϕ=0.8) condition at 0.1 MPa, 303K

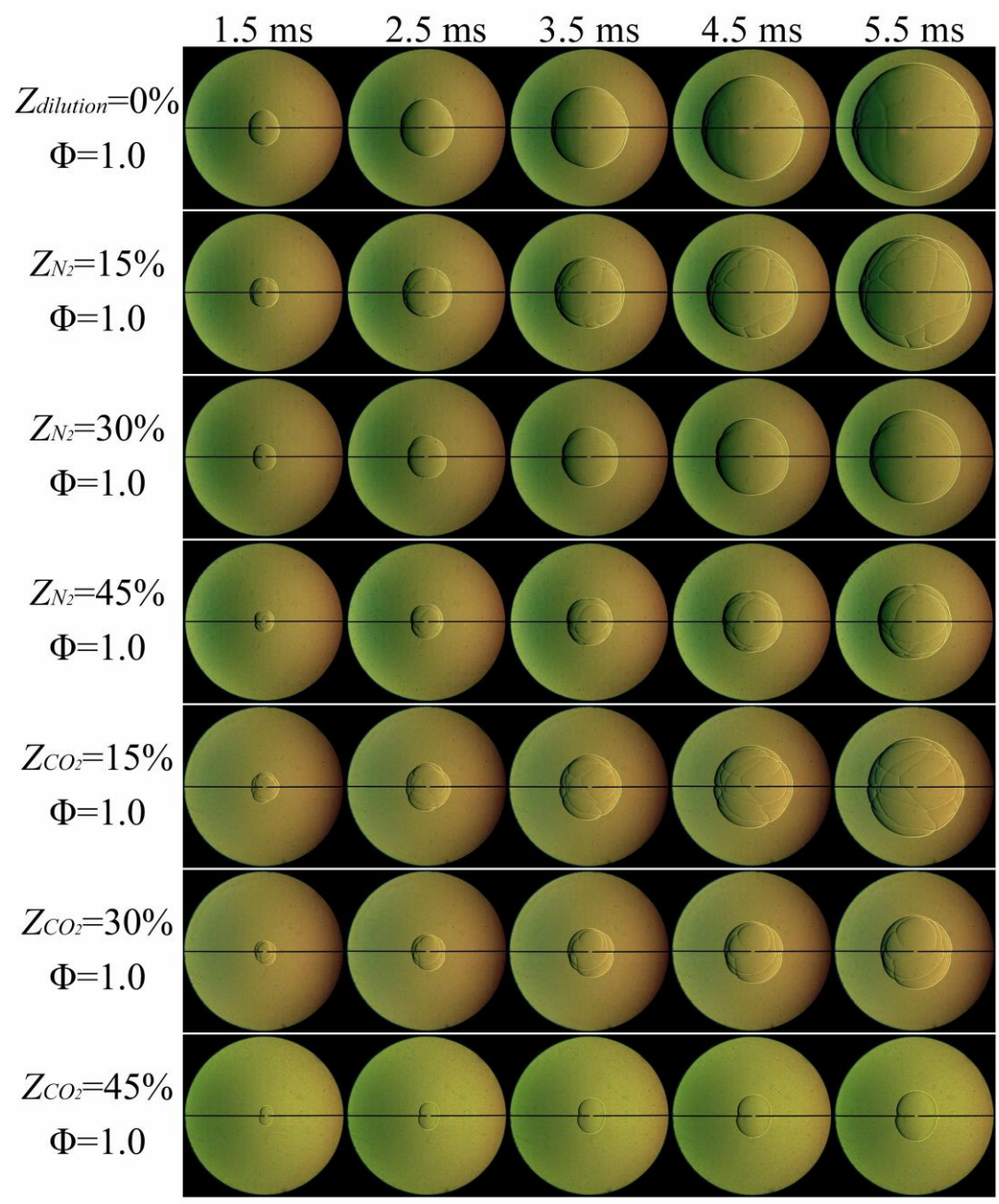

Figure 5.7 Schlieren photograph of N_2/CO_2 diluted $H_2/CO/CH_4$/air mixtures under fuel-stoichiometric (ϕ=1.0) condition at 0.1 MPa, 303K

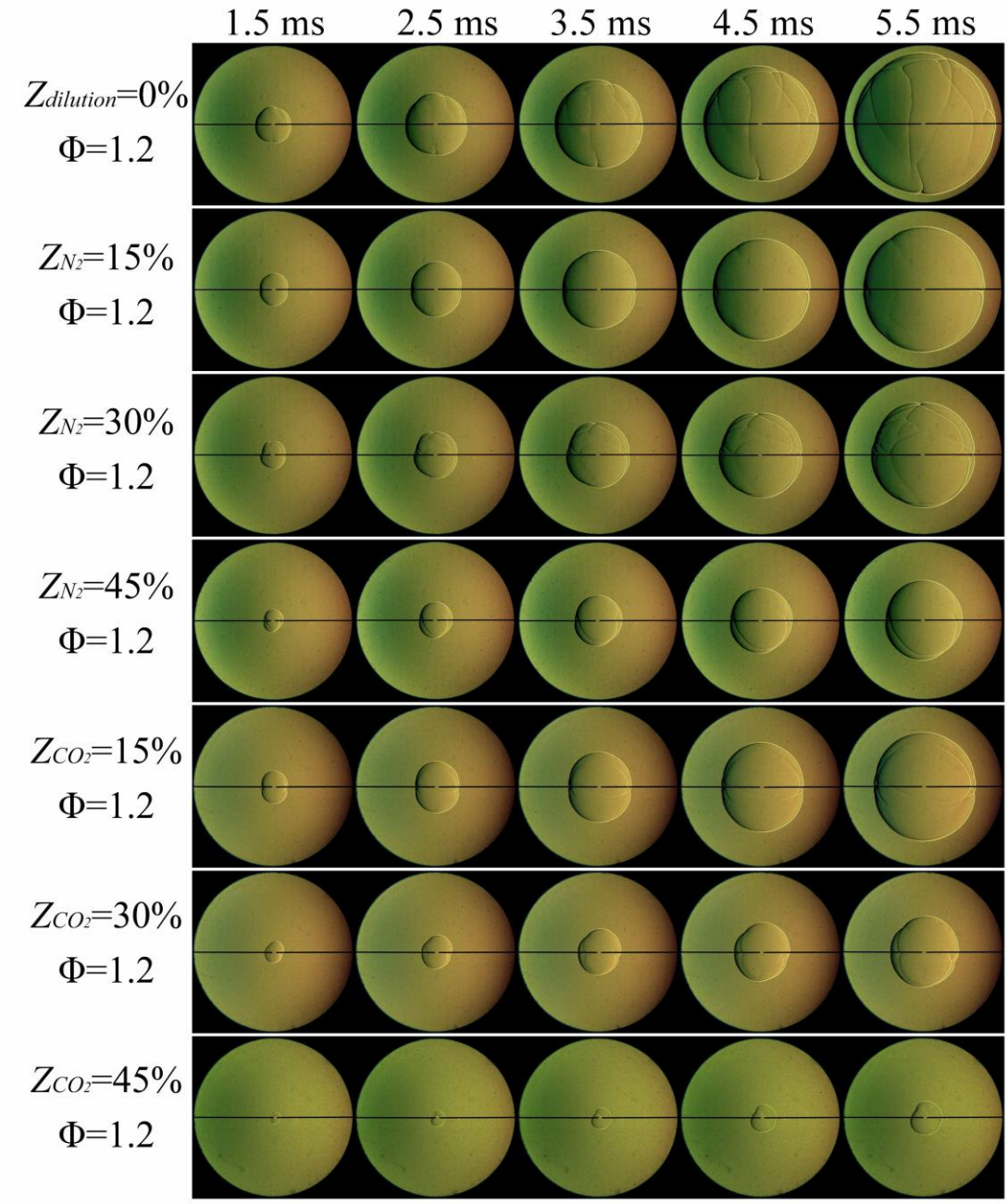

Figure 5.8 Schlieren photograph of N_2/CO_2 diluted $H_2/CO/CH_4$/air mixtures under fuel-rich (ϕ=1.2) condition at 0.1 MPa, 303K

It is obvious that with N_2/CO_2 addition, the flame propagation speed decreases significantly, and the propagation speed of the CO_2-diluted bio-syngas/air flame is lower than that of the N_2-diluted bio-syngas/air flame at all dilution ratios due to the

higher specific heat capacity and radiation of CO_2 than that of N_2. As shown in the figures, the flame front of diluted bio-syngas/air flame appears as smooth surface at atmospheric pressure under each operating condition, although some large cracks are observed due to ignition disturbance. It is difficult to tell which flame is more stable by referring to the number of curves/cracks. Therefore, the measured data of Markstein length are still required for analyzing the flame stability at atmospheric pressure.

5.2.2.2 Markstein length

Figure 5.9 gives the Markstein lengths of N_2/CO_2 diluted $H_2/CO/CH_4$/air premixed flames at the initial pressure of 0.1 MPa for various equivalence ratios and dilution ratios. As stated earlier, Markstein length represents the sensitivity of flame propagation to the stretch rate and also reflects the variation of flame instability. A larger Markstein length indicates that the flame front is less likely to form wrinkled flame front. It can be seen that the Markstein length increases with the increase of equivalence ratio for all the diluted flames. At fuel-lean condition, the Markstein length is even negative, which means that the flame front is more susceptible to the stretch rate effects [146]. It is seen from Figure 5.9(b) that with the N_2/CO_2 dilution, the Markstein length decreases at all dilution ratios. This indicates that the dilution makes the flame front more sensitive to the stretch rate effects and promotes the flame instability at atmospheric pressure. This observation is consistent with the

results presented by Vu et al. [168]. They reported that the addition of N_2/CO_2 causes the Markstein length to decrease, and normally the Markstein lengths of CO_2 diluted flames are lower than that of the N_2 diluted flames at the initial pressure of 0.1 MPa. Prathap et al. [147] also indicated that a fuel mixture with CO_2 dilution is more affected by preferential diffusion instabilities than that with N_2 dilution.

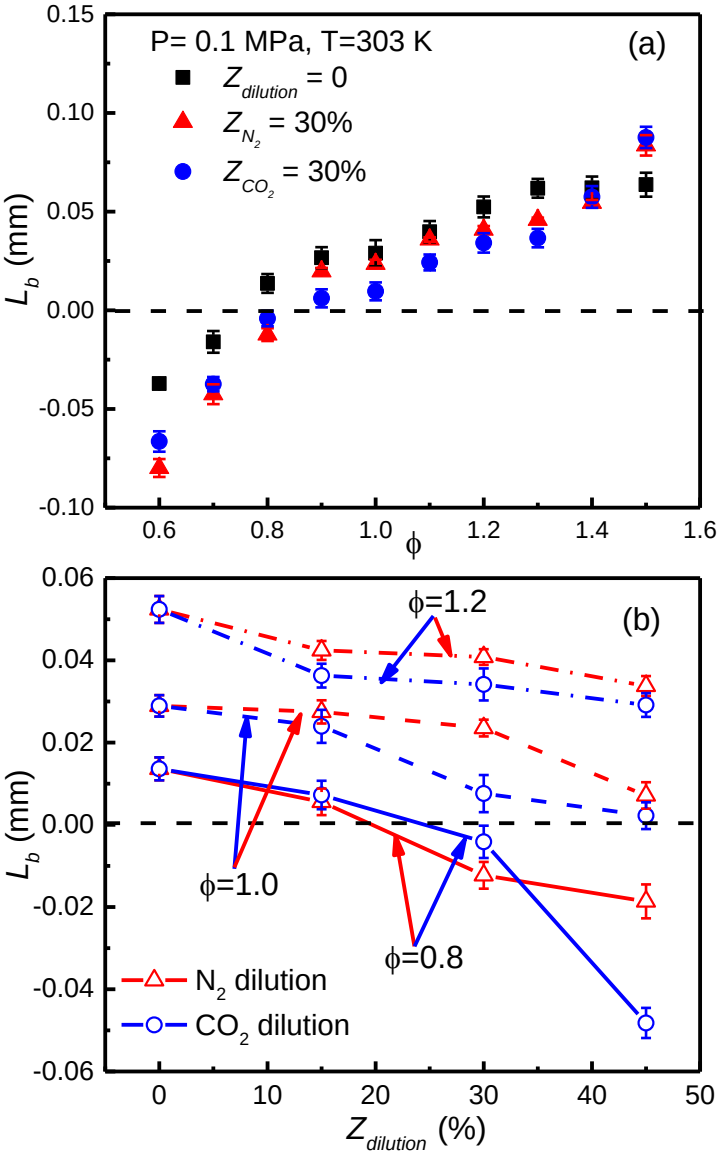

Figure 5.9 Markstein length at different dilution ratios for N_2/CO_2 diluted $H_2/CO/CH_4$/air mixtures

5.3 Effect of fuel composition variation on cellular instabilities at elevated initial pressures

5.3.1 Flame morphology

Figure 5.10 presents the schlieren photographs of H_2/CO/CH_4/air flames at different initial pressures under ϕ=0.8, T=303 K, αBasis condition. The effective Lewis number (Le_{eff}), the laminar flame thickness (l_f), and the thermal expansion ratio (σ) are provided along with the photographs. It can be seen that the flame front remains fairly smooth at atmospheric pressure except for some large wrinkles caused by ignition disturbance. With the increase of initial pressure, irregular wrinkles appeared at the flame surface. Moreover, the higher the initial pressure, the more advance the onset of cellular instability of the flame is observed. It is noted that the effective Lewis number does not change with the variation of initial pressure, indicating that the diffusional-thermal instability does not change with the increase of initial pressure. On the other hand, when the initial pressure is increased, the thermal expansion ratio slightly increases while the flame thickness decreases significantly. Therefore, the wrinkles formed at the flame surface as the initial pressure is increased must be dominated by the hydrodynamic instability.

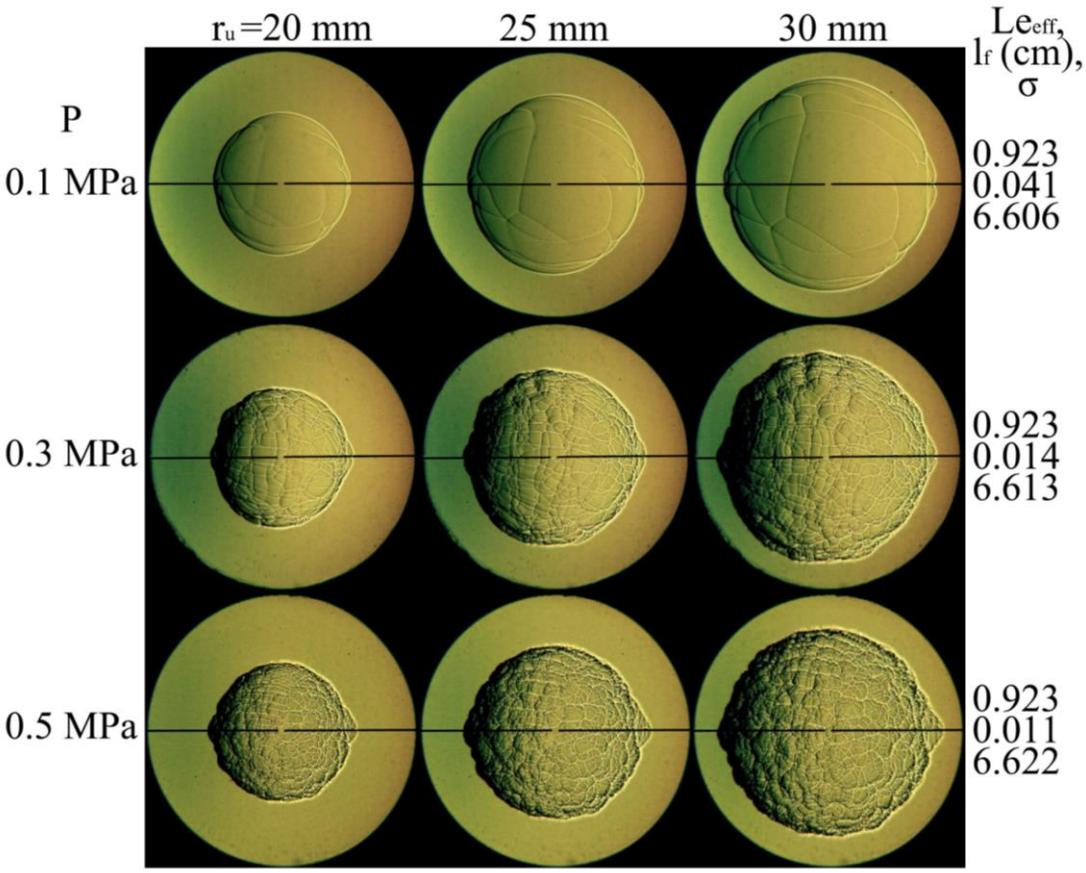

Figure 5.10 Schlieren photographs of H_2/CO/CH_4/air flames at different initial pressures (ϕ=0.8, T=303 K, αBasis)

Figure 5.11 shows the schlieren photographs of H_2/CO/CH_4/air flames at different fuel compositions under ϕ=0.8, T=303 K, P=0.3 MPa condition. As shown in the figure, the variation of composition of H_2/CO/CH_4/air mixture can have a strong influence on the cellular instabilities of the flame front at elevated initial pressure.

With the increase of H_2 fraction in the fuel mixture, it is seen that the cellular instabilities of the flame front are stronger and onset of the cellular flame structure occurs earlier at the αH_2-60 condition compared to that of the αBasis condition. The

effective Lewis number is decreased with H_2 addition as shown in the data on the right side of the figure, suggesting that the increase of H_2 fraction in the fuel mixture increases the diffusional-thermal instability. This is consistent with the result of Hu et al. [114], in which the flame becomes diffusional-thermally unstable at large hydrogen fraction. In addition, it is seen that both the laminar flame thickness and the thermal expansion ratio decrease with the increase of hydrogen concentration. According to a previous research [159], the laminar flame thickness plays a more significant role in affecting the hydrodynamic instability of the flame front than that of the thermal expansion ratio for a near-equidiffusive H_2/CO/CH_4 flame (Le~1) at elevated initial pressure. Therefore, the earlier onset of the cellular instability of the H_2-enriched flame is caused by the dominant role of enhanced diffusional-thermal instability due to the decrease of effective Lewis number and the less dominant role of hydrodynamic instability due to the decrease of laminar flame thickness [114, 273].

On the other hand, it is seen that with the increase of CO fraction in the fuel mixture, both the effective Lewis number and the laminar flame thickness are slightly increased and the thermal expansion ratio is slightly decreased, and consequently both the diffusional-thermal instability and hydrodynamic instability are inhibited with increasing CO concentration in the fuel mixture.

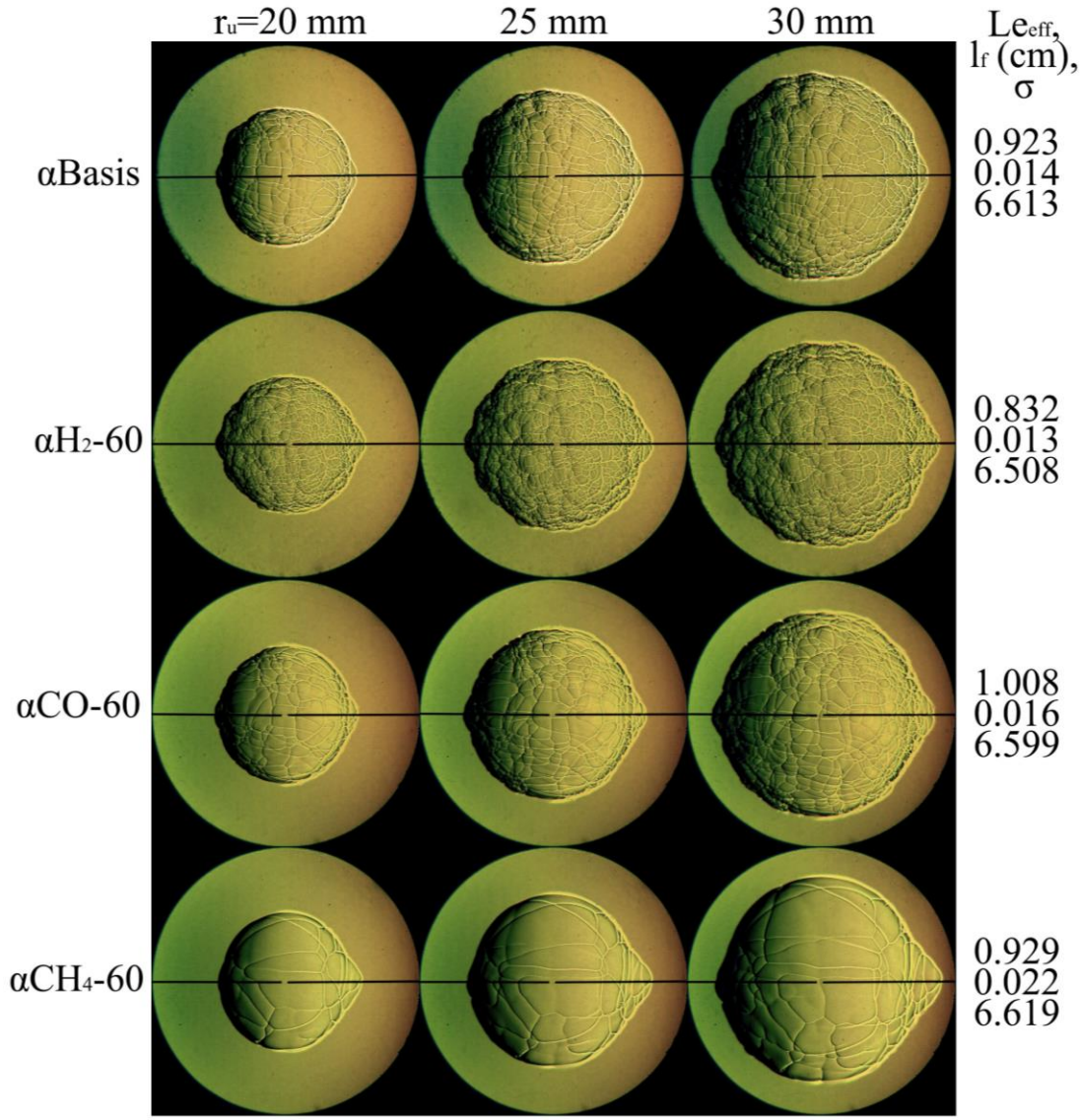

Figure 5.11 Schlieren photographs of H_2/CO/CH_4/air flames at different fuel compositions (ϕ=0.8, T=303 K, P=0.3 MPa)

Finally, a comparison of the schlieren photographs of the αCH_4-60 flame with the αBasis flame shows that the cellular instabilities of the flame front are significantly suppressed with increasing CH_4 concentration in the fuel mixture. In fact, the effective Lewis number is slightly increased with CH_4 addition, indicating that the diffusional-thermal instability can be suppressed. Concerning the hydrodynamic

instability, it is noted that the thermal expansion ratio varies little at different CH_4 fractions while the laminar flame thickness is increased with the increase of CH_4 concentration in the fuel mixture. Therefore, CH_4 addition to the bio-syngas/air mixture can suppress both the diffusional-thermal instability through the slight increase of the effective Lewis number and the hydrodynamic instability through the increase of the flame thickness.

5.3.2 Instability parameters

5.3.2.1 Effective Lewis number

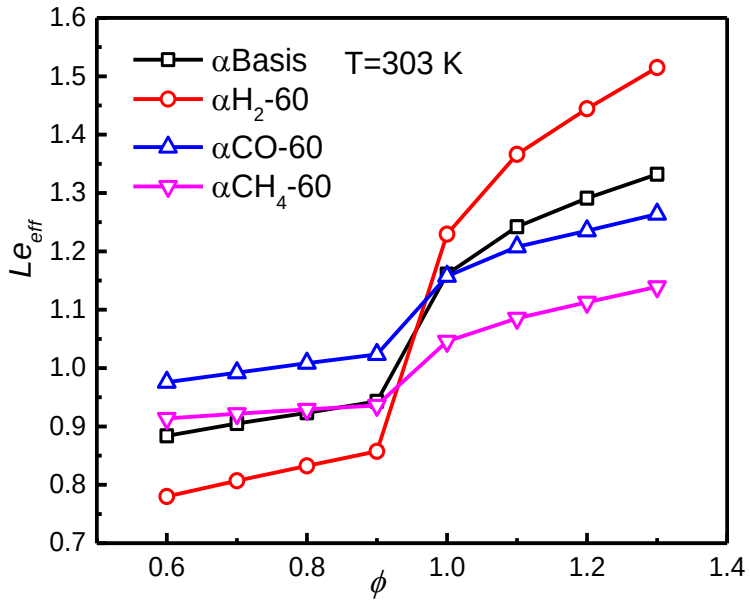

Figure 5.12 Effective Lewis numbers of H_2/CO/CH_4/air mixtures versus equivalence ratio at different fuel compositions

Figure 5.12 gives the effective Lewis numbers (Le_{eff}) of H_2/CO/CH_4/air mixtures versus equivalence ratio at different fuel compositions. As mentioned in section

3.5.2, the calculation of effective Lewis number in the present study takes both the fuel and oxidizer into account. Therefore, it is seen that the trends of Le_{eff} for different fuel compositions at the fuel-lean condition and fuel-rich condition are quite different but it always increases with the increase of equivalence ratio. This suggests that the diffusional-thermal instability can be inhibited with the increase of equivalence ratio at various fuel compositions of bio-syngas/air mixtures.

For fuel-lean condition, the three fuel components H_2/CO/CH_4 are deficient reactants in the mixture. By using the volume-based mixing rule, as mentioned in section 3.5.2, Equation (3-12), we can found that most of the effective Lewis numbers for all the reported fuel compositions are smaller than 1 and thus these flames are unconditionally diffusional-thermally unstable at fuel-lean condition. Moreover, compared to the αBasis condition, Le_{eff} decreases with the increase of H_2 fraction in the fuel mixture but increases with the increase of CH_4 or CO fraction in the fuel mixture, indicating that the diffusional-thermal instability is promoted with H_2 addition and suppressed with CH_4 or CO addition. For fuel-rich condition, since O_2 is a single deficient reactant in the mixture now, it is noted that all the effective Lewis numbers for all the reported fuel compositions are larger than 1, leading to the suppression of diffusional-thermal instability.

5.3.2.2 Thermal expansion ratio and laminar flame thickness

Figure 5.13 and Figure 5.14 give the thermal expansion ratios (σ) and laminar flame

thicknesses (l_f) of H_2/CO/CH_4/air flames versus equivalence ratio at different fuel compositions and the elevated initial pressure P=0.3 MPa. According to the hydrodynamic theory of Darrieus [154] and Landau [155], the flame is absolutely unstable to disturbance of all wavelengths. Since the growth rate is proportional to the density jump across the flame, namely thermal expansion ratio, the hydrodynamic instability is increased with increasing σ [225]. Next to the thermal expansion ratio, the laminar flame thickness is also expected to have a strong influence on the hydrodynamic instability, in which the thinner the flame, the stronger is the hydrodynamic instability. It is seen from Figure 5.13 that the thermal expansion ratio first increases with the increase of equivalence ratio and always reaches its peak value at around ϕ=1.0 regardless of the variation of fuel composition, after that it decreases with increasing equivalence ratio. On the other hand, as shown in Figure 5.14, the laminar flame thickness decreases with the increase of equivalence ratio and its decrement tends to be small gradually and even starts to increase for more rich mixture for the αCH_4-60 flame.

With the increase of H_2 fraction in the fuel mixture, it is noted that both the thermal expansion ratio and the flame thickness are decreased for all the tested equivalence ratios. As shown in Figure 5.11, it is obvious that increasing H_2 concentration in the fuel mixture can significantly promote cellular instability at elevated initial pressures. Although the thermal expansion ratio is decreased with H_2 addition, this suppressing effect on hydrodynamic instability is far lower than the promoting effect of

diffusional-thermal instability due to the decrease of effective Lewis number and hydrodynamic instability due to the decrease of flame thickness [274]. Moreover, with the increase of CO fraction in the fuel mixture, the thermal expansion ratio is slightly decreased and the flame thickness is slightly increased compared to that of the αBasis condition at all equivalence ratios. This indicates that adding CO to the fuel mixture can inhibit the hydrodynamic instability at elevated initial pressure. With the increase of CH_4 fraction in the fuel mixture, it is seen that the thermal expansion ratio is slightly increased which promotes the hydrodynamic instability, while the flame thickness is also significantly increased which strongly inhibits the hydrodynamic instability, with a net result of suppression of hydrodynamic instability at all reported equivalence ratios.

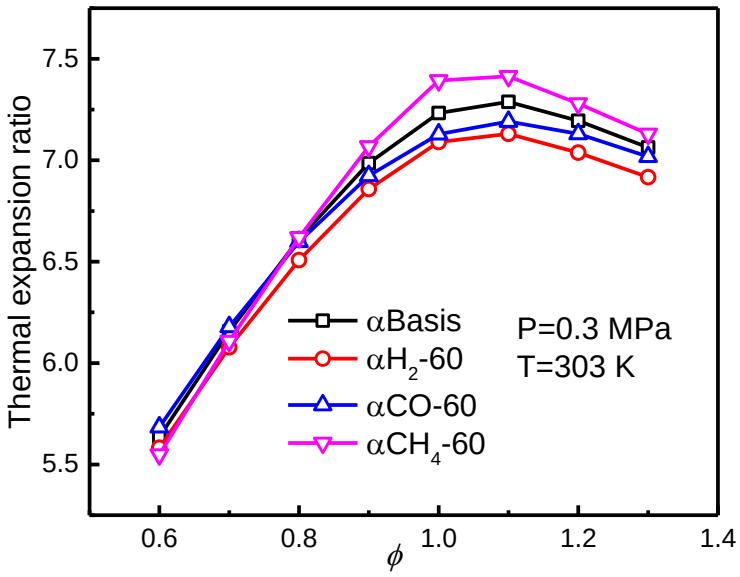

Figure 5.13 Thermal expansion ratios of H_2/CO/CH_4/air flames versus equivalence ratio at different fuel compositions

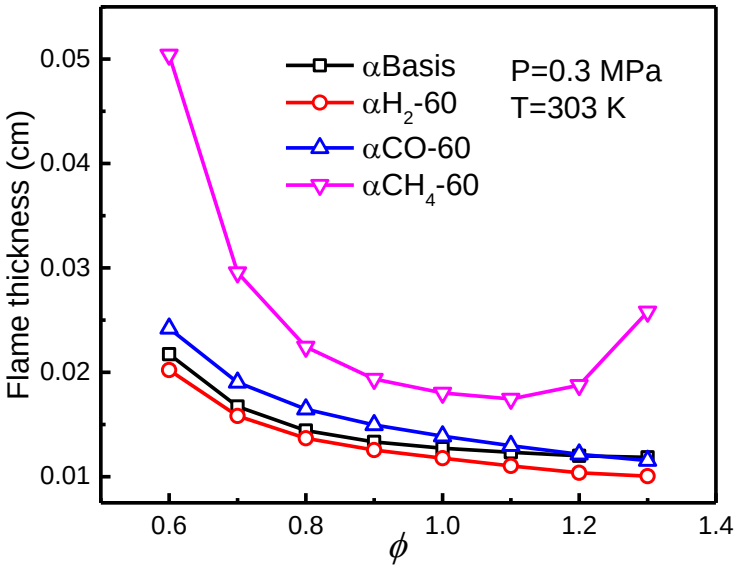

Figure 5.14 Laminar flame thicknesses of H_2/CO/CH_4/air flames versus equivalence ratio at different fuel compositions

5.3.3 Critical flame radius and Peclet number

As mentioned in section 3.5.2, critical flame radius R_{cr} and critical Peclet number Pe_{cr} are two important parameters to illustrate the onset of cellular instability, when the cellular structures can no longer be suppressed and cover the entire flame front surface. In the early stage of flame front evolution, the flame stretch rate is large enough to maintain the flame front to be stable. As the spherical flame front propagates outward, the flame stretch rate is decreased and large cracks appearing on the flame surface starts to branch gradually. Once beyond a certain flame radius, a coherent cellular structure appears on the whole flame surface spontaneously and uniformly. This experimental critical flame radius R_{cr}-*Exp* can be obtained from the schlieren photographs when cellular structures appeared uniformly over the flame front surface. Then, the experimental critical Peclet number, Pe_{cr}-*Exp*, can be

calculated through: $Pe_{cr}=R_{cr}/l_f$. On the other hand, as previously mentioned, Addabbo et al. [228] and Law et al. [170] proposed a theoretical model to predict the onset of cellular instability. The detailed expression of the critical Peclet number Pe_{cr} is shown in Equation (3-15) as: $Pe_{cr}=\omega^{-1}\{Q_1+\beta(Le_{eff}-1)Q_2/(\sigma-1)+PrQ_3\}$. Then, the corresponding theoretical critical flame radius can be obtained by: $R_{cr}=Pe_{cr}*l_f$.

Figure 5.15 and Figure 5.16 show the experimental and predicted critical flame radius and critical Peclet number of H_2/CO/CH_4/air flames versus equivalence ratio at different fuel compositions, respectively. It is seen that the theoretical results can predict the general trends of the experimental data, but not the absolute values, that is, there are some discrepancies between the experimental data and the predicted results using the theoretical model. There are two reasons for the discrepancies between the experimental and theoretical calculated results of critical flame radius and Peclet number. First, there should be inaccuracies when we obtained the experimental results directly from the flame images. Second, the theoretical model developed for predicting the onset of cellular instability is actually not fully developed and completed at the present state. Both of them contribute to the differences between the experimental and theoretical calculated results. As shown in Figure 5.15 and Figure 5.16, compared to the αBasis condition, both the experimental determined critical flame radius R_{cr}-*Exp* and the critical Peclet number Pe_{cr}-*Exp* decrease with the increase of H_2 fraction in the fuel mixture and increases

with the increase of CO fraction in the fuel mixture at all the reported equivalence ratios. This indicates that the moment at which the cellular structures distributing uniformly over the entire flame surface is advanced and the intrinsic flame instability is promoted with increasing H_2 concentration in the fuel mixture, while the moment is postponed and the intrinsic flame instability is suppressed with increasing CO concentration in the fuel mixture. Moreover, recall that with the increase of CH_4 fraction in the fuel mixture, the diffusional-thermal instability is slightly suppressed by a small increase of the effective Lewis number and the hydrodynamic instability is significantly suppressed by a significant increase of the laminar flame thickness. Therefore, the moment for the onset of cellular structure is also significantly delayed with CH_4 addition. Limited by the size of the combustion bomb chamber used in the present study, the experimental critical flame radius and critical Peclet number of the CH_4-enriched condition could not be obtained. However, as presented in Figure 5.15, the theoretical results show that the αCH_4-60 flame has the largest critical flame radius compared to the other flames, suggesting a strong inhibiting effect on the cellular instability of the flame front with CH_4 addition. Meanwhile, it can be noted that the equivalence ratio has different effects on the critical flame radius and critical Peclet number for various fuel compositions. It is obvious that the critical Peclet number increases with the increase of equivalence ratio for all the reported fuel compositions. However, the critical flame radius has little variation with the increase of equivalence ratio for the αBasis and

αH_2-60 conditions, while it decreases slightly with the increase of equivalence ratio for the αCO-60 and αCH_4-60 flames. This could be explained by the variation of laminar flame thickness with equivalence ratio. It is seen from Figure 5.14 that with the increase of equivalence ratio, the flame thickness decreases more significantly for the αCO-60 and αCH_4-60 conditions, implying that hydrodynamic instability has been promoted with increasing equivalence ratio for these two conditions. Combined the promoting effect of increasing equivalence ratio on the hydrodynamic instability and inhibiting effect on diffusional-thermal instability, the critical flame radius slightly decreases with the increase of equivalence ratio for the αCO-60 and αCH_4-60 conditions.

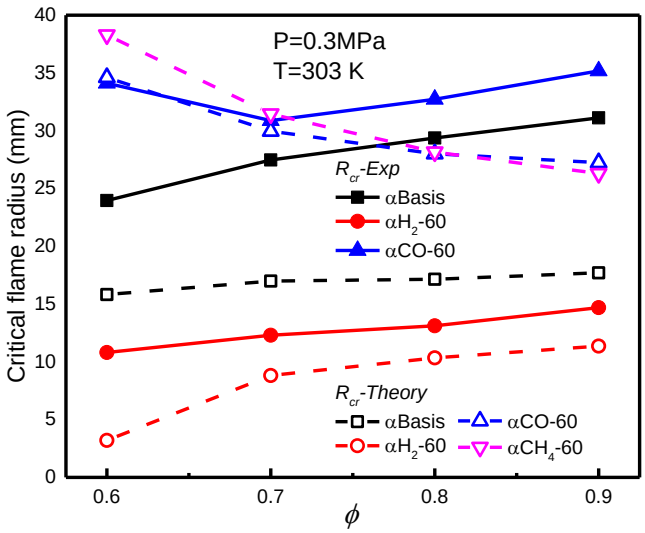

Figure 5.15 Critical flame radius of H_2/CO/CH_4/air flames versus equivalence ratio at different fuel compositions

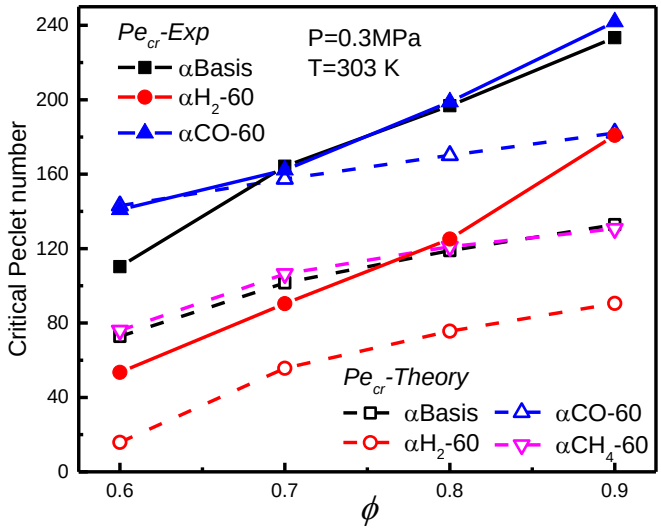

Figure 5.16 Critical Peclet number of H_2/CO/CH_4/air flames versus equivalence ratio at different fuel compositions

5.4 Effect of diluents (N_2/CO_2) on cellular instabilities at elevated initial pressures

5.4.1 Flame morphology

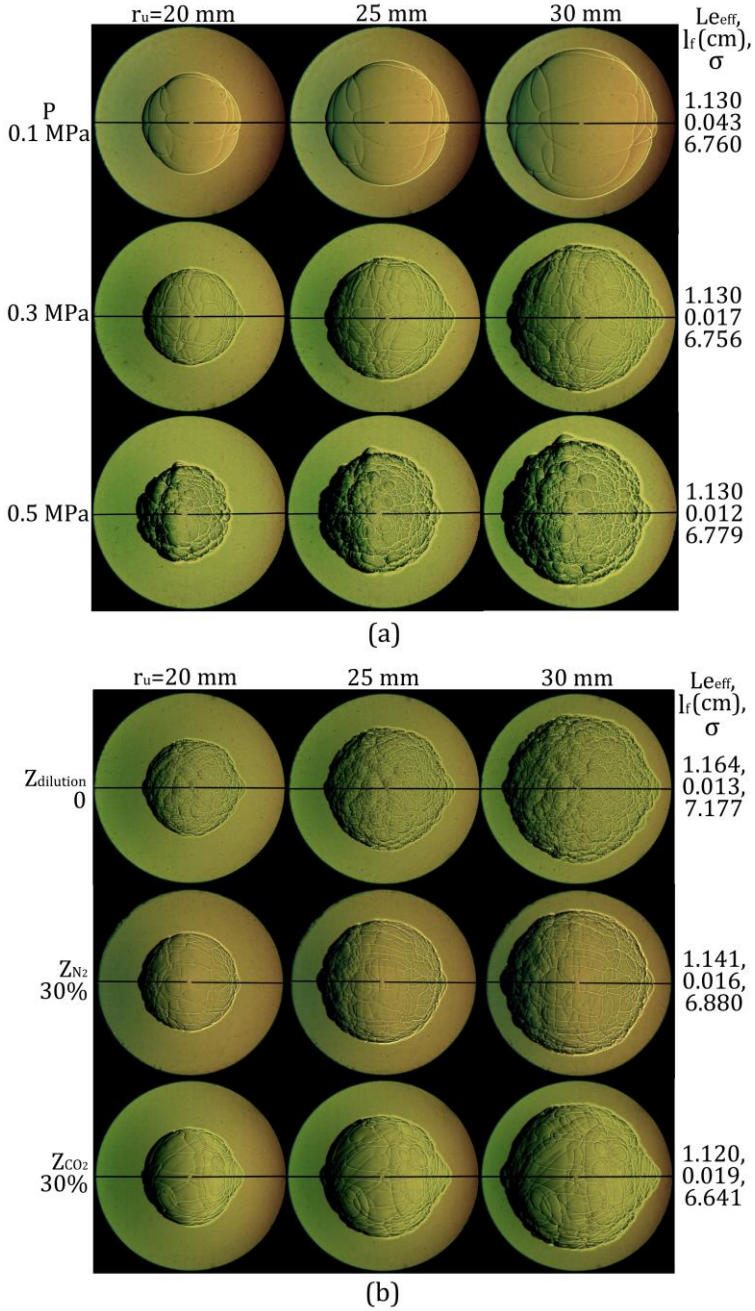

Figure 5.17 Schlieren photographs of stoichiometric N_2/ CO_2 diluted $H_2/CO/CH_4$/air mixture at T=303 K: (a) Pressure effect ($Z_{N2\text{-}CO2}$=30%, N_2:CO_2=1:1); (b) Dilution effect (P=0.3 MPa)

Figure 5.17 shows the schlieren photographs of stoichiometric N_2/CO_2 diluted $H_2/CO/CH_4$/air flames at different initial pressures and dilution ratios. The effective Lewis number (Le_{eff}), the flame thickness (l_f), and the thermal expansion ratio (σ) are also provided along with each photograph. It can be seen from Figure 5.17(a) that for N_2/CO_2 diluted $H_2/CO/CH_4$/air flames, the flame front also remains smooth at the initial pressure of 0.1 MPa. With the increase of initial pressure, the onset of cellular instability of the flame occurs at earlier position, which is similar to the non-diluted flames. The effect of diluents on the instability of flames at elevated initial pressures is shown in Figure 5.17(b). With N_2 or CO_2 dilution, the effective Lewis number decreases compared to the no dilution condition, which means that the diffusional-thermal instability of the flame is increased. However, it is seen that with N_2/CO_2 dilution, the flame thickness and thermal expansion ratio increases and decreases, respectively. These indicate that the hydrodynamic instability of the flame can be suppressed by the addition of N_2/CO_2. A comparison of the CO_2-diluted condition with N_2-diluted condition shows that CO_2 dilution has stronger effect in suppressing the flame instability at elevated initial pressures.

5.4.2 Instability parameters

5.4.2.1 Effective Lewis number

Figure 5.18 shows the effective Lewis numbers (Le_{eff}) of N_2/CO_2 diluted $H_2/CO/CH_4$/air mixtures at various equivalence ratios and dilution ratios. It is seen

that the effective Lewis number increases with the increase of equivalence ratio, which implies that the diffusional-thermal instability of the N_2/CO_2 diluted $H_2/CO/CH_4$/air flames can be suppressed by increasing the equivalence ratio. When the N_2/CO_2 diluent is added to the fuel mixture, the effective Lewis number slightly decreases with the increase of dilution ratio, and thereby the diffusional-thermal instability is promoted by N_2/CO_2 dilution. This is consistent with the results of Markstein length at atmospheric pressure, as shown in Figure 5.9, which shows that N_2/CO_2 dilution makes the flame more diffusional-thermally unstable. Moreover, it is seen that the effective Lewis numbers of CO_2-diluted mixtures decrease faster than those of the N_2-diluted mixtures, which means that CO_2 dilution has a stronger influence on the diffusional-thermal instability of the flame compared to that of N_2 dilution.

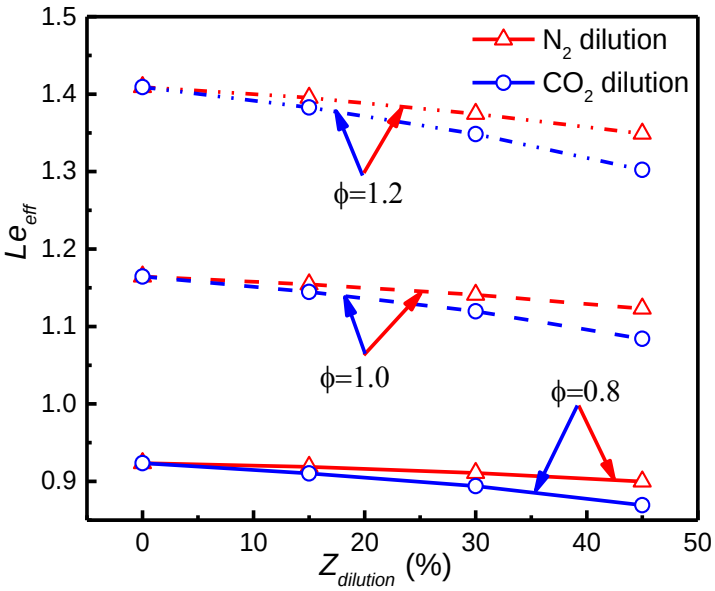

Figure 5.18 Effective Lewis numbers of N_2/CO_2 diluted $H_2/CO/CH_4$/air mixtures at various equivalence ratios and dilution ratios (T=303 K)

5.4.2.2 Thermal expansion ratio and laminar flame thickness

Figure 5.19 and Figure 5.20 give the thermal expansion ratios and the laminar flame thicknesses of N_2/CO_2 diluted $H_2/CO/CH_4$/air flames at P=0.3 MPa for different equivalence ratios and dilution ratios, respectively. As previously mentioned, these two parameters are critical to characterize the hydrodynamic instability of a flame. It is seen from Figure 5.19 that the thermal expansion ratios are higher under stoichiometric condition, compared to those under fuel-rich condition and fuel-lean condition. With an increase of the N_2/CO_2 dilution ratio, the thermal expansion ratio decreases obviously and the thermal expansion ratios of the CO_2-diluted flames decrease faster than those of the N_2-diluted flames. On the other hand, as shown in Figure 5.20, the flame thickness decreases with the increase of equivalence ratio and increases with N_2/CO_2 addition, respectively. Moreover, it is seen that the flame thicknesses of the CO_2-diluted flames are larger than those of N_2-diluted flames at all the dilution ratios. In general, the results indicate that at elevated initial pressures, CO_2 dilution is better in suppressing the hydrodynamic instability of a flame compared to N_2 dilution because of its strong ability in decreasing the thermal expansion ratio and increasing the flame thickness.

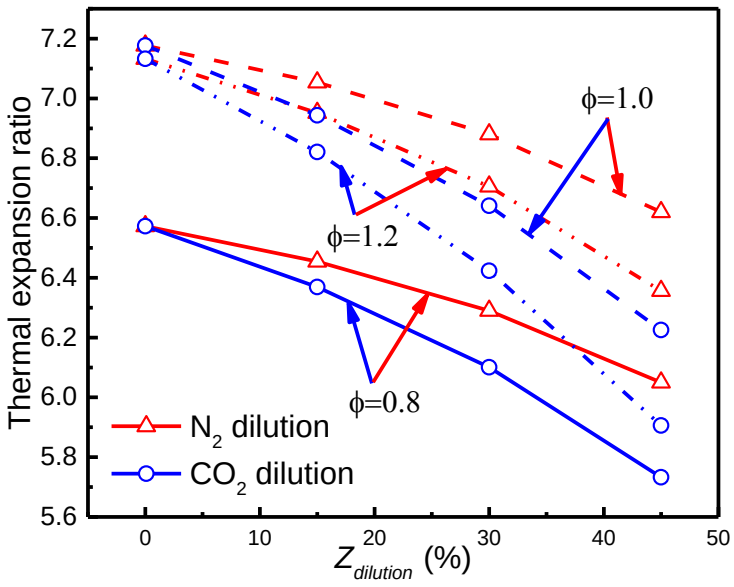

Figure 5.19 Thermal expansion ratios of N_2/CO_2 diluted $H_2/CO/CH_4$/air flames at various equivalence ratios and dilution ratios (P=0.3 MPa, T=303 K)

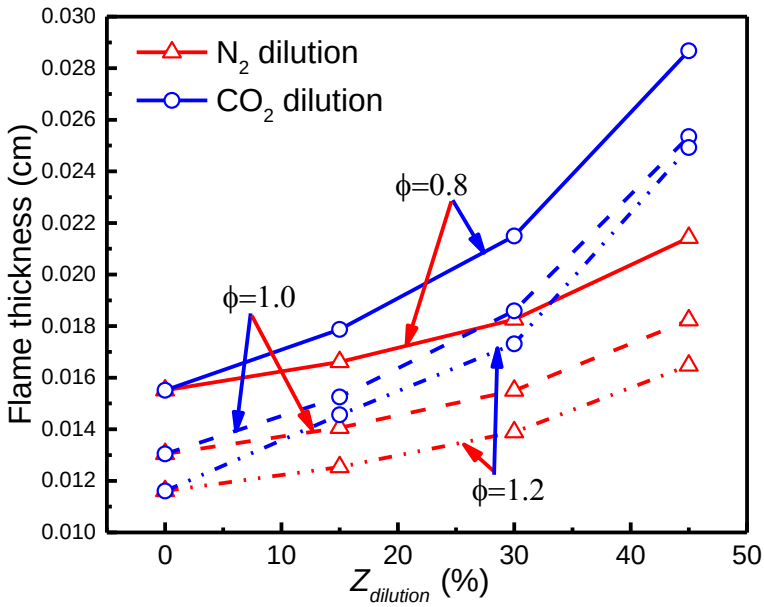

Figure 5.20 Laminar flame thicknesses of N_2/CO_2 diluted $H_2/CO/CH_4$/air flames at various equivalence ratios and dilution ratios (P=0.3 MPa, T=303 K)

5.4.3 Critical flame radius and Peclet number

As shown in Figure 5.21 and Figure 5.22, the critical Peclet number (Pe_{cr}) and the critical flame radius (R_{cr}) are also introduced to reveal the onset of cellular instability of N_2/CO_2 diluted $H_2/CO/CH_4$/air flame at P=0.3 MPa for various dilution ratios. The calculated results show similar behavior with the experimental results that with the increase of the N_2/CO_2 dilution ratio, the critical flame radius increases and the critical Peclet number decreases, respectively. This is due to the substantial increase of the flame thickness and decrease of the thermal expansion ratio with N_2/CO_2 addition as illustrated by the results shown in Figure 5.19 and Figure 5.20, respectively. Hence, the cellular instability of the flame is suppressed with N_2/CO_2 addition at elevated initial pressures as a combination result of diffusional-thermal instability and hydrodynamic instability, that is, adding N_2/CO_2 to the bio-syngas/air mixture can slightly promote the diffusion-thermal instability through a decrease in the effective Lewis number while significantly suppressed the hydrodynamic instability by the substantial increase in the flame thickness and decrease in the thermal expansion ratio. In addition, the results also illustrate that CO_2 dilution has a stronger inhibiting effect on the onset of cellular instability of the flame than N_2 dilution at elevated initial pressures as evidenced by the larger critical flame radius and smaller critical Peclet number at all dilution ratios associated with CO_2 dilution.

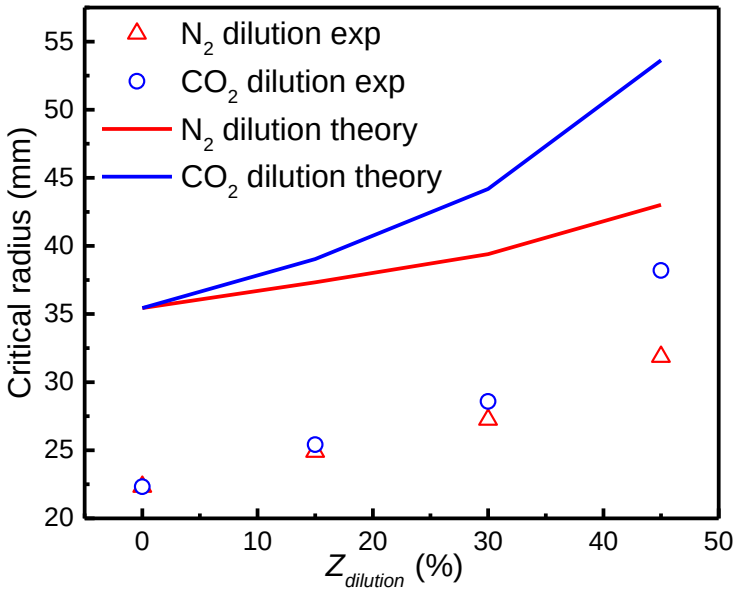

Figure 5.21 Critical flame radius of stoichiometric N_2/CO_2 diluted $H_2/CO/CH_4$/air flame at various dilution ratios (P=0.3 MPa, T=303 K)

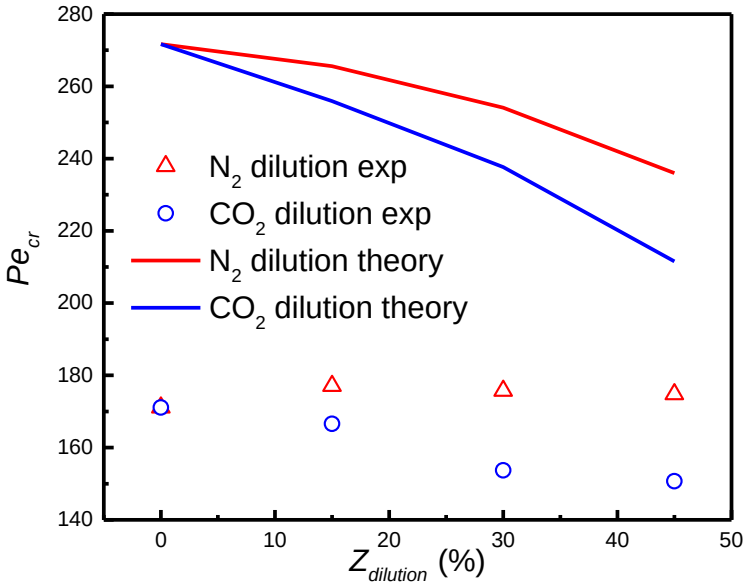

Figure 5.22 Critical Peclet number of stoichiometric N_2/CO_2 diluted $H_2/CO/CH_4$/air flame at various dilution ratios (P=0.3 MPa, T=303 K)

5.5 Summary

Experiments and theoretical calculations were conducted to study the intrinsic flame instabilities of outwardly expanding spherical flames of the bio-syngas/air mixtures at various fuel compositions, dilution ratios and equivalence ratios under atmospheric pressure and elevated initial pressures. The following results are obtained:

For the propagation of laminar flame front at atmospheric pressure, the results of flame morphology and Markstein length show that the flame front tends to be stable with the increase of equivalence ratio at atmospheric pressure. With the increase of H_2 fraction in the fuel mixture, the Markstein length decreases, indicating that the increase of H_2 concentration in the fuel mixture decreases the stability of the flame front. Moreover, adding CH_4 or CO to the fuel mixture slightly increases the Markstein length, and the increases of the CH_4-enriched conditions are more substantial than those of the CO-enriched conditions, suggesting that the flame front stability is slightly enhanced with CH_4 addition at atmospheric pressure. For the effect of different diluents (N_2/CO_2) on the propagation of laminar flame front at atmospheric pressure, the results show that the Markstein length decreases at all dilution ratios, suggesting that the addition of N_2/CO_2 makes the flame front more sensitive to the stretch rate effects and promotes the flame instability at atmospheric pressure. Moreover the CO_2-diluted mixture is more affected by preferential

diffusion instabilities than the N_2-diluted mixture.

For the propagation of laminar flame front at elevated initial pressures, the results clearly show that with the increase of initial pressure, irregular wrinkles appeared on the flame surface. Moreover, the higher the initial pressure, the more advance the onset of cellular instability of the flame is observed. The variation of composition of H_2/CO/CH_4/air mixture has a strong influence on the cellular instabilities of the flame front at elevated initial pressures. With the increase of H_2 fraction in the fuel mixture, the cellular instabilities (including the diffusional-thermal instability and the hydrodynamic instability) of the flame front are significantly promoted due to the decrease of effective Lewis number and flame thickness, moreover, the earlier onset of cellular flame structure is also observed. With the increase of CO fraction in the fuel mixture, both the effective Lewis number and the laminar flame thickness are slightly increased and the thermal expansion ratio is slightly decreased. Consequently, both the diffusional-thermal instability and hydrodynamic instability are inhibited and the moment for onset of cellular flame structure is postponed. Finally, the results show that with CH_4 addition, the cellular instabilities of the flame front are significantly suppressed. The moment for the onset of cellular instability of the flame front is also significantly delayed.

On the other hand, the results show that with N_2 or CO_2 dilution, the diffusional-thermal instability of the flame front is increased by a decrease of the

effective Lewis number, while the hydrodynamic instability of the flame front is significantly suppressed by an increase of the flame thickness and a decrease of the thermal expansion ratio, and thereby with a net result of suppression of cellular instability. Moreover, CO_2 dilution has stronger effect in suppressing the flame instability at elevated initial pressures than that of N_2 dilution.

CHAPTER 6 EXPLOSION CHARACTERISTICS OF BIO-SYNGAS/AIR MIXTURES

6.1 Introduction

The combustion process of a combustible fuel mixture is commonly accompanied by a lot of heat release. When the combustion process occurs in a confined vessel, the intense heat release will lead to a sharp increase in pressure inside the combustion chamber. If there is no suitable relief device to guard against the damage from gaseous explosion, when the pressure exceeds the acceptable upper limit of the combustion vessel, the high explosion pressure and rate of pressure rise will lead to serious hazards. Therefore, it is of great importance to know the explosion characteristics of bio-syngas with various fuel compositions to ensure safety in practical applications. This chapter presents the explosion characteristics of bio-syngas/air mixtures at different fuel compositions, dilution ratios and initial pressures over a wide range of equivalence ratios. The characteristic parameters such as explosion pressure (P_{max}), explosion time (t_c), maximum rate of pressure rise $(dP/dt)_{max}$ and deflagration index (K_G) were obtained to evaluate the hazards of bio-syngas/air mixtures explosion.

6.2 Controlling factor of explosion parameter

Theoretically, assuming that the combustible fuel mixture is approximately an ideal

gas during the explosion process and the flame propagation is a constant volume and adiabatic process, thus, at the beginning and end of the explosion, the mixture follows the ideal gas law. At the initial moment, that is,

$$P_0V=n_0RT_0 \tag{6-1}$$

where P_0 and T_0 are the initial pressure and temperature respectively; n_0 is the initial number of moles of the unburned fuel mixture. Adiabatic combustion results in a maximum pressure P'_{max} at the end of combustion, then we have,

$$P'_{max}V=n_{max}RT_{max} \tag{6-2}$$

where P'_{max} is the adiabatic explosion pressure; T_{max} is the maximum flame temperature, namely the adiabatic flame temperature in accordance to the assumption; n_{max} is the number of moles of the burned fuel mixture. Then, the relationship between the adiabatic explosion pressure P'_{max} and the initial pressure P_0 can be obtained by combining the above two equations,

$$P'_{max}=\frac{n_{max}}{n_0}\frac{T_{max}}{T_0}P_0 \tag{6-3}$$

It is seen from Equation (6-3) that the adiabatic explosion pressure P'_{max} mainly depends on the variation of number of molecules and temperature before and after the explosion. Thus, there exists a positive correlation between the explosion pressure and the adiabatic flame temperature. Moreover, it should be noticed that the experimental explosion pressure P_{max} is not only determined by the adiabatic explosion pressure P'_{max} but also the heat loss form the combustion chamber to the

surrounding. Thus, the experimental explosion pressure P_{max} is always lower than the adiabatic explosion pressure P'_{max} [203, 275].

Lewis and von Elbe [276] proposed that the increment of instant pressure P inside the combustion chamber is proportional to the mass of burned mixture,

$$\frac{m_b}{m} = 1 - \frac{m_u}{m} = \frac{P - P_0}{P'_{max} - P_0} \tag{6-4}$$

where m_b and m_u are the burned mass and unburned mass of the fuel mixture, respectively. By differentiating Equation (6-4) with respect to time, the formula of rate of pressure rise is obtained,

$$dP/dt = \frac{P'_{max} - P_0}{m}\left(-\frac{dm_u}{dt}\right) \tag{6-5}$$

For an outwardly expanding spherical flame, the consumption rate of unburned fuel mixture can be expressed by the mass burning rate,

$$\frac{dm_u}{dt} = -4\pi R_f^2 \rho_u S_L \tag{6-6}$$

where R_f is the flame radius; ρ_u is the density of the unburned fuel mixture; S_L is the laminar flame speed. Substitute Equation (6-6) into Equation (6-5), we can obtain,

$$dP/dt = \frac{P'_{max} - P_0}{m} \cdot 4\pi R_f^2 \rho_u S_L \tag{6-7}$$

From Equation (6-7), we can see that the rate of pressure rise not only depends on the explosion pressure but also on the mass burning rate of the unburned fuel mixture.

6.3 Data processing of pressure curve

Figure 6.1 shows the typical pressure evolution during explosion of a bio-syngas/air mixture in a confined vessel. Since the experimental pressure-time curve contained pressure oscillations, a smoothing filter was used to determine the mean pressure-time curve and its derivative before further processing. In this study, the explosion pressure evolution was filtered by means of the Savitzky-Golay method [277], using the ORIGIN software with a second order polynomial and 21 points (10 on the left and 10 the right) data window. This method has the advantage of producing a smoothed first derivative without filtering the data [182]. The *dP/dt* curve was obtained from the smoothed *P(t)* curve.

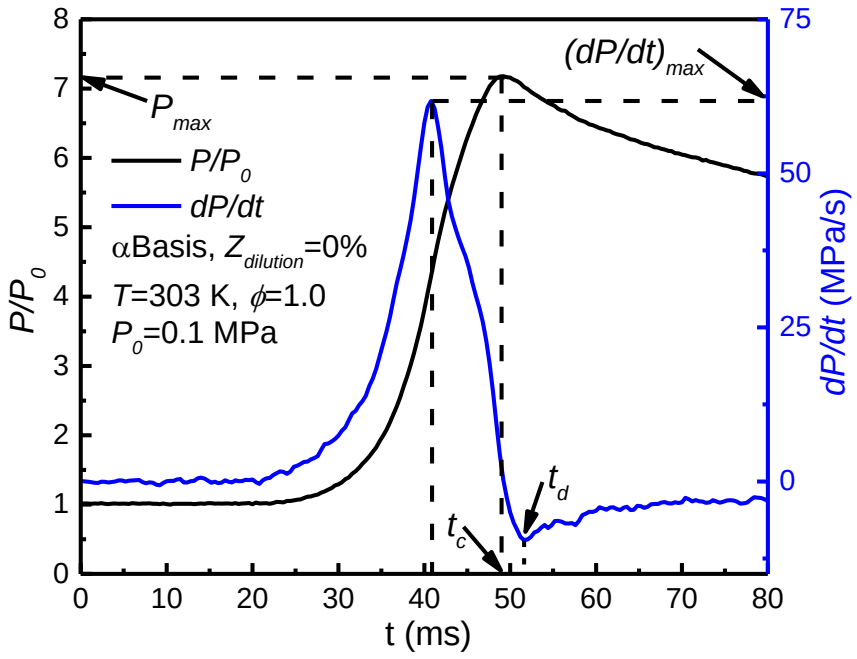

Figure 6.1 Definition of the explosion parameters and typical pressure evolution during explosion of a bio-syngas/air mixture

As observed in Figure 6.1, after ignition, the fuel mixture in the combustion chamber expands rapidly due to the large heat release from combustion, and the pressure increases progressively until the pressure rise rate reaches to its maximum value, then the pressure continues to increase with a decreasing pressure rise rate, and after the maximum pressure is achieved, the pressure begins to decrease accordingly due to the significant heat loss and the end of combustion.

It is seen that for the explosion experiments, the important explosion parameters such as explosion pressure (P_{max}), explosion time (t_c), and maximum rate of pressure rise $(dP/dt)_{max}$, can be obtained directly from the explosion pressure-time curves. The explosion pressure P_{max} is defined as the highest pressure reached during the explosion. The explosion time t_c is the time interval between ignition and the moment when P_{max} is achieved [193]. It is also defined as the combustion duration in previous studies [26, 184, 195]. A previous study indicated that the explosion time suggested the moment when the heat release due to the combustion is equal to the heat loss [203]. For a spherical combustion vessel, this moment occurs when the combustion process is ended and the flame front starts to collide with the combustion chamber wall. However, for a cylindrical combustion vessel, the explosion time is not associated with the moment when the combustion is ended [176]. In fact, the pressure increases with the propagation of the flame front and reaches its maximum value at the moment before the combustion ended when the flame front collided with the combustion chamber wall, which means the

combustion has not ended. Therefore, it is seen from Figure 6.1 that there exists a time t_d indicating the end of combustion, instead of t_c, for the cylindrical vessel used in the present study when the pressure rise rate reaches its minimum value. The maximum rate of pressure rise $(dP/dt)_{max}$ is defined as the highest value of pressure rise rate observed and also refers to the value of the maximum slope of the pressure-time curve. Previous studies [182, 278-281] showed that the maximum rates of pressure rise in confined vessels not only depend on the composition, pressure and temperature of the fuel/air mixture (factors which also determine the rate of heat release) but also are influenced by the volume and shape of the combustion vessel, the size, energy, and position of the ignition source (factors which determine the amount of generated heat as well as the heat losses during explosion). Thus, the deflagration index (K_G) is often introduced to eliminate the influence of the volume of the combustion vessel according to the cubic-root law:

$$K_G = \left(\frac{dP}{dt}\right)_{max} \times V^{1/3} \tag{6-8}$$

where V is the volume of the combustion vessel. This law was originally proposed for a spherical combustion vessel. It was also demonstrated that it can be applied in cylindrical vessel with the length to diameter ratio (L/D) lower than 2 [282]. In the present study, the L/D ratio is equal to 1.167, which conforms to the requirement. Since K_G is assumed to be independent of the size of the combustion vessel, and depends only on the properties of the fuel mixture (composition, initial pressure and temperature) now [282, 283], it can be used for evaluating the gas explosions in the

confined vessel used in the present study under different initial conditions. The higher the deflagration index is, the more intense and dangerous the combustion process will be. Consequently, the explosion will be more robust and damaging. In the present study, the deflagration index (K_G) is also calculated to evaluate the explosive consequence of the bio-syngas/air mixtures.

6.4 Dependence of pressure evolution on initial conditions

6.4.1 Dependence of pressure evolution on equivalence ratio

Figure 6.2 and Figure 6.3 give the pressure evolution and the rate of pressure rise during the combustion process of H_2/CO/CH_4/air mixtures under αBasis condition and atmospheric pressure at different equivalence ratios. All the pressures are normalized with respect to the initial pressure (P_0).

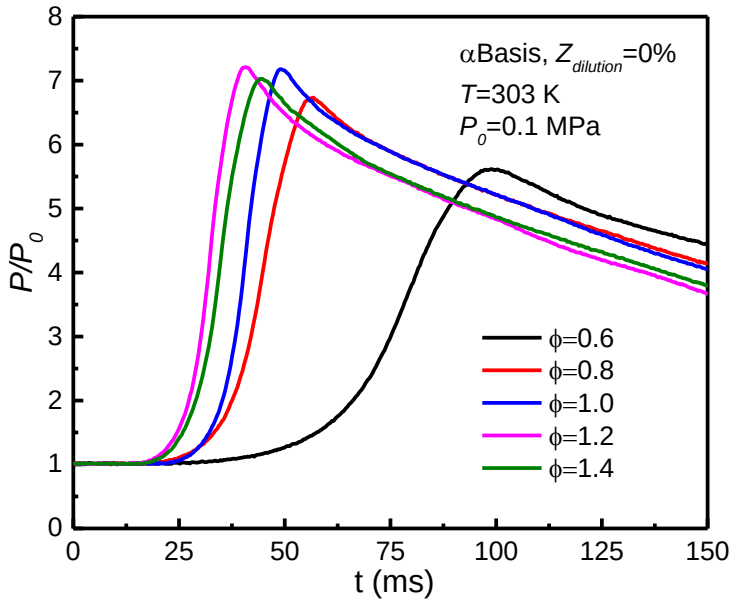

Figure 6.2 Pressure history for different equivalence ratios

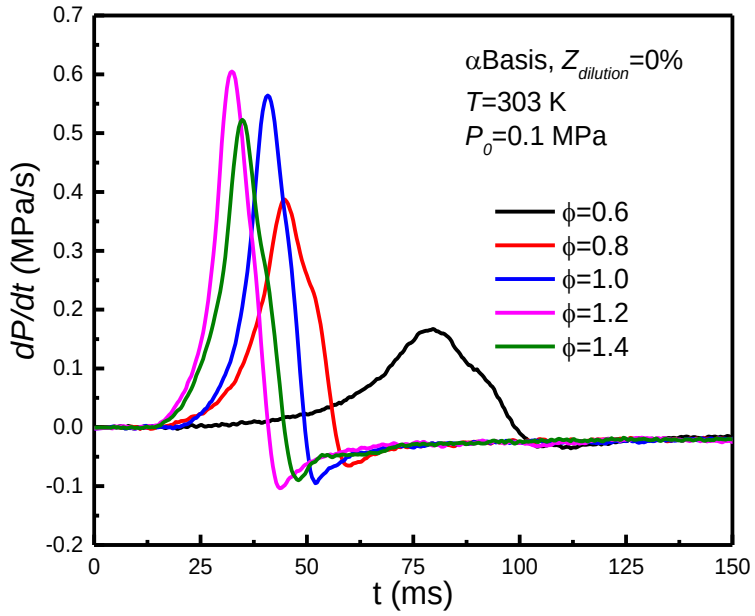

Figure 6.3 The rate of pressure rise for different equivalence ratios

It is seen from Figure 6.2 that the explosion pressure (P_{max}) increases with the increase of equivalence ratio and occurs slightly on the fuel rich side, ϕ=1.2. Law et al. [284] suggested that for hydrocarbon as well as H_2 and CO, the maximum value of the adiabatic flame temperature (T_{ad}) also peaks on the rich side of stoichiometry which is caused by the reduced heat release in the presence of product dissociation.

Figure 6.4 shows the adiabatic flame temperature and laminar flame speed of H_2/CO/CH_4/air mixtures under αBasis condition and atmospheric pressure at various equivalence ratios. A slight shift to the fuel rich side is also observed for the maximum adiabatic flame temperature. This suggests that there is a strong correlation between the explosion pressure and the adiabatic flame temperature, which also can be verified by Equation (6-3). Moreover, from Figure 6.3, we can see

that, for the very lean fuel mixture, ϕ=0.6, the rate of pressure rise during combustion is very slow because there is significantly excessive oxidizer provided in the fuel mixture. As the equivalence ratio increases, the heat release of the fuel mixture is increased due to the increase of the fuel concentration in the mixture, and the combustion becomes more violent, leading to a significant increase of pressure inside the vessel. It is noted that at ϕ=1.2, the rate of pressure rise reaches its maximum value due to the complete combustion of the fuel mixture. However, as the equivalence ratio is further increased, there is excessive fuel provided and the combustion is incomplete, leading to a decrease of pressure rise rate and explosion pressure.

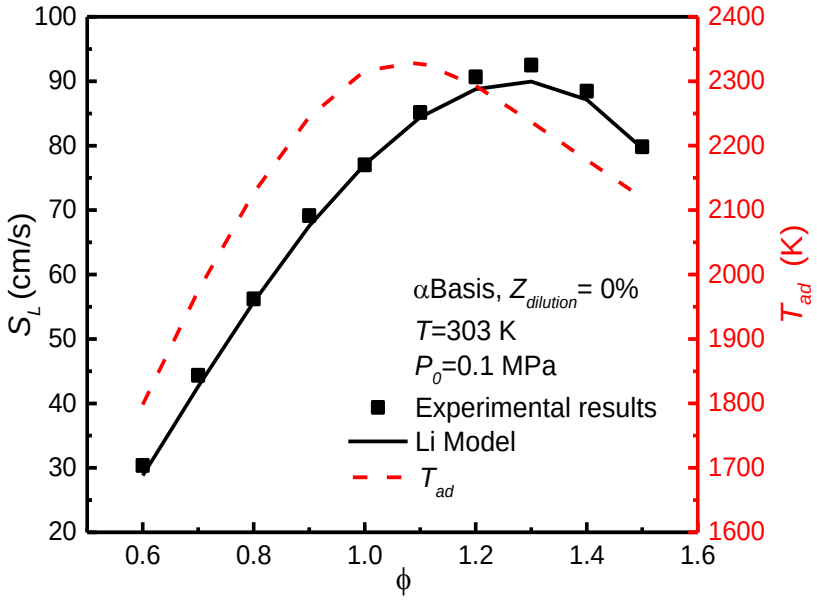

Figure 6.4 Laminar flame speed and adiabatic flame temperature of H_2/CO/CH_4/air mixtures at various equivalence ratios

6.4.2 Dependence of pressure evolution on initial pressure

Figure 6.5 and Figure 6.6 present the pressure-time curves and the rates of pressure rise at different initial pressures under αBasis condition, respectively. The pressure has been normalized with respect to the initial pressure (P_0).

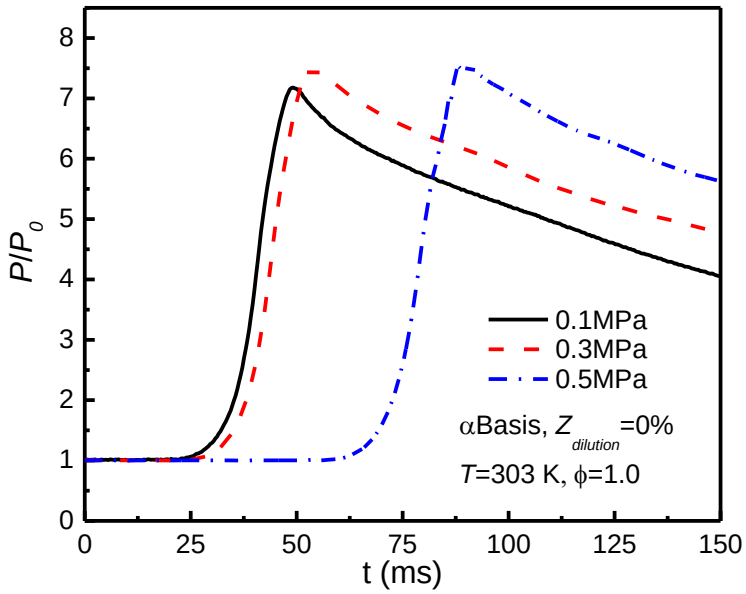

Figure 6.5 Pressure history for different initial pressures

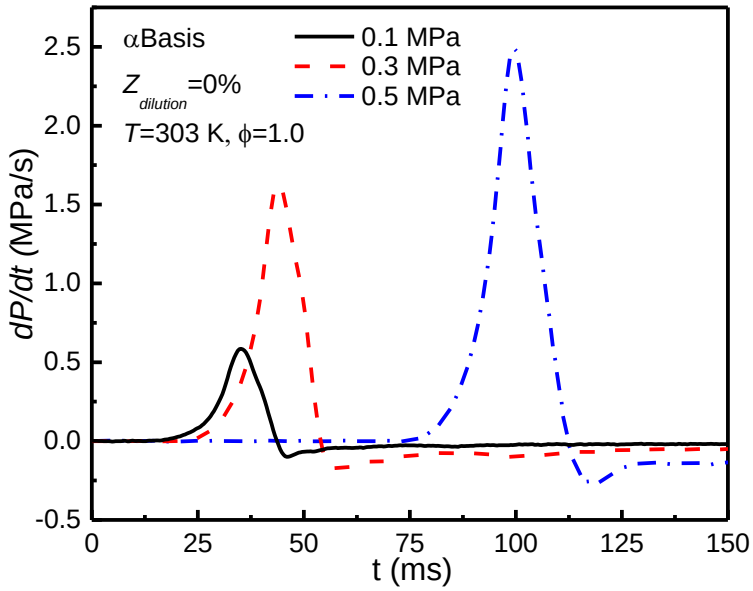

Figure 6.6 The rate of pressure rise for different initial pressures

Compared with the P_0=0.1 MPa condition, both the normalized explosion pressure (P_{max}) and time for reaching P_{max} slightly increase for the P_0=0.3 MPa condition, while for the P_0=0.5 MPa condition, the increases of the normalized explosion pressure (P_{max}) is still small but the increases of the time for reaching P_{max} is more substantial. Recall that the adiabatic flame temperature is not a strong function of pressure and it only slightly increases with increasing initial pressure as shown in Figure 4.17. Therefore, the maximum value of the normalized explosion pressure is also not sensitive to the initial pressure. On the other hand, as shown in Figure 4.16, the laminar flame speed is decreased with the increase of the initial pressure, leading to a significant increase of the time for reaching the explosion pressure, as well as to the time for reaching the maximum value of the pressure rise rate, as shown in Figure 6.6. Moreover, there is a significant increase in the rate of pressure rise with increasing initial pressure.

6.5 Explosion characteristics of different bio-syngas/air mixtures

6.5.1 Effect of fuel composition variation

Figure 6.7 gives the pressure-time curves of stoichiometric H_2/CO/CH_4/air mixtures for different fuel compositions. The corresponding adiabatic flame temperature and the laminar flame speed are given in Table 6-1. It is seen that the fuel composition variation has a significant influence on the explosion pressure evolution.

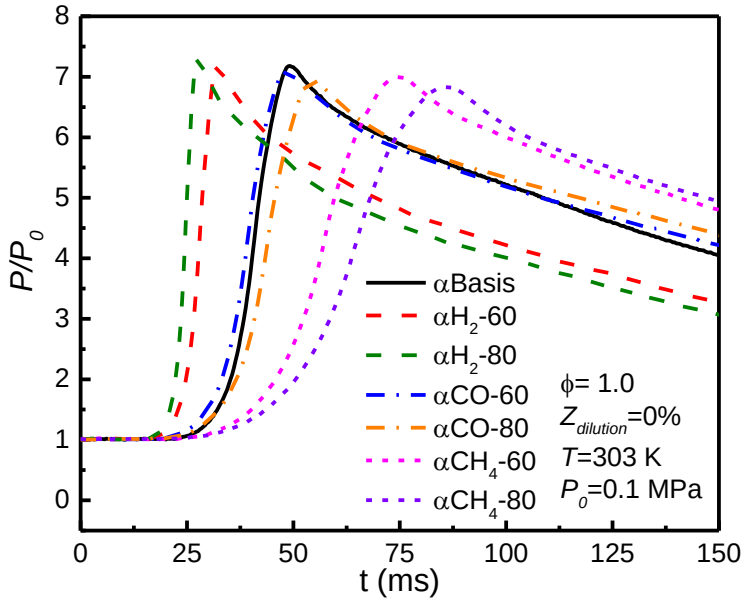

Figure 6.7 Pressure evolution during explosions of H_2/CO/CH_4/air mixtures for different fuel compositions

Table 6-1 T_{ad} and S_L of stoichiometric H_2/CO/CH_4/air mixtures for different fuel compositions

Fuel mixture	T_{ad} (K)	S_L (cm/s)
αBasis	2316.2	77.0
αH_2-60	2331.4	104.4
αH_2-80	2353.5	155.2
αCO-60	2335.1	76.8
αCO-80	2358.7	61.2
αCH_4-60	2259.1	45.3
αCH_4-80	2243.7	38.5

As shown in Table 6-1, with the increase of H_2 concentration in the fuel mixture, the adiabatic flame temperature increases slightly and the laminar flame speed increases significantly, resulting in a slight increase in the maximum explosion pressure and significant advancement of the timing of the peak pressure compared to that of the αBasis condition, as observed in Figure 6.7. On the contrary, with the increase of

CH_4 fraction in the fuel mixture, the maximum explosion pressure decreases and the timing of the peak pressure is retarded evidently. This is consistent with the results presented by Tang et al. [184], in which the addition of CH_4 to the fuel mixture could decrease the explosion pressure and delay the timing of the peak pressure due to the decrease of adiabatic flame temperature and laminar flame speed. For the CO-enriched cases, it is seen from Table 6-1 that the adiabatic flame temperature slightly increases with increasing CO concentration in the fuel mixture, and the increment is even higher than that of the H_2-enriched conditions. The increase in flame temperature, in principle, should have a positive effect on the flame burning velocity. However, it is clear that the difference between the laminar flame speed of αBasis condition (77.0 cm/s) and αCO-60 condition is small (76.8 cm/s), and the laminar flame speed decreases to 61.2 cm/s when the CO concentration is further increased to 80% at the αCO-80 condition. This indicates that the effect of CO concentration on the burning characteristics of bio-syngas cannot be solely determined based on the adiabatic flame temperature, but the competition between the thermal effect and the chemical effect contributes to this result [131, 261]. Compared to the αBasis condition, the αCO-60 condition has a comparable explosion pressure and the time for reaching the peak pressure is slightly advanced mainly due to the dominant role of thermal effect of CO addition, while for the αCO-80 condition, the concentration of CO is so high that the negative chemical effect is more significant, leading to a decrease of the explosion pressure and an

increase of the timing for the peak pressure.

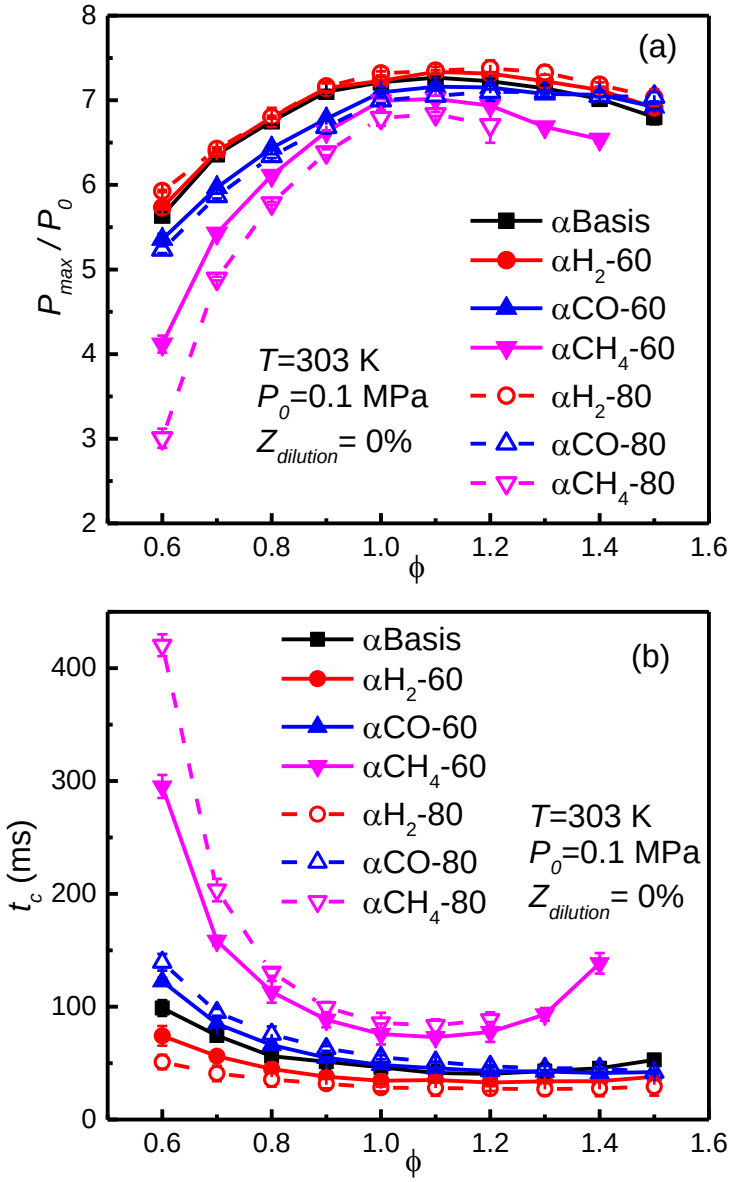

Figure 6.8 Normalized explosion pressure and explosion time versus equivalence ratio at different fuel compositions: (a) P_{max}/P_0; (b) t_c

Figure 6.8 presents the influence of fuel composition variation on the normalized explosion pressure (P_{max}/P_0) and the explosion time (t_c) versus equivalence ratio. As shown in Figure 6.8(a), the behavior of the normalized explosion pressure has

similar trend with the adiabatic flame temperature such that P_{max}/P_0 has its peak value at a slightly fuel rich equivalence ratio with ϕ=1.0-1.2 for all the presented conditions. For fuel-lean condition, there is a decrease of the explosion pressure which is caused by the decreasing combustion rates due to the lower fuel content per unit volume and lower combustion temperature at fuel-lean condition, while for fuel-rich condition, the lack of oxygen leads to incomplete combustion and then the decrease of explosion pressure [26]. Moreover, it is seen in Figure 6.8(b) that the explosion time, t_c, also decreases to its minimum value around ϕ=1.1. As mentioned earlier, the explosion time (t_c) corresponds to the occurrence of the maximum explosion pressure (P_{max}). Movileanu et al. [176] indicated that in the case of a cylindrical closed vessel with central ignition, the time for reaching the maximum explosion pressure always occurs at the moment before complete combustion of the fuel mixture. At this moment, the heat release rate due to the combustion equals to the heat loss caused by thermal convection, conduction, and radiation [203]. Thus, there exists a correlation between the explosion time and the laminar flame speed such that the higher the laminar flame speed, the faster the consumption of the combustible mixture in the combustion chamber, and then the shorter the explosion time. Compared with the αBasis condition, with the increase of H_2 content in the fuel mixture, P_{max}/P_0 slightly increases and t_c decreases as a result of the increase of both the adiabatic flame temperature and the laminar flame speed with H_2 enrichment [202]. For the CH_4-enriched condition, it has lower explosion pressure

and much longer explosion time. It is expected that the addition of CH_4 to the fuel mixture can significantly decrease the adiabatic flame temperature and laminar flame speed, resulting in the observed postponed pressure evolution [184]. However, it is seen that the differences in P_{max}/P_0 and t_c between the αBasis and the CO-enriched conditions are not significant. The main reason is that the addition of CO to the fuel mixture plays a small role in the chemical kinetic effect compared to that of the H_2 or CH_4 addition, resulting in an insignificant change in the laminar flame speed [261].

As mentioned earlier, the maximum rate of pressure rise and the deflagration index are indications of the hazards of the explosion. Figure 6.9 presents the maximum rate of pressure rise $(dP/dt)_{max}$ and the calculated deflagration index (K_G) versus equivalence ratio at different fuel compositions. It can be seen that both $(dP/dt)_{max}$ and K_G reach their maximum values at a slightly fuel rich equivalence ratio for all the presented conditions. The deflagration indices, K_G, are lower than 30 MPa.m.s^{-1} in all cases, suggesting that the bio-syngas (H_2/CO/CH_4) fuel compositions tested in this study are within a relatively safe level [27, 285]. According to Bradley et al. [286] and Movileanu et al. [287], the rate of pressure rise and the deflagration index in a confined vessel are closely related to the variation of the overall reaction rate in the reaction zone, which is the most important factor correlated to the laminar flame speed and the explosion pressure. Increase of the H_2 content in the fuel mixture can significantly increase the laminar flame speed and shorten the explosion time.

Therefore, there is a substantial increase in the maximum rate of pressure rise and the deflagration index for H_2-enriched conditions. For CH_4-enriched conditions, both $(dP/dt)_{max}$ and K_G decrease with the increase of CH_4 fraction in the fuel mixture. This is consistent with the results presented by Tran et al. [206], which shows that the addition of a small amount of hydrocarbon can significantly suppress the explosion hazard of a syngas/air mixture. Additionally, the maximum rate of pressure rise and the deflagration index change little for CO-enriched conditions compared to that of the αBasis condition, indicating that the increase of CO fraction in the fuel mixture plays a mild role in affecting the explosion hazard of bio-syngas. For the αCO-80 condition, the explosion hazard of the mixture is slightly suppressed at fuel-lean and stoichiometric equivalence ratios due to the slight decrease of the laminar flame speed [261].

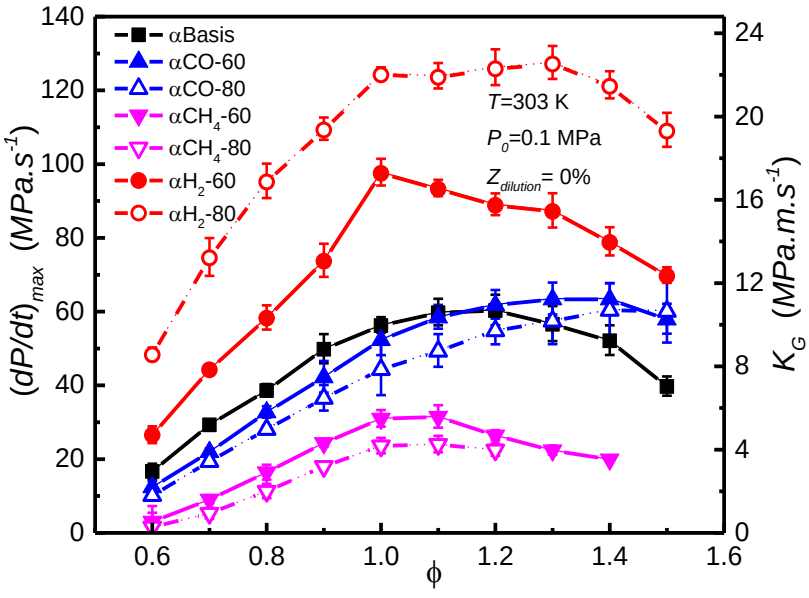

Figure 6.9 Maximum rate of pressure rise and deflagration index versus equivalence ratio at different fuel compositions

6.5.2 Effect of diluents (N_2/CO_2)

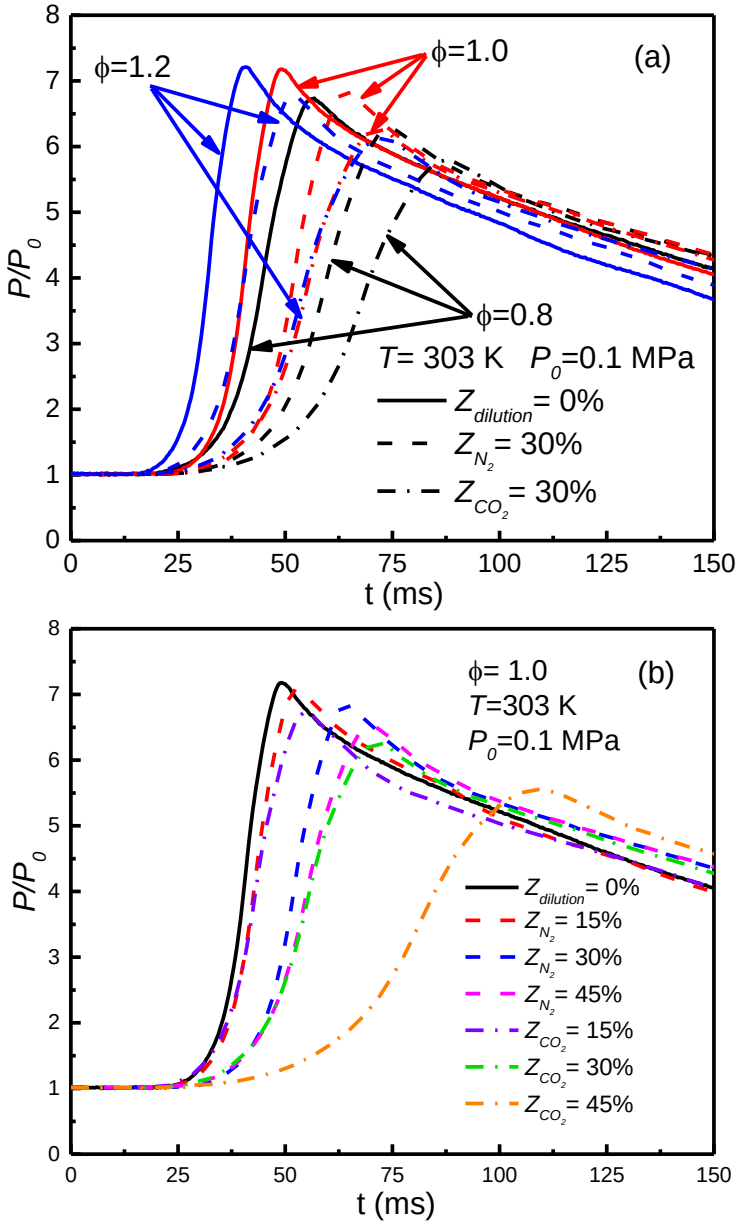

Figure 6.10 Pressure evolution during explosion of N_2/CO_2 diluted $H_2/CO/CH_4$/air mixtures at different (a) equivalence ratios; (b) dilution ratios

As mentioned earlier, bio-syngas usually contains a considerable amount of diluents, such as N_2 and CO_2. In some practical applications, these dilution gases are deliberately introduced to the unburned mixtures to reduce the NO_x emission [140].

Therefore, it is necessary for us to investigate the explosion characteristics of bio-syngas/air mixtures with N_2/CO_2 dilution. Figure 6.10 gives the pressure-time curves of $H_2/CO/CH_4$/air mixtures with N_2/CO_2 dilution at different equivalence ratios and dilution ratios. It can be seen from Figure 6.10(a) that the maximum explosion pressure decreases with N_2/CO_2 addition at all the reported equivalence ratios and the time for reaching the maximum explosion pressure increases with N_2/CO_2 addition. Additionally, Figure 6.10(b) shows that the maximum explosion pressure and the time for reaching peak pressure substantially decrease and increase with increasing dilution ratio.

Table 6-2 gives the calculated adiabatic flame temperatures using the Li mechanism and the experimental laminar flame speeds of stoichiometric N_2/CO_2 diluted $H_2/CO/CH_4$/air mixtures at different dilution ratios. It is seen that both of them decrease significantly with increasing dilution. Qiao et al. [288] indicated that the addition of diluents to a fuel mixture can reduce the laminar flame speed due to the increase of specific heat of the non-fuel gases per unit oxygen concentration. Hence, the maximum explosion pressure is decreased and the pressure rise becomes slower with increasing dilution in the bio-syngas/air mixture. Moreover, since both the adiabatic flame temperature and laminar flame speed of CO_2 diluted $H_2/CO/CH_4$/air mixture are lower than that of the N_2 diluted $H_2/CO/CH_4$/air mixture at each dilution ratio, it is obvious that CO_2 dilution has a stronger influence on the explosion of bio-syngas/air mixture than N_2 dilution. This is consistent with the results of

previous studies [287, 289] that CO_2 is more efficient in decreasing the explosion pressure and postponing the explosion time than that of N_2. This is mainly because CO_2 can significantly increase the specific heat of the fuel mixture in comparison to N_2, resulting in a substantial decrease of the flame temperature and the combustion rate.

Table 6-2 T_{ad} and S_L of stoichiometric N_2/CO_2 diluted $H_2/CO/CH_4$/air mixtures at different dilution ratios

Fuel mixture	T_{ad} (K)	S_L (cm/s)
$Z_{diluton}$=0%	2316.2	77.0
Z_{N2}=15%	2274.9	69.1
Z_{N2}=30%	2218.7	62.6
Z_{N2}=45%	2133.1	49.7
Z_{CO2}=15%	2240.5	63.8
Z_{CO2}=30%	2144.1	46.3
Z_{CO2}=45%	2009.9	29.6

Figure 6.11 presents the normalized explosion pressure (P_{max}/P_0) and the explosion time (t_c) of N_2/CO_2 diluted bio-syngas/air mixtures at various dilution ratios. It is apparent that P_{max}/P_0 decreases and t_c increases significantly with increasing dilution ratio in the fuel mixture. As dilution gases, the presence of N_2/CO_2 in the fuel mixture leads to a decrease of the fuel content and an increase of specific heat of the fuel mixture, leading to a much lower burning velocity and heat release rate during flame propagation. These contribute to the substantial decrease of explosion pressure and increase of explosion time with increasing dilution ratio. Compared to the N_2-diluted bio-syngas/air mixture, the CO_2-diluted bio-syngas/air mixture shows a

progressive decrease in P_{max}/P_0, and a significant increase in t_c at all the reported equivalence ratios, indicating that CO_2 addition can more effectively reduce the explosion severity of a bio-syngas/air mixture.

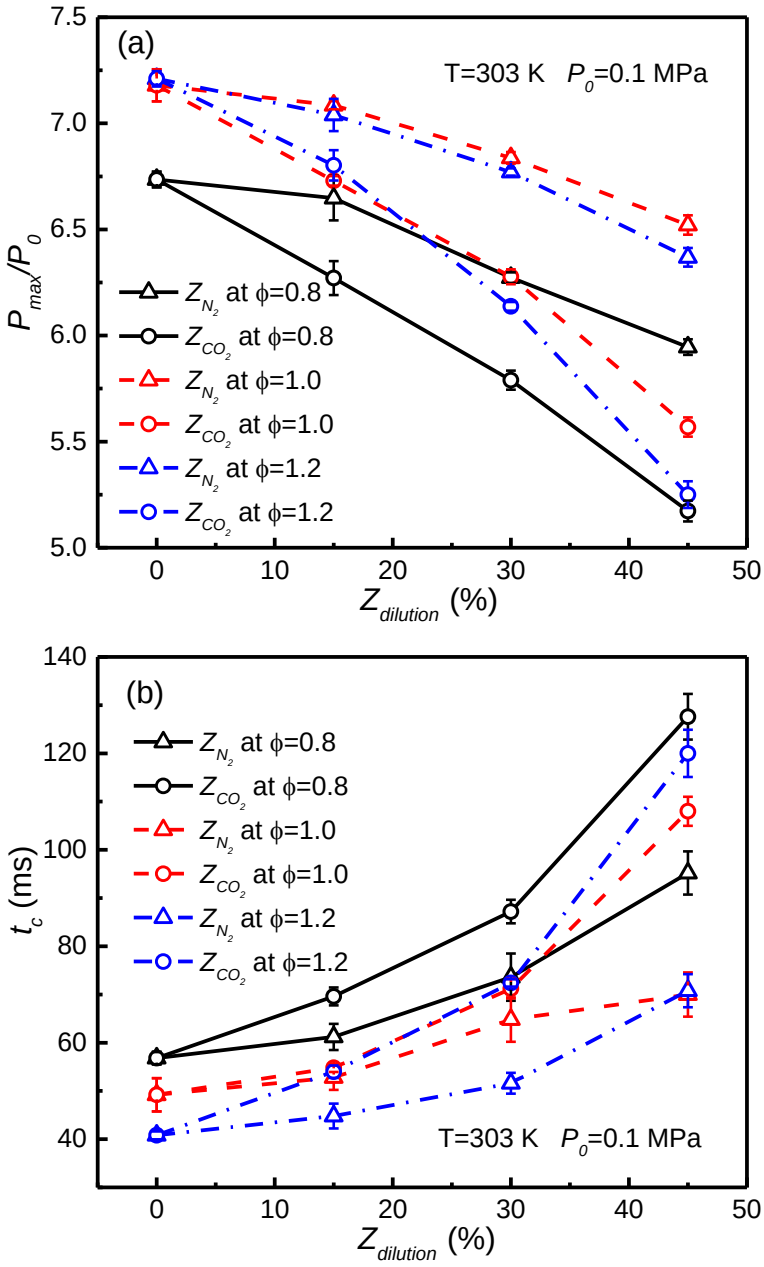

Figure 6.11 Normalized explosion pressure and explosion time of N_2/CO_2 diluted $H_2/CO/CH_4$/air mixture at various dilution ratios (a) P_{max}/P_0; (b) t_c

Moreover, the relationships between the normalized explosion pressure/explosion

time and dilution ratio can be depicted using a second order polynomial curve fitting method as $P_{max}/P_0 = C_1 + a_1 \cdot Z_{dilution} + a_2 \cdot Z_{dilution}^2$ and $t_c = C_2 + b_1 \cdot Z_{dilution} + b_2 \cdot Z_{dilution}^2$, respectively. Table 6-3 and Table 6-4 give the fitted parameters and the correlation coefficients. These equations can be useful for predicting the explosion pressure and explosion time of a bio-syngas/air mixture at different dilution ratios.

Table 6-3 Fitted parameters a_1, a_2, and C_1 of $P_{max}/P_0 = f(Z_{dilution})$ and correlation coefficients R^2 for the deflagration of bio-syngas/air mixture diluted with N_2/CO_2 at different equivalence ratios

	C_1	a_1	a_2	R^2
ϕ=0.8				
N_2	6.752±0.073	-0.006±0.008	-2.66E-4±1.67E-4	0.957
CO_2	6.729±0.026	-0.027±0.003	-1.69E-4±5.90E-5	0.998
ϕ=1.0				
N_2	7.183±0.019	-0.004±0.002	-2.48E-4±4.24E-5	0.996
CO_2	7.166±0.055	-0.022±0.006	-2.87E-4±1.26E-4	0.993
ϕ=1.2				
N_2	7.209±0.008	-0.007±0.008	-2.57E-4±1.76E-5	0.999
CO_2	7.212±0.007	-0.020±0.007	-5.32E-4±1.66E-5	0.999

Table 6-4 Fitted parameters b_1, b_2, and C_2 of $t_c = f(Z_{dilution})$ and correlation coefficients R^2 for the deflagration of bio-syngas/air mixture diluted with N_2/CO_2 at different equivalence ratios

	C_2	b_1	b_2	R^2
ϕ=0.8				
N_2	56.86±0.262	-0.009±0.028	-0.019±0.001	0.999
CO_2	57.70±3.923	0.153±0.420	0.031±0.009	0.983
ϕ=1.0				
N_2	48.59±2.659	0.359±0.285	0.003±0.006	0.920
CO_2	49.68±2.092	-0.275±0.224	0.035±0.005	0.993
ϕ=1.2				
N_2	41.28±2.092	-0.115±0.224	0.017±0.005	0.974
CO_2	42.00±5.231	-0.013±0.560	0.038±0.012	0.976

Figure 6.12 gives the maximum rate of pressure rise $(dP/dt)_{max}$ and the deflagration index (K_G) of N_2/CO_2 diluted bio-syngas/air mixtures at various dilution ratios. It is seen that $(dP/dt)_{max}$ and K_G are significantly decreased with increasing N_2/CO_2 dilution. Movileanu et al. [287] also observed that N_2 and CO_2 have strong influence on the maximum rate of pressure rise and the deflagration index. As mentioned earlier, the rate of pressure rise in a closed vessel has a strong correlation with the laminar flame speed and the explosion pressure [286]. The suppression influence of N_2/CO_2 dilution on $(dP/dt)_{max}$ and K_G can be explained by the change in thermo-physical properties of the unburned mixture and the overall reaction rate in the reaction zone with addition of N_2/CO_2 to the fuel mixture, contributing to the decrease of adiabatic flame temperature, the total amount of heat release, and the laminar flame speed of the diluted bio-syngas/air mixture. Previous studies [287, 289] stated that the addition of CO_2 has a stronger radiation effect and greater negative influence on the thermal effect than N_2 addition. Moreover, it should be noted that unlike N_2, CO_2 can be directly involved in the chemical reactions primarily through the reaction: $CO+OH \leftrightarrow CO_2+H$ in addition to acting as an inert gas in the fuel mixture [260]. Consequently, the CO_2-diluted fuel mixture has much lower laminar flame speed than that of the N_2-diluted fuel mixture, resulting in lower $(dP/dt)_{max}$ and K_G in all the reported equivalence ratios. An approximate linear correlation of the maximum rate of pressure rise $(dP/dt)_{max}$ and dilution ratio ($Z_{dilution}$) is observed and can be depicted as $(dP/dt)_{max} = C_3 + d_1 \cdot Z_{dilution}$, with the fitted

parameters given in Table 6-5. Such correlation is also useful for the determination of the maximum rate of pressure rise in any closed vessel within the investigated range of parameters.

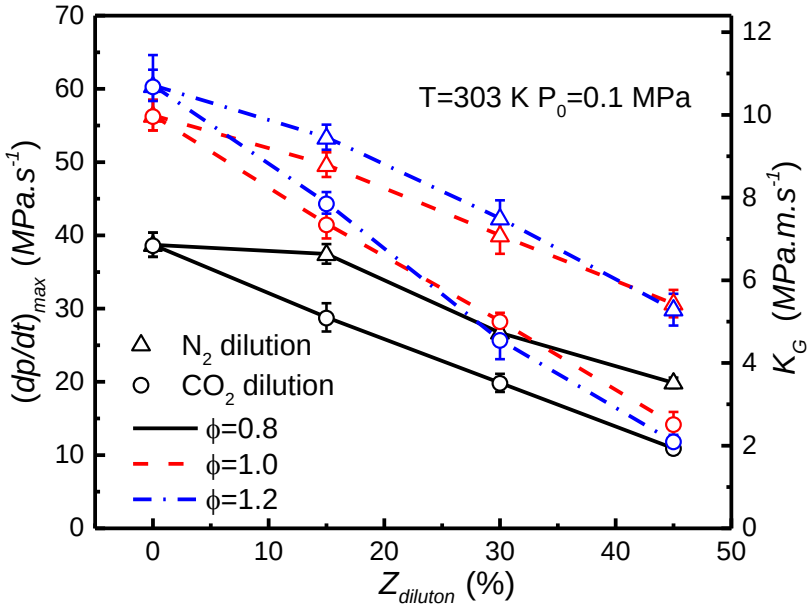

Figure 6.12 Maximum rate of pressure rise and deflagration index of N_2/CO_2 diluted $H_2/CO/CH_4$/air mixture at various dilution ratios

Table 6-5 Fitted parameters C_3, d_1 of $(dP/dt)_{max} = f(Z_{dilution})$ and correlation coefficients R^2 for the deflagration of bio-syngas/air mixture diluted with N_2/CO_2 at different equivalence ratios

	C_3	d_1	R^2
ϕ=0.8			
N_2	40.785±2.420	-0.449±0.080	0.896
CO_2	38.423±0.315	-0.615±0.011	0.999
ϕ=1.0			
N_2	57.214±0.870	-0.579±0.031	0.991
CO_2	56.105±0.386	-0.932±0.014	0.999
ϕ=1.2			
N_2	61.958±1.600	-0.686±0.050	0.979
CO_2	60.317±1.170	-1.097±0.041	0.996

6.6 Summary

In this chapter, the effects of fuel composition variation (H_2/CO/CH_4) and diluents (N_2/CO_2) on the explosion characteristics of bio-syngas/air mixtures were experimentally investigated in a constant volume combustion vessel over a wide range of fuel compositions and dilution ratios. Moreover, the dependence of pressure evolution on the initial pressure and equivalence ratio were also studied. The main results are summarized as follows:

It is found that the equivalence ratio has a strong influence on the pressure evolution during the explosion of a bio-syngas/air mixture. On the one hand, the explosion pressure increases with the increase of equivalence ratio and the maximum value of P_{max} occurs slightly on the rich side of the equivalence ratio. On the other hand, the maximum value of the normalized explosion pressure is not sensitive to the variation of initial pressure. However, the time for reaching the maximum explosion pressure and the maximum value of pressure rise rate significantly increases with the increase of initial pressure due to the decrease of the laminar flame speed.

For the effect of fuel composition variation, the results clearly show that the explosion pressure increases and the explosion time decreases with the increase of H_2 fraction in the fuel mixture. Moreover, there is a substantial increase in $(dP/dt)_{max}$ and K_G as the H_2 concentration is increased. This is mainly because the addition of H_2 can significantly increase the adiabatic flame temperature as well as the laminar

flame speed of the fuel mixture. However, the CH_4-enriched mixture has much lower explosion pressure and longer explosion time. $(dP/dt)_{max}$ and K_G also decrease with the increase of CH_4 fraction in the fuel mixture, indicating that increasing the concentration of CH_4 in the fuel mixture can significantly suppress the explosion hazard of a bio-syngas/air mixture. However, the explosion behaviors of CO-enriched mixtures change little compared to that of the basic condition, suggesting that increasing the concentration of CO in the fuel mixture plays a mild role in affecting the explosion characteristics of a bio-syngas.

With respect to the effect of diluents (N_2/CO_2), it is observed that when N_2/CO_2 is added to the fuel mixture, the explosion pressure decreases and the explosion time increases significantly with the increase of dilution ratio. The maximum rate of pressure rise and the deflagration index also progressively decrease with increasing dilution ratio. This is mainly because the addition of N_2/CO_2 to the fuel mixture can cause a decrease of the adiabatic flame temperature and the laminar flame speed due to the decrease of fuel content and total heat release. CO_2 is found to be more effective in suppressing the explosion hazard of a bio-syngas/air mixture than N_2 due to its stronger influence on the dilution effect, thermal effect, and chemical kinetic effect. In addition, corresponding correlations have been developed between the explosion pressure/explosion time/maximum rate of pressure rise and dilution ratio, which are useful for predicting the deflagration of bio-syngas/air mixture at various dilution ratios.

CHAPTER 7 CONCLUSIONS AND RECOMMENDATIONS

7.1 Conclusions of the present work

In this thesis, a detailed experimental and numerical investigation into the laminar premixed combustion and flame dynamics of bio-syngas fuels was conducted, with the main goal being to characterize the effect of fuel composition variation, different diluents, and initial conditions on their combustion behaviors. More specifically, this work first involved the experimental measurements of laminar flame speeds of bio-syngas under various operating conditions. The corresponding numerical simulation was also conducted by using the PREMIXED code in the CHEMKIN package with the Li mechanism to validate the chemical mechanism and clarify the thermal and chemical effects. Second, the intrinsic flame instabilities of the flame front of various bio-syngas/air mixtures were quantitatively analyzed by means of experimental measurements and theoretical analyses. Third, the explosion characteristics of various bio-syngas/air mixtures were also studied to evaluate the hazards of bio-syngas/air mixtures explosion. This study contributes several valuable insights and findings to improve the understanding on the combustion behaviors of bio-syngas fuels and provide some useful in information and guidelines for its application in practical combustors. The main conclusions drawn from this study are shown as follows:

7.1.1 Laminar flame speeds of bio-syngas/air mixtures

Experiments and numerical simulations were conducted to investigate the laminar flame speeds of bio-syngas/air mixtures under different fuel compositions (H_2/CO/CH_4), initial pressures (0.1 MPa/0.3 MPa/0.5 MPa), and different dilution ratios (N_2/CO_2, from 0% to 45%) at initial temperature of 303 K and wide range of equivalence ratios (0.6-1.5). For the effect of fuel composition variation, the experimental and predicted results using the Li mechanism show good agreement with each other, especially at fuel-lean conditions. With the increase of H_2 fraction in the fuel mixture, the overall reaction activity is strongly promoted, resulting in a significant increase in the laminar flame speed of H_2-enriched conditions compared to that of the αBasis condition. For the CO-enriched conditions, the laminar flame speed of the αCO-60 condition changes little compared to that of the αBasis condition, while the laminar flame speed of the αCO-80 condition is slightly decreased. It is observed that CO addition has more impact on the adiabatic flame temperature, but it plays a small role in the chemical kinetic effect compared to that of H_2 addition. For the CH_4-enriched conditions, the laminar flame speed decreases evidently compared to that of the αBasis condition, and is also lower than the CO-enriched conditions due to the combination of thermal and chemical kinetic effects of CH_4 addition.

For the effect of initial pressure study, the Li mechanism slightly overestimates the laminar flame speed for fuel-lean conditions, but slightly underestimates for the

fuel-rich conditions at elevated initial pressures. The laminar flame speed decreases with the increase of the initial pressure. This is mainly caused by the growing importance of the chain termination reactions in the overall reaction process and the increase of fuel mixture density as the initial pressure is increased.

For the effect of diluents study, the Li mechanism slightly underestimates the laminar flame speed of H_2/CO/CH_4/air mixture with N_2/CO_2 dilution at fuel-rich condition. As N_2/CO_2 is added to the fuel mixture, the laminar flame speed decreases obviously with the increase of dilution ratio. Furthermore, the results show that the reductions of laminar flame speeds for CO_2-diluted conditions are more substantial than that of the N_2-diluted conditions due to the stronger dilution effect, thermal-diffusion effect, and chemical effect of CO_2 dilution than that of N_2 dilution.

7.1.2 Laminar flame instabilities of bio-syngas/air mixtures

Experiments and theoretical calculations were conducted to study the intrinsic flame instabilities of outwardly expanding spherical flames of the bio-syngas/air mixtures at various fuel compositions, dilution ratios and equivalence ratios under atmospheric pressure and elevated initial pressures. For the propagation of laminar flame front at atmospheric pressure, the results of flame morphology and Markstein length show that the flame front tends to be stable with the increase of equivalence ratio at atmospheric pressure. With the increase of H_2 fraction in the fuel mixture, the Markstein length decreases compared to the other conditions, indicating that the

increase of H_2 concentration in the fuel mixture will decrease the stability of the flame front. Moreover, adding CH_4 or CO to the fuel mixture slightly increases the Markstein length, and the increases of the CH_4-enriched conditions are more substantial than that of the CO-enriched conditions, suggesting that the flame front stability is slightly enhanced with CH_4 addition at atmospheric pressure. For the effect of different diluents (N_2/CO_2) on the propagation of laminar flame front at atmospheric pressure, the results show that with N_2/CO_2 dilution, the Markstein length decreases at all dilution ratios, suggesting that the addition of N_2/CO_2 makes the flame front more sensitive to the stretch rate effects and promotes the flame instability at atmospheric pressure. Moreover, the CO_2-diluted mixture is more affected by preferential diffusion instabilities than that of the N_2-diluted mixture.

For the propagation of laminar flame front at elevated initial pressures, the results clearly show that with the increase of initial pressure, irregular wrinkles appear at the flame surface. Moreover, the higher the initial pressure, the more advance the onset of cellular instability of the flame is observed. The variation of fuel composition of H_2/CO/CH_4/air mixture has a strong influence on the cellular instabilities of the flame front at elevated initial pressure. With the increase of H_2 fraction in the fuel mixture, the cellular instabilities (including the diffusional-thermal instability and the hydrodynamic instability) of the flame front are significantly promoted due to the decrease of effective Lewis number and flame thickness, moreover, the earlier onset of cellular flame structure is also observed.

With the increase of CO fraction in the fuel mixture, both the effective Lewis number and the laminar flame thickness are slightly increased and the thermal expansion ratio is slightly decreased. Consequently, both the diffusional-thermal instability and hydrodynamic instability are inhibited and the moment for onset of cellular flame structure is postponed with increasing CO concentration in the fuel mixture. Finally, the results show that the cellular instabilities of the flame front are significantly suppressed with increasing CH_4 concentration in the fuel mixture. The moment for the onset of cellular instability of the flame front is also significantly delayed with CH_4 addition.

Regarding the effect of different diluents (N_2/CO_2) on the propagation of laminar flame front at elevated initial pressures, the results show that with N_2 or CO_2 dilution, the diffusional-thermal instability is increased by a decrease of the effective Lewis number, while the hydrodynamic instability is significantly suppressed by an increase of flame thickness and decrease of thermal expansion ratio, and thereby with a net result of suppression of cellular instability. Moreover, a comparison of the CO_2-diluted condition with N_2-diluted condition shows that CO_2 dilution has stronger effect in suppressing the flame instability at elevated initial pressure.

7.1.3 Explosion characteristics of bio-syngas/air mixtures

Experiments and theoretical calculations were conducted to study effects of fuel composition variation (H_2/CO/CH_4), dilution ratios (N_2/CO_2), and initial conditions on the explosion characteristics of bio-syngas/air mixtures. It is found that the

equivalence ratio has a strong influence on the pressure evolution during the explosion of bio-syngas/air mixtures, showing that the explosion pressure increases with the increase of equivalence ratio and the maximum value of P_{max} occurs slightly on the rich side of the equivalence ratio. On the other hand, the maximum value of normalized explosion pressure is not sensitive to the variation of initial pressure. However, the time for reaching the maximum explosion pressure significantly increases with the increase of initial pressure, so is the time for reaching the maximum value of pressure rise rate due to the decrease of laminar flame speed.

For the effect of fuel composition variation on the explosion characteristics of bio-syngas/air mixtures, the results clearly show that the explosion pressure increases and the explosion time decreases with the increase of H_2 fraction in the fuel mixture. Moreover, there is a substantial increase in $(dP/dt)_{max}$ and K_G as H_2 concentration is increased. This is mainly because the addition of H_2 can significantly increase the adiabatic flame temperature as well as the laminar flame speed of the fuel mixture. However, the CH_4-enriched mixture has much lower explosion pressure and longer explosion time. $(dP/dt)_{max}$ and K_G also decrease with the increase of CH_4 fraction in the fuel mixture, indicating that increasing concentration of CH_4 in the fuel mixture can significantly suppress the explosion hazard of a bio-syngas/air mixture. Additionally, the explosion behaviors of CO-enriched mixtures change little compared to that of the basic condition,

suggesting that increasing concentration of CO in the fuel mixture plays a mild role in affecting the explosion characteristics of bio-syngas.

For the effect of diluents (N_2/CO_2) on the explosion characteristics of bio-syngas/air mixtures, it is observed that when N_2/CO_2 is added to the fuel mixture, the explosion pressure decreases and the explosion time increases significantly with the increase of dilution ratio. The maximum rate of pressure rise and the deflagration index also progressively decrease with increasing N_2/CO_2 dilution. This is mainly because the addition of N_2/CO_2 to the fuel mixture can cause a decrease of adiabatic flame temperature and laminar flame speed due to the decrease of fuel content and total heat release. CO_2 is found to be more effective in suppressing the explosion hazard of a bio-syngas/air mixture than N_2 due to its stronger influence on the dilution effect, thermal effect, and chemical kinetic effect. In addition, corresponding correlations have been developed between the explosion pressure/explosion time/maximum rate of pressure rise and dilution ratio, which are useful for predicting the deflagration of bio-syngas/air mixture at various dilution ratios.

From the results of all the tested fuel mixtures in the present study, it can be concluded that H_2 addition can significantly increase the laminar flame speed of a bio-syngas/air mixture. The laminar flame front instability and explosion hazard are also strongly promoted by increasing H_2 fraction in the fuel mixture. But for the CH_4-enriched fuel mixtures, the combustion behaviors are quite the contrary, in

which CH_4 addition can evidently decrease the laminar flame speed and suppress the flame front instability as well as explosion hazard of a bio-syngas/air mixture. CO addition is found to play a mild role in affecting the laminar burning characteristics and explosion characteristics of a bio-syngas/air mixture. On the other hand, for the effect of different diluents, it can be concluded that bio-syngas with N_2/CO_2 dilution has much lower laminar flame speed, moreover, the intrinsic flame instability as well as explosion hazard are found to be suppressed compared to that of non-diluted bio-syngas. Unlike the single-component fuels, bio-syngas has multiple fuel components, which significantly increases the difficulty in controlling the combustion process. Therefore, the different combustion behaviors of diverse bio-syngas fuels need to be fully understood and considered for optimizing the combustion process of burning bio-syngas in practical combustors. Based on the experimental results of this study and the theoretical analysis on the effect of each fuel component on the combustion performance of bio-syngas, the potential bio-syngas users can predict the expected performance based on the composition of their bio-syngas and the requirements of their combustors to plan for the application and design of the combustors involved.

7.2 Recommendations

In this study, the fundamental investigation on the laminar premixed combustion and flame dynamics of bio-syngas has been systematically studied using a constant

volume combustion bomb system. Based on the results of the present study, the following are some recommendations for potential improvements and future work.

1. Our experimental data and numerical calculations using the Li mechanism show that there exist discrepancies in the laminar flame speeds of bio-syngas, especially at fuel-rich condition and elevated initial pressures. Previous researches [134, 139] found that the predicted results of laminar flame speeds of biomass derived gases using other chemical kinetic mechanisms such as the GRI 3.0 mechanism and San Diego mechanism also shown discrepancies compared to the experimental data. Therefore, it is necessary to continue to improve the accuracies of the prediction of laminar flame speeds using chemical kinetic mechanisms, especially at fuel-rich condition and elevated initial pressures.

2. On the other hand, it is important to recognize that although the effect of stretch rate and ignition disturbance have been eliminated in the extraction of experimental data for determining the laminar flame speed of bio-syngas in the present study, some degree of uncertainty may still exist in the rigor of the extrapolation methodologies (linear versus non-linear extrapolations) and the extraction range of the experimental data. More investigations are needed to improve the accuracy of the experimental data in the future. Moreover, due to the limitation of the experimental device used in the present study, the initial pressure can only be raised up to 0.5 MPa, it would be meaningful to measure

the accurate laminar flame speed of bio-syngas at high initial pressures and high initial temperatures since many practical combustors operate near these conditions.

3. For intrinsic flame instability study, although the existing linear theories of intrinsic flame instability can predict the onset of cellular flame structure by calculating the critical Peclet number and critical flame radius, there are large discrepancies between the experimental data and the predicted results as shown in Chapter 5. Therefore, efforts need be spent on further developing more accurate theoretical model for predicting the onset of cellular instabilities especially at elevated initial pressures. Massive experimental data concerning the evolution and development of the cellular flame structures on the flame surface for bio-syngas/air mixture are needed to support the completion of theoretical modeling. In addition, it would be meaningful to study the self-acceleration of cellular flames of bio-syngas/air flames at elevated initial pressure since previous studies [25, 175] have pointed out that the wrinkled flame front could accelerate the flame propagation speed and may even induce turbulent flame.

4. In the present study, the explosion characteristics of various bio-syngas/air mixtures were experimentally studied in a cylindrical constant volume combustion vessel. Numerical simulations and more theoretical analyses will help to validate the experimental data obtained using propagating spherical

flames. Moreover, as presented in Chapter 6, the correlations of $P_{max}/P_0=f(Z_{dilution})$, $t_c=f(Z_{dilution})$, and $(dP/dt)_{max}=f(Z_{dilution})$ have been developed for predicting the explosion behaviors of N_2/CO_2 diluted bio-syngas/air mixture at various dilution ratios. To improve the accuracy and reliability of the correlations, it would be useful to study a larger range of dilution ratios for providing more experimental data.

5. Since bio-syngas is expected to have the potential to substitute fossil fuel in heat and power generation, further attempts can be made on investigating the pollutant emission characteristics of burning various bio-syngas fuels. This will help us to have a comprehensive understanding and evaluation for the utilization of bio-syngas in practical combustion devices.

REFERENCE

[1] BP Statistical Review of World Energy 2018. https://wwwbpcom/en/global/corporate/energy-economics/statistical-review-of-world-energyhtml.

[2] BP Energy Outlook 2019 edition. https://wwwbpcom/en/global/corporate/energy-economics/energy-outlookhtml.

[3] Han J, Kim H. The reduction and control technology of tar during biomass gasification/pyrolysis: An overview. Renewable and Sustainable Energy Reviews. 2008;12:397-416.

[4] Bilandzija N, Voca N, Jelcic B, Jurisic V, Matin A, Grubor M, et al. Evaluation of Croatian agricultural solid biomass energy potential. Renewable and Sustainable Energy Reviews. 2018;93:225-30.

[5] Cardoen D, Joshi P, Diels L, Sarma PM, Pant D. Agriculture biomass in India: Part 1. Estimation and characterization. Resources, Conservation and Recycling. 2015;102:39-48.

[6] Demirbas A. Combustion characteristics of different biomass fuels. Progress in Energy and Combustion Science. 2004;30:219-30.

[7] Eldabbagh F, Ramesh A, Hawari J, Hutny W, Kozinski JA. Particle–metal interactions during combustion of pulp and paper biomass in a fluidized bed combustor. Combustion and Flame. 2005;142:249-57.

[8] Chaudhari S, Bej S, Bakhshi N, Dalai A. Steam gasification of biomass-derived char for the production of carbon monoxide-rich synthesis gas. Energy & Fuels. 2001;15:736-42.

[9] Chaudhari S, Dalai A, Bakhshi N. Production of hydrogen and/or syngas (H2+ CO) via steam gasification of biomass-derived chars. Energy & Fuels. 2003;17:1062-7.

[10] Hanaoka T, Inoue S, Uno S, Ogi T, Minowa T. Effect of woody biomass components on air-steam gasification. Biomass and Bioenergy. 2005;28:69-76.

[11] Lv P, Yuan Z, Ma L, Wu C, Chen Y, Zhu J. Hydrogen-rich gas production from biomass air and oxygen/steam gasification in a downdraft gasifier. Renewable Energy. 2007;32:2173-85.

[12] Lv P, Yuan Z, Wu C, Ma L, Chen Y, Tsubaki N. Bio-syngas production from biomass catalytic gasification. Energy Conversion and Management. 2007;48:1132-9.

[13] Panigrahi S, Dalai A, Chaudhari S, Bakhshi N. Synthesis gas production from steam gasification of biomass-derived oil. Energy & fuels. 2003;17:637-42.

[14] Tijmensen MJ, Faaij AP, Hamelinck CN, van Hardeveld MR. Exploration of the possibilities for production of Fischer Tropsch liquids and power via biomass gasification. Biomass and Bioenergy. 2002;23:129-52.

[15] Wang T, Chang J, Lv P. Synthesis gas production via biomass catalytic gasification with addition of biogas. Energy & fuels. 2005;19:637-44.

[16] Sutton D, Kelleher B, Ross JRH. Review of literature on catalysts for biomass gasification. Fuel Processing Technology. 2001;73:155-73.

[17] Cheng TS, Chang YC, Chao YC, Chen GB, Li YH, Wu CY. An experimental and numerical study on characteristics of laminar premixed H2/CO/CH4/air flames. International Journal of Hydrogen Energy. 2011;36:13207-17.

[18] Turns SR. An introduction to combustion: McGraw-hill New York; 1996.

[19] Law CK. Combustion physics: Cambridge University Press; 2010.

[20] Veynante D, Vervisch L. Turbulent combustion modeling. Progress in Energy and Combustion Science. 2002;28:193-266.

[21] Peters N. Turbulent combustion: Cambridge University Press; 2000.

[22] Clavin P. Dynamic behavior of premixed flame fronts in laminar and turbulent flows. Progress in Energy and Combustion Science. 1985;11:1-59.

[23] Xie Y, Wang X, Bi H, Yuan Y, Wang J, Huang Z, et al. A comprehensive review on laminar spherically premixed flame propagation of syngas. Fuel Processing Technology. 2018;181:97-114.

[24] Boughanem H, Trouvé A. The domain of influence of flame instabilities in turbulent premixed combustion. Symposium (International) on Combustion. 1998;27:971-8.

[25] Wu F, Jomaas G, Law CK. An experimental investigation on self-acceleration of cellular spherical flames. Proceedings of the Combustion Institute.

2013;34:937-45.

[26] Hu E, Tian H, Zhang X, Li X, Huang Z. Explosion characteristics of n-butanol/iso-octane-air mixtures. Fuel. 2017;188:90-7.

[27] Tang C, Huang Z, Jin C, He J, Wang J, Wang X, et al. Explosion characteristics of hydrogen–nitrogen–air mixtures at elevated pressures and temperatures. International Journal of Hydrogen Energy. 2009;34:554-61.

[28] Egolfopoulos FN, Hansen N, Ju Y, Kohse-Höinghaus K, Law CK, Qi F. Advances and challenges in laminar flame experiments and implications for combustion chemistry. Progress in Energy and Combustion Science. 2014;43:36-67.

[29] Echekki T, Mungal M. Flame speed measurements at the tip of a slot burner: Effects of flame curvature and hydrodynamic stretch. Symposium (International) on Combustion: Elsevier; 1991. p. 455-61.

[30] Wu C, Law CK. On the determination of laminar flame speeds from stretched flames. Symposium (International) on Combustion: Elsevier; 1985. p. 1941-9.

[31] Egolfopoulos F, Zhu D, Law CK. Experimental and numerical determination of laminar flame speeds: Mixtures of C2-hydrocarbons with oxygen and nitrogen. Symposium (International) on Combustion: Elsevier; 1991. p. 471-8.

[32] Vagelopoulos C, Egolfopoulos F, Law CK. Further considerations on the determination of laminar flame speeds with the counterflow twin-flame technique. Symposium (international) on Combustion: Elsevier; 1994. p. 1341-7.

[33] Veloo PS, Wang YL, Egolfopoulos FN, Westbrook CK. A comparative experimental and computational study of methanol, ethanol, and n-butanol flames. Combustion and Flame. 2010;157:1989-2004.

[34] Kee RJ, Miller JA, Evans GH, Dixon-Lewis G. A computational model of the structure and extinction of strained, opposed flow, premixed methane-air flames. Symposium (International) on Combustion: Elsevier; 1989. p. 1479-94.

[35] Botha J, Spalding DB. The laminar flame speed of propane/air mixtures with heat extraction from the flame. Proceedings of the Royal Society of London Series A Mathematical and Physical Sciences. 1954;225:71-96.

[36] De Goey L, Van Maaren A, Quax R. Stabilization of adiabatic premixed laminar flames on a flat flame burner. Combustion Science and Technology. 1993;92:201-7.

[37] Konnov AA, Dyakov IV. Measurement of propagation speeds in adiabatic cellular premixed flames of CH4+ O2+ CO2. Experimental Thermal and Fluid Science. 2005;29:901-7.

[38] Stevens F. The rate of flame propagation in gaseous explosive reactions1. Journal of the American Chemical Society. 1926;48:1896-906.

[39] Lewis B, Von Elbe G. Determination of the speed of flames and the temperature distribution in a spherical bomb from time‐pressure explosion records. The Journal of Chemical Physics. 1934;2:283-90.

[40] Clavin P, Williams F. Effects of molecular diffusion and of thermal expansion on the structure and dynamics of premixed flames in turbulent flows of large scale and low intensity. Journal of Fluid Mechanics. 1982;116:251-82.

[41] Matalon M, Matkowsky BJ. Flames as gasdynamic discontinuities. Journal of Fluid Mechanics. 1982;124:239-59.

[42] Bechtold J, Matalon M. Hydrodynamic and diffusion effects on the stability of spherically expanding flames. Combustion and Flame. 1987;67:77-90.

[43] Huang Z, Zhang Y, Zeng K, Liu B, Wang Q, Jiang D. Measurements of laminar burning velocities for natural gas–hydrogen–air mixtures. Combustion and Flame. 2006;146:302-11.

[44] Akhtar A, Krepl V, Ivanova T. A combined overview of combustion, pyrolysis, and gasification of biomass. Energy & fuels. 2018;32:7294-318.

[45] Rubin EM. Genomics of cellulosic biofuels. Nature. 2008;454:841.

[46] Goyal HB, Seal D, Saxena RC. Bio-fuels from thermochemical conversion of renewable resources: A review. Renewable and Sustainable Energy Reviews. 2008;12:504-17.

[47] Long H, Li X, Wang H, Jia J. Biomass resources and their bioenergy potential estimation: A review. Renewable and Sustainable Energy Reviews. 2013;26:344-52.

[48] Wang S, Dai G, Yang H, Luo Z. Lignocellulosic biomass pyrolysis mechanism: A state-of-the-art review. Progress in Energy and Combustion Science. 2017;62:33-86.

[49] Van Wyk JP. Biotechnology and the utilization of biowaste as a resource for bioproduct development. TRENDS in Biotechnology. 2001;19:172-7.

[50] Del Río JC, Marques G, Rencoret J, Martínez ÁT, Gutiérrez A. Occurrence of naturally acetylated lignin units. Journal of Agricultural and Food Chemistry. 2007;55:5461-8.

[51] Dasappa S. Thermochemical conversion of biomass. Transformation of Biomass: Theory to Practice. 2014:133-57.

[52] Rover M, Smith R, Brown RC. Enabling biomass combustion and co-firing through the use of Lignocol. Fuel. 2018;211:312-7.

[53] Jr JJB, Hughes EE, Tillman DA. Biomass cofiring at Seward Station. Biomass and Bioenergy. 2000;19:419-27.

[54] Brown RC. Thermochemical processing of biomass: conversion into fuels, Chemicals and Power: Wiley; 2019.

[55] Kwietniewska E, Tys J. Process characteristics, inhibition factors and methane yields of anaerobic digestion process, with particular focus on microalgal biomass fermentation. Renewable and Sustainable Energy Reviews. 2014;34:491-500.

[56] Limayem A, Ricke SC. Lignocellulosic biomass for bioethanol production: Current perspectives, potential issues and future prospects. Progress in Energy and Combustion Science. 2012;38:449-67.

[57] Mazaheri N, Akbarzadeh AH, Madadian E, Lefsrud M. Systematic review of research guidelines for numerical simulation of biomass gasification for bioenergy production. Energy Conversion and Management. 2019;183:671-88.

[58] Munasinghe PC, Khanal SK. Biomass-derived syngas fermentation into biofuels: Opportunities and challenges. Bioresour Technol. 2010;101:5013-22.

[59] García-Aparicio MP, Ballesteros I, González A, Oliva JM, Ballesteros M, Negro MJ. Effect of inhibitors released during steam-explosion pretreatment of barley straw on enzymatic hydrolysis. Applied Biochemistry and Biotechnology. 2006;129:278-88.

[60] Lehmann J, Joseph S. Biochar for environmental management: an introduction. Biochar for Environmental Management: Routledge; 2015. p. 33-46.

[61] Kumar A, Jones DD, Hanna MA. Thermochemical Biomass Gasification: A Review of the Current Status of the Technology. Energies. 2009;2:556-81.

[62] Molino A, Chianese S, Musmarra D. Biomass gasification technology: The

state of the art overview. Journal of Energy Chemistry. 2016;25:10-25.

[63] Klass DL. Biomass for Renewable Energy and Fuels. In: Cleveland CJ, editor. Encyclopedia of Energy. New York: Elsevier; 2004. p. 193-212.

[64] Henrich E, Weirich F. Pressurized entrained flow gasifiers for biomass. Environmental Engineering Science. 2004;21:53-64.

[65] Knoef H, Ahrenfeldt J. Handbook biomass gasification: BTG Biomass Technology Group The Netherlands; 2005.

[66] Sharma S, Sheth PN. Air–steam biomass gasification: Experiments, modeling and simulation. Energy Conversion and Management. 2016;110:307-18.

[67] Baruah D, Baruah DC. Modeling of biomass gasification: A review. Renewable and Sustainable Energy Reviews. 2014;39:806-15.

[68] Loha C, Chattopadhyay H, Chatterjee PK. Three dimensional kinetic modeling of fluidized bed biomass gasification. Chemical Engineering Science. 2014;109:53-64.

[69] Materazzi M, Lettieri P, Mazzei L, Taylor R, Chapman C. Thermodynamic modelling and evaluation of a two-stage thermal process for waste gasification. Fuel. 2013;108:356-69.

[70] Wang J, Cheng G, You Y, Xiao B, Liu S, He P, et al. Hydrogen-rich gas production by steam gasification of municipal solid waste (MSW) using NiO supported on modified dolomite. International Journal of Hydrogen Energy. 2012;37:6503-10.

[71] Wei L, Xu S, Zhang L, Liu C, Zhu H, Liu S. Steam gasification of biomass for hydrogen-rich gas in a free-fall reactor. International Journal of Hydrogen Energy. 2007;32:24-31.

[72] Lucas C, Szewczyk D, Blasiak W, Mochida S. High-temperature air and steam gasification of densified biofuels. Biomass and Bioenergy. 2004;27:563-75.

[73] Tang Y, Ma X, Wang Z, Wu Z, Yu Q. A study of the thermal degradation of six typical municipal waste components in CO2 and N2 atmospheres using TGA-FTIR. Thermochimica Acta. 2017;657:12-9.

[74] Azuara M, Sáiz E, Manso JA, García-Ramos FJ, Manyà JJ. Study on the effects of using a carbon dioxide atmosphere on the properties of vine shoots-derived

biochar. Journal of Analytical and Applied Pyrolysis. 2017;124:719-25.

[75] Gupta M, Pramanik S, Ravikrishna RV. Development of a syngas-fired catalytic combustion system for hybrid solar-thermal applications. Applied Thermal Engineering. 2016;109:1023-30.

[76] Kohsri S, Meechai A, Prapainainar C, Narataruksa P, Hunpinyo P, Sin G. Design and preliminary operation of a hybrid syngas/solar PV/battery power system for off-grid applications: A case study in Thailand. Chemical Engineering Research and Design. 2018;131:346-61.

[77] Hacker V, Faleschini G, Fuchs H, Fankhauser R, Simader G, Ghaemi M, et al. Usage of biomass gas for fuel cells by the SIR process. Journal of Power Sources. 1998;71:226-30.

[78] Donolo G, Simon GD, Fermeglia M. Steady state simulation of energy production from biomass by molten carbonate fuel cells. Journal of Power Sources. 2006;158:1282-9.

[79] Tomasi C, Baratieri M, Bosio B, Arato E, Baggio P. Process analysis of a molten carbonate fuel cell power plant fed with a biomass syngas. Journal of Power Sources. 2006;157:765-74.

[80] Morita H, Yoshiba F, Woudstra N, Hemmes K, Spliethoff H. Feasibility study of wood biomass gasification/molten carbonate fuel cell power system—comparative characterization of fuel cell and gas turbine systems. Journal of Power Sources. 2004;138:31-40.

[81] Indrawan N, Thapa S, Bhoi PR, Huhnke RL, Kumar A. Electricity power generation from co-gasification of municipal solid wastes and biomass: Generation and emission performance. Energy. 2018;162:764-75.

[82] Kohn MP, Lee J, Basinger ML, Castaldi MJ. Performance of an Internal Combustion Engine Operating on Landfill Gas and the Effect of Syngas Addition. Industrial & Engineering Chemistry Research. 2011;50:3570-9.

[83] Hagos FY, A. Aziz AR, Sulaiman SA. Methane enrichment of syngas (H2/CO) in a spark-ignition direct-injection engine: Combustion, performance and emissions comparison with syngas and Compressed Natural Gas. Energy. 2015;90:2006-15.

[84] Kan X, Zhou D, Yang W, Zhai X, Wang C-H. An investigation on utilization of biogas and syngas produced from biomass waste in premixed spark ignition engine. Applied Energy. 2018;212:210-22.

[85] Joshi MM, Lee S. Integrated gasification combined cycle—a review of IGCC technology. Energy Sources. 1996;18:537-68.

[86] Ståhl K, Neergaard M. IGCC power plant for biomass utilisation, Värnamo, Sweden. Biomass and Bioenergy. 1998;15:205-11.

[87] de Souza-Santos M. A feasibility study of an alternative power generation system based on biomass gasification/gas turbine concept. Fuel. 1999;78:529-38.

[88] Fagbenle RL, Oguaka ABC, Olakoyejo OT. A thermodynamic analysis of a biogas-fired integrated gasification steam injected gas turbine (BIG/STIG) plant. Applied Thermal Engineering. 2007;27:2220-5.

[89] Ge H, Zhang H, Guo W, Song T, Shen L. System simulation and experimental verification: Biomass-based integrated gasification combined cycle (BIGCC) coupling with chemical looping gasification (CLG) for power generation. Fuel. 2019;241:118-28.

[90] Mínguez M, Jiménez Á, Rodríguez J, González C, López I, Nieto R. Analysis of energetic and exergetic efficiency, and environmental benefits of biomass integrated gasification combined cycle technology. Waste Management & Research. 2013;31:401-12.

[91] Srinivas T, Reddy BV, Gupta AVSSKS. Thermal Performance Prediction of a Biomass Based Integrated Gasification Combined Cycle Plant. Journal of Energy Resources Technology. 2012;134:021002--9.

[92] Baratieri M, Baggio P, Bosio B, Grigiante M, Longo GA. The use of biomass syngas in IC engines and CCGT plants: A comparative analysis. Applied Thermal Engineering. 2009;29:3309-18.

[93] Tchapda A, Pisupati S. A Review of Thermal Co-Conversion of Coal and Biomass/Waste. Energies. 2014;7:1098-148.

[94] Caputo J, Hacker J. Biomass cofiring: a transition to a low-carbon future. Environmental and Energy Study Institute: Washington, DC, USA. 2009.

[95] Mann M, Spath P. A life cycle assessment of biomass cofiring in a coal-fired power plant. Clean Products and Processes. 2001;3:81-91.

[96] Reichling JP, Kulacki FA. Comparative analysis of Fischer–Tropsch and integrated gasification combined cycle biomass utilization. Energy. 2011;36:6529-35.

[97] Bhattacharya A, Datta A. Effects of supplementary biomass firing on the performance of combined cycle power generation: A comparison between NGCC and IGCC plants. Biomass and Bioenergy. 2013;54:239-49.

[98] Wu Z, OuYang D. Technical-economical Analysis on Co-gasification of Coal and Biomass Based on the IGCC System with a Two-staged Gasifier. Energy Procedia. 2017;142:774-9.

[99] Thallam Thattai A, Oldenbroek V, Schoenmakers L, Woudstra T, Aravind PV. Experimental model validation and thermodynamic assessment on high percentage (up to 70%) biomass co-gasification at the 253MWe integrated gasification combined cycle power plant in Buggenum, The Netherlands. Applied Energy. 2016;168:381-93.

[100] Kwon OC, Faeth GM. Flame/stretch interactions of premixed hydrogen-fueled flames: measurements and predictions. Combustion and Flame. 2001;124:590-610.

[101] Hu E, Huang Z, He J, Miao H. Experimental and numerical study on laminar burning velocities and flame instabilities of hydrogen–air mixtures at elevated pressures and temperatures. International Journal of Hydrogen Energy. 2009;34:8741-55.

[102] Lamoureux N, Djebaıli-Chaumeix N, Paillard C-E. Laminar flame velocity determination for H2–air–He–CO2 mixtures using the spherical bomb method. Experimental Thermal and Fluid Science. 2003;27:385-93.

[103] Hu E, Li X, Meng X, Chen Y, Cheng Y, Xie Y, et al. Laminar flame speeds and ignition delay times of methane–air mixtures at elevated temperatures and pressures. Fuel. 2015;158:1-10.

[104] Liao S, Jiang D, Cheng Q. Determination of laminar burning velocities for natural gas. Fuel. 2004;83:1247-50.

[105] Gu XJ, Haq MZ, Lawes M, Woolley R. Laminar burning velocity and Markstein lengths of methane–air mixtures. Combustion and Flame. 2000;121:41-58.

[106] Liao S, Jiang D, Gao J, Huang Z. Measurements of Markstein numbers and laminar burning velocities for natural gas− air mixtures. Energy & fuels. 2004;18:316-26.

[107] Li Q, Fu J, Wu X, Tang C, Huang Z. Laminar Flame Speeds of DMF/Iso-octane-Air-N2/CO2Mixtures. Energy & Fuels. 2012;26:917-25.

[108] Li Q, Hu E, Cheng Y, Huang Z. Measurements of laminar flame speeds and flame instability analysis of 2-methyl-1-butanol–air mixtures. Fuel. 2013;112:263-71.

[109] Li Q, Jin W, Huang Z. Laminar Flame Characteristics of C1–C5 Primary Alcohol-Isooctane Blends at Elevated Temperature. Energies. 2016;9:511.

[110] Li Q, Tang C, Cheng Y, Guan L, Huang Z. Laminar Flame Speeds and Kinetic Modeling ofn-Pentanol and Its Isomers. Energy & Fuels. 2015;29:5334-48.

[111] Miao J, Leung CW, Huang Z, Cheung CS, Yu H, Xie Y. Laminar burning velocities, Markstein lengths, and flame thickness of liquefied petroleum gas with hydrogen enrichment. International Journal of Hydrogen Energy. 2014;39:13020-30.

[112] Hu E, Huang Z, He J, Jin C, Zheng J. Experimental and numerical study on laminar burning characteristics of premixed methane–hydrogen–air flames. International Journal of Hydrogen Energy. 2009;34:4876-88.

[113] Hu E, Huang Z, He J, Miao H. Experimental and numerical study on lean premixed methane–hydrogen–air flames at elevated pressures and temperatures. International Journal of Hydrogen Energy. 2009;34:6951-60.

[114] Hu E, Huang Z, He J, Zheng J, Miao H. Measurements of laminar burning velocities and onset of cellular instabilities of methane–hydrogen–air flames at elevated pressures and temperatures. International Journal of Hydrogen Energy. 2009;34:5574-84.

[115] Halter F, Chauveau C, Djebaili-Chaumeix N, Gökalp I. Characterization of the effects of pressure and hydrogen concentration on laminar burning velocities of methane–hydrogen–air mixtures. Proceedings of the Combustion Institute. 2005;30:201-8.

[116] Law C, Kwon O. Effects of hydrocarbon substitution on atmospheric hydrogen–air flame propagation. International Journal of Hydrogen Energy. 2004;29:867-79.

[117] Hu E, Fu J, Pan L, Jiang X, Huang Z, Zhang Y. Experimental and numerical study on the effect of composition on laminar burning velocities of H2/CO/N2/CO2/air mixtures. International Journal of Hydrogen Energy. 2012;37:18509-19.

[118] Burbano HJ, Pareja J, Amell AA. Laminar burning velocities and flame stability analysis of syngas mixtures at sub-atmospheric pressures. International

Journal of Hydrogen Energy. 2011;36:3243-52.

[119] Li H-M, Li G-X, Sun Z-Y, Zhai Y, Zhou Z-H. Measurement of the laminar burning velocities and markstein lengths of lean and stoichiometric syngas premixed flames under various hydrogen fractions. International Journal of Hydrogen Energy. 2014;39:17371-80.

[120] Das AK, Kumar K, Sung C-J. Laminar flame speeds of moist syngas mixtures. Combustion and Flame. 2011;158:345-53.

[121] Varghese RJ, Kolekar H, Hariharan V, Kumar S. Effect of CO content on laminar burning velocities of syngas-air premixed flames at elevated temperatures. Fuel. 2018;214:144-53.

[122] Zhang W, Gou X, Kong W, Chen Z. Laminar flame speeds of lean high-hydrogen syngas at normal and elevated pressures. Fuel. 2016;181:958-63.

[123] Dong C, Zhou Q, Zhao Q, Zhang Y, Xu T, Hui S. Experimental study on the laminar flame speed of hydrogen/carbon monoxide/air mixtures. Fuel. 2009;88:1858-63.

[124] Sánchez AL, Williams FA. Recent advances in understanding of flammability characteristics of hydrogen. Progress in Energy and Combustion Science. 2014;41:1-55.

[125] Tang CL, Huang ZH, Law CK. Determination, correlation, and mechanistic interpretation of effects of hydrogen addition on laminar flame speeds of hydrocarbon–air mixtures. Proceedings of the Combustion Institute. 2011;33:921-8.

[126] Rightley M, Williams F. Burning velocities of CO flames. Combustion and flame. 1997;110:285-97.

[127] Troe J. Modeling the temperature and pressure dependence of the reaction HO+ CO ixHOCO ixH+ CO2. Symposium (International) on Combustion: Elsevier; 1998. p. 167-75.

[128] Ai Y, Zhou Z, Chen Z, Kong W. Laminar flame speed and Markstein length of syngas at normal and elevated pressures and temperatures. Fuel. 2014;137:339-45.

[129] Lee MC, Yoon J, Joo S, Kim J, Hwang J, Yoon Y. Investigation into the cause of high multi-mode combustion instability of H2/CO/CH4 syngas in a partially premixed gas turbine model combustor. Proceedings of the Combustion Institute. 2015;35:3263-71.

[130] Vagelopoulos CM, Egolfopoulos FN. Laminar flame speeds and extinction strain rates of mixtures of carbon monoxide with hydrogen, methane, and air. Symposium (International) on Combustion. 1994;25:1317-23.

[131] Wu CY, Chao YC, Cheng TS, Chen CP, Ho CT. Effects of CO addition on the characteristics of laminar premixed CH4/air opposed-jet flames. Combustion and Flame. 2009;156:362-73.

[132] Yan B, Wu Y, Liu C, Yu J, Li B, Li Z, et al. Experimental and modeling study of laminar burning velocity of biomass derived gases/air mixtures. International Journal of Hydrogen Energy. 2011;36:3769-77.

[133] Monteiro E, Bellenoue M, Sotton J, Moreira NA, Malheiro S. Laminar burning velocities and Markstein numbers of syngas–air mixtures. Fuel. 2010;89:1985-91.

[134] Liu C, Yan B, Chen G, Bai XS. Structures and burning velocity of biomass derived gas flames. International Journal of Hydrogen Energy. 2010;35:542-55.

[135] Liu J, Zhang X, Wang T, Hou X, Zhang J, Zheng S. Numerical study of the chemical, thermal and diffusion effects of H2 and CO addition on the laminar flame speeds of methane–air mixture. International Journal of Hydrogen Energy. 2015;40:8475-83.

[136] Zhang K, Jiang X. An investigation of fuel variability effect on bio-syngas combustion using uncertainty quantification. Fuel. 2018;220:283-95.

[137] Smith GP, Golden DM, Frenklach M, Moriarty NW, Eiteneer B, Goldenberg M,et al. GRI 3.0, http://www.me.berkeley.edu/gri_mech/.

[138] Chemical Kinetic Mechanism for Combustion Applications Center for Energy Research (Combustion Division), University of California at San Diego http:// maewebucsdedu/combustion/.

[139] Vu TM, Song WS, Park J, Bae DS, You HS. Measurements of propagation speeds and flame instabilities in biomass derived gas–air premixed flames. International Journal of Hydrogen Energy. 2011;36:12058-67.

[140] Zhang Y, Shen W, Zhang H, Wu Y, Lu J. Effects of inert dilution on the propagation and extinction of lean premixed syngas/air flames. Fuel. 2015;157:115-21.

[141] Hermanns R, Konnov AA, Bastiaans R, De Goey L. Laminar burning

velocities of diluted hydrogen− oxygen− nitrogen mixtures. Energy & Fuels. 2007;21:1977-81.

[142] Hu E, Jiang X, Huang Z, Iida N. Numerical Study on the Effects of Diluents on the Laminar Burning Velocity of Methane–Air Mixtures. Energy & Fuels. 2012;26:4242-52.

[143] Mitu M, Prodan M, Giurcan V, Razus D, Oancea D. Influence of inert gas addition on propagation indices of methane–air deflagrations. Process Safety and Environmental Protection. 2016;102:513-22.

[144] Weng WB, Wang ZH, He Y, Whiddon R, Zhou YJ, Li ZS, et al. Effect of N2/CO2 dilution on laminar burning velocity of H2–CO–O2 oxy-fuel premixed flame. International Journal of Hydrogen Energy. 2015;40:1203-11.

[145] Xie Y, Wang J, Xu N, Yu S, Huang Z. Comparative study on the effect of CO2 and H2O dilution on laminar burning characteristics of CO/H2/air mixtures. International Journal of Hydrogen Energy. 2014;39:3450-8.

[146] Prathap C, Ray A, Ravi MR. Investigation of nitrogen dilution effects on the laminar burning velocity and flame stability of syngas fuel at atmospheric condition. Combustion and Flame. 2008;155:145-60.

[147] Prathap C, Ray A, Ravi MR. Effects of dilution with carbon dioxide on the laminar burning velocity and flame stability of H2–CO mixtures at atmospheric condition. Combustion and Flame. 2012;159:482-92.

[148] Shang R, Zhang Y, Zhu M, Zhang Z, Zhang D, Li G. Laminar flame speed of CO2 and N2 diluted H2/CO/air flames. International Journal of Hydrogen Energy. 2016;41:15056-67.

[149] Liu F, Guo H, Smallwood GJ. The chemical effect of CO2 replacement of N2 in air on the burning velocity of CH4 and H2 premixed flames. Combustion and Flame. 2003;133:495-7.

[150] Smithells A, Ingle H. XV.—The structure and chemistry of flames. Journal of the Chemical Society, Transactions. 1892;61:204-16.

[151] Smith FA, Pickering SF. Bunsen Flames of Unusual Structure1. Industrial & Engineering Chemistry. 1928;20:1012-3.

[152] Markstein G. Experimental studies of flame-front instability. AGARDograph: Elsevier; 1964. p. 75-105.

[153] Vu TM, Park J, Kwon OB, Kim JS. Effects of hydrocarbon addition on cellular instabilities in expanding syngas–air spherical premixed flames. International Journal of Hydrogen Energy. 2009;34:6961-9.

[154] Darrieus G. Propagation d'un front de flamme. La Technique Moderne. 1938;30:18.

[155] Landau L. On the theory of slow combustion. Acta Physicochim (USSR). 1944;19:77-85.

[156] Markstein GH. Nonsteady flame propagation: AGARDograph: Elsevier; 2014.

[157] Sivashinsky G. Diffusional-thermal theory of cellular flames. Combustion Science and Technology. 1977;15:137-45.

[158] Sharp DH. Overview of Rayleigh-taylor instability. Los Alamos National Lab., NM (USA); 1983.

[159] Lapalme D, Halter F, Mounaïm-Rousselle C, Seers P. Characterization of thermodiffusive and hydrodynamic mechanisms on the cellular instability of syngas fuel blended with CH4 or CO2. Combustion and Flame. 2018;193:481-90.

[160] Beeckmann J, Hesse R, Kruse S, Berens A, Peters N, Pitsch H, et al. Propagation speed and stability of spherically expanding hydrogen/air flames: Experimental study and asymptotics. Proceedings of the Combustion Institute. 2017;36:1531-8.

[161] Kim W, Imamura T, Mogi T, Dobashi R. Experimental investigation on the onset of cellular instabilities and acceleration of expanding spherical flames. International Journal of Hydrogen Energy. 2017;42:14821-8.

[162] Kim W, Sato Y, Johzaki T, Endo T, Shimokuri D, Miyoshi A. Experimental study on self-acceleration in expanding spherical hydrogen-air flames. International Journal of Hydrogen Energy. 2018;43:12556-64.

[163] Matsugi A, Terashima H. Diffusive-thermal effect on local chemical structures in premixed hydrogen–air flames. Combustion and Flame. 2017;179:238-41.

[164] Tse SD, Zhu DL, Law CK. Morphology and burning rates of expanding spherical flames in H2/O2/inert mixtures up to 60 atmospheres. Proceedings of the Combustion Institute. 2000;28:1793-800.

[165] Jiang Y-H, Li G-X, Li H-M, Li L, Tian L-L. Study on the influence of flame

inherent instabilities on crack propagation of expanding premixed flame. Fuel. 2018;233:504-12.

[166] Cai X, Wang J, Zhao H, Zhang M, Huang Z. Flame morphology and self-acceleration of syngas spherically expanding flames. International Journal of Hydrogen Energy. 2018;43:17531-41.

[167] Li H-M, Li G-X, Jiang Y-H. Laminar burning velocities and flame instabilities of diluted H2/CO/air mixtures under different hydrogen fractions. International Journal of Hydrogen Energy. 2018;43:16344-54.

[168] Vu TM, Park J, Kwon OB, Bae DS, Yun JH, Keel SI. Effects of diluents on cellular instabilities in outwardly propagating spherical syngas–air premixed flames. International Journal of Hydrogen Energy. 2010;35:3868-80.

[169] Law CK, Kwon OC. Effects of hydrocarbon substitution on atmospheric hydrogen–air flame propagation. International Journal of Hydrogen Energy. 2004;29:867-79.

[170] Law CK, Jomaas G, Bechtold JK. Cellular instabilities of expanding hydrogen/propane spherical flames at elevated pressures: theory and experiment. Proceedings of the Combustion Institute. 2005;30:159-67.

[171] Okafor EC, Nagano Y, Kitagawa T. Experimental and theoretical analysis of cellular instability in lean H2-CH4-air flames at elevated pressures. International Journal of Hydrogen Energy. 2016;41:6581-92.

[172] Vu TM, Park J, Kim JS, Kwon OB, Yun JH, Keel SI. Experimental study on cellular instabilities in hydrocarbon/hydrogen/carbon monoxide–air premixed flames. International Journal of Hydrogen Energy. 2011;36:6914-24.

[173] Lapalme D, Lemaire R, Seers P. Assessment of the method for calculating the Lewis number of H2/CO/CH4 mixtures and comparison with experimental results. International Journal of Hydrogen Energy. 2017;42:8314-28.

[174] Zhang X, Tang C, Yu H, Huang Z. Flame-front instabilities of outwardly expanding isooctane/n-butanol blend–air flames at elevated pressures. Energy & Fuels. 2014;28:2258-66.

[175] Xie Y, Wang J, Cai X, Huang Z. Self-acceleration of cellular flames and laminar flame speed of syngas/air mixtures at elevated pressures. International Journal of Hydrogen Energy. 2016;41:18250-8.

[176] Movileanu C, Gosa V, Razus D. Explosion of gaseous ethylene–air mixtures in closed cylindrical vessels with central ignition. Journal of Hazardous Materials. 2012;235-236:108-15.

[177] Kindracki J, Kobiera A, Rarata G, Wolanski P. Influence of ignition position and obstacles on explosion development in methane–air mixture in closed vessels. Journal of Loss Prevention in the Process Industries. 2007;20:551-61.

[178] Park DJ, Lee YS, Green AR. Prediction for vented explosions in chambers with multiple obstacles. Journal of Hazardous Materials. 2008;155:183-92.

[179] Park DJ, Lee YS, Green AR. Experiments on the effects of multiple obstacles in vented explosion chambers. Journal of Hazardous Materials. 2008;153:340-50.

[180] Razus D, Brinzea V, Mitu M, Movileanu C, Oancea D. Temperature and pressure influence on maximum rates of pressure rise during explosions of propane–air mixtures in a spherical vessel. Journal of Hazardous Materials. 2011;190:891-6.

[181] Razus D, Brinzea V, Mitu M, Oancea D. Temperature and pressure influence on explosion pressures of closed vessel propane–air deflagrations. Journal of Hazardous Materials. 2010;174:548-55.

[182] Razus D, Movileanua C, Oancea D. The rate of pressure rise of gaseous propylene–air explosions in spherical and cylindrical enclosures. Journal of hazardous materials. 2007;139:1-8.

[183] Faghih M, Gou X, Chen Z. The explosion characteristics of methane, hydrogen and their mixtures: A computational study. Journal of Loss Prevention in the Process Industries. 2016;40:131-8.

[184] Tang C, Zhang S, Si Z, Huang Z, Zhang K, Jin Z. High methane natural gas/air explosion characteristics in confined vessel. Journal of Hazardous Materials. 2014;278:520-8.

[185] Crowl DA, Jo Y-D. The hazards and risks of hydrogen. Journal of Loss Prevention in the Process Industries. 2007;20:158-64.

[186] Dahoe AE. Laminar burning velocities of hydrogen–air mixtures from closed vessel gas explosions. Journal of Loss Prevention in the Process Industries. 2005;18:152-66.

[187] Jo YD, Crowl DA. Explosion characteristics of hydrogen‐air mixtures in a spherical vessel. Process Safety Progress. 2010;29:216-23.

[188] Ng HD, Ju Y, Lee JH. Assessment of detonation hazards in high-pressure hydrogen storage from chemical sensitivity analysis. International Journal of Hydrogen Energy. 2007;32:93-9.

[189] Cammarota F, Di Benedetto A, Russo P, Salzano E. Experimental analysis of gas explosions at non-atmospheric initial conditions in cylindrical vessel. Process Safety and Environmental Protection. 2010;88:341-9.

[190] Mogi T, Horiguchi S. Explosion and detonation characteristics of dimethyl ether. Journal of Hazardous Materials. 2009;164:114-9.

[191] Razus D, Brinzea V, Mitu M, Movileanu C, Oancea D. Inerting effect of the combustion products on the confined deflagration of liquefied petroleum gas–air mixtures. Journal of Loss Prevention in the Process Industries. 2009;22:463-8.

[192] Razus D, Brinzea V, Mitu M, Oancea D. Explosion characteristics of LPG–air mixtures in closed vessels. Journal of Hazardous Materials. 2009;165:1248-52.

[193] Razus D, Movileanu C, Brinzea V, Oancea D. Explosion pressures of hydrocarbon–air mixtures in closed vessels. Journal of Hazardous Materials. 2006;135:58-65.

[194] Razus D, Oancea D, Movileanu C. Burning velocity evaluation from pressure evolution during the early stage of closed-vessel explosions. Journal of Loss Prevention in the Process Industries. 2006;19:334-42.

[195] Zhang B, Xiu G, Bai C. Explosion characteristics of argon/nitrogen diluted natural gas–air mixtures. Fuel. 2014;124:125-32.

[196] Zhang Q, Li W, Tan R, Duan Y. Combustion parameters of gaseous epoxypropane/air in a confined vessel. Fuel. 2013;105:512-7.

[197] Gieras M, Klemens R, Rarata G, Wolański P. Determination of explosion parameters of methane-air mixtures in the chamber of 40 dm3 at normal and elevated temperature. Journal of Loss Prevention in the Process Industries. 2006;19:263-70.

[198] Emami SD, Rajabi M, Che Hassan CR, Hamid MDA, Kasmani RM, Mazangi M. Experimental study on premixed hydrogen/air and hydrogen–methane/air mixtures explosion in 90 degree bend pipeline. International Journal of Hydrogen Energy. 2013;38:14115-20.

[199] Li Q, Lin B, Dai H, Zhao S. Explosion characteristics of H2/CH4/air and

CH4/coal dust/air mixtures. Powder Technology. 2012;229:222-8.

[200] Salzano E, Cammarota F, Di Benedetto A, Di Sarli V. Explosion behavior of hydrogen–methane/air mixtures. Journal of Loss Prevention in the Process Industries. 2012;25:443-7.

[201] Ning J, Wang C, Lu J. Explosion characteristics of coal gas under various initial temperatures and pressures. Shock Waves. 2006;15:461-72.

[202] Tran M-V, Scribano G, Chong CT, Ho TX, Huynh TC. Experimental and numerical investigation of explosive behavior of syngas/air mixtures. International Journal of Hydrogen Energy. 2018;43:8152-60.

[203] Xie Y, Wang J, Cai X, Huang Z. Pressure history in the explosion of moist syngas/air mixtures. Fuel. 2016;185:18-25.

[204] Yu M, Yang X, Zheng K, Zheng L, Wen X. Experimental study of premixed syngas/air flame deflagration in a closed duct. International Journal of Hydrogen Energy. 2018;43:13676-86.

[205] Dupont L, Accorsi A. Explosion characteristics of synthesised biogas at various temperatures. Journal of Hazardous Materials. 2006;136:520-5.

[206] Tran M-V, Scribano G, Chong CT, Ho TX. Influence of hydrocarbon additions and dilutions on explosion behavior of syngas/air mixtures. International Journal of Hydrogen Energy. 2017;42:27416-27.

[207] Lu X, Hu E, Li X, Ku J, Huang Z. Non-monotonic behaviors of laminar burning velocities of H2/O2/He mixtures at elevated pressures and temperatures. International Journal of Hydrogen Energy. 2017;42:22036-45.

[208] Kéromnès A, Metcalfe WK, Heufer KA, Donohoe N, Das AK, Sung C-J, et al. An experimental and detailed chemical kinetic modeling study of hydrogen and syngas mixture oxidation at elevated pressures. Combustion and Flame. 2013;160:995-1011.

[209] Broustail G, Halter F, Seers P, Moréac G, Mounaïm-Rousselle C. Experimental determination of laminar burning velocity for butanol/iso-octane and ethanol/iso-octane blends for different initial pressures. Fuel. 2013;106:310-7.

[210] Bradley D, Gaskell PH, Gu XJ. Burning velocities, markstein lengths, and flame quenching for spherical methane-air flames: A computational study. Combustion and Flame. 1996;104:176-98.

[211] Law CK, Sung CJ. Structure, aerodynamics, and geometry of premixed flamelets. Progress in Energy and Combustion Science. 2000;26:459-505.

[212] Chen Z. On the accuracy of laminar flame speeds measured from outwardly propagating spherical flames: Methane/air at normal temperature and pressure. Combustion and Flame. 2015;162:2442-53.

[213] Lamoureux N, Djebaïli-Chaumeix N, Paillard CE. Laminar flame velocity determination for H2–air–He–CO2 mixtures using the spherical bomb method. Experimental Thermal and Fluid Science. 2003;27:385-93.

[214] Broustail G, Seers P, Halter F, Moréac G, Mounaïm-Rousselle C. Experimental determination of laminar burning velocity for butanol and ethanol iso-octane blends. Fuel. 2011;90:1-6.

[215] Burke MP, Chen Z, Ju Y, Dryer FL. Effect of cylindrical confinement on the determination of laminar flame speeds using outwardly propagating flames. Combustion and Flame. 2009;156:771-9.

[216] Kelley AP, Law CK. Nonlinear effects in the extraction of laminar flame speeds from expanding spherical flames. Combustion and Flame. 2009;156:1844-51.

[217] Chen Z. Effects of radiation and compression on propagating spherical flames of methane/air mixtures near the lean flammability limit. Combustion and Flame. 2010;157:2267-76.

[218] Rozenchan G, Zhu D, Law CK, Tse S. Outward propagation, burning velocities, and chemical effects of methane flames up to 60 atm. Proceedings of the Combustion Institute. 2002;29:1461-70.

[219] Chen Z, Qin X, Ju Y, Zhao Z, Chaos M, Dryer FL. High temperature ignition and combustion enhancement by dimethyl ether addition to methane–air mixtures. Proceedings of the Combustion Institute. 2007;31:1215-22.

[220] Li X, Hu E, Meng X, Peng C, Lu X, Huang Z. Effect of Lewis Number on Nonlinear Extrapolation Methods from Expanding Spherical Flames. Combustion Science and Technology. 2017;189:1510-26.

[221] Markstein GH. Experimental and theoretical studies of flame-front stability. Journal of the Aeronautical Sciences. 1951;18:199-209.

[222] Frankel M, Sivashinsky G. On effects due to thermal expansion and Lewis

number in spherical flame propagation. Combustion science and technology. 1983;31:131-8.

[223] Chen Z. On the extraction of laminar flame speed and Markstein length from outwardly propagating spherical flames. Combustion and Flame. 2011;158:291-300.

[224] Wu F, Liang W, Chen Z, Ju Y, Law CK. Uncertainty in stretch extrapolation of laminar flame speed from expanding spherical flames. Proceedings of the Combustion Institute. 2015;35:663-70.

[225] Kwon OC, Rozenchan G, Law CK. Cellular instabilities and self-acceleration of outwardly propagating spherical flames. Proceedings of the Combustion Institute. 2002;29:1775-83.

[226] Muppala SPR, Nakahara M, Aluri NK, Kido H, Wen JX, Papalexandris MV. Experimental and analytical investigation of the turbulent burning velocity of two-component fuel mixtures of hydrogen, methane and propane. International Journal of Hydrogen Energy. 2009;34:9258-65.

[227] Dinkelacker F, Manickam B, Muppala SPR. Modelling and simulation of lean premixed turbulent methane/hydrogen/air flames with an effective Lewis number approach. Combustion and Flame. 2011;158:1742-9.

[228] Addabbo R, Bechtold JK, Matalon M. Wrinkling of spherically expanding flames. Proceedings of the Combustion Institute. 2002;29:1527-35.

[229] Chen Z, Burke MP, Ju Y. Effects of Lewis number and ignition energy on the determination of laminar flame speed using propagating spherical flames. Proceedings of the Combustion Institute. 2009;32:1253-60.

[230] Kim HH, Won SH, Santner J, Chen Z, Ju Y. Measurements of the critical initiation radius and unsteady propagation of n-decane/air premixed flames. Proceedings of the Combustion Institute. 2013;34:929-36.

[231] Ronney PD, Wachman HY. Effect of gravity on laminar premixed gas combustion I: Flammability limits and burning velocities. Combustion and Flame. 1985;62:107-19.

[232] Qiao L, Gu Y, Dahm WJA, Oran ES, Faeth GM. Near-limit laminar burning velocities of microgravity premixed hydrogen flames with chemically-passive fire suppressants. Proceedings of the Combustion Institute. 2007;31:2701-9.

[233] Jayachandran J, Zhao R, Egolfopoulos FN. Determination of laminar flame

speeds using stagnation and spherically expanding flames: Molecular transport and radiation effects. Combustion and Flame. 2014;161:2305-16.

[234] Yu H, Han W, Santner J, Gou X, Sohn CH, Ju Y, et al. Radiation-induced uncertainty in laminar flame speed measured from propagating spherical flames. Combustion and Flame. 2014;161:2815-24.

[235] Santner J, Haas FM, Ju Y, Dryer FL. Uncertainties in interpretation of high pressure spherical flame propagation rates due to thermal radiation. Combustion and Flame. 2014;161:147-53.

[236] Chen Z, Qin X, Xu B, Ju Y, Liu F. Studies of radiation absorption on flame speed and flammability limit of CO2 diluted methane flames at elevated pressures. Proceedings of the Combustion Institute. 2007;31:2693-700.

[237] Bradley D, Lawes M, Liu K, Verhelst S, Woolley R. Laminar burning velocities of lean hydrogen–air mixtures at pressures up to 1.0 MPa. Combustion and Flame. 2007;149:162-72.

[238] Jomaas G, Law C, Bechtold J. On transition to cellularity in expanding spherical flames. Journal of fluid mechanics. 2007;583:1-26.

[239] Bonhomme A, Selle L, Poinsot T. Curvature and confinement effects for flame speed measurements in laminar spherical and cylindrical flames. Combustion and Flame. 2013;160:1208-14.

[240] Chen Z, Burke MP, Ju Y. Effects of compression and stretch on the determination of laminar flame speeds using propagating spherical flames. Combustion Theory and Modelling. 2009;13:343-64.

[241] Wang D, Ji C, Wang S, Yang J, Meng H. Numerical Study of Geometric Effects on Burning Velocity Measurement by Constant Volume Method. Combustion Science and Technology. 2019:1-18.

[242] Li X, You X, Wu F, Law CK. Uncertainty analysis of the kinetic model prediction for high-pressure H2/CO combustion. Proceedings of the Combustion Institute. 2015;35:617-24.

[243] Santner J, Haas FM, Dryer FL, Ju Y. High temperature oxidation of formaldehyde and formyl radical: A study of 1,3,5-trioxane laminar burning velocities. Proceedings of the Combustion Institute. 2015;35:687-94.

[244] Varea E, Beeckmann J, Pitsch H, Chen Z, Renou B. Determination of burning

velocities from spherically expanding H2/air flames. Proceedings of the Combustion Institute. 2015;35:711-9.

[245] Kelley AP, Bechtold JK, Law CK. Premixed flame propagation in a confining vessel with weak pressure rise. Journal of Fluid Mechanics. 2012;691:26-51.

[246] Halter F, Tahtouh T, Mounaïm-Rousselle C. Nonlinear effects of stretch on the flame front propagation. Combustion and Flame. 2010;157:1825-32.

[247] Moffat RJ. Describing the uncertainties in experimental results. Experimental Thermal and Fluid Science. 1988;1:3-17.

[248] Lowry W, de Vries J, Krejci M, Petersen E, Serinyel Z, Metcalfe W, et al. Laminar flame speed measurements and modeling of pure alkanes and alkane blends at elevated pressures. Journal of Engineering for Gas Turbines and Power. 2011;133:091501.

[249] Zhang Y, Shen W, Fan M, Zhang H, Li S. Laminar flame speed studies of lean premixed H2/CO/air flames. Combustion and Flame. 2014;161:2492-5.

[250] Li Q, Tang C, Cheng Y, Guan L, Huang Z. Laminar flame speeds and kinetic modeling of n-pentanol and its isomers. Energy & Fuels. 2015;29:5334-48.

[251] Krejci M, Vissotski A, Ravi S, Metcalfe W, Keromnes A, Curran H, et al. Laminar flame speed measurements of moist syngas fuel blends at elevated pressures and temperatures. Spring Technical Meeting of the Central States Section of the Combustion Institute 2012.

[252] Cai X, Wang J, Zhang W, Xie Y, Zhang M, Huang Z. Effects of oxygen enrichment on laminar burning velocities and Markstein lengths of CH4/O2/N2 flames at elevated pressures. Fuel. 2016;184:466-73.

[253] Kee RJ, Grcar JF, Smooke MD, Miller J, Meeks E. PREMIX: a Fortran program for modeling steady laminar one-dimensional premixed flames. Sandia National Laboratories Report. 1985.

[254] Kee RJ, Rupley FM, Meeks E, Miller JA. CHEMKIN-III: A FORTRAN chemical kinetics package for the analysis of gas-phase chemical and plasma kinetics. Sandia National Laboratories Report SAND96-8216. 1996.

[255] Kee RJ, Dixon-Lewis G, Warnatz J, Coltrin ME, Miller JA. A Fortran computer code package for the evaluation of gas-phase multicomponent transport properties. Sandia National Laboratories Report SAND86-8246.

1986;13:80401-1887.

[256] Li J, Zhao Z, Kazakov A, Chaos M, Dryer FL, Scire JJ. A comprehensive kinetic mechanism for CO, CH2O, and CH3OH combustion. International Journal of Chemical Kinetics. 2007;39:109-36.

[257] Mueller M, Kim T, Yetter R, Dryer F. Flow reactor studies and kinetic modeling of the H2/O2 reaction. International Journal of Chemical Kinetics. 1999;31:113-25.

[258] Li J, Zhao Z, Kazakov A, Dryer FL. An updated comprehensive kinetic model of hydrogen combustion. International Journal of Chemical Kinetics. 2004;36:566-75.

[259] Xie Y, Wang J, Xu N, Yu S, Zhang M, Huang Z. Thermal and Chemical Effects of Water Addition on Laminar Burning Velocity of Syngas. Energy & Fuels. 2014;28:3391-8.

[260] Zhou Q, Cheung CS, Leung CW, Li X, Huang Z. Effects of diluents on laminar burning characteristics of bio-syngas at elevated pressure. Fuel. 2019;248:8-15.

[261] Zhou Q, Cheung CS, Leung CW, Li X, Li X, Huang Z. Effects of fuel composition and initial pressure on laminar flame speed of H2/CO/CH4 bio-syngas. Fuel. 2019;238:149-58.

[262] Zhang X, Huang Z, Zhang Z, Zheng J, Yu W, Jiang D. Measurements of laminar burning velocities and flame stability analysis for dissociated methanol–air–diluent mixtures at elevated temperatures and pressures. International Journal of Hydrogen Energy. 2009;34:4862-75.

[263] STANJAN transport properties calculator Available at: http:// navierengrcolostateedu/~dandy/code/code-2/indexhtml.

[264] Kee R, Rupley F, Miller J. CHEMKIN: The Chemkin Thermodynamic Database. Rep. SAND87-8215. Sandia National Laboratories, Livermore (CA), USA. 1987.

[265] Kuo KK. Principles of Combustion2005.

[266] Chaos M, Dryer FL. Syngas combustion kinetics and applications. Combustion Science and Technology. 2008;180:1053-96.

[267] Law C. Propagation, structure, and limit phenomena of laminar flames at elevated pressures. Combustion Science and Technology. 2006;178:335-60.

[268] Egolfopoulos FN, Law CK. Chain mechanisms in the overall reaction orders in laminar flame propagation. Combustion and Flame. 1990;80:7-16.

[269] Singh D, Nishiie T, Tanvir S, Qiao L. An experimental and kinetic study of syngas/air combustion at elevated temperatures and the effect of water addition. Fuel. 2012;94:448-56.

[270] Westbrook CK, Dryer FL. Chemical kinetic modeling of hydrocarbon combustion. Progress in Energy and Combustion Science. 1984;10:1-57.

[271] Manton J, von Elbe G, Lewis B. Burning-velocity measurements in a spherical vessel with central ignition. Symposium (International) on Combustion: Elsevier; 1953. p. 358-63.

[272] Markstein G. Non-steady flame Propagation,(1964). P22, Pergarmon, New York.

[273] Tang C, He J, Huang Z, Jin C, Wang J, Wang X, et al. Measurements of laminar burning velocities and Markstein lengths of propane–hydrogen–air mixtures at elevated pressures and temperatures. International Journal of Hydrogen Energy. 2008;33:7274-85.

[274] Wang JH, Xie YL, Cai X, Nie YH, Peng C, Huang ZH. Effect of H2O Addition on the Flame Front Evolution of Syngas Spherical Propagation Flames. Combustion Science and Technology. 2016;188:1054-72.

[275] Van den Bulck E. Closed algebraic expressions for the adiabatic limit value of the explosion constant in closed volume combustion. Journal of Loss Prevention in the Process Industries. 2005;18:35-42.

[276] Lewis B, von Elbe G. Combustion, Flames and Explosions of Gases 3rd edn (New York: Academic). 1987.

[277] Savitzky A, Golay MJ. Smoothing and differentiation of data by simplified least squares procedures. Analytical chemistry. 1964;36:1627-39.

[278] Cashdollar KL, Zlochower IA, Green GM, Thomas RA, Hertzberg M. Flammability of methane, propane, and hydrogen gases. Journal of Loss Prevention in the Process Industries. 2000;13:327-40.

[279] Nagy J, Conn JW, Verakis HC. Explosion development in a spherical vessel: US Department of the Interior, Bureau of Mines; 1969.

[280] Phylaktou H, Andrews G. Gas explosions in long closed vessels. Combustion Science and Technology. 1991;77:27-39.

[281] Phylaktou H, Andrews G, Herath P. Fast flame speeds and rates of pressure rise in the initial period of gas explosions in large L/D cylindrical enclosures. Journal of Loss Prevention in the Process Industries. 1990;3:355-64.

[282] NFPA 68. Guide for venting deflagrations. National Fire Protection Agency; 2002.

[283] Bartknecht W, Zwahlen G. Explosionsschutz: Grundlagen und Anwendung: Springer; 1993.

[284] Law CK, Makino A, Lu TF. On the off-stoichiometric peaking of adiabatic flame temperature. Combustion and Flame. 2006;145:808-19.

[285] Association NFP. NFPA 68: Standard on explosion protection by deflagration venting: National Fire Protection Association; 2007.

[286] Bradley D, Mitcheson A. Mathematical solutions for explosions in spherical vessels. Combustion and Flame. 1976;26:201-17.

[287] Movileanu C, Razus D, Oancea D. Additive effects on the rate of pressure rise for ethylene–air deflagrations in closed vessels. Fuel. 2013;111:194-200.

[288] Qiao L, Kim CH, Faeth GM. Suppression effects of diluents on laminar premixed hydrogen/oxygen/nitrogen flames. Combustion and Flame. 2005;143:79-96.

[289] Di Benedetto A, Di Sarli V, Salzano E, Cammarota F, Russo G. Explosion behavior of CH4/O2/N2/CO2 and H2/O2/N2/CO2 mixtures. International Journal of Hydrogen Energy. 2009;34:6970-8.